Role of Calcium in Cerebellar Learning and Function

De Rol van Calcium bij Cerebellair Leren en Funktioneren

Proefschrift

Ter verkrijging van de graad van doctor aan de
Erasmus Universiteit Rotterdam
op gezag van de
rector magnificus

Prof. Dr. H.G. Schmidt

en volgens besluit van het College voor Promoties.

De openbare verdediging zal plaatsvinden op
Woensdag 15 Juni 2011 om 09:30 uur

door

Zhenyu Gao

geboren te Shanghai, China

Promotiecommissie

Promotor:	Prof. dr. C.I. De Zeeuw
Overige leden:	Prof. dr. J.G.G. Borst
	Prof. dr. Y. Elgersma
	Dr. A.B. Houtsmuller
Copromoter:	Dr. F.E. Hoebeek

The work presented in this thesis was performed in the Department of Neuroscience at the Erasmus MC in Rotterdam, The Netherlands and was supported by Prinses Beatrix Fonds. The publication of this thesis was financially supported by J.E. Jurriaanse Stichting.

Printed by Off Page

For my parents

TABLE OF CONTENTS

CHAPTER 1

INTRODUCTION

General introduction

The cerebellum, which means little brain in Latin, occupies most of the posterior cranial fossa and connects with the dorsal brainstem (Kandel et al., 2000). The cerebellar cortex is one of the most foliated brain structures, which accounts for 10% of the total volume and over half of the total neurons in the central nervous system of higher vertebrates (Llinas et al., 2004). The unique position and structure of cerebellum has inspired neuroscientists over the past century to dedicate their research and imagination to uncover the function of the cerebellum. In the late 19th century, the cerebellum was suggested to be involved in controlling the spatial accuracy and temporal coordination of motor movement, based on clinical studies on cerebellar specific lesion patients. Further studies suggested that the learning and memory of motor movements may also be stored in cerebellum (for review see Dow and Moruzzi, 1958). Meanwhile, in the late 19th and early 20th century, the Italian scientist Camillo Golgi as well as his Spanish colleague and life-long competitor Santiago Ramón y Cajal (who shared the Nobel Prize for Physiology and Medicine in 1906) carried out their pioneer research on the detailed cellular organization of the cerebellum (and other parts of the central nervous system). Their studies provided the initial description of the cerebellar circuit.

In the 1960's a legendary group of scientists, including John C. Eccles, David Marr, James S. Albus, and Masao Ito, compiled the emerging anatomical and electrophysiological data of various cerebellar neurons and proposed an influential theory about how the cerebellum functions. This theory suggests that the cerebellum functions as a neuronal machine that decodes and encodes vast amount of inputs at high spatial and temporal resolution (Eccles, 1967; Marr, 1969; Albus, 1971; Ito, 2006). The essence of this theory, which is best known as the *Marr-Albus-Ito* hypothesis, has inspired new generations of cerebellar scientists to focus their research on the cellular and molecular mechanisms that enable motor learning in the cerebellum. Over the years, various types of short- and long-term synaptic plasticity as well as intrinsic plasticity have been revealed and most of them play a role in motor learning. Genetically manipulated animal models proved valuable in dissecting the molecular pathways that control these forms of synaptic plasticity. Such studies not only complement but also challenge the classic cerebellar learning theory, which promote the future discussion on how the cerebellum encodes information and changes this processing of inputs such that the output is adapted to the novel situation.

One of the fundamental features of various synaptic plasticity and neuronal activity during motor learning is calcium dependency. The calcium ion (Ca^{2+}) is one of the common second messengers in the central nervous system. How Ca^{2+} dependent signaling cascades control synaptic transmission and synaptic plasticity are probably two of the most studied topics in current neuroscience research. The current thesis will focus on how Ca^{2+}-dependent signaling affects synaptic and cellular functions in the cerebellum thereby this thesis contributes to the discussion of cerebellar functioning in a wide spectrum, ranging from Ca^{2+}-dependent signaling cascades to cerebellar motor performance and learning. Subsequently, this thesis will focus on the deficits of one of the main Ca^{2+}-sources in neurons: the voltage-gated Ca^{2+}-channels, and explain the consequences of Ca^{2+}-channelopathy in a

Ca^{2+}-channel mutant mouse model. Finally, this thesis will summarize our recent research and discuss the current scopes of the role of Ca^{2+}-dependent cascades in cerebellar learning and functions.

1.1 Cerebellum circuitry and functions

The cerebellum as a whole consists of three functional regions: the outermost is the cerebellar cortex, which contains most of the cerebellar neurons and connections; the middle is the white matter that consists of the input and output fibers; and the innermost cerebellar nuclei. The cerebellar cortex in higher vertebrates can be divided into three anatomical and functional distinct regions. The central part, which is called vermis, receives visual, auditory, vestibular and somatosensory inputs and projects the fastigial nucleus to the cerebral cortex and brain stem. The cerebellar hemispheres, which are located aside from the vermis, receive inputs from the cerebral cortex and send output to various motor related regions. The most primitive and phylogenetically preserved part of the cerebellum is the flocculonodular lobe. The nodulus receives input directly from vestibular projections and the flocculonodular lobe sends its output primarily to the vestibular nuclei. It is generally believed that the flocculonodular region is involved exclusively in controlling body balance and eye movement in high vertebrates. The anatomy and connectivity of flocculonodular cerebellum is one of the most extensively studied cerebellar regions, and is also one of the regions of interest in this thesis (Figure 1).

1.1.1 Anatomical pathways within the cerebellar cortex

Despite some anatomical variations, the cerebellar cortex consists of a well-organized homogenous neuronal circuitry that can be divided in three layers: the granular layer, the molecular layer and the Purkinje cell layer. The main input-output pathway in the cerebellar cortex travels these three layers: mossy fibers (MF) that derive from various brain regions contact granule cells (GrCs) in the granular layer, GrCs and climbing fiber (CF) from inferior olive contact Purkinje cells (PCs) in the molecular layer and the output of the cerebellar cortex is formed in the Purkinje cell layer. In addition to these excitatory connections, local inhibitory interneurons like stellate cells, basket cells, Golgi cells and Lugaro cells are superimposed in various layers of the cerebellar cortex (Figure 1). Although some variations have been reported, such as the presence of excitatory unipolar-brush cells in the granule layer, each neuronal component has a predetermined location in the cortical structure. The granular layer consists of GrCs, Golgi cells and Lugaro cells. The molecular layer is populated by the fan-shaped dendritic trees of PCs, stellate/basket cells (i.e., molecular layer interneurons (MLI)), vast amounts of GrC axons (ascending GrC axons and parallel fibers (PFs)) and the axons of olivary neurons (e.g., CFs). The Purkinje cell layer consists almost exclusively of PC somata. In addition to the neuronal components all three cortical layers contain glia and astrocytes, which are believed not only to support the function of the network, but also to control neuronal activity at various levels (Lee et al., 2010). Overall,

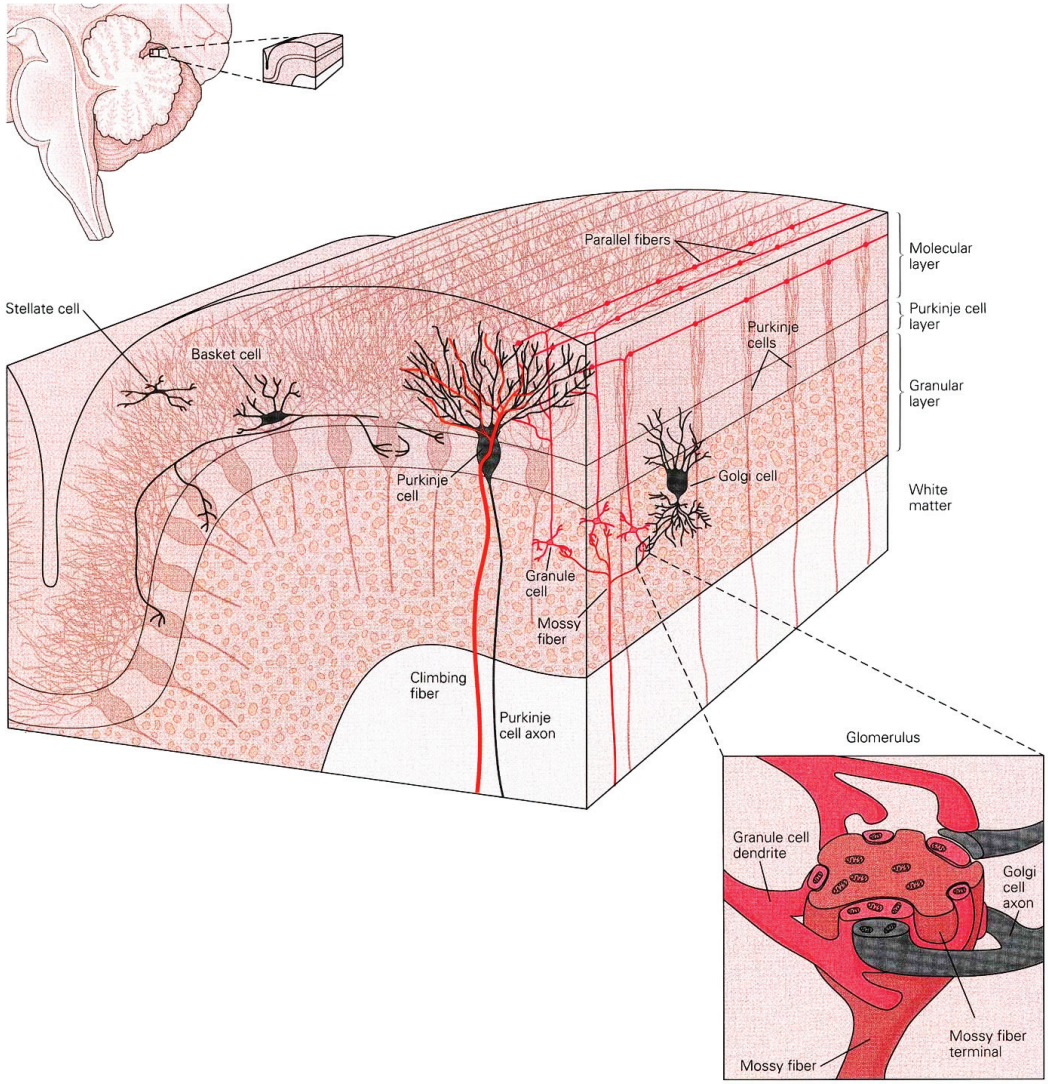

Figure 1. Cerebellar cotical neurons are organized into three distinct layers

The mossy fiber and climbing fiber pathways are the two inputs into the cerebellum. Granule cells and Purkinje cells form the major input-output pathway in the cerebellar cortex, whereas inhibitory interneurons, stellate cells, basket cells and Golgi cells are superimposed into the main pathway. The detail of a cerebellar glomerulus in the granular layer that contains a mossy fiber terminal as well as granule cell and Golgi cell terminals is also shown. Adapted form Kandel et al., 2000.

the granule layer is seen as the input layer, the molecular layer as the intermediate layer and the Purkinje cell layer as the output layer.

The granular layer

In rodents and higher-order mammals, GrCs account for more than half of all neurons in the central nervous system to even more than 70% (~10^{11}) of the total neurons in humans (Eccles, 1969). Surprisingly, the morphological features of the GrCs, e.g., small neurons

(~5-10 µm), 4 short claw-like dendrites and a single axon that bifurcates into parallel fibers, have been highly preserved during phylogeny (Eccles, 1969). The connectivity of GrCs is consistent across several species. The dendritic claws of several GrCs wrap around single MF axon terminals ('rosettes'), which together with glia and GoC axon terminals form a glomerulus. Each cerebellar GrC receives on average input from 4 MFs; one MF per GrC dendrite. It is most likely this limited input per GrC that accounts for their abundance: in order to cope with all the information encoded by MFs the cerebellar cortex needs a great number of GrCs. The output of the GrC is formed by both its ascending part and the bifurcated PFs, which contact Golgi cell dendrites, PC spiny branchlets and molecular layer interneurons.

The excitatory (glutamatergic) input from MFs to GrCs is balanced by inhibitory input (GABAergic) from Golgi cells. Activity in Golgi cells induces release of GABA into the confined space of the glomerulus. Postsynaptically, GABA is bound by both synaptic and extrasynaptic $GABA_A$ receptors, which are thought to mediate phasic and tonic inhibition, respectively (Brickley et al., 1996; Nusser et al., 1998). Thus, whereas most neurons receive inhibitory input (peri-) somatically, GrC are actively inhibited by maintaining GABA conductance at their dendrites by Golgi cells. In turn, Golgi cells are excited directly by GrCs through their ascending axon terminals and PFs. This excitatory drive is often characterized as the slow excitatory input to GoCs, whereas the direct innervations of Golgi cell by MFs is referred to as the fast excitatory input. This connectivity functions as an inhibitory feedback loop, in that MF activity first elicits GrC and Golgi cell activity, but then the Golgi cell activity suppresses the GrC activity, which eventually reduces the excitatory input from GrCs to Golgi cells (see also Chapter 2). In addition to this inhibitory feedback loop, the granular layer of vermal regions and vestibulocerebellar lobules is also characterized by feed-forward excitation from unipolar-brush cells. These neurons are excited by glutamate released from MF terminals and in turn excite various GrCs by release of glutamate. In addition to GrCs, Golgi cells and unipolar-brush cells, Lugaro cells are also positioned in the granular layer, albeit the most superior part. Lugaro cells contact ~5-15 PCs somata in the near vicinity by means of bi-polarly organized dendrites. Lugaro cell axons run perpendicular to PFs and are believed to contact GoCs dendrites in the proximal half of the molecular layer (Dieudonne and Dumoulin, 2000) and also PC dendrites (Dean et al., 2003). The sparse spontaneous activity of Lugaro cells is controlled by serotonin and evokes a mixed GABA-ergic / glycinergic inhibition of target neurons (Dieudonne and Dumoulin, 2000; Dumoulin et al., 2001).

The molecular layer

Several axonal structures arise from the granular layer into the molecular layer to contact dendrites of Molecular layer interneurons, Golgi cells and / or PCs. The most predominant axon in the molecular layer is the GrC axon. Both the ascending GrC axon and the resulting PFs travel through the molecular layer. PFs transverse through the molecular layer and form only few synapses per target neurons (i.e., <2 per PC), whereas ascending GrC axons form various contacts per target neuron (i.e., ~10-20 per PC) (Harvey and Napper, 1991; Gundappa-Sulur et al., 1999). This difference in connectivity founded the dispute between

the beam-theory and patch-theory (Braitenberg and Atwood, 1958; Eccles, 1967; Eccles et al., 1972; Bower and Woolston, 1983). Although some consensus has been reached due to detailed anatomical and electrophysiological characterization of these synapses, it remains unclear how the output of GrCs is transmitted to Purkinje cells. Also the anatomical and functional connectivity to the other GrC target neurons is not yet clarified. Imaging studies may prove the best way to decipher how GrC activity affects other neurons, as recently shown by the Ebner lab (Wang et al., 2011).

Another predominant axon in the molecular layer is the CFs, which arises from the inferior olivary nucleus in the ventral brainstem. Each inferior olive axon forms ~10 collaterals, all of which innervate sagitally-oriented strips of cerebellar cortex (Voogd et al., 1996) and branch intensely. In the adult brain, each Purkinje cell is contacted by ~1500 CF synapses formed by a single collateral of the inferior olive axon (Dittman and Regehr, 1998). As a result of this widespread branching, the activation of a CF results in the release of glutamate from hundreds of presynaptic sites and the subsequent postsynaptic depolarization that covers large parts of the PC dendritic tree (Konnerth et al., 1992; Miyakawa et al., 1992; Midtgaard et al., 1993). Despite the presence of glutamate transporters like vesicular glutamate transporter type 2 (vGlut2) and excitatory amino acid transporter 4 (EAAT4) near CF–PC synapses (Satake et al., 2010; Miyazaki and Watanabe, 2011) the glutamate spills over from the synaptic cleft. Outside of the CF-PC synapse, glutamate is believed not only to activate dendritic glutamate receptors of MLIs (Szapiro and Barbour, 2007), but also to suppress GABA-release from axon terminals of MLIs on PCs (Satake et al., 2010). In addition, CF collaterals may also contact with Golgi cell soma or dendrites (Palay and Chan-Palay, 1974). Although this collateral connection is currently unexplored, its impact for cerebellar scientists would be substantial and thus worthwhile investigating.

Molecular layer interneurons can be subdivided in stellate and basket cells. Although some reports indicate that both cell types are electrophysiologically similar (Kreiner and Jaeger, 2004; Barmack and Yakhnitsa, 2008; Ruigrok, 2010), their connectivity indicates otherwise: Stellate cells synapse upon distal PC dendrites, whereas basket cells synapse upon the PC soma and form a specialized terminal that wraps the axon hillock. The activity of stellate and basket cell are driven by intrinsic pacemaking activity (Hausser and Clark, 1997) and modulated by excitatory input from GrCs and via spillover from climbing fiber terminals (Szapiro and Barbour, 2007) and by inhibitory input from other Molecular layer interneurons. The output of Molecular layer interneurons controls the timing of action potential firing in PCs (Hausser and Clark, 1997).

The Purkinje cell layer

The PC somata form a mono-layer between the granular layer and molecular layer. This position indicates that numerous fibers pass through of which the GrC axons and CFs are the most predominant. The dendrites of Lugaro and Golgi cells penetrate the PC layer, as well as recurrent PC axon collaterals. The latter fibers branch off to innervate neighboring PCs in young (<P18) mice, but are believed to innervate mostly non-PCs, like basket cells, in older mice and cats (O'Donoghue et al., 1989; Watt et al., 2009). In turn, basket

cells axons also transverse the PC layer to form a pinceau-like axon terminal (e.g., basket) around the perisomatic axonal region of PCs. Together the PC axon collaterals and basket cell axons could form an inhibitory feed-back and feed-forward loop in adult mice, since the innervated basket cells could very well innervate the initial PCs, or its direct neighbors, respectively.

1.1.2 Neuronal activity in the cerebellar cortex

The activity patterns of the various types of neurons in rodents have recently been described in detail (Barmack and Yakhnitsa, 2008; Ruigrok et al., 2011). These studies show that all types of neurons in the cerebellar cortex have specific firing patterns and respond in different ways to, for instance, sensory input from the eye. Each of these firing patterns will have a distinct effect on target neurons. The detailed discussion of all such effects is outside the scope of this thesis. Instead, we will focus on how the output of the cerebellar cortex is shaped by the PCs spiking activity.

PCs are intrinsically active; even freshly dissociated PCs somata fire action potentials at frequencies comparable to those recorded in slices and *in vivo* (Hausser and Clark, 1997; Raman and Bean, 1999; Goossens et al., 2001). This pronounced pacemaking activity is driven by a specific mixture of transient, persistent and resurgent Na^+-currents, which are counterbalanced by voltage-gated K^+-currents (Raman and Bean, 1999). In addition, voltage-gated Ca^{2+}-influx and the resulting Ca^{2+}-dependent K^+-currents also shape action potential firing patterns (Edgerton and Reinhart, 2003; Womack et al., 2004) (see section 1.2.2 for a more detailed description). Inhibition-activated cation-mediated depolarizing currents ('I_H'-currents) are reported to modulate PC activity (Nolan et al., 2003).

Action potential firing in adult PCs is modulated by excitatory GrC and olivary input and by inhibitory stellate and basket cell inputs. All of these afferents except for the latter synapse in the PC dendritic tree. To exert their effects on action potential generation, which occurs in the axon hillock, these synaptic events need to propagate from the dendritic site. The effect of specific distributions of voltage-gated cation channels on propagation from dendrite to soma is complemented by an effect of dendritic morphology (and *vice versa*) (Roth and Hausser, 2001; Branco and Hausser, 2009; Branco et al., 2010) and the continuous bombardment of the PC dendritic tree by numerous synaptic inputs. For instance, the propagation of the CF induced depolarization in the PC dendritic tree is severely affect by inhibitory inputs (Callaway et al., 1995). This inhibitory shunt conductance has been shown to shape the precision and spike rate of PCs (Hausser and Clark, 1997; Jaeger et al., 1997). Thus, propagation in the PC dendritic tree is dependent on the origin of the signal as well as the morphology and the electrophysiological status of the dendritic structure (i.e., depolarized or hyperpolarized membrane potential). In other words, the incorporation of dendritic signaling into the spontaneous pacemaking activity greatly increases the information content of each action potential (and each pause).

Despite the vast amount of information that is encoded into each PC action po-

tential, these events are named ‘simple spikes’ when recorded extracellularly *in vivo*. The true meaning of this nomenclature becomes evident when one considers the other type of activity that characterizes PCs *in vivo*, which is called ‘complex spike’ (Figure 2). This latter spiking event is not related to the intrinsic pacemaking activity, but originates from the activation of a CF. Upon the activation of a CF, the PC receives vast amount of excitatory synaptic input in the perisomatic area of PCs, which initiates a cascade of events in an all-or-none fashion (see (Schmolesky et al., 2002) for review). Upon the depolarization of the

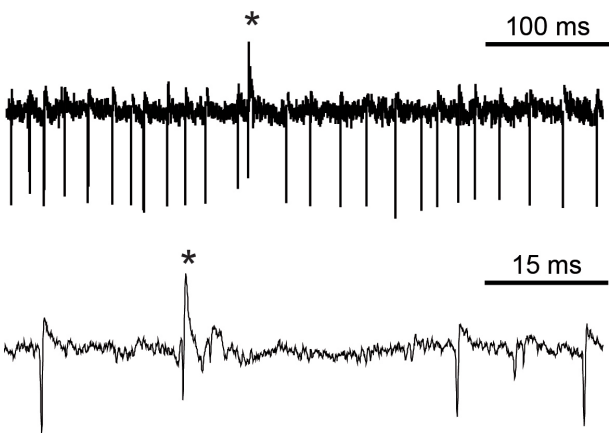

Figure 2. Simple spike and complex spike (*) firing in the extracellular Purkinje cell activity recordings.

dendritic tree due to the opening of voltage-gated Ca^{2+}- channels, NMDA-mediated Ca^{2+}-influx and Ca^{2+}-release from internal Ca^{2+}-store. In soma, this input generates an initial fast, Na^{+}-mediated action potential in the axon hillock. Recent evidence indicates that the subsequent spikelets that seem to ride the Ca^{2+}-mediated plateau, which is caused by the dendritic depolarization, also originate from the axon hillock (Davie et al., 2008). Complex spikes in PCs faithfully represent each signal in the CF, especially since CF axons tend to fire in high-frequency burst (Maruta et al., 2007; Mathy et al., 2009). The local dendritic effects of each complex spike, however, tend to differ extensively due to the inhibitory input from stellate cells (Callaway et al., 1995) and regional differences in expression of metabotropic glutamate receptors (Wang et al., 2011). Together with the differential expression of ion-channels and variation in dendritic morphology these variables may also account for the differential complex spike waveforms recorded in the soma (see (Schmolesky et al., 2002) for examples).

1.1.3 Cerebellar motor control and learning paradigms

The cerebellum is involved in many types of behavior and more functions are ascribed to the hindbrain every year. Yet, the core function of the cerebellum is sensorimotor control. The cerebellum receives vast amounts of sensory data through the MF and CF systems, which is subsequently processed and forwarded via the cerebellar and/or vestibular nuclei to, for instance, premotor nuclei in the brain stem like the red nucleus (Teune et al., 2000). Also parts of the thalamus that are related to motor function (ventro-anterior and ventro-

lateral nuclei) and connected to the motor cortices are innervated by the cerebellar nuclei (Sawyer et al., 1994; Teune et al., 2000).

One of the most investigated motor functions is the compensatory eye movements. Species with a retinal fovea (area of retina with increased density of specialized cells) are equipped with other types of eye movements, like smooth pursuit, that are related to compensatory eye movements. In species that lack a fovea, like rodents, the most studied compensatory eye movements are optokinetic reflex (OKR), vestibulo-ocular reflex (VOR) and visually-enhanced VOR (VVOR) (Figure 3a). OKR is performed when the surrounding is in motion – the eyes follow the surrounding. VOR is performed when the rodent is in motion in darkness – the eyes move in the opposite direction as the head. VVOR is performed when the rodent is in motion in a lighted surrounding – the eyes follow the surrounding and compensate for the movement of the head. The neuronal circuit of these responses centers on the vestibulocerebellar cortex (Figure 3b), e.g., lobules IX and X. More specifically, the two visual reflexes (OKR and VVOR) are dependent on the flocculus, whereas the VOR can be performed without the flocculus (Takemori, 1975; Robinson, 1976; Zee et al., 1981; Ito, 1982; Lisberger et al., 1984; Barmack and Pettorossi, 1985; Nagao, 1989). Rodents' lobules IX and X receive MF inputs from pontine nuclei as well as from primary (only uvula and nodulus) and secondary vestibular afferents (Voogd et al., 1996). The information propagated by these MFs is mixed with the intrinsic activity of neurons in the cerebellar cortex and the activity in the inferior olive nucleus via the CFs. PCs in the vestibulocerebellum innervate neurons in the vestibular nuclei either directly or via neurons in the lateral cerebellar (dentate) nuclei (Voogd et al., 1996; Figure 3).

The flocculus is subdivided in several zones; vertical axis zones and horizontal axis zones. These zones are functionally different in that the neurons of each zone predominantly encode eye movement around the vertical axis and a horizontal axis (Stahl and Simpson, 1995; Schonewille et al., 2006). The orientation of these axes is related to the position of the vestibular sensory organs, e.g., the semicircular canals in the inner ear. The anterior and posterior semicircular canals innervate superior and inferior rectus and oblique eye muscles to evoke eye movements in the vertical plane around horizontal axes. The horizontal canals innervate the medial and lateral rectus muscles and thereby evoke eye movements in the horizontal plane around the vertical axis. Whereas the vertical axis is predefined, the horizontal axis can be rotated. Rotations of the head around horizontal axes that are perpendicular to the orientation of the anterior (45° ipsilateral azimuth) and posterior (135° ipsilateral azimuth) semicircular canal are most effective in evoking an eye movement. The floccular PCs in the horizontal axes zones (HA PCs) respond with modulation of spiking frequency most sensitively to eye movements around a horizontal axis 135° ipsilateral azimuth. Similarly, rotations of the eye around a vertical axis also evoke a response in PCs within vertical axes zones (VA PCs). As natural eye movements will be a mixture of horizontal and vertical axes, both HA and VA PCs will be involved in the coordination of such complex movements.

The optokinetic and vestibular stimuli that we use in our experiments are oriented around the vertical axis. To evoke optokinetic reflexes we rotate a black-and-white check-

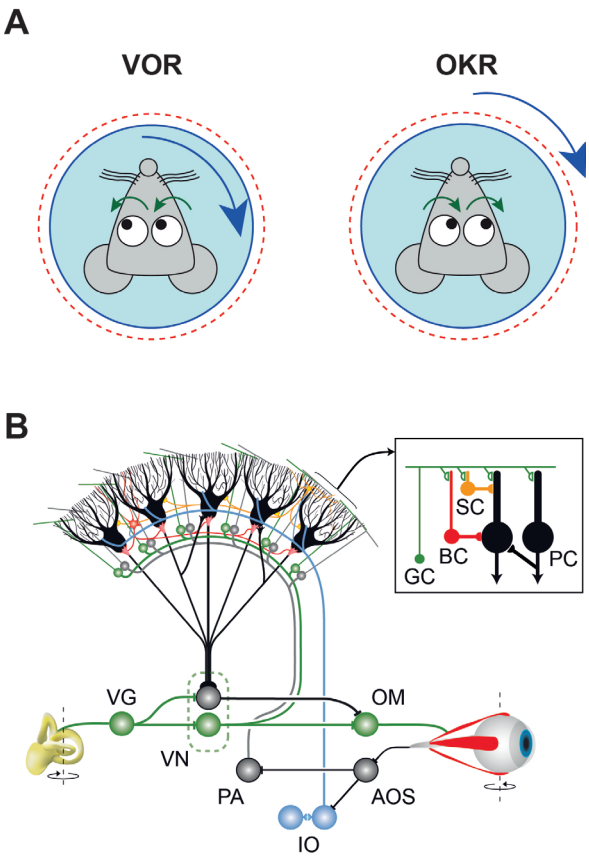

Figure 3.

A. Schematic drawings of the eye movements of the mouse in response to VOR and OKR stimulation paradigms.

B. Schematic drawing of intra- and extracerebellar connections that are involved in vestibuloocular and optokinetic reflexes. Floccular Purkinje cells receive inputs from the vestibular and ocular systems via mossy fiber projections during vestibuloocular and/or optokinetic reflexes. The climbing fiber activity, which is triggered by retinal slip signal, through the inferior olive projections, is also involved. AOS (accessory optic system), IO (inferior olive), OM (oculomotor neurons), PA (Potine areas),VG (vestibular ganglion cells) and VN (vestibular nuclei).

ered surrounding around the head-fixed mouse with a constant amplitude (5°) or constant velocity (8°/s) at various frequencies (0.1 – 1.6 Hz). In mice the OKR acts as a low-pass filter, in that at low frequencies the responses are near optimal, but start lagging when the frequencies increase. In contrast, the VOR, which we record in the dark by rotating the mouse around the vertical axis with a constant amplitude (5°) at various frequencies (0.1 – 1.0 Hz), acts as a high-pass filter; at high frequencies the responses are better than at low frequencies. When mice are rotated in a lighted, stable surrounding, their OKR and VOR response are combined; their visually-enhanced VOR (VVOR) performs almost equally well at all tested frequencies (0.1 – 1.0 Hz) and amplitudes (5° and 10°). The amplitude of VOR can be modified to adapt the combination of such visual and vestibular input. The details of the VOR adaptation will be described in later chapters.

1.2 The role of calcium in cerebellar functions

Ca^{2+} entry into the cytoplasm is critical for a variety of neuronal functions, including action potential firing, neurotransmitter release, induction of short- and long-term synaptic plasticity, as well as gene transcription (Ahn et al., 1999; Raman and Bean, 1999; Coesmans et al., 2004; Catterall and Few, 2008; Fioravante and Regehr, 2011). The Ca^{2+}-signaling

cascades that control these neuronal functions are generally initiated by a transient increase of the cytoplasmic Ca^{2+}-concentration that can occur via three main sources: the Ca^{2+}-influx through Ca^{2+}-permeable glutamate receptors, release of Ca^{2+} from internal Ca^{2+}-stores and through voltage-gated Ca^{2+}-(Ca_V) channels.

In this thesis we will primarily focus on the Ca^{2+}-signaling cascades mediated by Ca_V-channels and will discuss the functional importance for synaptic transmission, synaptic plasticity, action potential firing and, finally, the pathogenesis of Ca_V-channel malfunction. The Ca_V-channels can be categorized based on their physiological and pharmacological properties into P/Q-type, N-type, R-type, L-type and T-type of Ca_V channels (Dunlap et al., 1995). P/Q-, N-, L- and R-type Ca_V-channels require a strong depolarization of the membrane potential to be activated and thus are high-voltage-activated Ca_V-channels. In contrast, T-type Ca_V-channels are more readily activated at near resting membrane potentials,

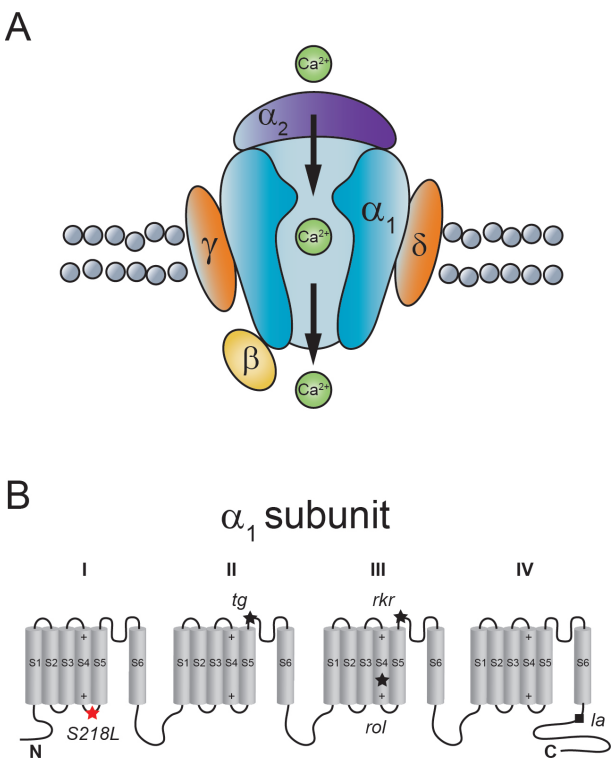

Figure 4

A. Scheme showing the subunits of a voltage gated calcium channel. The α1 subunit forms the pore of Ca^{2+} entry.

B. Mutations in the *cacna1a* gene which are associated with ataxia in mouse models. *S218L* (S218L knock-in mutant), *tg* (Tottering), *rkr* (Rocker), *rol* (Rolling Nagoya) and *la* (Leaner).

and thus are low-voltage-activated Ca_V-channels. Despite the variety of channel properties, all Ca_V-channel subtypes share similar structural features. They are composed by four or five distinct subunits (Dunlap et al., 1995; Catterall, 2000), which include a single α1-subunit. Alpha1-subunits of Ca_V-channels are formed by four homologous transmembrane sections, each of which consists of six transmembrane (S1-S6) helices and an intracellular loop between S5 and S6. The S1 to S4 helices serve as the voltage sensor, whereas the four transmembrane domains between S5 and S6 form the pore of the channel. The α1-subunits are encoded by a group of distinct genes in mammals (for review see Snutch and Reiner, 1992; Catterall, 2000): *cacna1a* encodes the α1-subunit of P/Q-type channels; *cacna1b* encodes the α1-subunit of N-type channels, *cacna1c/d/f* encode the α1-subunit of L-type channels, *cacna1e* encodes the α1-subunit of R-type channels and *cncna1g/h/i* encode for the α1-subunit of T-type channels.

P/Q-type channels can be effectively blocked by spider venom ω-Agatoxin-IVA (Mintz et al., 1992b). It is predominantly expressed at presynaptic terminals and somato-

dendritic membranes (Westenbroek et al., 1995). In the cerebellar cortex, P/Q-type channels are particularly enriched in PC, GrC and other neurons; the P-type, which in fact represents cerebellar Purkinje type, gates the majority of Ca^{2+}-influx in PCs (Llinas and Sugimori, 1980; Llinas et al., 1989; Mintz et al., 1992b); whereas the splicing variant Q-type channels are highly abundant in cerebellar GrCs (Randall and Tsien, 1995; Bourinet et al., 1999). Cav2.2-channels gate N-type Ca^{2+}-currents that can be sensitive to ω-Conotoxin-GVIA (Dubel et al., 1992; Williams et al., 1992); whereas $Ca_V2.3$-channels mediate R-type Ca^{2+}-currents that can be effectively inhibited by SNX-482 (Tottene et al., 2000). Both N-type and R-type Ca^{2+} -channels are widely expressed in the synaptic terminals and neuronal dendrites of various cerebellar neurons that control the neurotransmitter release and Ca^{2+}-transients in the dendrites (Tottene et al., 2000; Matsushita et al., 2002; Cavelier et al., 2008; Myoga and Regehr, 2011).

1.2.1 The role of calcium in synaptic transmission

It has been shown that P/Q-type Ca_V-channels mediate the bulk of fast transmitter release at various synapses in the cerebellum. At PF-PC synapses, blockage of P/Q-type Ca_V-channels suppresses more than 90% of the total synaptic transmission, whereas the remaining component is primarily mediated by N-type Ca_V-channels (Mintz et al., 1995; Matsushita et al., 2002). Previous studies estimated that P/Q-type Ca_V-channels account for more than half of the total number Ca_V-channels at presynaptic terminals and are extremely efficient in triggering transmitter release, probably due to their close physical association with SNARE proteins (Kaeser et al., 2011). However the release probability at PF-PC synapses remains relatively low (Dittman and Regehr, 1998; Dittman et al., 2000; Isope and Barbour, 2002), compared to more reliable CF-PC synapses (Dittman and Regehr, 1998). This low release probability at PF-PC synapses is likely due to the relatively low level of Ca^{2+}-influx at presynaptic terminals, because artificially elevating the external Ca^{2+}-concentration significantly increases PF-EPSC amplitudes (Matsushita et al., 2002). In line with these data, high frequency PFs stimulation results in a paired-pulse facilitation of Ca^{2+}-influx (Adams et al., 2010). Considering that GrCs remain silent most of the times and operate in short bursts at high frequency when activated (Chadderton et al., 2004; Barmack and Yakhnitsa, 2008; Ruigrok, 2010), it seems plausible to hypothesize that the PF-PC synapses are designed to work as a high pass filter, in that only high-frequency bursts of granule cell activity would have a direct impact on PCs. Interestingly, although P/Q-type Ca_V-channels are highly abundant throughout the soma, dendrite and axonal terminals of PCs, in adult GrC they are exclusively located at GrC axonal terminals but not in soma or dendrite (D'Angelo et al., 1997).

At CF-PC synapses, P/Q-type Ca_V channels also account for more than half of the transmitter release (Mintz et al., 1995; Matsushita et al., 2002). At this synapse, simultaneous transmitter release upon presynaptic Ca^{2+}-influx results in an all-or-none excitatory postsynaptic potential that can reach up to several nA in PCs. A consecutive stimulation results in a significant reduction in the CF-EPSC amplitude, due to fast depletion of readily

release pool and/or desensitization of post-synaptic AMPA receptors (Dittman and Regehr, 1998; Harrison and Jahr, 2003). Thus, it is likely that at this synapses fluctuations in the presynaptic calcium influx have less impact on the final transmitter release. This is in line with the data that alternating the external Ca^{2+}-concentration from 2 to 4 mM only induces minor change in the CF-EPSC amplitude (Matsushita et al., 2002). In addition, in various loss-of-function Ca_V channel mutants (see section 1.2.4), CF-EPSCs often do not change or even paradoxical increased amplitude, whereas PF-EPSCs are consistently reduced (Matsushita et al., 2002). These differences in the transmitter release properties are in line with the specific functions of PF and CF to PC synapses.

PC typically receives vast amounts of PF inputs but only a single CF input. As GrCs often fire action potentials in bursts, a graded Ca^{2+}-transient in response to alternating firing frequencies and durations could considerably change the synaptic transmission and thus the input strength of individual GrCs. CF input, on the other hand, occurs at relatively low frequency (~1 Hz on average). Also, the all-or-none response of CF input into PCs seems to implicate that modulation of the Ca^{2+}-transient is likely to have a minimal impact on the synaptic transmission and thus spiking output of PCs. However, we cannot fully exclude the significance of Ca^{2+}-modulation in CF-PC synaptic transmission due to the influence of post-synaptic Ca^{2+}-influx based on the following reasons: First, PCs respond to CF input as complex spikes. The generation and modulation of complex spike waveforms largely depend on the Ca^{2+}-influx in PCs (as reviewed by Schmolesky et al., 2002); although any change in the Ca^{2+}-influx might have small impact on transmitter release, it may dramatically change the complex spike waveforms. Second, it has been shown that CF-PC input can also undergo long-term plasticity (Hansel and Linden, 2000) and thereby alter the CF-mediated Ca^{2+}-influx in PCs. Third, inferior olivary neurons also tend to fire in bursts (Maruta et al., 2007; Mathy et al., 2009). The burst firing of olivary neurons may serve as a fail proof mechanism that ensures a complex spike in PCs. Although recently data also suggests that such burst firing also results in changes in complex spike length and probably also heterosynaptic influences on LTD at PF-PC synapses (Mathy et al., 2009).

Similar to excitatory synapses in cerebellum, synaptic transmission at various inhibitory synapses is also mediated by P/Q-type Ca_V-channels. Ca^{2+}-dependent GABA release is predominantly mediated by P/Q type Ca_V-channels at the molecular layer interneuron-PC, the molecular layer interneuron-molecular layer interneuron and adult PC-cerebellar nuclei synapses (Forti et al., 2000; Iwasaki et al., 2000; Stephens et al., 2001; Lonchamp et al., 2009; Bouhours et al., 2011; Mark et al., 2011). The detailed description of transmitter release at these synapses is out of the scope of this thesis. In summary, the dense expressions of P/Q-type CaV-channels at various cerebellar synapses emphasize the importance of P/Q-type Ca_V-channels in proper cerebellar function. More details about malfunction of Ca_V-channels and pathological consequences will be discussed in section 1.2.4.

1.2.2 The role of calcium in neuronal spiking patterns

The P/Q-type Ca_V-channels carry more than 90% of the total high-voltage-activated Ca^{2+}-currents in PCs (Mintz et al., 1992a). The impact of such Ca^{2+}-current on Purkinje cell spiking patterns has been extensively studied. Raman and Bean described the ionic mechanisms of spontaneous spiking in dissociated PCs (Raman and Bean, 1999). One interesting phenomenon is that although Ca^{2+}-influx via P/Q-type Ca_V-channels during action potential firing has a depolarizing force on membrane potential, the net effect of this current is outward (hyperpolarizing) (Raman and Bean, 1999). Thus, the electrical effect of Ca^{2+}-current is apparently dominated by rapidly activated Ca^{2+}-dependent K^+-currents. This net hyperpolarizing effect of $Ca_V2.1$-channels is confirmed in acute cerebellar slices and shown to be mediated by large-conductance (BK) and small-conductance (SK) Ca^{2+}-dependent K^+-channels (Schmolesky et al., 2002; Edgerton and Reinhart, 2003; Swensen and Bean, 2003; Womack and Khodakhah, 2003; Davie et al., 2008).

Detailed models that combine morphological and electrophysiological features of PCs suggest that the interaction between Ca^{2+}- and Ca^{2+}-dependent K^+-channels have to be well balanced to maintain PC firing patterns (De Schutter and Bower, 1994; Anwar et al., 2010). Blockage of Ca^{2+}-influx disrupts the continuous spiking from PCs by inducing an initial burst of action potentials and a subsequent depolarizing plateau that prevents action potential firing (Edgerton and Reinhart, 2003; Walter et al., 2006). Pharmacological blockage of either SK or BK channels reveals similar effects in PC spiking. When SK channels are blocked, the PC firing pattern becomes irregular, alternating between bursts of spontaneous action potentials and quiescent periods (Edgerton and Reinhart, 2003; Womack and Khodakhah, 2003). Affecting BK channels also disrupts the PC firing, by increasing the spontaneous firing frequency and promoting the occurrence of burst firing patterns (Edgerton and Reinhart, 2003; Womack et al., 2009). Both the SK- and BK-channels control Purkinje cell spiking patterns by modulating the after-hyperpolarization (AHP). BK-channels probably contribute to the majority of the fast AHP whereas the SK-channels are involved in both the fast and slow AHP. The involvement of Ca^{2+}-dependent K^+-channels in maintaining proper cerebellar function also holds true in vivo. Both the global and PC-specific deletion of BK-channels results in irregular PC firing and pronounced ataxia (Sausbier et al., 2004; Chen et al., 2010), much alike the phenotypes found in various *cacna1a* loss-of-function mutants (see section 1.2.4). Both the irregular PC firing patterns and ataxic phenotypes in *cacna1a* loss-of-function mutants can be partially rescued by enhancing Ca^{2+}-dependent K^+-channel functions (Walter et al., 2006; Alvina and Khodakhah, 2010), which indicates that an optimal balance between Ca^{2+}- and Ca^{2+}-dependent K^+-channels is critical for proper functioning of the cerebellar cortex.

In addition to the impact on PC intrinsic spike firing, which originates primarily in the peri-somatic region, BK-channels also participate in regulating dendritic activities in PCs. The spontaneous burst firing in PCs from acute slices can be modulated by locally affecting dendritic BK-channels (Womack and Khodakhah, 2004). Blocking BK-channels also increases the intracellular Ca^{2+}-concentration in PCs by promoting Ca^{2+}-spreading in the dendrites, which in turn enhances the release of endocannabinoid from dendrites and thereby promote short-term plasticity at PF-PC synapses (Rancz and Hausser, 2006).

1.2.3 The role of calcium in synaptic plasticity

Both parallel and climbing fiber activity induces Ca^{2+}-transients in Purkinje cells that trigger various types of synaptic plasticity. PF inputs induce local Ca^{2+}-transient that are often restricted within spines or small sections of dendrites (Eilers et al., 1995a; Eilers et al., 1995b). Synaptic transmission at PF-PC synapses is mainly mediated by GluR2 containing, Ca^{2+}-impermeable types of AMPA receptors (Tempia et al., 1996). Thus the Ca^{2+}-transient in response to PF input is primarily mediated by Ca^{2+}-influx through P/Q-type Ca_V-channels, in response to local depolarization after AMPA receptor activation (Eilers et al., 1995a). At low stimulation intensities, the Ca^{2}-transients have a linear correlation with the strength of PF input (Wang et al., 2000). Such a local signaling of PF input provides significant benefits of input specificity, considering a single PC is designed to receive and process > 150,000 GrC-inputs. However, it has been shown that with more intense stimulation, PF inputs also result in a supralinear increase in Ca^{2+}-concentration (Hartell, 1996; Canepari and Vogt, 2008), which was previously considered to only occur in response to conjunct PF and CF inputs (Wang et al., 2000). This PF-only supralinear Ca^{2+}-influx is probably controlled by mGluR1-induced Ca^{2+}-release from internal Ca^{2+}-store. Several studies showed that repetitive PF stimulation produces a complex Ca^{2+}-signal, with a fast component dependent on AMPA receptor induced depolarization, and a slower component that requires mGluR1 activation (Finch and Augustine, 1998; Takechi et al., 1998). Whether the supralinear Ca^{2+}-transients in responses to PF input can be observed *in vivo* remains to be elucidated.

CF input elicits all-or-none responses, e.g., complex spikes, in PCs, which are manifested by high amplitude Ca^{2+}-transients that spread throughout the entire PC dendritic tree (Tank et al., 1988). The climbing fiber induced Ca^{2+}-transients originate primarily from P/Q-type Ca_V-channels, whereas NMDA-mediated Ca^{2+}-influx as well as Ca^{2+}-release from internal stores also contribute to this postsynaptic response (Dzubay and Otis, 2002; Piochon et al., 2010). The global Ca^{2+}-influx after CF stimulation is initially generated in the soma and spreads into PCs dendrites and spines. Because of the high Ca_V-channel density in the dendritic spines, the peak concentration of Ca^{2+} occurs in the spines even earlier than in the dendrite (Schmidt et al., 2003). During conjunctive PF and CF stimulation, Ca^{2+}-transients saturate in the spines in response to the mGluR1 activation induced Ca^{2+}-release from endoplasmic reticulum (ER) (Wang et al., 2000). It has been shown that mGluR1 physically binds with type-1 IP_3 receptors, which plays a dominant role in gating Ca^{2+}-release from the ER in PCs (Tu et al., 1998; Sharp et al., 1999). Since IP_3Rs and ER are not evenly distributed in PC dendrites (Volpe et al., 1993), the mGluR1-induced Ca^{2+}-release from internal stores could act locally. Thus, ER may serve as a remote Ca^{2+}-supplier throughout PC dendrites for regional Ca^{2+}-release. Support for this theory comes from the fact that Myosin5a-dependent translocation of ER into PC spines is essential for mGluR1-dependent Ca^{2+}-transient modulations and PF-PC LTD (Miyata et al., 2000; Wagner et al., 2011). The regional specificity of Ca^{2+}-transients in spines and dendrites determines the input specificity of long-term plasticity in neurons. In PCs, CF-induced Ca^{2+}-transients alone does not induce long term plasticity at PF-PC synapses, however LTD can be regionally

induced only at those synapses when coincident PF and CF inputs are applied (Reynolds and Hartell, 2000). Similarly, restriction of dendritic Ca^{2+}-transients result in input specific LTD at PF-stellate cell synapses (Soler-Llavina and Sabatini, 2006).

Ca^{2+}-transients facilitate synaptic plasticity by activating several key enzymes in neurons, such as protein kinase-C (PKC), Ca^{2+}/Calmodulin-dependent kinase type II (CaMKII) and protein-phosphatase 2B (PP2B; calcineurin). The former two enzymes are essential for the expression of PF-PC LTD and the latter is essential for LTP. PKC-dependent phosphorylation of the S880 amino acid residue at the C terminal of GluR2-subunits of AMPA receptors is essential for LTD induction at PF-PC synapses (De Zeeuw et al., 1998). The recognition of such phosphorylation is mediated by the binding of protein interacting with C-kinase 1 (PICK1) to AMPA receptors (Steinberg et al., 2006). Both α- and βCaMKII have been shown to be essential molecules for PF-PC LTD (Hansel et al., 2006; chapter 6.1). PP2B on the other hand competes with CaMKII and promotes LTP in PCs (Belmeguenai and Hansel, 2005; Belmeguenai et al., 2010).

Although the involvement of Ca^{2+}-activated CaMKII cascades in cerebellar learning and plasticity has only been characterized in the last decade, CaMKII has been identified as one of the best candidates being the 'memory molecule' 20 years ago (Silva et al., 1992a; Silva et al., 1992b; Lisman et al., 1997; Lisman et al., 2002). CaMKII is one of the most abundant proteins in the central nervous system and accounts for more than 2% of the total amount of protein (Erondu and Kennedy, 1985). Four different isoforms of CaMKII, α, β, γ and δ are found in the brain, among which the α- and β-isoforms are the most prominent forms (for review see Colbran and Brown, 2004). Alpha- and βCaMKII are almost completely homologous in that they both contain: a catalytic domain that fulfills the enzymatic role of CaMKII; a regulatory domain that controls the activation/inactivation of CaMKII; and an association domain (Hudmon and Schulman, 2002). The enzymatic role of CaMKII is characterized by its ability of self-activate by autophosphorylation. The activation of CaMKII is triggered by phosphorylation of Thr286 (for αCaMKII) or Thr287 (for βCaMKII) in the regulatory domain, which converts each CaMKII isoform into its active state that subsequently phosphorylates the neighbor subunits within the holoenzyme (Hanson et al., 1994). The autophosphorylation extends the activation state well beyond the duration of the Ca^{2+}-transient (Lisman et al., 2002; Colbran and Brown, 2004).

Alpha- and βCaMKII also show functional differences. For instance, βCaMKII has an F-actin binding domain (Shen et al., 1998) and slower translocation time constant in the postsynaptic density (Shen and Meyer, 1999). Also, the Ca^{2+}-sensitivity of βCaMKII is ~6-fold higher than of αCaMKII (Brocke et al., 1999) and the distribution pattern of both isoforms is different in various brain regions. For instance, αCaMKII is the most abundant isoform in forebrain (the ratio of α to βCaMKII is 3:1), whereas βCaMKII dominates in the cerebellum (α:β of 1:4) (Miller and Kennedy, 1985). The peculiar ratio of α and β isoforms in the cerebellum is due to the neuronal type specific distribution of CaMKII isoforms. αCaMKII is present exclusively in PCs and βCaMKII is commonly found in various cerebellar neurons (Hansel et al., 2006). The unique combination of α and βCaMKII in PCs is likely to serve particular functions in synaptic plasticity.

1.2.4 How deficits in calcium homeostasis mediate ataxia

Since the P/Q-type Ca_V-channels play a vital role in maintaining normal neuronal function, aberrations in the P/Q-type Ca_V-channel function could lead to a severe dysfunction of neuronal networks. In the cerebellum, such Ca^{2+}-channelopathy is manifested by various groups of ataxias. For instance, episodic ataxia type 2 (EA2) and Spinal cereberal ataxia type 6 (SCA6) have been tightly linked with a group of mutations in the *cacna1a* gene (Figure 4). Several mouse models that harbor aberrant P/Q-type Ca_V-channels have been extensively studied. The most extreme models are the mouse strains that lack expression of the α1A subunit, which results in severe phenotypes including ataxia and dystonia. In the first strain mice die at 3–4 weeks (Jun et al., 1999). The second strain permitted observation of late-onset cerebellar neurodegeneration (Fletcher et al., 2001). It has been shown that the morphology of the cerebellum, the connectivity between PF-PC and CF-PC synapses, the synaptic transmission at PF-PC, CF-PC, MLI-PC and PC-CN synapses is altered in the $Ca_v2.1^{-/-}$ mice (Miyazaki et al., 2004; Lonchamp et al., 2009; Mark et al., 2011).

The early onset of cerebellar phenotypes in the $Ca_v2.1^{-/-}$ mice makes it difficult to study the development and pathological consequences of Ca_V channelopathies and to correlate with the clinical data from EA2 patients. A group of spontaneous *cacna1a* mutant mice has proven to be more relevant for the translation of results from mice to human. These mutant mice, e.g., tottering **(***tg*), rolling Nagoya (*rol*), rocker (*rkr*) and leaner (*la*), each harbor a missense mutation in the voltage-sensing domain of the α1A-subunit (for *tg*, *rol* and *rkr*), or a splicing variance that altered the c-terminal of the α1A-subunit (for *la*). In these mutants, consequently, the P/Q-type Ca_V-channel functions are impaired to various extents. The reductions of Ca^{2+}-current densities in PCs vary from 40% to 70% compared with wild type littermates (Wakamori et al., 1998; Mori et al., 2000; Zwingman et al., 2001). In concordance, these mutants all show certain levels of progressive ataxia. *Tg* and *rkr* mice have relative mild form of ataxia, *rol* mice are more severely affected and *la* mice show the most pronounced ataxia phenotype (for review see (Plomp J 2009)). In addition to the cerebellar ataxia these mutants show a mixture of other neurological symptoms, like dystonia, paroxysmal dyskinesia and absence seizures.

Previous studies show that the mutants with mild forms of ataxia, like those in *tg* and *rol* mice, are not associated with early onset of neuronal degeneration. No change in the PCs densities are found in *tg*, *rol* or *rkr* mice at 4 month of age, however a progressive loss of PCs in parasagittal patterns has been reported in *la* mutants at similar age (Herrup and Wilczynski, 1982). A late onset progressive form of PC degeneration has been found in older than 1 year *tg* mice (Sawada et al., 2009). Interestingly, the PC degeneration in both *la* and *tg* are not homogeneous but rather colocalized with zebrin expression patterns. Thus the susceptibility of PC degeneration might be determined by various other protein expression patterns. To what extent the ataxic phenotypes associate with degenerating PCs or malfunction of neurons remain to be determined, although it is obvious that ataxia can be found without clear loss of PCs.

At the ultrastructural level, loss-of-function *cacna1a* mutants often have dys-

morphed PC synapses. Similar to what was found in global $Ca_V2.1^{-/-}$ mice (Jun et al., 1999), in *tg*, *rol* and *la* mice the PF-PC synapses are formed in unnatural locations, like on secondary Purkinje cell dendrites and multiple PC spines contact single PF varicosity (Rhyu et al., 1999). In addition, adult PCs receive input from multiple CFs, of which all but one CF should have been eliminated during the second post-natal week (Hashimoto et al., 2009). In addition to the effects on synaptic connectivity, these *cacna1a* mutations also affect the PC morphology, in that the branching of the PC dendritic tree is reduced and PC axons form swellings (Rhyu et al., 1999; Ovsepian and Friel, 2008).

Electrophysiological evidences provide more details on the relation between aberrant neuronal activities in loss-of-function *cacna1a* mutants and ataxia. Presynaptic reductions in P/Q-type Ca^{2+}-currents result in smaller amplitudes of PF-EPSCs in *tg*, *rol, rkr* and *la* Purkinje cells, whereas increased paired pulse facilitation ratio of two consecutive PF-EPSCs are found in *rol* and *la*, but not *tg* and *rkr* mice (Matsushita et al., 2002; Kodama et al., 2006; Liu and Friel, 2008). Although synaptic transmission between CF and PC is also mediated by P/Q-type Ca_V channels, the amplitude of CF-EPSC is normal in tg and even enhanced in *rol* and *la* mice (Matsushita et al., 2002; Kodama et al., 2006; Liu and Friel, 2008). This is probably due, to a large extent, to a saturated release probability and an increased postsynaptic AMPA receptor density at this synapses (Matsushita et al., 2002). Phenotypes of synaptic transmission at inhibitory MLI to PC synapses show a more complex mixture of alterations, varying from probably normal input in ducky mutant to enhanced inhibitory input in *la* mice (Walter et al., 2006; Ovsepian and Friel, 2008; Lonchamp et al., 2009). These variable effects may well be induced by both pre- and post-synaptic factors. Presynaptically, inhibiting Ca^{2+} influx using cadium does not completely abolish the GABA release, but rather reduces it to ~ 50%. This is probably due to the Ca^{2+} independent, BEST1 channel mediated GABA release from glia cells (Lee et al., 2010). Postsynaptically, alterations in the Purkinje cell dendritic morphology significantly increase the input resistance of PCs, result in larger inhibitory currents (Ovsepian and Friel, 2008). Beside the alterations in synaptic transmission, irregular PC pacemaking activity has also been shown to be associated with ataxic behavior. (Walter et al., 2006) showed more irregular of PC intrinsic firing patterns in *la* and *ducky* mice, due to the altered balance between Ca^{2+}-influx and Ca^{2+}-activated K^+-channels. Interestingly enough, enhancing SK-channel function by EBIO application not only improved the regularity of PC intrinsic firing pattern, but also improved the motor performance in *la* and ducky and reduced the occurrence of dyskinesia in *tg* mice. These findings are consistent with increased irregularity of simple spike firing of floccular PCs in awake *tg* mice (Hoebeek et al., 2005). Although *tg* PCs showed a normal average simple spike modulation during optokinetic stimulation, the irregularity of simple spike firing minimized the precision of compensatory eye movements in *tg* mice (Hoebeek et al., 2005).

In summary, recent studies unambiguously show the strong correlation between the reduction of Ca^{2+}-influx in various mutants and ataxic phenotypes. The alteration of P/Q-type Ca_V-channel function results in a series of morphological and electrophysiological aberrations that cause behavioral deficits. Those mouse mutant models all, despite the phenotypical variances, share similar pathological origins, in that all these mutations lead

to severe reduction in Ca^{2+}-current density in neurons. Such a compromised channel function has been thought to be a predominant cause of ataxia. Interestingly enough, a recently generated knock-in mouse mutant, which harbors a single mutation of serine 218 to leucine (S218L) in the α1A subunit, show prominent ataxic phenotype but an increased Ca^{2+}-influx through mutant channels (van den Maagdenberg et al., 2010 and Ch. 7). Apparently the suboptimal functioning of $Ca_V2.1$ channels induces ataxia, regardless of whether the mutation induces a loss- or gain-of-function**.**

1.3 Scope of the Thesis

The current thesis centers on the role of calcium in cerebellar functioning; how calcium influx in axon terminals mediates neurotransmitter release, how calcium influx postsynaptically controls several forms of synaptic plasticity and how aberrant calcium channel functioning disrupts the output of the cerebellar cortex. Chapter 2 introduces and reviews the currently known forms of synaptic plasticity in the cerebellar cortex and their molecular mechanisms. In addition, the functional connections between all types of neurons are reviewed. From the discussed literature it becomes evident that calcium homeostasis has a central role in each of these plastic events.

In Chapter 3 we use the fact that neurotransmission between GrCs and PCs is particularly dependent on Ca^{2+}-influx through P/Q-type voltage-gated Ca^{2+}-channels to study the essence of such a vast amount of GrCs when most of these neurons is known to be silent most of the time. By GrC-specific deletion we found that we can selectively block the output of ~70% of all GrCs. Surprisingly, these mice show now behavioral deficits or gross abnormalities in GrC excitability or of any downstream target neuron. *In vivo* we found that the PCs showed more regular PC firing patterns, which we relate to the absence of motor learning consolidation.

Chapter 4 describes what the role is of synaptic plasticity of the GrC–PC synapses in controlling the core function of the cerebellum, like motor behavior. Since more than 4 decades one of the leading hypotheses is that long-term depression at the PF-PC synapses accounts for the adaptation of motor behavior. This well-known *Marr-Albus-Ito* hypothesis is challenged in this chapter by two studies, which show that not long-term depression but long-term potentiation at the GrC-PC synapses is essential for motor learning in adult mice.

Chapter 5 identifies the synaptic inhibitory input from molecular layer interneurons to PC as one of the main neuronal substrates of consolidation of motor learning. Previously, the inhibitory input from stellate and basket cells was thought to control the timing of action potential firing in PCs, and although this synapse was known to be plastic in a Ca^{2+}-dependent manner, a true role in motor learning was not yet described. Here we show that the lack of synaptic inhibitory input to PC enhances the regularity of PC firing and thereby disrupts that consolidation of newly acquired motor tasks.

Chapter 6 explores the molecular pathways of the abovementioned forms of plasticity in the PCs and thereby focuses on the role of CaMKII. The α-isoform of this particular enzyme was shown to control long-term depression at the excitatory GrC-PC synapse, but it role in inhibitory plasticity, or that of the β-isoform in both types of plasticity remained unclear. Our results reveal how the lack of βCaMKII alters the function of the residual αCaMKII in PCs. For both excitatory and inhibitory plasticity the effect of αCaMKII activation reversed; GrC-PC LTP protocols induced LTD and vice versa and SC-PC LTP suppression protocols induced LTP. For both synaptic contacts the absence of βCaMKII switched the plasticity induction rules from cerebellar to hippocampal.

Chapter 7 describes how a gain-of-function mutation in the pore-forming subunit of

P/Q-type calcium channels disrupts the output of the cerebellar cortex and thereby mediates cerebellar ataxia. Previous studies showed a similar pathogenesis for loss-of-function mutations. Our study reveals a remarkable similarity in the effects of gain-of-function mutations and loss-of-function mutations and also describes how these opposite effects eventually both induce cerebellar malfunctioning and ataxia.

Chapter 8 discusses the results described in the current thesis.

References

Adams PJ, Rungta RL, Garcia E, van den Maagdenberg AM, MacVicar BA, Snutch TP (2010) Contribution of calcium-dependent facilitation to synaptic plasticity revealed by migraine mutations in the P/Q-type calcium channel. Proc Natl Acad Sci U S A 107:18694-18699.

Ahn S, Ginty DD, Linden DJ (1999) A late phase of cerebellar long-term depression requires activation of CaMKIV and CREB. Neuron 23:559-568.

Albus JS (1971) A theory of cerebellar function. Math Biosci 10:25-61.

Alvina K, Khodakhah K (2010) KCa channels as therapeutic targets in episodic ataxia type-2. J Neurosci 30:7249-7257.

Anwar H, Hong S, De Schutter E (2010) Controlling Ca(2+)-Activated K (+) Channels with Models of Ca (2+) Buffering in Purkinje Cells. Cerebellum.

Barmack NH, Pettorossi VE (1985) Effects of unilateral lesions of the flocculus on optokinetic and vestibuloocular reflexes of the rabbit. J Neurophysiol 53:481-496.

Barmack NH, Yakhnitsa V (2008) Functions of interneurons in mouse cerebellum. J Neurosci 28:1140-1152.

Belmeguenai A, Hansel C (2005) A role for protein phosphatases 1, 2A, and 2B in cerebellar long-term potentiation. J Neurosci 25:10768-10772.

Belmeguenai A, Hosy E, Bengtsson F, Pedroarena CM, Piochon C, Teuling E, He Q, Ohtsuki G, De Jeu MT, Elgersma Y, De Zeeuw CI, Jorntell H, Hansel C (2010) Intrinsic plasticity complements long-term potentiation in parallel fiber input gain control in cerebellar Purkinje cells. J Neurosci 30:13630-13643.

Bouhours B, Trigo FF, Marty A (2011) Somatic Depolarization Enhances GABA Release in Cerebellar Interneurons via a Calcium/Protein Kinase C Pathway. J Neurosci 31:5804-5815.

Bourinet E, Soong TW, Sutton K, Slaymaker S, Mathews E, Monteil A, Zamponi GW, Nargeot J, Snutch TP (1999) Splicing of alpha 1A subunit gene generates phenotypic variants of P- and Q-type calcium channels. Nat Neurosci 2:407-415.

Bower JM, Woolston DC (1983) Congruence of spatial organization of tactile projections to granule cell and Purkinje cell layers of cerebellar hemispheres of the albino rat: vertical organization of cerebellar cortex. J Neurophysiol 49:745-766.

Braitenberg V, Atwood RP (1958) Morphological observations on the cerebellar cortex. J Comp Neurol 109:1-33.

Branco T, Hausser M (2009) The selfish spike: local and global resets of dendritic excitability. Neuron 61:815-817.

Branco T, Clark BA, Hausser M (2010) Dendritic discrimination of temporal input sequences in cortical neurons. Science 329:1671-1675.

Brickley SG, Cull-Candy SG, Farrant M (1996) Development of a tonic form of synaptic inhibition in rat cerebellar granule cells resulting from persistent activation of GABAA receptors. J Physiol 497 (Pt 3):753-759.

Brocke L, Chiang LW, Wagner PD, Schulman H (1999) Functional implications of the subunit composition of neuronal CaM kinase II. J Biol Chem 274:22713-22722.

Callaway JC, Lasser-Ross N, Ross WN (1995) IPSPs strongly inhibit climbing fiber-acti-

vated [Ca2+]i increases in the dendrites of cerebellar Purkinje neurons. J Neurosci 15:2777-2787.
Canepari M, Vogt KE (2008) Dendritic spike saturation of endogenous calcium buffer and induction of postsynaptic cerebellar LTP. PLoS One 3:e4011.
Catterall WA (2000) Structure and regulation of voltage-gated Ca2+ channels. Annu Rev Cell Dev Biol 16:521-555.
Catterall WA, Few AP (2008) Calcium channel regulation and presynaptic plasticity. Neuron 59:882-901.
Cavelier P, Lohof AM, Lonchamp E, Beekenkamp H, Mariani J, Bossu JL (2008) Participation of low-threshold Ca2+ spike in the Purkinje cells complex spike. Neuroreport 19:299-303.
Chadderton P, Margrie TW, Hausser M (2004) Integration of quanta in cerebellar granule cells during sensory processing. Nature 428:856-860.
Chen X, Kovalchuk Y, Adelsberger H, Henning HA, Sausbier M, Wietzorrek G, Ruth P, Yarom Y, Konnerth A (2010) Disruption of the olivo-cerebellar circuit by Purkinje neuron-specific ablation of BK channels. Proc Natl Acad Sci U S A 107:12323-12328.
Coesmans M, Weber JT, De Zeeuw CI, Hansel C (2004) Bidirectional parallel fiber plasticity in the cerebellum under climbing fiber control. Neuron 44:691-700.
Colbran RJ, Brown AM (2004) Calcium/calmodulin-dependent protein kinase II and synaptic plasticity. Curr Opin Neurobiol 14:318-327.
D'Angelo E, De Filippi G, Rossi P, Taglietti V (1997) Synaptic activation of Ca2+ action potentials in immature rat cerebellar granule cells in situ. J Neurophysiol 78:1631-1642.
Davie JT, Clark BA, Hausser M (2008) The origin of the complex spike in cerebellar Purkinje cells. J Neurosci 28:7599-7609.
De Schutter E, Bower JM (1994) An active membrane model of the cerebellar Purkinje cell. I. Simulation of current clamps in slice. J Neurophysiol 71:375-400.
De Zeeuw CI, Hansel C, Bian F, Koekkoek SK, van Alphen AM, Linden DJ, Oberdick J (1998) Expression of a protein kinase C inhibitor in Purkinje cells blocks cerebellar LTD and adaptation of the vestibulo-ocular reflex. Neuron 20:495-508.
Dean I, Robertson SJ, Edwards FA (2003) Serotonin drives a novel GABAergic synaptic current recorded in rat cerebellar purkinje cells: a Lugaro cell to Purkinje cell synapse. J Neurosci 23:4457-4469.
Dieudonne S, Dumoulin A (2000) Serotonin-driven long-range inhibitory connections in the cerebellar cortex. J Neurosci 20:1837-1848.
Dittman JS, Regehr WG (1998) Calcium dependence and recovery kinetics of presynaptic depression at the climbing fiber to Purkinje cell synapse. J Neurosci 18:6147-6162.
Dittman JS, Kreitzer AC, Regehr WG (2000) Interplay between facilitation, depression, and residual calcium at three presynaptic terminals. J Neurosci 20:1374-1385.
Dow RS, Moruzzi G (1958) The physiology and pathology of the cerebellum. Minneapolis,: University of Minnesota Press.
Dubel SJ, Starr TV, Hell J, Ahlijanian MK, Enyeart JJ, Catterall WA, Snutch TP (1992) Molecular cloning of the alpha-1 subunit of an omega-conotoxin-sensitive calcium

channel. Proc Natl Acad Sci U S A 89:5058-5062.
Dumoulin A, Triller A, Dieudonne S (2001) IPSC kinetics at identified GABAergic and mixed GABAergic and glycinergic synapses onto cerebellar Golgi cells. J Neurosci 21:6045-6057.
Dunlap K, Luebke JI, Turner TJ (1995) Exocytotic Ca2+ channels in mammalian central neurons. Trends in neurosciences 18:89-98.
Dzubay JA, Otis TS (2002) Climbing fiber activation of metabotropic glutamate receptors on cerebellar purkinje neurons. Neuron 36:1159-1167.
Eccles JC (1967) The cerebellum as a neuronal machine. New York,: Springer.
Eccles JC (1969) The development of the cerebellum of vertebrates in relation to the control of movement. Naturwissenschaften 56:525-534.
Eccles JC, Sabah NH, Schmidt RF, Taborikova H (1972) Cutaneous mechanoreceptors influencing impulse discharges in cerebellar cortex. II. In Purkyne cells by mossy fiber input. Exp Brain Res 15:261-277.
Edgerton JR, Reinhart PH (2003) Distinct contributions of small and large conductance Ca2+-activated K+ channels to rat Purkinje neuron function. J Physiol 548:53-69.
Eilers J, Augustine GJ, Konnerth A (1995a) Subthreshold synaptic Ca2+ signalling in fine dendrites and spines of cerebellar Purkinje neurons. Nature 373:155-158.
Eilers J, Callewaert G, Armstrong C, Konnerth A (1995b) Calcium signaling in a narrow somatic submembrane shell during synaptic activity in cerebellar Purkinje neurons. Proc Natl Acad Sci U S A 92:10272-10276.
Erondu NE, Kennedy MB (1985) Regional distribution of type II Ca2+/calmodulin-dependent protein kinase in rat brain. J Neurosci 5:3270-3277.
Finch EA, Augustine GJ (1998) Local calcium signalling by inositol-1,4,5-trisphosphate in Purkinje cell dendrites. Nature 396:753-756.
Fioravante D, Regehr WG (2011) Short-term forms of presynaptic plasticity. Curr Opin Neurobiol.
Fletcher CF, Tottene A, Lennon VA, Wilson SM, Dubel SJ, Paylor R, Hosford DA, Tessarollo L, McEnery MW, Pietrobon D, Copeland NG, Jenkins NA (2001) Dystonia and cerebellar atrophy in Cacna1a null mice lacking P/Q calcium channel activity. FASEB J 15:1288-1290.
Forti L, Pouzat C, Llano I (2000) Action potential-evoked Ca2+ signals and calcium channels in axons of developing rat cerebellar interneurones. J Physiol 527 Pt 1:33-48.
Goossens J, Daniel H, Rancillac A, van der Steen J, Oberdick J, Crepel F, De Zeeuw CI, Frens MA (2001) Expression of protein kinase C inhibitor blocks cerebellar long-term depression without affecting Purkinje cell excitability in alert mice. J Neurosci 21:5813-5823.
Gundappa-Sulur G, De Schutter E, Bower JM (1999) Ascending granule cell axon: an important component of cerebellar cortical circuitry. J Comp Neurol 408:580-596.
Hansel C, Linden DJ (2000) Long-term depression of the cerebellar climbing fiber--Purkinje neuron synapse. Neuron 26:473-482.
Hansel C, de Jeu M, Belmeguenai A, Houtman SH, Buitendijk GH, Andreev D, De Zeeuw CI, Elgersma Y (2006) alphaCaMKII Is essential for cerebellar LTD and motor learning. Neuron 51:835-843.

Hanson PI, Meyer T, Stryer L, Schulman H (1994) Dual role of calmodulin in autophosphorylation of multifunctional CaM kinase may underlie decoding of calcium signals. Neuron 12:943-956.

Harrison J, Jahr CE (2003) Receptor occupancy limits synaptic depression at climbing fiber synapses. J Neurosci 23:377-383.

Hartell NA (1996) Strong activation of parallel fibers produces localized calcium transients and a form of LTD that spreads to distant synapses. Neuron 16:601-610.

Harvey RJ, Napper RM (1991) Quantitative studies on the mammalian cerebellum. Prog Neurobiol 36:437-463.

Hashimoto K, Ichikawa R, Kitamura K, Watanabe M, Kano M (2009) Translocation of a "winner" climbing fiber to the Purkinje cell dendrite and subsequent elimination of "losers" from the soma in developing cerebellum. Neuron 63:106-118.

Hausser M, Clark BA (1997) Tonic synaptic inhibition modulates neuronal output pattern and spatiotemporal synaptic integration. Neuron 19:665-678.

Herrup K, Wilczynski SL (1982) Cerebellar cell degeneration in the leaner mutant mouse. Neuroscience 7:2185-2196.

Hoebeek FE, Stahl JS, van Alphen AM, Schonewille M, Luo C, Rutteman M, van den Maagdenberg AM, Molenaar PC, Goossens HH, Frens MA, De Zeeuw CI (2005) Increased noise level of purkinje cell activities minimizes impact of their modulation during sensorimotor control. Neuron 45:953-965.

Hudmon A, Schulman H (2002) Structure-function of the multifunctional Ca2+/calmodulin-dependent protein kinase II. Biochem J 364:593-611.

Isope P, Barbour B (2002) Properties of unitary granule cell-->Purkinje cell synapses in adult rat cerebellar slices. J Neurosci 22:9668-9678.

Ito M (1982) Modifiability of cerebellar neuronal networks related to adaptive control of vestibulo-ocular reflex. Electroencephalogr Clin Neurophysiol Suppl 36:139-146.

Ito M (2006) Cerebellar circuitry as a neuronal machine. Prog Neurobiol 78:272-303.

Iwasaki S, Momiyama A, Uchitel OD, Takahashi T (2000) Developmental changes in calcium channel types mediating central synaptic transmission. J Neurosci 20:59-65.

Jaeger D, De Schutter E, Bower JM (1997) The role of synaptic and voltage-gated currents in the control of Purkinje cell spiking: a modeling study. J Neurosci 17:91-106.

Jun K, Piedras-Renteria ES, Smith SM, Wheeler DB, Lee SB, Lee TG, Chin H, Adams ME, Scheller RH, Tsien RW, Shin HS (1999) Ablation of P/Q-type Ca(2+) channel currents, altered synaptic transmission, and progressive ataxia in mice lacking the alpha(1A)-subunit. Proc Natl Acad Sci U S A 96:15245-15250.

Kaeser PS, Deng L, Wang Y, Dulubova I, Liu X, Rizo J, Sudhof TC (2011) RIM proteins tether Ca2+ channels to presynaptic active zones via a direct PDZ-domain interaction. Cell 144:282-295.

Kandel ER, Schwartz JH, Jessell TM (2000) Principles of neural science, 4th Edition. New York: McGraw-Hill, Health Professions Division.

Kodama T, Itsukaichi-Nishida Y, Fukazawa Y, Wakamori M, Miyata M, Molnar E, Mori Y, Shigemoto R, Imoto K (2006) A CaV2.1 calcium channel mutation rocker reduces the number of postsynaptic AMPA receptors in parallel fiber-Purkinje cell synapses. Eur J Neurosci 24:2993-3007.

Konnerth A, Dreessen J, Augustine GJ (1992) Brief dendritic calcium signals initiate long-lasting synaptic depression in cerebellar Purkinje cells. Proc Natl Acad Sci U S A 89:7051-7055.

Kreiner L, Jaeger D (2004) Synaptic shunting by a baseline of synaptic conductances modulates responses to inhibitory input volleys in cerebellar Purkinje cells. Cerebellum 3:112-125.

Lee S, Yoon BE, Berglund K, Oh SJ, Park H, Shin HS, Augustine GJ, Lee CJ (2010) Channel-mediated tonic GABA release from glia. Science 330:790-796.

Lisberger SG, Miles FA, Zee DS (1984) Signals used to compute errors in monkey vestibuloocular reflex: possible role of flocculus. J Neurophysiol 52:1140-1153.

Lisman J, Schulman H, Cline H (2002) The molecular basis of CaMKII function in synaptic and behavioural memory. Nat Rev Neurosci 3:175-190.

Lisman J, Malenka RC, Nicoll RA, Malinow R (1997) Learning mechanisms: the case for CaM-KII. Science 276:2001-2002.

Liu S, Friel DD (2008) Impact of the leaner P/Q-type Ca2+ channel mutation on excitatory synaptic transmission in cerebellar Purkinje cells. J Physiol 586:4501-4515.

Llinas R, Sugimori M (1980) Electrophysiological properties of in vitro Purkinje cell somata in mammalian cerebellar slices. J Physiol 305:171-195.

Llinas RR, Sugimori M, Cherksey B (1989) Voltage-dependent calcium conductances in mammalian neurons. The P channel. Ann N Y Acad Sci 560:103-111.

Llinas RR, Walton KD, Lang EJ (2004) Ch. 7 Cerebellum. In: The synaptic organization of the brain, 5th Edition (Shepherd GM, ed), pp xiv, 719 p. Oxford ; New York: Oxford University Press.

Lonchamp E, Dupont JL, Doussau F, Shin HS, Poulain B, Bossu JL (2009) Deletion of Cav2.1(alpha1(A)) subunit of Ca2+-channels impairs synaptic GABA and glutamate release in the mouse cerebellar cortex in cultured slices. Eur J Neurosci 30:2293-2307.

Mark MD, Maejima T, Kuckelsberg D, Yoo JW, Hyde RA, Shah V, Gutierrez D, Moreno RL, Kruse W, Noebels JL, Herlitze S (2011) Delayed Postnatal Loss of P/Q-Type Calcium Channels Recapitulates the Absence Epilepsy, Dyskinesia, and Ataxia Phenotypes of Genomic Cacna1A Mutations. J Neurosci 31:4311-4326.

Marr D (1969) A theory of cerebellar cortex. J Physiol 202:437-470.

Maruta J, Hensbroek RA, Simpson JI (2007) Intraburst and interburst signaling by climbing fibers. J Neurosci 27:11263-11270.

Mathy A, Ho SS, Davie JT, Duguid IC, Clark BA, Hausser M (2009) Encoding of oscillations by axonal bursts in inferior olive neurons. Neuron 62:388-399.

Matsushita K, Wakamori M, Rhyu IJ, Arii T, Oda S, Mori Y, Imoto K (2002) Bidirectional alterations in cerebellar synaptic transmission of tottering and rolling Ca2+ channel mutant mice. J Neurosci 22:4388-4398.

Midtgaard J, Lasser-Ross N, Ross WN (1993) Spatial distribution of Ca2+ influx in turtle Purkinje cell dendrites in vitro: role of a transient outward current. J Neurophysiol 70:2455-2469.

Miller SG, Kennedy MB (1985) Distinct forebrain and cerebellar isozymes of type II Ca2+/calmodulin-dependent protein kinase associate differently with the postsynaptic

density fraction. J Biol Chem 260:9039-9046.
Mintz IM, Adams ME, Bean BP (1992a) P-type calcium channels in rat central and peripheral neurons. Neuron 9:85-95.
Mintz IM, Sabatini BL, Regehr WG (1995) Calcium control of transmitter release at a cerebellar synapse. Neuron 15:675-688.
Mintz IM, Venema VJ, Swiderek KM, Lee TD, Bean BP, Adams ME (1992b) P-type calcium channels blocked by the spider toxin omega-Aga-IVA. Nature 355:827-829.
Miyakawa H, Lev-Ram V, Lasser-Ross N, Ross WN (1992) Calcium transients evoked by climbing fiber and parallel fiber synaptic inputs in guinea pig cerebellar Purkinje neurons. J Neurophysiol 68:1178-1189.
Miyata M, Finch EA, Khiroug L, Hashimoto K, Hayasaka S, Oda SI, Inouye M, Takagishi Y, Augustine GJ, Kano M (2000) Local calcium release in dendritic spines required for long-term synaptic depression. Neuron 28:233-244.
Miyazaki T, Watanabe M (2011) Development of an anatomical technique for visualizing the mode of climbing fiber innervation in Purkinje cells and its application to mutant mice lacking GluRdelta2 and Ca(v)2.1. Anat Sci Int 86:10-18.
Miyazaki T, Hashimoto K, Shin HS, Kano M, Watanabe M (2004) P/Q-type Ca2+ channel alpha1A regulates synaptic competition on developing cerebellar Purkinje cells. J Neurosci 24:1734-1743.
Mori Y, Wakamori M, Oda S, Fletcher CF, Sekiguchi N, Mori E, Copeland NG, Jenkins NA, Matsushita K, Matsuyama Z, Imoto K (2000) Reduced voltage sensitivity of activation of P/Q-type Ca2+ channels is associated with the ataxic mouse mutation rolling Nagoya (tg(rol)). J Neurosci 20:5654-5662.
Myoga MH, Regehr WG (2011) Calcium microdomains near R-type calcium channels control the induction of presynaptic long-term potentiation at parallel fiber to purkinje cell synapses. J Neurosci 31:5235-5243.
Nagao S (1989) Role of cerebellar flocculus in adaptive interaction between optokinetic eye movement response and vestibulo-ocular reflex in pigmented rabbits. Exp Brain Res 77:541-551.
Nolan MF, Malleret G, Lee KH, Gibbs E, Dudman JT, Santoro B, Yin D, Thompson RF, Siegelbaum SA, Kandel ER, Morozov A (2003) The hyperpolarization-activated HCN1 channel is important for motor learning and neuronal integration by cerebellar Purkinje cells. Cell 115:551-564.
Nusser Z, Sieghart W, Somogyi P (1998) Segregation of different GABAA receptors to synaptic and extrasynaptic membranes of cerebellar granule cells. J Neurosci 18:1693-1703.
O'Donoghue DL, King JS, Bishop GA (1989) Physiological and anatomical studies of the interactions between Purkinje cells and basket cells in the cat's cerebellar cortex: evidence for a unitary relationship. J Neurosci 9:2141-2150.
Ovsepian SV, Friel DD (2008) The leaner P/Q-type calcium channel mutation renders cerebellar Purkinje neurons hyper-excitable and eliminates Ca2+-Na+ spike bursts. Eur J Neurosci 27:93-103.
Palay SL, Chan-Palay V (1974) Cerebellar cortex: cytology and organization. Berlin, Heidelberg, New York,: Springer.

Piochon C, Levenes C, Ohtsuki G, Hansel C (2010) Purkinje cell NMDA receptors assume a key role in synaptic gain control in the mature cerebellum. J Neurosci 30:15330-15335.

Raman IM, Bean BP (1999) Ionic currents underlying spontaneous action potentials in isolated cerebellar Purkinje neurons. J Neurosci 19:1663-1674.

Rancz EA, Hausser M (2006) Dendritic calcium spikes are tunable triggers of cannabinoid release and short-term synaptic plasticity in cerebellar Purkinje neurons. J Neurosci 26:5428-5437.

Randall A, Tsien RW (1995) Pharmacological dissection of multiple types of Ca2+ channel currents in rat cerebellar granule neurons. J Neurosci 15:2995-3012.

Reynolds T, Hartell NA (2000) An evaluation of the synapse specificity of long-term depression induced in rat cerebellar slices. J Physiol 527 Pt 3:563-577.

Rhyu IJ, Abbott LC, Walker DB, Sotelo C (1999) An ultrastructural study of granule cell/Purkinje cell synapses in tottering (tg/tg), leaner (tg(la)/tg(la)) and compound heterozygous tottering/leaner (tg/tg(la)) mice. Neuroscience 90:717-728.

Robinson DA (1976) Adaptive gain control of vestibuloocular reflex by the cerebellum. J Neurophysiol 39:954-969.

Roth A, Hausser M (2001) Compartmental models of rat cerebellar Purkinje cells based on simultaneous somatic and dendritic patch-clamp recordings. J Physiol 535:445-472.

Ruigrok TJ (2010) Ins and Outs of Cerebellar Modules. Cerebellum.

Ruigrok TJ, Hensbroek RA, Simpson JI (2011) Spontaneous activity signatures of morphologically identified interneurons in the vestibulocerebellum. J Neurosci 31:712-724.

Satake S, Song SY, Konishi S, Imoto K (2010) Glutamate transporter EAAT4 in Purkinje cells controls intersynaptic diffusion of climbing fiber transmitter mediating inhibition of GABA release from interneurons. Eur J Neurosci 32:1843-1853.

Sausbier M, Hu H, Arntz C, Feil S, Kamm S, Adelsberger H, Sausbier U, Sailer CA, Feil R, Hofmann F, Korth M, Shipston MJ, Knaus HG, Wolfer DP, Pedroarena CM, Storm JF, Ruth P (2004) Cerebellar ataxia and Purkinje cell dysfunction caused by Ca2+-activated K+ channel deficiency. Proc Natl Acad Sci U S A 101:9474-9478.

Sawada K, Kalam Azad A, Sakata-Haga H, Lee NS, Jeong YG, Fukui Y (2009) Striking pattern of Purkinje cell loss in cerebellum of an ataxic mutant mouse, tottering. Acta Neurobiol Exp (Wars) 69:138-145.

Sawyer SF, Young SJ, Groves PM, Tepper JM (1994) Cerebellar-responsive neurons in the thalamic ventroanterior-ventrolateral complex of rats: in vivo electrophysiology. Neuroscience 63:711-724.

Schmidt H, Brown EB, Schwaller B, Eilers J (2003) Diffusional mobility of parvalbumin in spiny dendrites of cerebellar Purkinje neurons quantified by fluorescence recovery after photobleaching. Biophys J 84:2599-2608.

Schmolesky MT, Weber JT, De Zeeuw CI, Hansel C (2002) The making of a complex spike: ionic composition and plasticity. Ann N Y Acad Sci 978:359-390.

Schonewille M, Luo C, Ruigrok TJ, Voogd J, Schmolesky MT, Rutteman M, Hoebeek FE, De Jeu MT, De Zeeuw CI (2006) Zonal organization of the mouse flocculus: physi-

ology, input, and output. J Comp Neurol 497:670-682.
Sharp AH, Nucifora FC, Jr., Blondel O, Sheppard CA, Zhang C, Snyder SH, Russell JT, Ryugo DK, Ross CA (1999) Differential cellular expression of isoforms of inositol 1,4,5-triphosphate receptors in neurons and glia in brain. J Comp Neurol 406:207-220.
Shen K, Meyer T (1999) Dynamic control of CaMKII translocation and localization in hippocampal neurons by NMDA receptor stimulation. Science 284:162-166.
Shen K, Teruel MN, Subramanian K, Meyer T (1998) CaMKIIbeta functions as an F-actin targeting module that localizes CaMKIIalpha/beta heterooligomers to dendritic spines. Neuron 21:593-606.
Silva AJ, Paylor R, Wehner JM, Tonegawa S (1992a) Impaired spatial learning in alpha-calcium-calmodulin kinase II mutant mice. Science 257:206-211.
Silva AJ, Stevens CF, Tonegawa S, Wang Y (1992b) Deficient hippocampal long-term potentiation in alpha-calcium-calmodulin kinase II mutant mice. Science 257:201-206.
Snutch TP, Reiner PB (1992) Ca2+ channels: diversity of form and function. Curr Opin Neurobiol 2:247-253.
Soler-Llavina GJ, Sabatini BL (2006) Synapse-specific plasticity and compartmentalized signaling in cerebellar stellate cells. Nat Neurosci 9:798-806.
Stahl JS, Simpson JI (1995) Dynamics of rabbit vestibular nucleus neurons and the influence of the flocculus. J Neurophysiol 73:1396-1413.
Steinberg JP, Takamiya K, Shen Y, Xia J, Rubio ME, Yu S, Jin W, Thomas GM, Linden DJ, Huganir RL (2006) Targeted in vivo mutations of the AMPA receptor subunit GluR2 and its interacting protein PICK1 eliminate cerebellar long-term depression. Neuron 49:845-860.
Stephens GJ, Morris NP, Fyffe RE, Robertson B (2001) The Cav2.1/alpha1A (P/Q-type) voltage-dependent calcium channel mediates inhibitory neurotransmission onto mouse cerebellar Purkinje cells. Eur J Neurosci 13:1902-1912.
Swensen AM, Bean BP (2003) Ionic mechanisms of burst firing in dissociated Purkinje neurons. J Neurosci 23:9650-9663.
Szapiro G, Barbour B (2007) Multiple climbing fibers signal to molecular layer interneurons exclusively via glutamate spillover. Nat Neurosci 10:735-742.
Takechi H, Eilers J, Konnerth A (1998) A new class of synaptic response involving calcium release in dendritic spines. Nature 396:757-760.
Takemori S (1975) Visual suppression of vestibular nystagmus after cerebellar lesions. Ann Otol Rhinol Laryngol 84:318-326.
Tank DW, Sugimori M, Connor JA, Llinas RR (1988) Spatially resolved calcium dynamics of mammalian Purkinje cells in cerebellar slice. Science 242:773-777.
Tempia F, Kano M, Schneggenburger R, Schirra C, Garaschuk O, Plant T, Konnerth A (1996) Fractional calcium current through neuronal AMPA-receptor channels with a low calcium permeability. J Neurosci 16:456-466.
Teune TM, van der Burg J, van der Moer J, Voogd J, Ruigrok TJ (2000) Topography of cerebellar nuclear projections to the brain stem in the rat. Prog Brain Res 124:141-172.

Tottene A, Volsen S, Pietrobon D (2000) alpha(1E) subunits form the pore of three cerebellar R-type calcium channels with different pharmacological and permeation properties. J Neurosci 20:171-178.

Tu JC, Xiao B, Yuan JP, Lanahan AA, Leoffert K, Li M, Linden DJ, Worley PF (1998) Homer binds a novel proline-rich motif and links group 1 metabotropic glutamate receptors with IP3 receptors. Neuron 21:717-726.

van den Maagdenberg AM, Pizzorusso T, Kaja S, Terpolilli N, Shapovalova M, Hoebeek FE, Barrett CF, Gherardini L, van de Ven RC, Todorov B, Broos LA, Tottene A, Gao Z, Fodor M, De Zeeuw CI, Frants RR, Plesnila N, Plomp JJ, Pietrobon D, Ferrari MD (2010) High cortical spreading depression susceptibility and migraine-associated symptoms in Ca(v)2.1 S218L mice. Ann Neurol 67:85-98.

Volpe P, Nori A, Martini A, Sacchetto R, Villa A (1993) Multiple/heterogeneous Ca2+ stores in cerebellum Purkinje neurons. Comp Biochem Physiol Comp Physiol 105:205-211.

Voogd J, Gerrits NM, Ruigrok TJ (1996) Organization of the vestibulocerebellum. Ann N Y Acad Sci 781:553-579.

Wagner W, Brenowitz SD, Hammer JA, 3rd (2011) Myosin-Va transports the endoplasmic reticulum into the dendritic spines of Purkinje neurons. Nat Cell Biol 13:40-48.

Wakamori M, Yamazaki K, Matsunodaira H, Teramoto T, Tanaka I, Niidome T, Sawada K, Nishizawa Y, Sekiguchi N, Mori E, Mori Y, Imoto K (1998) Single tottering mutations responsible for the neuropathic phenotype of the P-type calcium channel. J Biol Chem 273:34857-34867.

Walter JT, Alvina K, Womack MD, Chevez C, Khodakhah K (2006) Decreases in the precision of Purkinje cell pacemaking cause cerebellar dysfunction and ataxia. Nat Neurosci 9:389-397.

Wang SS, Denk W, Hausser M (2000) Coincidence detection in single dendritic spines mediated by calcium release. Nat Neurosci 3:1266-1273.

Wang X, Chen G, Gao W, Ebner TJ (2011) Parasagittally Aligned, mGluR1-Dependent Patches are Evoked at Long Latencies by Parallel Fiber Stimulation in the Mouse Cerebellar Cortex In Vivo. J Neurophysiol.

Watt AJ, Cuntz H, Mori M, Nusser Z, Sjostrom PJ, Hausser M (2009) Traveling waves in developing cerebellar cortex mediated by asymmetrical Purkinje cell connectivity. Nat Neurosci 12:463-473.

Westenbroek RE, Sakurai T, Elliott EM, Hell JW, Starr TV, Snutch TP, Catterall WA (1995) Immunochemical identification and subcellular distribution of the alpha 1A subunits of brain calcium channels. J Neurosci 15:6403-6418.

Williams ME, Brust PF, Feldman DH, Patthi S, Simerson S, Maroufi A, McCue AF, Velicelebi G, Ellis SB, Harpold MM (1992) Structure and functional expression of an omega-conotoxin-sensitive human N-type calcium channel. Science 257:389-395.

Womack MD, Khodakhah K (2003) Somatic and dendritic small-conductance calcium-activated potassium channels regulate the output of cerebellar purkinje neurons. J Neurosci 23:2600-2607.

Womack MD, Khodakhah K (2004) Dendritic control of spontaneous bursting in cerebellar Purkinje cells. J Neurosci 24:3511-3521.

Womack MD, Chevez C, Khodakhah K (2004) Calcium-activated potassium channels are selectively coupled to P/Q-type calcium channels in cerebellar Purkinje neurons. J Neurosci 24:8818-8822.

Womack MD, Hoang C, Khodakhah K (2009) Large conductance calcium-activated potassium channels affect both spontaneous firing and intracellular calcium concentration in cerebellar Purkinje neurons. Neuroscience 162:989-1000.

Zee DS, Yamazaki A, Butler PH, Gucer G (1981) Effects of ablation of flocculus and paraflocculus of eye movements in primate. J Neurophysiol 46:878-899.

Zwingman TA, Neumann PE, Noebels JL, Herrup K (2001) Rocker is a new variant of the voltage-dependent calcium channel gene Cacna1a. J Neurosci 21:1169-1178.

Chapter 2

Cerebellar Cortical Plasticity Cut into Cellular Components

Adapted from submitted review

Zhenyu Gao, Boeke van Beugen, and Chris.I. De Zeeuw

General introduction

Voluntary movements are initiated in the cerebral cortex, while involuntary movements are mostly reflexes triggered by events that evoke responses in one of our sensory organs. Both types of movements can be initiated without a cerebellum, but proper execution of these movements as well as adaptive modification of them requires an intact cerebellum. These functions are in line with the position and connectivity of the cerebellum in that it is superimposed on, but not an essential part of, the brain systems that are required for the initiation and occurrence of movements (Figure 1). The cerebellum itself is also composed of layered networks: The cerebellar cortex is superimposed on the cerebellar and vestibular nuclei to which it projects and via which it exerts all its effects (Figure 1); the granular layer of the cerebellar cortex contains the mossy fiber - granule cell pathway on which the Golgi cells and unipolar brush cells (UBCs) are superimposed; and in the molecular layer there is another group of interneurons formed by the stellate cells and basket cells that are superimposed on the Purkinje cells. The layered character of the networks in the cerebellar cortex makes it ideal to dissect them into cellular components and to subsequently analyze their individual contributions at the level of the functional network involved. Such an approach follows the concepts that implementing new functions during evolution of the central nervous system is often realized by imposing new networks onto existing circuitries and/or by expanding their development (Nieuwenhuys, 1967; Simat et al., 2007b). Specific teleological functions may thus well be attributed to the separate network layers in the cerebellar cortex and their target neurons in the cerebellar and vestibular nuclei. Interestingly, both the neurons in the cerebellar cortex ánd the neurons in the cerebellar and vestibular nuclei are with various forms of synaptic and intrinsic plasticity (for reviews see (Hansel et al., 2001; Bagnall and du Lac, 2006; Pugh and Raman, 2009), and both are innervated by axons from the mossy fiber and climbing fiber system (Figure 1). This configuration raises the intriguing possibility that the various forms of plasticity induced in the cortex and nuclei are not independent, but finely regulated in a coordinated and temporally related fashion (Pugh and Raman, 2009) and that some of the processing and memory formation in the cerebellar cortex ultimately is also consolidated and stored in the cerebellar and vestibular nuclei (Kassardjian et al., 2005; Shutoh et al., 2006; Kellett et al., 2010).

Plasticity at granule cells and superimposed interneurons

Mossy fiber to granule cell synapse

The mossy fibers form one of the two main afferent systems to the cerebellar cortex (Figure 1; connections indicated in brown). They are derived from a large variety of nuclei in the brainstem (Voogd et al., 2010). A single mossy fiber can divide across different folia into multiple branches, each of which provides multiple rosettes, and a single mossy fiber rosette targets tens of granule cells within the cerebellar glomerulus (Palay and Chan-Palay, 1974; Jakab and Hamori, 1988). Thereby the mossy fiber system provides a source of enormous divergence creating a sparse and diverse distribution of information to the granular layer in the cerebellar cortex. The mossy fiber to granule cell synapse shows robust plas-

ticity in that long-term potentiation (LTP) can be readily induced (D'Angelo et al., 1997). This form of LTP is presynaptic, dependent on activation of NMDA and metabotropic glutamate receptors, and can be reversed by presynaptic long-term depression (LTD) (Maffei et al., 2002; Gall et al., 2005) for review see (D'Angelo and De Zeeuw, 2009). Mossy fiber to granule cell LTP and LTD are both Hebbian in that they depend on persistent presynaptic activity and subsequent Ca^{2+} influx in the postsynaptic granule cell (Figure 2). Mossy fiber bursts with a duration longer than 250 ms generally lead to a large Ca^{2+} increase and LTP, whereas those with shorter durations result in small Ca^{2+} increases and LTD (Gall et al., 2005) (Table 1). Hence, plasticity at the mossy fiber to granule cell synapse follows a Ca^{2+}-dependent, bidirectional induction mechanism according to the Bienenstock-Cooper-Munro (BCM) rule (Bienenstock et al., 1982). The balance between LTP and LTD may have important implications for the timing and duration of spike activity in the granule cells (Nieus et al., 2006). According to the Time-Window hypothesis (Kistler and De Zeeuw, 2003; D'Angelo and De Zeeuw, 2009), a higher level of LTP will result in an earlier and more precise onset and a higher number of spikes in the window of granule cell activity following mossy fiber activation. Importantly, the high-frequency transmission at the mossy fiber to granule cell synapse can be sustained despite prominent spillover effects in the glomerulus, the surrounding of which is formed by enwrapping glial sheaths (Palay and Chan-Palay, 1974; DiGregorio et al., 2002). Normally, an accumulation of glutamate leads to desensitization of α-amino-3-hydroxy-5-methyl-isoxazole-4-propionic acid (AMPA) receptors, but this synapse shows a relatively strong resistance to desensitization and does not show prominent signs of postsynaptic short-term depression (DiGregorio et al., 2007).

Inputs to Golgi cells

Golgi cells, which form a heterogeneous group of interneurons in the granular layer, have long apical, often sagittally oriented, dendrites that arborize far into the molecular layer, and shorter proximal dendrites that remain within the granular layer (Palay and Chan-Palay, 1974; Simat et al., 2007a; Sillitoe et al., 2008). Their activity is directly controlled by synaptic inputs from mossy fibers, parallel fibers and molecular layer interneurons (Palay and Chan-Palay, 1974; Dieudonne, 1998; Dumoulin et al., 2001; Nakanishi, 2009), and probably influenced more indirectly by climbing fibers (Schulman and Bloom, 1981; Xu and Edgley, 2008). Whereas plasticity at the mossy fiber to Golgi cell synapse and that at the molecular layer interneuron to Golgi cell synapse remain to be investigated (Kanichay and Silver, 2008; Nakanishi, 2009), the parallel fiber to Golgi cell synapse has been subject of studies on both short-term and long-term plasticity. Paired-pulse facilitation (PPF) and short-term depression (STD) can be induced presynaptically following short bursts of parallel fiber stimulation, but endocannabinoid (eCB) - dependent synaptically-evoked suppression of excitation (SSE), depolarization-induced suppression of excitation (DSE), and posttetanic potentiation (PTP) are difficult to obtain at the parallel fiber to Golgi cell synapse (Beierlein et al., 2007). Instead, high-frequency parallel fiber burst stimulation results in mGluR2 and PKA, but not NMDA, dependent LTD that is postsynaptically expressed (Robberechts et al., 2010) (Table 1). Whether this form of homosynaptic LTD is sufficiently potent to modulate the spiking output of Golgi cells *in vivo* remains to be shown, especially since the efficacy of the parallel fiber to Golgi cell input is already rela-

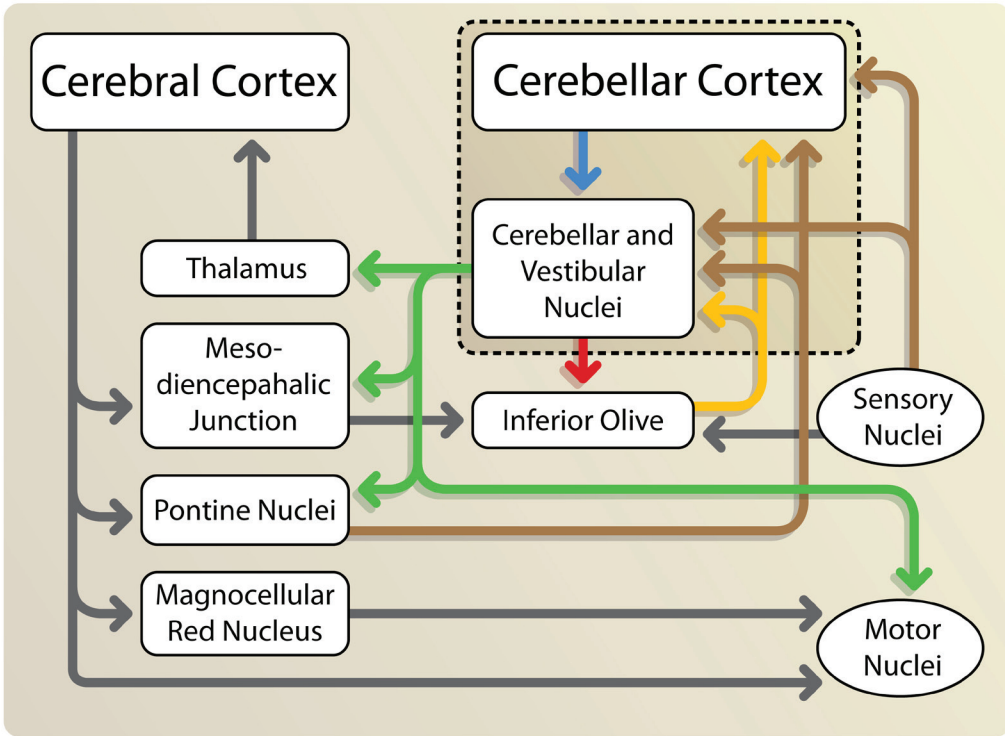

Figure 1 Schematic overview depicting the position of the cerebellum with respect to other parts of the central nervous system.

Pathways directly involved in olivocerebellar processing are shown in individual colors, while the remaining pathways are indicated in dark grey. Input to the cerebellum (dashed border) is conveyed by mossy fibers (brown) and climbing fibers (yellow). Ultimately, these two pathways converge within the cerebellar cortex, from which Purkinje cells project to the cerebellar and vestibular nuclei (blue). From these nuclei, projections are provided to the inferior olive (red) and other extra-cerebellar sites (green). Please note that the direct projections from the cerebellar and vestibular nuclei to the motor nuclei only reflect the direct projections towards the oculomotor nuclei; otherwise there are no direct connections to motor nuclei to the best of our knowledge.

tively weak at its baseline level (Dieudonne, 1998) and the potential range for change in synaptic strength is relatively moderate compared to that at for example the parallel fiber to Purkinje cell synapse . From this point of view the impact of climbing fiber activity on the spike rate of Golgi cells during peripheral activation is more compelling (Xu and Edgley, 2008). The inhibitory component of the often biphasic excitatory-inhibitory response of Golgi cells in crus I/II to peripheral stimulation is strongly attenuated when conjunctive climbing fiber activation is applied. However, the cellular mechanism by which the climbing fibers impose these effects onto the Golgi cell remains to be identified. In principle, it could be heterosynaptic potentiation of the parallel fiber to Golgi cell synapse, similar to that described for the parallel fiber to molecular layer interneuron synapse (Jorntell and Ekerot, 2003; Bender et al., 2009), and/or heterosynaptic depression of the molecular layer interneuron to Golgi cell synapse, similar to that described for the molecular layer interneuron to Purkinje cell synapse (Mittmann and Hausser, 2007). Alternatively, the climbing fibers might have more indirect impact on Golgi cell spiking patterns by affecting the Golgi cell to Golgi cell inhibition mediated through electrotonic coupling (Dugue et al., 2009;

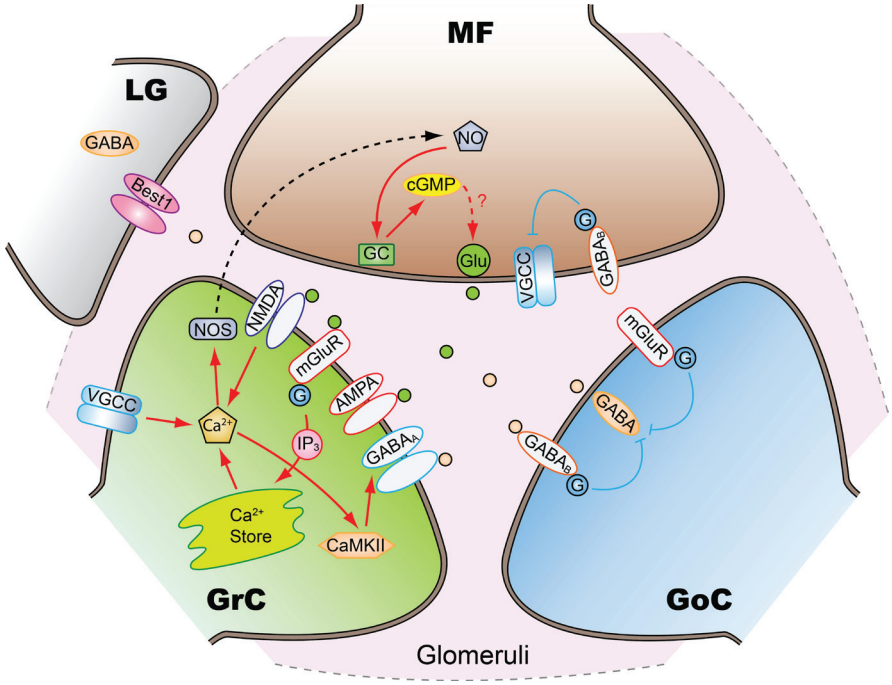

Figure 2 Molecular mechanisms underlying plasticity in granular layer.

Glutamate release from mossy fiber (MF) and GABA release from Golgi cell terminals (GoC) and lamella of glia (LG) trigger various signaling cascades of synaptic plasticity inside the so-called mossy fiber – glomerulus (dashed border). In granule cells (GrC) the glutamate release will evoke an increase in Ca^{2+} via an influx through NMDA receptors and voltage gated Ca^{2+} channels (VGCCs) and via Ca^{2+} release from internal Ca^{2+} stores. The increase in Ca^{2+} triggers retrograde signaling of NO into the MF terminal, which facilitates a presynaptic form of long-term plasticity via guanylate cyclase (GC) and cyclic guanosine mono-phosphate (cGMP) pathways. In addition, the increase in Ca^{2+} activates Ca^{2+}/calmodulin activated kinase II (CaMKII) and facilitates the response of $GABA_A$ receptors to GABA. Within the glomerulus GABA release can also, via spillover, suppress transmitter release presynaptically via activation of $GABA_B$ receptors mediated pathways. Red arrows indicate potentiation cascades, dashed black arrow indicates trans-synaptic diffusion of NO, and blue lines indicate the suppression interactions. Best1 and IP_3 indicate Bestrophin 1 anion channel and inositol-trisphosphate, respectively. See main text for further explanation.

Vervaeke et al., 2010), or on the tonic inhibition provided by GABA release from the lamellar astrocytes within the glomeruli (Lee et al., 2010).

Golgi cell output

Golgi cells have an extensive axonal tree innervating hundreds to thousands of granule cells (Palkovits et al., 1971) and in the vestibulocerebellum also tens of UBCs (Dugue et al., 2005). About two-thirds of the Golgi cells use both GABA and glycine as their neurotransmitter, while two smaller subgroups use either GABA or glycine (Simat et al., 2007a). Interestingly, Golgi cell inhibition of granule cells is mediated by GABA receptors only, while that of UBCs is dominated by glycinergic currents raising the possibility that in the vestibulocerebellum postsynaptic selection of the coreleased transmitters is used to achieve target-specific signaling (Dugue et al., 2005). Most of the Golgi cell axon terminals make synaptic contacts with the granule cell dendrites in the periphery of the cerebellar

Table 1; Summary of all forms of plasticity in cerebellar cortex. N/A indicates not applicable. LTP, LTD, IP and RP indicate long-term potentiation, long-term depression, intrinsic plasticity and rebound potentiation, respectively. SSE, DSE and PTP indicate endocannabinoid (eCB)-dependent synaptically-evoked suppression of excitation, depolarization-induced suppression of excitation, and post-tetanic potentiation, respectively. Arrows up or down indicate final effect on synaptic strength or excitability.

	Cell type	Synapse /cell	Main receptors	Short term plasticity	Key cascades	References	Long term plasticity Direction	Pre/ post	Typical protocol	Key cascades	Selective References
Granule cell network	Granule cell (GrC)	Golgi-GrC	$GABA_A$	Depression	$GABA_B$/ mGluR	Mapelli *et al.*,2009	N/A				
		MF-GrC	AMPA/NMDA	Depression	$GABA_B$/ mGluR	Mitchell and Silver 2000	LTP ↑	pre	MF burst long	NMDAR/PKA	D'angelo *et al.*, 1997
							LTD ↓	pre	MF burst short	NMDAR PKA	Gall *et al.*, 2005
		UBC-GrC	AMPA/NMDA	N/A			N/A				
		Intrinsic excitability		N/A			IP ↑		MF burst	NMDAR PKA	Armano *et al.*, 2000
	Golgi cell (GoC)	PF-GoC	AMPA/NMDA /Kainate	No PTP		Beierlein *et al.*, 2007	LTD ↓	post	100 Hz PF	PKA mGluR2	Robberechts *et al.*, 2010
		MF-GoC	AMPA/NMDA	N/A			N/A				
		CF-GoC	mGluR2	N/A			N/A				
		Lugaro-GoC	$GABA_A$ /glycine	N/A			N/A				
		MLI-GoC	$GABA_A$	N/A			N/A				
		Intrinsic excitability		N/A			N/A				
	Uni polar brush cell (UBC)	GoC-UBC	$GABA_A$ /glycine	N/A			N/A				
		MF-UBC	AMPA/NMDA	N/A			N/A				
		Intrinsic excitability		N/A			N/A				
Purkinje cell network	Purkinje cell (PC)	PF-PC	AMPA	SSE/DSE	eCB	Beierlein and Regehr 2006	LTP ↑	pre	4-8 Hz PF	cAMP/PKA/NO	Salin *et al.*, 1996
							LTD ↓	pre	4 Hz PF	CB1R/NMDA	Qiu and Knopfel, 2009
							LTP ↑	post	1 Hz PF	PP NSF	Lev-Ram *et al.*, 2003 Coesmans *et al.*, 2004
							LTD ↓	post	1Hz PF+CF	PKC/PICK1/PKA PKG/CaMKII/CRF NMDA/mGluR etc.	for review see Ito, 2001 and text
		MLI-PC	$GABA_A$	DSI	eCB	Diana and Marty, 2003	RP ↑	post	CF stimu PC depo	CaMKII	Kano *et al.*, 1992
						Yoshida *et al.*, 2002	LTD ↓	N/A	1Hz MLI+CF	N/A	Mittmann and Hausser, 2007
							DPI ↑	pre	CF stimu PC depo	NMDA	Duguid and Smart, 2004
		CF-PC	AMPA/NMDA	N/A			LTD ↓	post	5 Hz CF	mGluR/PKA/PKC CRF	Hansel and Linden, 2000
		Intrinsic excitability		N/A			IP ↑		1-100 Hz PF	PKA/SK CK2/PP2B	Schonewille *et al.*, 2010 Belmeguenai *et al.*, 2010
	Molecular layer interneuron (MLI)	MLI-MLI	$GABA_A$	N/A			LTP ↑	pre	100 Hz PF	NMDAR/PKA	Lachamp *et al.*, 2009
		PF-MLI	AMPA/NMDA	SSE/DSE	eCB	Beierlein and Regehr 2006	LTD ↓	pre	30 Hz PF	mGluR1/CB1R	Soler-Llavina and Sabatini 2006
							LTP ↑ LTD ↓	post	2-4 Hz PF	NO/mGluR /cAMP	Rancillac and Crépel 2002
							AMPAR switch	post	50 Hz PF	mGluR/PKC PICK1	Liu and Cull-Candy, 2000
		Intrinsic excitability		N/A			N/A				

glomerulus that is formed around the mossy fiber terminal innervating the same dendrites. The granule cell dendrites express different combinations of $GABA_A$ receptor subunits at different locations with putatively different functions (Brickley et al., 1996, 1999). The receptors with the α1 subunit are primarily localized in the synaptic cleft and might determine the amplitude of the phasic inhibition exerted by the Golgi cells, while those with the α6 subunit, which are sensitive to low concentration of GABA, are distributed both inside and outside the postsynaptic densities and could thus determine the strength of tonic inhibition following spillover due to GABA release from either the Golgi cells (Nusser et al., 1998; Rossi and Hamann, 1998; Rossi et al., 2003) or astrocytes (Lee et al., 2010). In addition to the postsynaptic effects, tonic inhibition by GABA within the glomerulus may also regulate transmitter release at the presynaptic site (Kulik et al., 2002) and thus affect short-term plasticity (Figure 2). Indeed, blocking presynaptic $GABA_B$ receptors increases release probability at the Golgi cell to granule cell synapse, increases the amplitude of the first granule cell IPSC evoked by Golgi cell stimulation, and accentuates short-term depression of these IPSCs in response to a train of Golgi cell stimulation (Mapelli et al., 2009). Interestingly, GABA release from the Golgi cell terminal onto the granule cell can also be suppressed by mossy fiber activity upon the activation of mGluRs on the Golgi cell axon terminals (Mitchell and Silver, 2000). Since these $GABA_B$ and mGluR mediated effects in the Golgi terminals are both particularly prominent following high-frequency stimulation, one may argue that they compensate for frequency-dependent depression of granule cell EPSCs following mossy fiber activation and that they further facilitate proper control of the time-window of granule cell activity that is required for creating optimal spatiotemporal spiking patterns in the granular layer (D'Angelo and De Zeeuw, 2009). In other words, presynaptic control of release probability of GABA at the Golgi cell terminal can be regarded as a mechanism to regulate the precision of the onset of feedforward inhibition of the granule cells. Since the Golgi cell feedforward inhibition can probably limit the discharge of connected granule cells within just about 5 ms (D'Angelo and De Zeeuw, 2009), low ambient GABA might well delimit the time-window during which granule cell spikes have the highest probability of being generated.

Input and output of unipolar brush cells

UBCs are small glutamatergic neurons that are prominently distributed in the granular layer of the vermis and flocculonodular lobe (for review see (Mugnaini et al., 2011). They have a single brush-like dendrite, which receives input from mostly a single mossy fiber terminal, and they give rise to an axon, which branches locally in the granular layer and provides itself multiple, intrinsic mossy fibers contacting granule cells and other UBCs (Nunzi and Mugnaini, 2000). Interestingly, the mossy fiber to UBC synapse is relatively large compared to the mossy fiber to granule cell synapse (Floris et al., 1994); it contains large areas of extensive synaptic appositions with multiple release sites and a continuous distribution of postsynaptic ionotropic glutamate receptors (Jaarsma et al., 1995; Rossi et al., 1995). Moreover, due to the tortuous three-dimensional space of the synapse, glutamate, and possibly also acetylcholine (Jaarsma et al., 1996), released from the mossy fiber terminal can become entrapped inside the synaptic cleft for a substantial period of time. This entrapment is likely to result in rebinding of the neurotransmitter and thereby long-lasting, repetitive

postsynaptic activation (Kinney et al., 1997). Indeed, activation of the mossy fiber to UBC input evokes unique biphasic responses consisting of a fast high-frequency component mediated by AMPA/Kainate(KA) receptors, and a slow, but long-lasting, component primarily mediated by AMPA and NMDA receptors (Rossi et al., 1995; Billups et al., 2002). This activation pattern is in line with the finding that fast high-frequency bursts in UBCs can be triggered at low-threshold by fast inactivating T-type Ca^{2+}-channels that generate powerful Ca^{2+} transients mainly in the dendritic brush, while their tonic firing mode is mainly sustained by slowly inactivating L-type Ca^{2+}-channels that are probably distributed more equally over the somatodendritic compartments (Diana et al., 2007; Russo et al., 2007; Birnstiel et al., 2009). Mossy fiber inputs that evoke a prolonged depolarization in UBCs are probably sufficient to inactivate T-type channels and thereby cause a period of hyperpolarization. In addition, mossy fiber activation can have an inhibitory effect on UBCs through activation of group 2 mGluRs, which are expressed at the periphery of the postsynaptic density (Jaarsma et al., 1998) and trigger a G-protein-coupled inward rectifying potassium conductance (Russo et al., 2008). Thus, excitation of UBCs may be tempered by closure of inward calcium currents as well as through activation of extrasynaptic mGluRs that increase background potassium conductances.

Since the size of the cleft of mossy fiber to UBC synapses varies greatly (Mugnaini et al., 2011), the duration of the sustained postsynaptic activation probably also varies substantially (Rossi et al., 1995; Kinney et al., 1997). Together with the fact that the quantity of many of the conductances present in UBCs, including the calcium currents mentioned above, vary substantially (Birnstiel et al., 2009), this will further enhance the diversity of granule cell coding in the temporal domain. Potentially, various forms of plasticity may further fine-tune and divert the duration of sustained activity in each individual UBC. The fast AMPA/KA receptor mediated responses show depression at short inter-stimulus intervals, suggesting fast depletion of available receptors in the synaptic cleft, while the responses of the slower, "steady-state" currents can be both facilitated and depressed dependent on the duration of inter-stimulus intervals (Rossi et al., 1995). In addition, these plastic effects at the mossy fiber to UBC synapse are likely to be influenced by the glycinergic inhibition provided by Golgi cell terminals, which impinge onto both the brush and soma of the UBC (Mugnaini et al., 1997; Dugue et al., 2005). Moreover, activation of the voltage-dependent calcium conductances described above may also elicit long-term changes by controlling the insertion cycle of receptors that affect postsynaptic plasticity (Malinow and Malenka, 2002), by modulating intrinsic excitability (Kassardjian et al., 2005), and/or by mediating activity-dependent changes that control gene expression in the nucleus (Bading et al., 1993; Sekerkova et al., 2005). Thus, the hardware of the UBC network as well as its modifiable elements appear well designed to provide feedforward excitation imposing precisely determined prolonged activity in granule cells over time courses varying from hundreds to thousands of milliseconds following activation by the extrinsic mossy fibers (Rossi et al., 1995; Dino et al., 2000; Billups et al., 2002).

Intrinsic plasticity of granule cells

Plasticity can be expressed by altering the composition of the molecular machinery at syn-

apses, but also by changing the density and/or identity of conductances at other parts of the neuronal membrane (Aizenman and Linden, 2000; Zhang and Linden, 2003; Schulz, 2006). Such intrinsic plasticity can affect the excitability of a dendritic tree partially or completely, and its induction is often preceded by synaptic potentiation (Schulz, 2006). Likewise in granule cells, theta-bursts of mossy fiber stimulation cannot only induce presynaptic LTP as outlined above, but they can also lead to enhanced intrinsic excitability of granule cells (Armano et al., 2000). Whether both changes occur at the same time depends on the strength of the stimulation (Table 1); when the mossy fiber input evokes a strong depolarizing charge on the granule cell the increase in intrinsic excitability will occur together with presynaptic LTP; instead, when the stimulation evokes only a weak change in the membrane potential, plastic effects will be largely restricted to changes in intrinsic excitability (Armano et al., 2000). The enhanced granule cell excitability results from an increased input resistance and lowered spike threshold, which enhance the EPSPs and thereby facilitate additional spike output. Further modification of spike output may be due to changes in intrinsic excitability resulting from NMDA and GABA activation in granule cells (Armano et al., 2000; Bender et al., 2009) (Figure 2). Thus, even though granule cells have low background firing rates due to tonic inhibition, sensory activation can in principle cause bursting in granule cells such that mossy fiber input is transmitted with high reliability to Purkinje cells (Chadderton et al., 2004).

Plasticity at Purkinje cells and superimposed interneurons

Parallel fiber to Purkinje cell synapse

All four forms of long-term plasticity that can possibly occur at a synapse have been described for this synapse; in historical order these include postsynaptic LTD (Ito and Kano, 1982), presynaptic LTP (Salin et al., 1996), postsynaptic LTP (Lev-Ram et al., 2002; Coesmans et al., 2004) and presynaptic LTD (Qiu and Knopfel, 2009). While all these forms of plasticity can be readily induced at the parallel fiber to Purkinje cell synapse, it can be questioned whether any of them can be induced at the synapses between the ascending part of the granule cell axons and Purkinje cells (Sims and Hartell, 2006).

Postsynaptic LTD at the parallel fiber to Purkinje cell synapse is typically induced by paired stimulation of parallel fibers and climbing fibers. This combined stimulation induces a large Ca^{2+} influx and activates both AMPA and mGluR1 receptors (Figure 3), which in turn facilitate phospholipase C to produce inositol 1,4,5-triphosphate (IP_3) (Linden and Connor, 1991; Linden et al., 1991; Hartell, 1994; Khodakhah and Armstrong, 1997). Boosted by IP_3- and Ca^{2+}-mediated calcium release from the endoplasmatic reticulum the postsynaptic Ca^{2+}-transient becomes supralinear (Wang et al., 2000), which in turn activates PKCα (Leitges et al., 2004) and alpha-calcium/calmodulin-dependent protein kinase II (αCaMKII) (Hansel et al., 2006). Ultimately, PKCα phosphorylates Ser-880 of the GluR2 subunit (Chung et al., 2003), which causes dissociation of the GluR2-subunit-containing AMPA receptors from the ‘glutamate receptor interacting protein’ (GRIP) (Matsuda et al., 1999) and facilitates their interaction with PSD-protein ‘protein interacting with

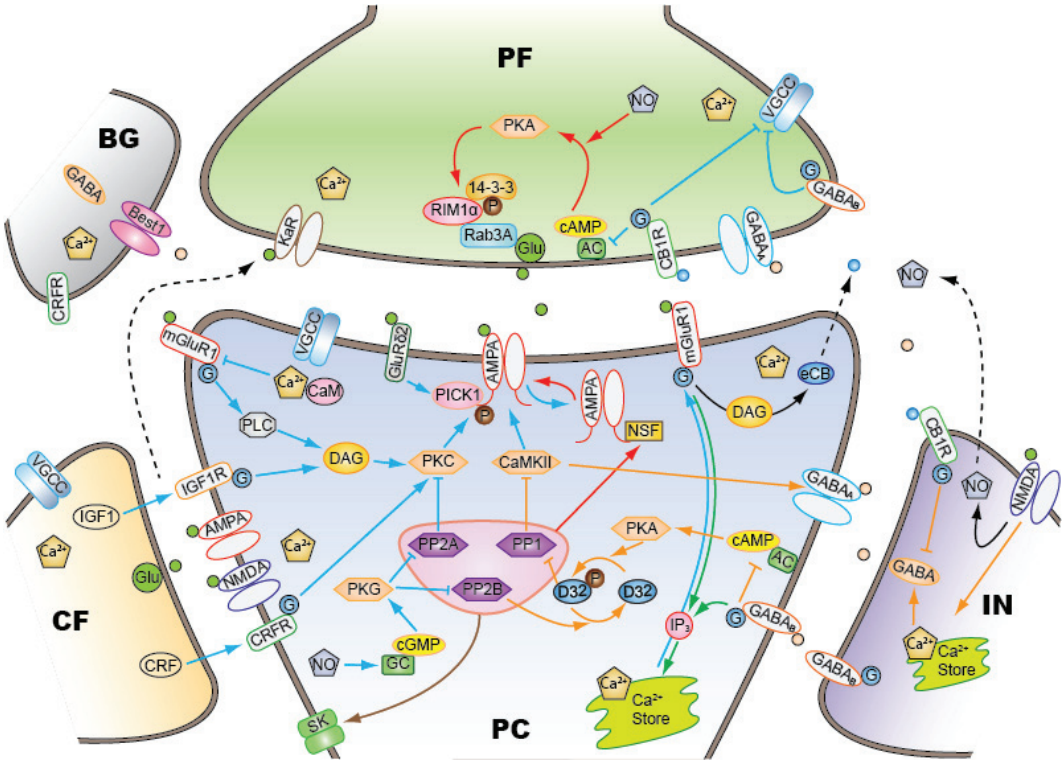

Figure 3 Molecular mechanisms underlying plasticity in molecular layer.

The schematic drawing presents the main molecules and pathways that are involved in the various forms of synaptic plasticity that can occur at the parallel fiber (PF), climbing fiber (CF), and molecular layer interneuron (IN) to Purkinje cell (PC) synapses. For clarity of illustration, the PC is simplified into single compartment. Pathways that are involved in long-term depression at PF-PC synapses are marked in blue; while pathways that are involved in long-term potentiation at PF-PC synapses are marked in red (arrows indicate stimulating impact, whereas lines with perpendicular stop at end indicate inhibitory impact). Yellow arrows indicate long-term plasticity pathways at inhibitory IN-PC synapses, green arrows indicate interacting pathways between inhibitory and excitatory synapses, and brown arrow indicates molecular cascade for intrinsic plasticity. All freely defuse messenger pathways are marked by black arrows (solid arrow for intracellular traffic and dashed arrows for transmembraneous and extracellular traffic). AC indicates adenylyl cyclase; Best1, bestrophin 1 anion channel; CaMKII, Calcium/calmodulin activated kinase II; cAMP, cyclic adenosine mono-phosphate; CB1R, cannabinoid receptor 1; cGMP, cyclic guanosine mono-phosphate; CRF, corticotropin-releasing factor; CRFR, corticotropin-releasing factor receptor; D32, DARPP-32; DAG, diacyl glycerol; eCB, endocannabinoid; GC, guanylate cyclase; Glu, glutamate; IGF1, insulin-like growth factor 1; IGF1R, insulin-like growth factor 1 receptors; IP3, inositol trisphosphate; KaR, Kainate receptor; NSF, N-ethylmaleimide-sensitive factor; PICK1, protein interacting with C kinase 1; PKA, protein kinase A; PKC, protein kinase C; PKG, protein kinase G; PLC, phospholipase C; PP1, protein phosphatase 1; PP2A, protein phosphatase 2A; PP2B, protein phosphatase 2B; RIM1α, Rab3-interacting molecule 1alpha; SK, small conductance Ca^{2+} activated K^{+} channel; and VGCC, voltage gated Ca^{2+} channel.

C kinase 1' (PICK1) (Xia et al., 2000) allowing internalization via a clathrin-dependent process (Wang and Linden, 2000; Xia et al., 2000). Probably, this process is facilitated by the Purkinje cell specific GluRδ2 subunit, which directly interacts with PICK1 (Yawata et al., 2006). Other molecular factors that act at the interface between Purkinje cells and their surrounding can also contribute to the induction of postsynaptic parallel fiber LTD; these include nitric oxide (NO), endocannabinoids, corticotropin-releasing factor (CRF), and NMDA receptors (Figure 3). The possibility that the NO - cyclic guanylate monophos-

phate (cGMP) cascade plays a role in LTD induction (Crepel and Jaillard, 1990; Shibuki and Okada, 1991; Ito, 2001) is supported by the findings that LTD can be prevented by inhibition of consecutive steps within the NO-activated soluble guanylate cyclase (sGS) - cGMP-dependent protein kinase (PKG) pathway (Hartell, 1996; Lev-Ram et al., 1997) and that postsynaptic NO uncaging can replace parallel fiber stimulation and thus bypass activation of AMPAR and mGluR1 as occurs in the classical LTD induction protocol (Lev-Ram et al., 1995; Lev-Ram et al., 1997). Possibly, phosphorylation of G substrate by PKG in the NO pathway suppresses the activity of protein phosphatases PP1 and PP2B (Ito, 2001), thereby controlling the balance between kinases and phosphatases involved in the various forms of plasticity in Purkinje cells (Figure 3). Since NO cannot be formed inside Purkinje cells due to their lack of nitric oxide synthase (NOS), NO probably acts as an anterogade messenger from outside, possibly from molecular layer interneurons (Shibuki and Okada, 1991; Shin and Linden, 2005). Nevertheless, LTD can be induced in cultures of isolated Purkinje neurons, in which all potential donors of NO are abolished (Linden and Connor, 1992), indicating that NO may contribute to, yet is not an essential factor for, postsynaptic LTD at the parallel fiber to Purkinje cell synapse. Endocannabinoids, which are commonly associated with different forms of instant, short-term alterations of synaptic efficacy at both parallel fiber and interneuron terminals (for reviews see (Safo et al., 2006; Le Guen and De Zeeuw, 2010), probably also have an essential role in controlling LTD at the parallel fiber to Purkinje cell synapse (Safo and Regehr, 2005). LTD induction can be blocked by a cannabinoid receptor (CB1R) antagonist or by inhibiting the synthesis of the endocannabinoid 2-arachidonyl glycerol (2-AG), and it is absent in mice lacking the CB1R (Safo and Regehr, 2005). When CB1Rs are activated by an agonist, both NO and postsynaptic calcium transients are still essential for LTD induction, which indicates that the endocannabinoid signaling pathway acts upstream of these factors (Safo and Regehr, 2005). Postsynaptic release of endocannabinoids in Purkinje cell spines, which is like post-synaptic LTD also facilitated by climbing fiber activation, results either directly from Ca^{2+} transients through voltage-gated calcium channels (VGCCs) or from a mGluR1-mediated cascade, which activates phospholipase C (Figure 3). The latter process allows the formation of diacylglycerol (DAG), which is converted into the endocannabinoid 2-AG by DAG lipase. Presynaptically at the parallel fiber terminal, endocannabinoids exert their effect by binding to the CB1R, which markedly attenuates the calcium influx and consequently reduces neurotransmitter release. The reduced calcium influx may result from a direct inhibition from CB1R activation on N-, P/Q- and R-type calcium channels (Brown et al., 2003; Brown et al., 2004) and/or more indirectly from G_i/G_o protein coupled activation of K^+ channels, which can affect VGCCs (Crepel and Ben-Ari, 1996). Thus, the factors involved in endocannabinoid signaling as well as their ultimate presynaptic (Beierlein and Regehr, 2006) and postsynaptic effects suggest a role for endocannabinoids in controlling parallel fiber to Purkinje cell LTD. Instead, CRF may play a permissive role in inducing parallel fiber to Purkinje cell LTD (Miyata et al., 1999). LTD induction can be effectively blocked by specific CRF receptor antagonists and LTD does not occur in CRF-deprived cerebella, while it can be rescued by CRF replenishment. LTD induced by CRF application is mediated by protein kinase C (PKC), but does not depend on changes in Ca2+ signaling or cyclic GMP (cGMP) production. Since, CRF has been shown to be distributed in many,

but not all, climbing fiber zones in both higher and lower mammals (Cha and Foote, 1988; Cummings et al., 1988; King et al., 1997; Sawada et al., 2008), it will be interesting to find out to what extent the induction of parallel fiber to Purkinje cell LTD is also limited to those zones, just like it may be inversely related to the zonal expression of zebrin and the glutamate transporter EAAT4 (Wadiche and Jahr, 2005; Paukert et al., 2010) or like it may be related to the zonal distribution of the promoter of IP_3-receptor IP3R1 (Khodakhah and Armstrong, 1997; Furutama et al., 2010). Finally, functional NMDA receptors have recently been demonstrated to be present postsynaptically at the climbing fiber to Purkinje cell synapse in adult rodents and to also contribute to parallel fiber LTD (Piochon et al., 2007). When NMDARs are blocked, postsynaptic parallel fiber LTD is prevented, yet postsynaptic parallel fiber LTP remains unaffected. Possibly, a decrease in the dentritic calcium transient following the impairment of NMDA mediated calcium influx is responsible for the impact on LTD. Bypassing NMDAR-activity by substituting climbing fiber activity with a brief depolarizing step of the Purkinje cell still elicits parallel fiber LTD in adult mice (Piochon et al., 2010). Thus, even though NMDARs may contribute to the induction of parallel fiber LTD in slices of adults, one cannot exclude the possibility that their role in vivo can to some extent be bypassed.

Presynaptically, plasticity at the parallel fiber to Purkinje cell synapse is dominated by potentiating effects and control thereof by endocannabinoids (for review see (Le Guen and De Zeeuw, 2010). Presynaptic LTP, which is independent of postsynaptic activity, can be elicited by a relatively short period of activity in parallel fibers, typically 120 pulses at 4 - 8 Hz (Salin et al., 1996). This stimulus train will induce a presynaptic calcium influx that will activate a pathway involving Ca^{2+}/calmodulin-sensitive adenyl cyclase, which in turn will lead to a rise in cAMP that activates cAMP-dependent PKA (Salin et al., 1996; Storm et al., 1998). PKA activation will further increase the presynaptic Ca^{2+}-transients thereby probably further strengthening the potentiation (Qiu and Knopfel, 2007). In addition, NO released from other synapses may contribute via diffusion to the induction of presynaptic LTP in unactivated parallel fiber terminals (Jacoby et al., 2001). Possibly, this release is initiated by activation of NMDARs at sites other than parallel fibers (Jacoby et al., 2001; Qiu and Knopfel, 2007). Whether phosphorylation of $RIM1_{\alpha}$, a protein in the active zone, is critical for presynaptic LTP remains to be shown as contradicting results have been found *in vitro* (Lonart et al., 2003) and *in vivo* (Kaeser et al., 2008). Possibly, a short-lasting form of presynaptic potentiation, which can be induced by a periodic burst pattern of homosynaptic stimulation of parallel fibers and lasts for tens of minutes, can facilitate the initiation of presynaptic LTP at the parallel fiber to Purkinje cell synapse (Goto et al., 2006). In contrast, activation of CB1Rs following climbing fiber evoked release of endocannabinoids will suppress adenyl cyclase 1, and thereby attenuate cAMP-dependent PKA activity and induction of presynaptic LTP (Ameri, 1999; van Beugen et al., 2006).

Initially, presynaptic LTP was presumed to act as a reversal mechanism for postsynaptic LTD. This view was refined when postsynaptic LTP was discovered (Lev-Ram et al., 2002) and it was demonstrated that postsynaptic LTD and postsynaptic LTP could reverse one another (Lev-Ram et al., 2003; Coesmans et al., 2004). Postsynaptic LTP, which can be most reliably induced by parallel fiber stimulation alone at 1 Hz for 5 min, can be

blocked when an extra-cellular NO-buffer is added. Moreover, uncaging of postsynaptic NO is sufficient to induce postsynaptic LTP, which suggests that NO acts as an anterogade messenger. Further downstream activation of soluble guanylate cyclase (sGC), which is essential for postsynaptic LTD, is not necessary for postsynaptic LTP induction. Although at a much smaller concentration than for LTD, a postsynaptic calcium transient is still needed for postsynaptic LTP (Coesmans et al., 2004). Subsequent activation of calcium/calmodulin-activated protein phosphatase 2B (PP2B) synergistically activates protein phosphatase 1 (PP1). This activation occurs by releasing the block of PP1 by inhibitor-1 (I-1), the activity of which is under control of PP2B as well as cAMP-activated PKA (Figure 3). Indeed, selectively inhibiting phosphatases PP1, PP2A or PP2B does prevent postsynaptic LTP (Belmeguenai and Hansel, 2005). Trafficking of AMPAR into the synapse, which is the structural correlate of LTP expression, is controlled by calcium sensitive n-ethylmaleimid-sensitive factor (NSF) (Steinberg et al., 2004; Gardner et al., 2005; Hanley, 2007). The protocols for LTP and LTD induction show remarkable similarity, with congruent climbing fiber activity being the only difference. Thus, the climbing fiber is able to reverse both forms of postsynaptic plasticity in either direction (Coesmans et al., 2004). This property can be replaced by altering postsynaptic calcium transients, indicating that the effective postsynaptic calcium transient determines the direction of plasticity at the parallel fiber to Purkinje cell synapse, following the 'inverted BCM-rule', where low and high calcium transients result in LTP and LTD, respectively (Coesmans et al., 2004). Further evidence that calcium-sensitive phosphatases and kinases work synergistically to direct postsynaptic plasticity towards LTP and LTD, respectively, was given by analyses of the βCaMKII knock-out mutant (van Woerden et al., 2009). In this mutant the outcome of the LTP and LTD stimulation protocols gave opposite results, which could be restored by inhibiting the opposing pathway (kinases and phosphatases, respectively).

Recently, (Qiu and Knopfel, 2009) have reported a form of presynaptic LTD that is expressed at the parallel fibers. Strikingly, this type of plasticity, which is most efficiently induced with a parallel fiber stimulation protocol that is similar to that for presynaptic LTP, can only be revealed when presynaptic LTP is pharmacologically prevented by inhibiting PKA or NO. It requires activation of cannabinoid CB1 receptors in a NMDAR, but not mGluR1, dependent fashion. Thus, in principle bidirectional mechanisms exist for both postsynaptic ánd presynaptic plasticity at the parallel fiber to Purkinje cell synapse, but it remains to be shown whether presynaptic LTD can serve a relevant function.

Parallel fiber to molecular layer interneuron synapse

At the parallel fiber to molecular layer interneuron synapse both LTP and LTD can be induced. Low frequency stimulation of parallel fibers alone can induce LTD, whereas parallel fiber stimulation combined with stellate cell depolarization, which in principle could be mediated by climbing fiber activation through spillover (Figure 3), shifts the synaptic plasticity towards LTP (Rancillac and Crepel, 2004). These forms of LTD and LTP induction depend on mGluR activation and the presence of NO or cAMP, respectively (Figure 3). LTD induction can be further facilitated by high frequency parallel fiber stimulation (30 Hz), which activates mGluR1 and CB1 receptors by promoting Ca^{2+} entry through

Ca^{2+} permeable AMPA receptors (Soler-Llavina and Sabatini, 2006). The synaptic changes reach a high level of input specificity, because the LTD expression is restricted to activated synapses due to high Ca^{2+} buffering and general restriction of molecular mobility. Interestingly, the enhanced Ca^{2+} entry does not only change the efficacy of synaptic transmission, but it also drives a rapid replacement of the Ca^{2+} permeable AMPA receptors with GluR2 containing, Ca^{2+} impermeable AMPA receptors (Liu and Cull-Candy, 2000). Thus this molecular modification of the receptor provides a self-regulating feedback that further reduces Ca^{2+} entry, and hence limits the level of GluR2-containing receptors indicating that postsynaptic LTD at the parallel fiber to molecular layer interneuron synapse is a form of plasticity that is limiting itself and thereby indirectly promoting LTP. The switch can be modulated by activation of not only mGluR but also extrasynaptic NMDA receptors and it requires PKC activation and interaction with GRIP and PICK (Liu and Cull-Candy, 2002, 2005; Sun and June Liu, 2007). Therefore, it appears feasible that insertion of GluR2-containing receptors and removal of GluR2-lacking receptors at the synapse are mediated by exocytosis and endocytosis, respectively. Even though the structural change in the AMPA receptor and its cell physiological impact on EPSC amplitude and facilitation properties can last for hours, it can be induced by a single stimulus. A single fear-inducing stimulus *in vivo* has been shown to increase both the expression and incorporation of GluR2 containing AMPA receptors in stellate cells (Liu et al., 2010). Long-term changes at the parallel fiber to molecular layer interneuron synapse *in vivo* are probably also reflected by changes in the cutaneous receptive fields of stellate cells following parallel fiber stimulation (Jorntell and Ekerot, 2002, 2003). Parallel fiber burst stimulation leads to a long-lasting decrease in the size of receptive fields of the interneurons, whereas conjunctive parallel fiber and climbing fiber stimulation leads to an increase of the parallel fiber input to stellate cells. The decrease in receptive fields following parallel fiber stimulation alone is in line with the theoretical consequence of synaptic LTD at the parallel fiber to molecular layer interneuron synapse, while the increase following combined stimulation may reflect LTP at these synapses. Presumably, the climbing fibers evoke their potentiating effects by activating AMPA- and NMDA-type glutamate receptors on interneurons via spillover of transmitters (Szapiro and Barbour, 2007). Apart from this form of LTP that is postsynaptically expressed at the parallel fiber to molecular layer interneuron synapse, there is also a form of LTP at the same synapse that is presynaptically expressed (Bender et al., 2009). This form of LTP operates at least in part through an increase in multivesicular release. GABA release from molecular layer interneurons can activate parallel fiber $GABA_A$ receptors, and this, in turn, can increase release probability at the parallel fiber to molecular layer interneuron synapse (Pugh and Jahr, 2011). Thus, LTP at these synapses implicates a positive feedback mechanism whereby transmission from granule cells to molecular layer interneurons will be strengthened during granule cell spike bursts. It will be interesting to find out to what extent this form of presynaptic LTP can be facilitated by climbing fiber activation of molecular layer interneurons and to what extent it will also affect activity at the parallel fiber to Golgi cell synapse, which in principle could be modified simultaneously by the very same process.

Molecular layer interneuron to Purkinje cell synapse

Purkinje cells receive their inhibitory input presumably mainly from molecular layer inter-

neurons (Palay and Chan-Palay, 1974). Even though climbing fiber activity directly suppresses GABA release of molecular layer interneurons at their synaptic input to Purkinje cells via spillover of glutamate (Satake et al., 2000; Satake et al., 2006), climbing fiber activation of Purkinje cells at relatively low frequency can potentiate the amplitude of spontaneous IPSCs or of IPSCs evoked by molecular layer interneuron activity (Kano et al., 1992; Kano et al., 1996; Kawaguchi and Hirano, 2002). This long-lasting potentiation, also called rebound potentiation, is caused by a Ca^{2+} dependent upregulation of $GABA_A$ receptor function (Kano et al., 1992; Kano et al., 1996; Kawaguchi and Hirano, 2007). The transient elevation of intracellular Ca^{2+}, which is due to activation of voltage-dependent calcium channels and IP3-mediated calcium release from internal stores (Hashimoto and Kano, 2001), activates CaMKII, which in turn regulates $GABA_A$ transmission (Kano et al., 1996). The binding of $GABA_AR\Delta2$ with $GABA_AR$-associated protein (GABARAP) is probably critical for both the induction and maintenance of rebound potentiation (Kawaguchi and Hirano, 2007). Inhibition of GABARAP binding to the $GABA_AR\Delta2$ subunit or expression of a GABARAP mutant, which is unable to associate with tubulin or to undergo conformational alteration, does not only suppress the sustained phases of rebound potentiation but also depresses its early phase. Although rebound potentiation enhances $GABA_A$ transmission in a synaptic unspecific manner, the potentiation can be inhibited at individual synapses in an input-specific way by conjunctive activation of molecular layer interneurons. This input-specific inhibition involves activation of $GABA_B$ receptors and phosphatases 1 and 2B, PKA and DARPP-32 (Kawaguchi and Hirano, 2002). At present, it is still unclear how rebound potentiation is expressed. Future studies will have to elucidate to what extent its expression is mediated by a modulation of $GABA_A$ receptors, a switch in subunits or an increased insertion of receptors. In any case, rebound potentiation provides a potent mechanism for global enhancement of inhibition of Purkinje cells, whereas the threshold for this enhancement can be determined at the level of individual synapses by means of local interneuron activity. In addition to the rebound potentiation, synaptic transmission between molecular layer interneurons and Purkinje cells can also be modulated by the short term Depolarization induced Suppression/Potentiation of Inhibition (DSI/DPI) (Yoshida et al., 2002; Diana and Marty, 2003; Duguid and Smart, 2004), as well as the long term depression (Mittmann and Hausser, 2007). These mechanisms may contribute to determine the inhibition on Purkinje cells.

Climbing fiber to Purkinje cell synapse

During the first postnatal weeks Purkinje cells are innervated by multiple climbing fibers (Hashimoto et al., 2009). Through a process of synapse elimination and axonal pruning, only a single projection will prevail. The remaining connection is established by ~1500 synapses distributed over the entire Purkinje cell dendritic tree with a decreasing gradient from proximal to distal (Crepel and Mariani, 1976). When activated, the climbing fiber will elicit a characteristic large and robust postsynaptic, all-or-none response, that, when observed in whole-cell current-clamp, reveals an initial fast, AMPA-mediated Na^+-spike followed by a slow depolarization on top of which 1-4, partially by Ca^{2+} driven, spikelets can occur (Schmolesky et al., 2002); this response is also known as the ‘complex spike’. When observed in voltage-clamp, closely spaced stimuli reveal paired pulse depression (PPD)

indicating that most of the available neurotransmitter is released with just a single pulse. The calcium transient that can be evoked in the Purkinje cell dendritic tree by climbing fiber activation can last for hundreds of milliseconds (Knopfel et al., 1991). As indicated above this transient results at least in part from opening of VGCCs and from mGluR1/IP3-mediated calcium release from internal stores; yet, in adults, but not in young animals, part of the initial calcium influx might also originate from activation of NMDA receptors at the climbing fiber to Purkinje cell synapse (Piochon et al., 2007; Renzi et al., 2007; Bidoret et al., 2009). Interestingly, elimination of the multiple climbing fiber innervations in young animals is probably partly mediated by induction of homosynaptic postsynaptic LTP at the "winning" climbing fiber to Purkinje cell synapse (Bosman et al., 2008) and presynaptic LTD at the "loosing" climbing fiber to Purkinje cell synapses (Ohtsuki and Hirano, 2008). Induction and expression of postsynaptic climbing fiber LTP (but not of presynaptic climbing fiber LTD) requires postsynaptic Ca^{2+} signaling and involves an increase in the single channel conductance of the postsynaptic AMPA receptors, respectively.

One can also induce postsynaptic LTD at the climbing fiber to Purkinje cell synapse (Hansel and Linden, 2000); a brief stimulation of the climbing fiber at 5 Hz for 30 seconds leads to an attenuation of the EPSCs by ~20%. This form of climbing fiber plasticity, which can also be evoked after the elimination of multiple climbing fibers is completed, requires mGluR1 activation, postsynaptic calcium signaling, activation of PKC and/or PKA, and ultimately internalization of AMPARs (Hansel and Linden, 2000; Schmolesky et al., 2002; Shen et al., 2002; Weber et al., 2003). The molecular cascade for induction and expression is thus remarkably similar to that of heterosynaptic parallel fiber LTD. Nevertheless, the effect is purely homosynaptic and does not spread to parallel fiber to Purkinje cell synapses (Hansel and Linden, 2000). Climbing fiber LTD results in a decrease in the climbing fiber evoked dendritic calcium transient, a reduction in the amplitude of the first slow spikelet and a calcium dependent reduction in the afterhyperpolarization following a complex spike (Hansel and Linden, 2000; Schmolesky et al., 2002; Shen et al., 2002; Weber et al., 2003). Since climbing fiber LTD leads to a decrease in AMPAR-mediated currents, which in turn results in a decrease in VGCC - mediated dendritic calcium transients, one might consider this form of plasticity as an autoregulating form of plasticity, which may serve to protect the Purkinje cell from an overdose of calcium influx following a high-frequency climbing fiber input. Interestingly, induction of climbing fiber LTD requires, just like LTD at the parallel fiber to Purkinje cell synapse, release of CRF, and all main cell physiological effects of climbing fiber LTD can be mimicked by application of CRF to Purkinje cells (Schmolesky et al., 2007). Moreover, these non-plastic, direct effects of CRF can, like climbing fiber LTD itself, be counteracted by PKA and PKC antagonists. Thus, it will be relevant to find out to what extent climbing fiber LTD merely reflects a direct effect upon release of CRF and to what extent it represents a true form of plasticity, in which the long-term consequences reflect processes beyond this direct effect. Likewise, since CRF is, as indicated above, not present in all climbing fiber zones (King et al., 1997; Sawada et al., 2008), it will be interesting to find out whether climbing fiber LTD is limited to the CRF expressing zones. Finally, as stimulation of climbing fibers or olivary neurons induces neuronal-glial transmission with Bergmann glia cells and promotes CRF-R1 expression in their lamellar

processes (Tian et al., 2008; Balakrishnan and Bellamy, 2009), which are known to release GABA through the calcium- and volume-activated, anionic Bestrophin 1 (Best1) channels (Lee et al., 2010), it will also be interesting to find out to what extent Bergmann glia activity plays an active role in plasticity at the climbing fiber to Purkinje cell synapse (Crepel and Mariani, 1976; Knopfel et al., 1991; Hansel and Linden, 2000; Schmolesky et al., 2002; Shen et al., 2002; Weber et al., 2003; Piochon et al., 2007; Renzi et al., 2007; Bosman et al., 2008; Ohtsuki and Hirano, 2008; Tian et al., 2008; Balakrishnan and Bellamy, 2009; Bidoret et al., 2009; Hashimoto et al., 2009) (Figure 3).

Intrinsic plasticity of Purkinje cells

Schreurs and colleagues (1998) were one of the first to show changes in excitability of Purkinje cells. More specifically, they showed that paired presentations of tone and periorbital electrical stimulation as used in classical delay conditioning increased the dendritic membrane excitability of Purkinje cells by modifying a potassium channel-mediated transient hyperpolarization and afterhyperpolarization. More recently, it was demonstrated that Purkinje cell excitability can be enhanced by somatic current injections or by parallel fiber stimulation at frequencies ranging from 1 to 100 Hz (Belmeguenai et al., 2010; Schonewille et al., 2010). Interestingly, the lower frequencies of this range correspond to those that can induce postsynaptic LTP at the parallel fiber to Purkinje cell synapse described above (Coesmans et al., 2004), whereas the higher ones are in line with those that can induce LTP at the molecular layer interneuron to molecular layer interneuron synapse (Lachamp et al., 2009). Analogous to parallel fiber LTP, the signaling cascade of Purkinje cell intrinsic plasticity requires postsynaptic calcium signaling followed by activation of the phosphatases PP1, PP2A and PP2B (Figure 3). Further activation of PKA and casein kinase 2 (CK2) are essential for expression, ultimately leading to a down regulation of SK channel mediated conductances (Belmeguenai et al., 2010). The reduction in SK channels only accounts for part of the observed effect suggesting that other mediators also play a role. Importantly, parallel fiber LTP by itself promotes induction of intrinsic plasticity, but intrinsic plasticity in turn inhibits expression of parallel fiber LTP. Thus, parallel fiber LTP may be the initiator, while intrinsic plasticity downstream may stabilize the appropriate level of excitability and provide feedback to regulate the synaptic weight of the parallel fiber to Purkinje cell synapses involved. In this respect, it is important to note that regulation of intrinsic excitability can also show various levels of input specificity (Schulz, 2006). It can for example control the excitability of a particular part of a dendrite, but alternatively, it may also regulate the level of parallel fiber to Purkinje cell LTP at larger parts of the dendritic tree including those that were not involved in the initial induction; in the latter fashion LTP at the activated parallel fibers would inhibit parallel fiber LTP at the unactivated fibers through intrinsic plasticity. In this respect LTD at the climbing fiber to Purkinje cell synapse may also play a role; it may affect intrinsic excitability at large parts of the Purkinje cell dendritic tree by evoking a calcium dependent change in the afterhyperpolarization in the period shortly following a complex spike (Schmolesky et al., 2007). Ultimately, enhanced excitability of Purkinje cells or parts of its dendritic tree could lead to an increase in firing frequency *in vivo* during spontaneous activity and/or during particular patterns of activation.

References

Aizenman CD, Linden DJ (2000) Rapid, synaptically driven increases in the intrinsic excitability of cerebellar deep nuclear neurons. Nat Neurosci 3:109-111.

Ameri A (1999) The effects of cannabinoids on the brain. Prog Neurobiol 58:315-348.

Armano S, Rossi P, Taglietti V, D'Angelo E (2000) Long-term potentiation of intrinsic excitability at the mossy fiber-granule cell synapse of rat cerebellum. J Neurosci 20:5208-5216.

Bading H, Ginty DD, Greenberg ME (1993) Regulation of gene expression in hippocampal neurons by distinct calcium signaling pathways. Science 260:181-186.

Bagnall MW, du Lac S (2006) A new locus for synaptic plasticity in cerebellar circuits. Neuron 51:5-7.

Balakrishnan S, Bellamy TC (2009) Depression of parallel and climbing fiber transmission to Bergmann glia is input specific and correlates with increased precision of synaptic transmission. Glia 57:393-401.

Beierlein M, Regehr WG (2006) Local interneurons regulate synaptic strength by retrograde release of endocannabinoids. J Neurosci 26:9935-9943.

Beierlein M, Fioravante D, Regehr WG (2007) Differential expression of posttetanic potentiation and retrograde signaling mediate target-dependent short-term synaptic plasticity. Neuron 54:949-959.

Belmeguenai A, Hansel C (2005) A role for protein phosphatases 1, 2A, and 2B in cerebellar long-term potentiation. J Neurosci 25:10768-10772.

Belmeguenai A, Hosy E, Bengtsson F, Pedroarena CM, Piochon C, Teuling E, He Q, Ohtsuki G, De Jeu MT, Elgersma Y, De Zeeuw CI, Jorntell H, Hansel C (2010) Intrinsic plasticity complements long-term potentiation in parallel fiber input gain control in cerebellar Purkinje cells. J Neurosci 30:13630-13643.

Bender VA, Pugh JR, Jahr CE (2009) Presynaptically expressed long-term potentiation increases multivesicular release at parallel fiber synapses. J Neurosci 29:10974-10978.

Bidoret C, Ayon A, Barbour B, Casado M (2009) Presynaptic NR2A-containing NMDA receptors implement a high-pass filter synaptic plasticity rule. Proc Natl Acad Sci U S A 106:14126-14131.

Bienenstock EL, Cooper LN, Munro PW (1982) Theory for the development of neuron selectivity: orientation specificity and binocular interaction in visual cortex. J Neurosci 2:32-48.

Billups D, Liu YB, Birnstiel S, Slater NT (2002) NMDA receptor-mediated currents in rat cerebellar granule and unipolar brush cells. J Neurophysiol 87:1948-1959.

Birnstiel S, Slater NT, McCrimmon DR, Mugnaini E, Hartell NA (2009) Voltage-dependent calcium signaling in rat cerebellar unipolar brush cells. Neuroscience 162:702-712.

Bosman LW, Takechi H, Hartmann J, Eilers J, Konnerth A (2008) Homosynaptic long-term synaptic potentiation of the "winner" climbing fiber synapse in developing Purkinje cells. J Neurosci 28:798-807.

Brickley SG, Cull-Candy SG, Farrant M (1996) Development of a tonic form of synaptic inhibition in rat cerebellar granule cells resulting from persistent activation of GABAA receptors. J Physiol 497 (Pt 3):753-759.

Brickley SG, Cull-Candy SG, Farrant M (1999) Single-channel properties of synaptic and extrasynaptic GABAA receptors suggest differential targeting of receptor subtypes. J Neurosci 19:2960-2973.

Brown SP, Brenowitz SD, Regehr WG (2003) Brief presynaptic bursts evoke synapse-specific retrograde inhibition mediated by endogenous cannabinoids. Nat Neurosci 6:1048-1057.

Brown SP, Safo PK, Regehr WG (2004) Endocannabinoids inhibit transmission at granule cell to Purkinje cell synapses by modulating three types of presynaptic calcium channels. J Neurosci 24:5623-5631.

Cha CI, Foote SL (1988) Corticotropin-releasing factor in olivocerebellar climbing-fiber system of monkey (Saimiri sciureus and Macaca fascicularis): parasagittal and regional organization visualized by immunohistochemistry. J Neurosci 8:4121-4137.

Chadderton P, Margrie TW, Hausser M (2004) Integration of quanta in cerebellar granule cells during sensory processing. Nature 428:856-860.

Chung HJ, Steinberg JP, Huganir RL, Linden DJ (2003) Requirement of AMPA receptor GluR2 phosphorylation for cerebellar long-term depression. Science 300:1751-1755.

Coesmans M, Weber JT, De Zeeuw CI, Hansel C (2004) Bidirectional parallel fiber plasticity in the cerebellum under climbing fiber control. Neuron 44:691-700.

Crepel F, Mariani J (1976) Multiple innervation of Purkinje cells by climbing fibers in the cerebellum of the Weaver Mutant Mouse. J Neurobiol 7:579-582.

Crepel F, Jaillard D (1990) Protein kinases, nitric oxide and long-term depression of synapses in the cerebellum. Neuroreport 1:133-136.

Crepel V, Ben-Ari Y (1996) Intracellular injection of a Ca2+ chelator prevents generation of anoxic LTP. J Neurophysiol 75:770-779.

Cummings S, Sharp B, Elde R (1988) Corticotropin-releasing factor in cerebellar afferent systems: a combined immunohistochemistry and retrograde transport study. J Neurosci 8:543-554.

D‘Angelo E, De Zeeuw CI (2009) Timing and plasticity in the cerebellum: focus on the granular layer. Trends in neurosciences 32:30-40.

D‘Angelo E, De Filippi G, Rossi P, Taglietti V (1997) Synaptic activation of Ca2+ action potentials in immature rat cerebellar granule cells in situ. J Neurophysiol 78:1631-1642.

Diana MA, Marty A (2003) Characterization of depolarization-induced suppression of inhibition using paired interneuron--Purkinje cell recordings. J Neurosci 23:5906-5918.

Diana MA, Otsu Y, Maton G, Collin T, Chat M, Dieudonne S (2007) T-type and L-type Ca2+ conductances define and encode the bimodal firing pattern of vestibulocerebellar unipolar brush cells. J Neurosci 27:3823-3838.

Dieudonne S (1998) Submillisecond kinetics and low efficacy of parallel fibre-Golgi cell synaptic currents in the rat cerebellum. J Physiol 510 (Pt 3):845-866.

DiGregorio DA, Nusser Z, Silver RA (2002) Spillover of glutamate onto synaptic AMPA receptors enhances fast transmission at a cerebellar synapse. Neuron 35:521-533.

DiGregorio DA, Rothman JS, Nielsen TA, Silver RA (2007) Desensitization properties of AMPA receptors at the cerebellar mossy fiber granule cell synapse. J Neurosci

27:8344-8357.

Dino MR, Schuerger RJ, Liu Y, Slater NT, Mugnaini E (2000) Unipolar brush cell: a potential feedforward excitatory interneuron of the cerebellum. Neuroscience 98:625-636.

Dugue GP, Dumoulin A, Triller A, Dieudonne S (2005) Target-dependent use of co-released inhibitory transmitters at central synapses. J Neurosci 25:6490-6498.

Dugue GP, Brunel N, Hakim V, Schwartz E, Chat M, Levesque M, Courtemanche R, Lena C, Dieudonne S (2009) Electrical coupling mediates tunable low-frequency oscillations and resonance in the cerebellar Golgi cell network. Neuron 61:126-139.

Duguid IC, Smart TG (2004) Retrograde activation of presynaptic NMDA receptors enhances GABA release at cerebellar interneuron-Purkinje cell synapses. Nat Neurosci 7:525-533.

Dumoulin A, Triller A, Dieudonne S (2001) IPSC kinetics at identified GABAergic and mixed GABAergic and glycinergic synapses onto cerebellar Golgi cells. J Neurosci 21:6045-6057.

Floris A, Dino M, Jacobowitz DM, Mugnaini E (1994) The unipolar brush cells of the rat cerebellar cortex and cochlear nucleus are calretinin-positive: a study by light and electron microscopic immunocytochemistry. Anat Embryol (Berl) 189:495-520.

Furutama D, Morita N, Takano R, Sekine Y, Sadakata T, Shinoda Y, Hayashi K, Mishima Y, Mikoshiba K, Hawkes R, Furuichi T (2010) Expression of the IP3R1 promoter-driven nls-lacZ transgene in Purkinje cell parasagittal arrays of developing mouse cerebellum. J Neurosci Res 88:2810-2825.

Gall D, Prestori F, Sola E, D'Errico A, Roussel C, Forti L, Rossi P, D'Angelo E (2005) Intracellular calcium regulation by burst discharge determines bidirectional long-term synaptic plasticity at the cerebellum input stage. J Neurosci 25:4813-4822.

Gardner SM, Takamiya K, Xia J, Suh JG, Johnson R, Yu S, Huganir RL (2005) Calcium-permeable AMPA receptor plasticity is mediated by subunit-specific interactions with PICK1 and NSF. Neuron 45:903-915.

Goto J, Inoue T, Kuruma A, Mikoshiba K (2006) Short-term potentiation at the parallel fiber-Purkinje cell synapse. Neurosci Res 55:28-33.

Hanley JG (2007) NSF binds calcium to regulate its interaction with AMPA receptor subunit GluR2. J Neurochem 101:1644-1650.

Hansel C, Linden DJ (2000) Long-term depression of the cerebellar climbing fiber--Purkinje neuron synapse. Neuron 26:473-482.

Hansel C, Linden DJ, D'Angelo E (2001) Beyond parallel fiber LTD: the diversity of synaptic and non-synaptic plasticity in the cerebellum. Nat Neurosci 4:467-475.

Hansel C, de Jeu M, Belmeguenai A, Houtman SH, Buitendijk GH, Andreev D, De Zeeuw CI, Elgersma Y (2006) alphaCaMKII Is essential for cerebellar LTD and motor learning. Neuron 51:835-843.

Hartell NA (1994) Induction of cerebellar long-term depression requires activation of glutamate metabotropic receptors. Neuroreport 5:913-916.

Hartell NA (1996) Inhibition of cGMP breakdown promotes the induction of cerebellar long-term depression. J Neurosci 16:2881-2890.

Hashimoto K, Kano M (2001) [Calcium dependent forms of synaptic plasticity in cerebellar Purkinje cells]. Clin Calcium 11:1432-1439.

Hashimoto K, Yoshida T, Sakimura K, Mishina M, Watanabe M, Kano M (2009) Influence of parallel fiber-Purkinje cell synapse formation on postnatal development of climbing fiber-Purkinje cell synapses in the cerebellum. Neuroscience 162:601-611.

Ito M (2001) Cerebellar long-term depression: characterization, signal transduction, and functional roles. Physiol Rev 81:1143-1195.

Ito M, Kano M (1982) Long-lasting depression of parallel fiber-Purkinje cell transmission induced by conjunctive stimulation of parallel fibers and climbing fibers in the cerebellar cortex. Neuroscience letters 33:253-258.

Jaarsma D, Wenthold RJ, Mugnaini E (1995) Glutamate receptor subunits at mossy fiber-unipolar brush cell synapses: light and electron microscopic immunocytochemical study in cerebellar cortex of rat and cat. J Comp Neurol 357:145-160.

Jaarsma D, Dino MR, Cozzari C, Mugnaini E (1996) Cerebellar choline acetyltransferase positive mossy fibres and their granule and unipolar brush cell targets: a model for central cholinergic nicotinic neurotransmission. J Neurocytol 25:829-842.

Jaarsma D, Dino MR, Ohishi H, Shigemoto R, Mugnaini E (1998) Metabotropic glutamate receptors are associated with non-synaptic appendages of unipolar brush cells in rat cerebellar cortex and cochlear nuclear complex. J Neurocytol 27:303-327.

Jacoby S, Sims RE, Hartell NA (2001) Nitric oxide is required for the induction and heterosynaptic spread of long-term potentiation in rat cerebellar slices. J Physiol 535:825-839.

Jakab RL, Hamori J (1988) Quantitative morphology and synaptology of cerebellar glomeruli in the rat. Anat Embryol (Berl) 179:81-88.

Jorntell H, Ekerot CF (2002) Reciprocal bidirectional plasticity of parallel fiber receptive fields in cerebellar Purkinje cells and their afferent interneurons. Neuron 34:797-806.

Jorntell H, Ekerot CF (2003) Receptive field plasticity profoundly alters the cutaneous parallel fiber synaptic input to cerebellar interneurons in vivo. J Neurosci 23:9620-9631.

Kaeser PS, Kwon HB, Blundell J, Chevaleyre V, Morishita W, Malenka RC, Powell CM, Castillo PE, Sudhof TC (2008) RIM1alpha phosphorylation at serine-413 by protein kinase A is not required for presynaptic long-term plasticity or learning. Proc Natl Acad Sci U S A 105:14680-14685.

Kanichay RT, Silver RA (2008) Synaptic and cellular properties of the feedforward inhibitory circuit within the input layer of the cerebellar cortex. J Neurosci 28:8955-8967.

Kano M, Fukunaga K, Konnerth A (1996) Ca(2+)-induced rebound potentiation of gamma-aminobutyric acid-mediated currents requires activation of Ca2+/calmodulin-dependent kinase II. Proc Natl Acad Sci U S A 93:13351-13356.

Kano M, Rexhausen U, Dreessen J, Konnerth A (1992) Synaptic excitation produces a long-lasting rebound potentiation of inhibitory synaptic signals in cerebellar Purkinje cells. Nature 356:601-604.

Kassardjian CD, Tan YF, Chung JY, Heskin R, Peterson MJ, Broussard DM (2005) The site of a motor memory shifts with consolidation. J Neurosci 25:7979-7985.

Kawaguchi SY, Hirano T (2002) Signaling cascade regulating long-term potentiation of

GABA(A) receptor responsiveness in cerebellar Purkinje neurons. J Neurosci 22:3969-3976.

Kawaguchi SY, Hirano T (2007) Sustained structural change of GABA(A) receptor-associated protein underlies long-term potentiation at inhibitory synapses on a cerebellar Purkinje neuron. J Neurosci 27:6788-6799.

Kellett DO, Fukunaga I, Chen-Kubota E, Dean P, Yeo CH (2010) Memory consolidation in the cerebellar cortex. PLoS One 5:e11737.

Khodakhah K, Armstrong CM (1997) Induction of long-term depression and rebound potentiation by inositol trisphosphate in cerebellar Purkinje neurons. Proc Natl Acad Sci U S A 94:14009-14014.

King JS, Madtes P, Jr., Bishop GA, Overbeck TL (1997) The distribution of corticotropin-releasing factor (CRF), CRF binding sites and CRF1 receptor mRNA in the mouse cerebellum. Prog Brain Res 114:55-66.

Kinney GA, Overstreet LS, Slater NT (1997) Prolonged physiological entrapment of glutamate in the synaptic cleft of cerebellar unipolar brush cells. J Neurophysiol 78:1320-1333.

Kistler WM, De Zeeuw CI (2003) Time windows and reverberating loops: a reverse-engineering approach to cerebellar function. Cerebellum 2:44-54.

Knopfel T, Vranesic I, Staub C, Gahwiler BH (1991) Climbing Fibre Responses in Olivocerebellar Slice Cultures. II. Dynamics of Cytosolic Calcium in Purkinje Cells. Eur J Neurosci 3:343-348.

Kulik A, Nakadate K, Nyiri G, Notomi T, Malitschek B, Bettler B, Shigemoto R (2002) Distinct localization of GABA(B) receptors relative to synaptic sites in the rat cerebellum and ventrobasal thalamus. Eur J Neurosci 15:291-307.

Lachamp PM, Liu Y, Liu SJ (2009) Glutamatergic modulation of cerebellar interneuron activity is mediated by an enhancement of GABA release and requires protein kinase A/RIM1alpha signaling. J Neurosci 29:381-392.

Le Guen MC, De Zeeuw CI (2010) Presynaptic plasticity at cerebellar parallel fiber terminals. Funct Neurol 25:141-151.

Lee S, Yoon BE, Berglund K, Oh SJ, Park H, Shin HS, Augustine GJ, Lee CJ (2010) Channel-mediated tonic GABA release from glia. Science 330:790-796.

Leitges M, Kovac J, Plomann M, Linden DJ (2004) A unique PDZ ligand in PKCalpha confers induction of cerebellar long-term synaptic depression. Neuron 44:585-594.

Lev-Ram V, Wong ST, Storm DR, Tsien RY (2002) A new form of cerebellar long-term potentiation is postsynaptic and depends on nitric oxide but not cAMP. Proc Natl Acad Sci U S A 99:8389-8393.

Lev-Ram V, Mehta SB, Kleinfeld D, Tsien RY (2003) Reversing cerebellar long-term depression. Proc Natl Acad Sci U S A 100:15989-15993.

Lev-Ram V, Makings LR, Keitz PF, Kao JP, Tsien RY (1995) Long-term depression in cerebellar Purkinje neurons results from coincidence of nitric oxide and depolarization-induced Ca2+ transients. Neuron 15:407-415.

Lev-Ram V, Jiang T, Wood J, Lawrence DS, Tsien RY (1997) Synergies and coincidence requirements between NO, cGMP, and Ca2+ in the induction of cerebellar long-term depression. Neuron 18:1025-1038.

Linden DJ, Connor JA (1991) Participation of postsynaptic PKC in cerebellar long-term

depression in culture. Science 254:1656-1659.

Linden DJ, Connor JA (1992) Long-term Depression of Glutamate Currents in Cultured Cerebellar Purkinje Neurons Does Not Require Nitric Oxide Signalling. Eur J Neurosci 4:10-15.

Linden DJ, Dickinson MH, Smeyne M, Connor JA (1991) A long-term depression of AMPA currents in cultured cerebellar Purkinje neurons. Neuron 7:81-89.

Liu SJ, Cull-Candy SG (2002) Activity-dependent change in AMPA receptor properties in cerebellar stellate cells. J Neurosci 22:3881-3889.

Liu SJ, Cull-Candy SG (2005) Subunit interaction with PICK and GRIP controls Ca2+ permeability of AMPARs at cerebellar synapses. Nat Neurosci 8:768-775.

Liu SQ, Cull-Candy SG (2000) Synaptic activity at calcium-permeable AMPA receptors induces a switch in receptor subtype. Nature 405:454-458.

Liu Y, Formisano L, Savtchouk I, Takayasu Y, Szabo G, Zukin RS, Liu SJ (2010) A single fear-inducing stimulus induces a transcription-dependent switch in synaptic AMPAR phenotype. Nat Neurosci 13:223-231.

Lonart G, Schoch S, Kaeser PS, Larkin CJ, Sudhof TC, Linden DJ (2003) Phosphorylation of RIM1alpha by PKA triggers presynaptic long-term potentiation at cerebellar parallel fiber synapses. Cell 115:49-60.

Maffei A, Prestori F, Rossi P, Taglietti V, D'Angelo E (2002) Presynaptic current changes at the mossy fiber-granule cell synapse of cerebellum during LTP. J Neurophysiol 88:627-638.

Malinow R, Malenka RC (2002) AMPA receptor trafficking and synaptic plasticity. Annu Rev Neurosci 25:103-126.

Mapelli L, Rossi P, Nieus T, D'Angelo E (2009) Tonic activation of GABAB receptors reduces release probability at inhibitory connections in the cerebellar glomerulus. J Neurophysiol 101:3089-3099.

Matsuda S, Mikawa S, Hirai H (1999) Phosphorylation of serine-880 in GluR2 by protein kinase C prevents its C terminus from binding with glutamate receptor-interacting protein. J Neurochem 73:1765-1768.

Mitchell SJ, Silver RA (2000) Glutamate spillover suppresses inhibition by activating presynaptic mGluRs. Nature 404:498-502.

Mittmann W, Hausser M (2007) Linking synaptic plasticity and spike output at excitatory and inhibitory synapses onto cerebellar Purkinje cells. J Neurosci 27:5559-5570.

Miyata M, Okada D, Hashimoto K, Kano M, Ito M (1999) Corticotropin-releasing factor plays a permissive role in cerebellar long-term depression. Neuron 22:763-775.

Mugnaini E, Dino MR, Jaarsma D (1997) The unipolar brush cells of the mammalian cerebellum and cochlear nucleus: cytology and microcircuitry. Prog Brain Res 114:131-150.

Mugnaini E, Sekerkova G, Martina M (2011) The unipolar brush cell: a remarkable neuron finally receiving deserved attention. Brain Res Rev 66:220-245.

Nakanishi S (2009) Genetic manipulation study of information processing in the cerebellum. Neuroscience 162:723-731.

Nieus T, Sola E, Mapelli J, Saftenku E, Rossi P, D'Angelo E (2006) LTP regulates burst initiation and frequency at mossy fiber-granule cell synapses of rat cerebellum: experimental observations and theoretical predictions. J Neurophysiol 95:686-699.

Nieuwenhuys R (1967) Comparative anatomy of the cerebellum. Prog Brain Res 25:1-93.

Nunzi MG, Mugnaini E (2000) Unipolar brush cell axons form a large system of intrinsic mossy fibers in the postnatal vestibulocerebellum. J Comp Neurol 422:55-65.

Nusser Z, Sieghart W, Somogyi P (1998) Segregation of different GABAA receptors to synaptic and extrasynaptic membranes of cerebellar granule cells. J Neurosci 18:1693-1703.

Ohtsuki G, Hirano T (2008) Bidirectional plasticity at developing climbing fiber-Purkinje neuron synapses. Eur J Neurosci 28:2393-2400.

Palay SL, Chan-Palay V (1974) Cerebellar cortex: cytology and organization. Berlin, Heidelberg, New York,: Springer.

Palkovits M, Magyar P, Szentagothai J (1971) Quantitative histological analysis of the cerebellar cortex in the cat. II. Cell numbers and densities in the granular layer. Brain Res 32:15-30.

Paukert M, Huang YH, Tanaka K, Rothstein JD, Bergles DE (2010) Zones of enhanced glutamate release from climbing fibers in the mammalian cerebellum. J Neurosci 30:7290-7299.

Piochon C, Levenes C, Ohtsuki G, Hansel C (2010) Purkinje cell NMDA receptors assume a key role in synaptic gain control in the mature cerebellum. J Neurosci 30:15330-15335.

Piochon C, Irinopoulou T, Brusciano D, Bailly Y, Mariani J, Levenes C (2007) NMDA receptor contribution to the climbing fiber response in the adult mouse Purkinje cell. J Neurosci 27:10797-10809.

Pugh JR, Raman IM (2009) Nothing can be coincidence: synaptic inhibition and plasticity in the cerebellar nuclei. Trends in neurosciences 32:170-177.

Pugh JR, Jahr CE (2011) Axonal GABAA receptors increase cerebellar granule cell excitability and synaptic activity. J Neurosci 31:565-574.

Qiu DL, Knopfel T (2007) An NMDA receptor/nitric oxide cascade in presynaptic parallel fiber-Purkinje neuron long-term potentiation. J Neurosci 27:3408-3415.

Qiu DL, Knopfel T (2009) Presynaptically expressed long-term depression at cerebellar parallel fiber synapses. Pflugers Arch 457:865-875.

Rancillac A, Crepel F (2004) Synapses between parallel fibres and stellate cells express long-term changes in synaptic efficacy in rat cerebellum. J Physiol 554:707-720.

Renzi M, Farrant M, Cull-Candy SG (2007) Climbing-fibre activation of NMDA receptors in Purkinje cells of adult mice. J Physiol 585:91-101.

Robberechts Q, Wijnants M, Giugliano M, De Schutter E (2010) Long-term depression at parallel fiber to Golgi cell synapses. J Neurophysiol 104:3413-3423.

Rossi DJ, Hamann M (1998) Spillover-mediated transmission at inhibitory synapses promoted by high affinity alpha6 subunit GABA(A) receptors and glomerular geometry. Neuron 20:783-795.

Rossi DJ, Hamann M, Attwell D (2003) Multiple modes of GABAergic inhibition of rat cerebellar granule cells. J Physiol 548:97-110.

Rossi DJ, Alford S, Mugnaini E, Slater NT (1995) Properties of transmission at a giant glutamatergic synapse in cerebellum: the mossy fiber-unipolar brush cell synapse. J Neurophysiol 74:24-42.

Russo MJ, Mugnaini E, Martina M (2007) Intrinsic properties and mechanisms of spontaneous firing in mouse cerebellar unipolar brush cells. J Physiol 581:709-724.

Russo MJ, Yau HJ, Nunzi MG, Mugnaini E, Martina M (2008) Dynamic metabotropic control of intrinsic firing in cerebellar unipolar brush cells. J Neurophysiol 100:3351-3360.

Safo PK, Regehr WG (2005) Endocannabinoids control the induction of cerebellar LTD. Neuron 48:647-659.

Safo PK, Cravatt BF, Regehr WG (2006) Retrograde endocannabinoid signaling in the cerebellar cortex. Cerebellum 5:134-145.

Salin PA, Malenka RC, Nicoll RA (1996) Cyclic AMP mediates a presynaptic form of LTP at cerebellar parallel fiber synapses. Neuron 16:797-803.

Satake S, Saitow F, Yamada J, Konishi S (2000) Synaptic activation of AMPA receptors inhibits GABA release from cerebellar interneurons. Nat Neurosci 3:551-558.

Satake S, Song SY, Cao Q, Satoh H, Rusakov DA, Yanagawa Y, Ling EA, Imoto K, Konishi S (2006) Characterization of AMPA receptors targeted by the climbing fiber transmitter mediating presynaptic inhibition of GABAergic transmission at cerebellar interneuron-Purkinje cell synapses. J Neurosci 26:2278-2289.

Sawada K, Fukui Y, Hawkes R (2008) Spatial distribution of corticotropin-releasing factor immunopositive climbing fibers in the mouse cerebellum: analysis by whole mount immunohistochemistry. Brain Res 1222:106-117.

Schmolesky MT, Weber JT, De Zeeuw CI, Hansel C (2002) The making of a complex spike: ionic composition and plasticity. Ann N Y Acad Sci 978:359-390.

Schmolesky MT, De Ruiter MM, De Zeeuw CI, Hansel C (2007) The neuropeptide corticotropin-releasing factor regulates excitatory transmission and plasticity at the climbing fibre-Purkinje cell synapse. Eur J Neurosci 25:1460-1466.

Schonewille M, Belmeguenai A, Koekkoek SK, Houtman SH, Boele HJ, van Beugen BJ, Gao Z, Badura A, Ohtsuki G, Amerika WE, Hosy E, Hoebeek FE, Elgersma Y, Hansel C, De Zeeuw CI (2010) Purkinje cell-specific knockout of the protein phosphatase PP2B impairs potentiation and cerebellar motor learning. Neuron 67:618-628.

Schulman JA, Bloom FE (1981) Golgi cells of the cerebellum are inhibited by inferior olive activity. Brain Res 210:350-355.

Schulz DJ (2006) Plasticity and stability in neuronal output via changes in intrinsic excitability: it's what's inside that counts. J Exp Biol 209:4821-4827.

Sekerkova G, Ilijic E, Mugnaini E, Baker JF (2005) Otolith organ or semicircular canal stimulation induces c-fos expression in unipolar brush cells and granule cells of cat and squirrel monkey. Exp Brain Res 164:286-300.

Shen Y, Hansel C, Linden DJ (2002) Glutamate release during LTD at cerebellar climbing fiber-Purkinje cell synapses. Nat Neurosci 5:725-726.

Shibuki K, Okada D (1991) Endogenous nitric oxide release required for long-term synaptic depression in the cerebellum. Nature 349:326-328.

Shin JH, Linden DJ (2005) An NMDA receptor/nitric oxide cascade is involved in cerebellar LTD but is not localized to the parallel fiber terminal. J Neurophysiol 94:4281-4289.

Shutoh F, Ohki M, Kitazawa H, Itohara S, Nagao S (2006) Memory trace of motor learning

shifts transsynaptically from cerebellar cortex to nuclei for consolidation. Neuroscience 139:767-777.

Sillitoe RV, Chung SH, Fritschy JM, Hoy M, Hawkes R (2008) Golgi cell dendrites are restricted by Purkinje cell stripe boundaries in the adult mouse cerebellar cortex. J Neurosci 28:2820-2826.

Simat M, Parpan F, Fritschy JM (2007a) Heterogeneity of glycinergic and gabaergic interneurons in the granule cell layer of mouse cerebellum. J Comp Neurol 500:71-83.

Simat M, Ambrosetti L, Lardi-Studler B, Fritschy JM (2007b) GABAergic synaptogenesis marks the onset of differentiation of basket and stellate cells in mouse cerebellum. Eur J Neurosci 26:2239-2256.

Sims RE, Hartell NA (2006) Differential susceptibility to synaptic plasticity reveals a functional specialization of ascending axon and parallel fiber synapses to cerebellar Purkinje cells. J Neurosci 26:5153-5159.

Soler-Llavina GJ, Sabatini BL (2006) Synapse-specific plasticity and compartmentalized signaling in cerebellar stellate cells. Nat Neurosci 9:798-806.

Steinberg JP, Huganir RL, Linden DJ (2004) N-ethylmaleimide-sensitive factor is required for the synaptic incorporation and removal of AMPA receptors during cerebellar long-term depression. Proc Natl Acad Sci U S A 101:18212-18216.

Storm DR, Hansel C, Hacker B, Parent A, Linden DJ (1998) Impaired cerebellar long-term potentiation in type I adenylyl cyclase mutant mice. Neuron 20:1199-1210.

Sun L, June Liu S (2007) Activation of extrasynaptic NMDA receptors induces a PKC-dependent switch in AMPA receptor subtypes in mouse cerebellar stellate cells. J Physiol 583:537-553.

Szapiro G, Barbour B (2007) Multiple climbing fibers signal to molecular layer interneurons exclusively via glutamate spillover. Nat Neurosci 10:735-742.

Tian JB, King JS, Bishop GA (2008) Stimulation of the inferior olivary complex alters the distribution of the type 1 corticotropin releasing factor receptor in the adult rat cerebellar cortex. Neuroscience 153:308-317.

van Beugen BJ, Nagaraja RY, Hansel C (2006) Climbing fiber-evoked endocannabinoid signaling heterosynaptically suppresses presynaptic cerebellar long-term potentiation. J Neurosci 26:8289-8294.

van Woerden GM, Hoebeek FE, Gao Z, Nagaraja RY, Hoogenraad CC, Kushner SA, Hansel C, De Zeeuw CI, Elgersma Y (2009) betaCaMKII controls the direction of plasticity at parallel fiber-Purkinje cell synapses. Nat Neurosci 12:823-825.

Vervaeke K, Lorincz A, Gleeson P, Farinella M, Nusser Z, Silver RA (2010) Rapid desynchronization of an electrically coupled interneuron network with sparse excitatory synaptic input. Neuron 67:435-451.

Voogd J, Schraa-Tam CK, van der Geest JN, De Zeeuw CI (2010) Visuomotor Cerebellum in Human and Nonhuman Primates. Cerebellum.

Wadiche JI, Jahr CE (2005) Patterned expression of Purkinje cell glutamate transporters controls synaptic plasticity. Nat Neurosci 8:1329-1334.

Wang SS, Denk W, Hausser M (2000) Coincidence detection in single dendritic spines mediated by calcium release. Nat Neurosci 3:1266-1273.

Wang YT, Linden DJ (2000) Expression of cerebellar long-term depression requires postsynaptic clathrin-mediated endocytosis. Neuron 25:635-647.

Weber JT, De Zeeuw CI, Linden DJ, Hansel C (2003) Long-term depression of climbing fiber-evoked calcium transients in Purkinje cell dendrites. Proc Natl Acad Sci U S A 100:2878-2883.

Xia J, Chung HJ, Wihler C, Huganir RL, Linden DJ (2000) Cerebellar long-term depression requires PKC-regulated interactions between GluR2/3 and PDZ domain-containing proteins. Neuron 28:499-510.

Xu W, Edgley SA (2008) Climbing fibre-dependent changes in Golgi cell responses to peripheral stimulation. J Physiol 586:4951-4959.

Yawata S, Tsuchida H, Kengaku M, Hirano T (2006) Membrane-proximal region of glutamate receptor delta2 subunit is critical for long-term depression and interaction with protein interacting with C kinase 1 in a cerebellar Purkinje neuron. J Neurosci 26:3626-3633.

Yoshida T, Hashimoto K, Zimmer A, Maejima T, Araishi K, Kano M (2002) The cannabinoid CB1 receptor mediates retrograde signals for depolarization-induced suppression of inhibition in cerebellar Purkinje cells. J Neurosci 22:1690-1697.

Zhang W, Linden DJ (2003) The other side of the engram: experience-driven changes in neuronal intrinsic excitability. Nat Rev Neurosci 4:885-900.

Chapter 3

Silencing the majority: The essence of cerebellar granule cells

Submitted

Zhenyu Gao, Freek E. Hoebeek, Elisa Galliano, Martijn Schonewille, Boyan Todorov, Andreea S. Pop, Egidio D'Angelo, Arn M.J.M. van den Maagdenberg, and Chris I. De Zeeuw

Abstract

Over half of all neurons in the central nervous system of vertebrates are cerebellar granule cells (GCs) (Williams and Herrup, 1988; Jakab and Hamori, 1988). Besides this striking abundance, their unique morphology, characterized by four short dendrites each of which is innervated by a single mossy fibre, has been highly preserved throughout vertebrate phylogeny (Eccles, 1969). It has been hypothesized that both the abundance and unique morphology of GCs allow the cerebellum to combine the advantages of sparse coding with high sensitivity for individual afferents (Eccles, 1969; Marr, 1969; Silver, 2010). Yet, it remains to be shown whether the extreme abundance of GCs is indeed required for creating selective activity patterns, and if so, what behavioural function they might serve. Here, we silenced the output of most, but not all, GCs by selectively eliminating their P/Q-type ($Ca_V2.1$) Ca^{2+}-channels, which mediate the bulk of their neurotransmitter release (Mintz et al., 1992). Reducing the GC input to both interneurons and Purkinje cells (PCs) increased the regularity of the output of the cerebellar cortex, i.e., simple spike activities, without adapting the average firing rate. Moreover, while silencing the output of GCs did not result in a change in motor performance or short-term motor learning, it severely impaired overnight consolidation of newly acquired motor tasks. Our data demonstrate that minimizing the main excitatory drive of the cerebellar cortex does neither decrease the firing frequency of its sole output neuron, the PC, nor induce severe cerebellar motor deficits such as ataxia. Instead, it specifically prevents temporal pattern formation in PCs and consolidation of cerebellar motor learning. Thus about half of the neurons in our brain are required not merely to perform, but to stabilize sophisticated memories.

Although cerebellar granule cells (GCs) are the most abundant neurons in the central nervous system and constitute one of the two main input stages of the cerebellar cortex (Fig. 1a), it is unclear why there are so many GCs, especially since they fire at low frequency most of the time (Chadderton et al., 2004, Barmack and Yakhnitsa, 2008). To address this long-standing question, previous investigations studied cerebellar motor behaviour when the output of the granule layer was completely abolished either by eliminating all the GCs themselves (Sidman et al., 1965, De Zeeuw et al., 2004), or by completely blocking neurotransmitter release from all GCs (Wada et al., 2007; Kim et al., 2009). However, such all-or-none types of blockades stop all information transfer from granular cell layer to Purkinje cells (PCs) and induce severe symptoms including ataxia, hypotonia and/or tremor preventing specific analysis of cerebellar motor learning (De Zeeuw et al., 2004; Kim et al., 2009). Thus, in order to fully understand the evolutionary preservation of the abundance of cerebellar GCs, a preferable strategy would be to robustly reduce, but not completely eliminate, the GC output. Here we used the incompetence of the conditional transgenic Cre-LoxP system (Tymms and Kola, 2001) to silence the output of most, but not all, GCs. We crossed GC-specific Cre-mice ($\alpha6^{Cre}$; Aller et al., 2003) with floxed *Cacna1a* mice (Todorov et al., 2006) to eliminate neurotransmitter release from the vast majority of

GC axon terminals (Mintz et al., 1992; D'Angelo et al., 1997) (Supplementary Fig. 1a and b). The animals were viable and by eye not distinguishable from their wild type littermates, and the morphology of their GCs and parallel fibre to PC synapses did not show any abnormality (Supplementary Fig. 1, Supplementary Tables 1 and 2). Consistent with our working hypothesis, electrical stimulation of GC parallel fibres elicited significantly smaller responses in both PCs ($P < 0.001$) and stellate cells (SCs) ($P < 0.04$) in $\alpha6^{Cre}$-*Cacna1a* KO mice (Fig. 1a, b, e, f), whereas passive GC membrane properties, and responses to somatic current injections and mossy fibres (MF) stimulations showed no significant differences (Supplementary Fig. 2, Supplementary Table 3). Paired whole-cell recordings of GCs and PCs confirmed that the overall electrical connectivity of GC-PC pairs was significantly reduced by about 70% ($P = 0.03$), but they also revealed that the unitary GC-PC response in $\alpha6^{Cre}$-*Cacna1a* KOs is normal ($P = 0.33$) (Fig. 1c, d), which indicates that the remaining GC input to PCs in $\alpha6^{Cre}$-*Cacna1a* KO mice is likely to originate from unaffected, Cre-negative GCs (Supplementary Fig. 1c). Along the same line, $\alpha6^{Cre}$-*Cacna1a* KO mice showed normal paired-pulse facilitation values at GC-PC synapses, which suggests that in functional GC axon terminals the Ca^{2+}-homeostasis is normal (Supplementary Fig. 3a). Together with the finding that there was no compensatory increase in non-P/Q-type Ca^{2+}-channel mediated neurotransmitter release from GCs in $\alpha6^{Cre}$-*Cacna1a* KO mice (Supplementary Fig. 3b-d), our findings demonstrate that the vast majority of GC output was successfully silenced and the remainder was functionally intact.

Chronic disturbances of synaptic output can potentially change the intrinsic activity of downstream target neurons (Daoudal and Debanne, 2003). To test whether such a secondary cellular effect might be present in $\alpha6^{Cre}$-*Cacna1a* KO mice we investigated the intrinsic excitability of their PCs and SCs. Both types of neurons displayed a normal intrinsic excitability (Supplementary Fig. 4 and Supplementary Table 4). Still, as molecular layer interneurons are also affected by the decreased GC output in $\alpha6^{Cre}$-*Cacna1a* KOs (Fig. 1c, d), their inhibitory input to PCs could in principle also be affected (Wulff et al., 2009). Yet, $\alpha6^{Cre}$-*Cacna1a* PCs showed no significant differences in the amplitude, frequency and kinetics of spontaneous IPSCs (Supplementary Table 5). In sum, our results in $\alpha6^{Cre}$-*Cacna1a* KO mice show little evidence for secondary effects on the activity of neurons downstream of GCs.

To assess the impact of silencing the majority of GC-PC pathway on cerebellar functioning, we first studied the electrophysiological properties of the output of the cerebellar cortex by recording single-unit activity of PCs in alert animals (Fig. 2a). The simple spike activities in $\alpha6^{Cre}$-*Cacna1a* KO mice showed an increased level of regularity ($P = 0.01$), whereas their average firing frequency as well as their climbing fibre pause were unaffected ($P = 0.12$ and $P = 0.59$, respectively) (Fig. 2b, c). In contrast, the complex spike activities showed both a normal firing frequency ánd regularity (P-values > 0.5; Fig. 2d) indicating that the olivary feedback loop probably functions properly. We next studied the behavioural consequences of our genetic manipulation in $\alpha6^{Cre}$-*Cacna1a* KO mice by testing compensatory eye movements, which are known to be a sensitive measure of subtle changes in cerebellar functioning (Wulff et al., 2009, Chapter 4, 5). Remarkably, $\alpha6^{Cre}$-*Cacna1a* KO mice showed no significant changes in the compensatory eye movements (Fig. 3) indicating that minimizing the input of the GCs to PCs has no obvious impact on basic motor performance.

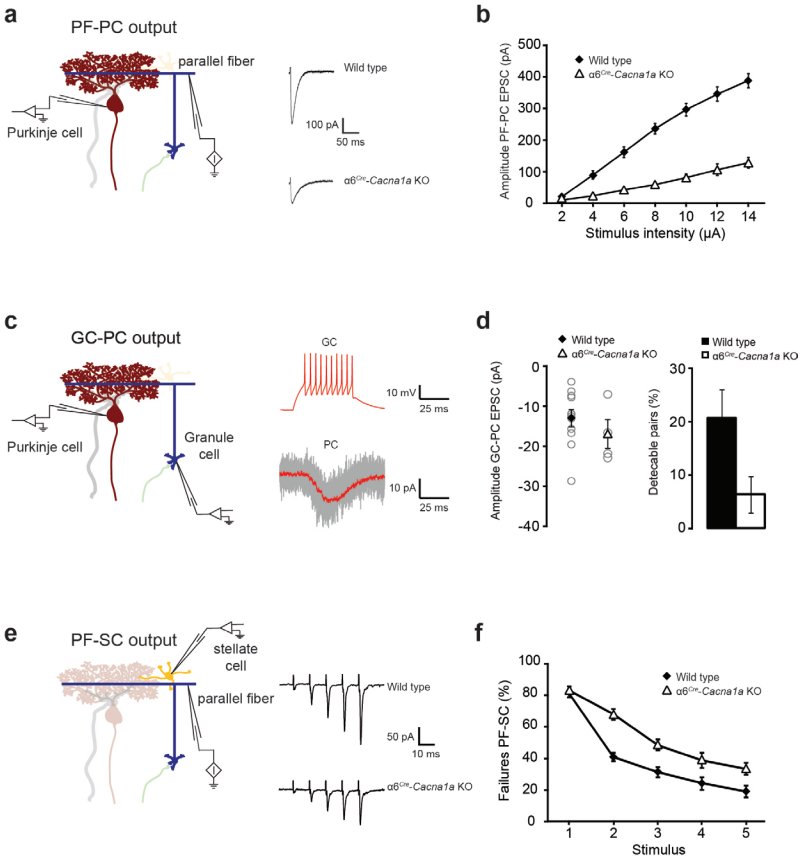

Figure 1. Output of cerebellar granule cells is minimized in α6^{Cre}-*Cacna1a* KO mice. a, c, e, Schematic representations of connectivity within the cerebellar cortex and the respective positions of recording and stimulus pipettes. **a**, Parallel fibre – Purkinje cell (PF-PC) output. Insets: typical responses recorded from PCs while stimulating PFs with a single stimulation pulse of 10 μA for wild type (top) and α6^{Cre}-*Cacna1a* KO mice (bottom). **b**, Average amplitude of the excitatory postsynaptic currents (EPSCs) to stimuli of increasing intensity for wild type (black diamond, n = 13) and α6^{Cre}-*Cacna1a* KO mice (white triangle, n = 9) are significant higher at intensities > 2 μA (all P-values < 0.001). **c**, Granule cell – Purkinje cell output (GC-PC). Insets: Top: representative traces of a connected GC-PC pair from a wild type animal. A train of action potentials of ~200 Hz elicited by somatic current injection in the GC (red trace) induced postsynaptic responses in the PC. Bottom: Red trace indicates the averaged response of 10 repetitive sweeps (gray traces) of GC–PC EPSC. **d**, Left: summary of unitary EPSC amplitudes in PCs evoked by single GC activation for wild type (open circles and black diamond, n = 11) and α6^{Cre}-*Cacna1a* KO (open circles and white triangle, n = 4) using paired GC-PC whole-cell recordings. Right: Percentage of pairs with detectable EPSC responses among all successful double recordings. **e**, Parallel fibre – stellate cell (PF-SC) output. Insets: typical averages of 30 repetitive PF-SC EPSC recordings in response to train stimuli (5 pulses at 100 Hz) for wild type (top) and α6^{Cre}-*Cacna1a* KO mice (bottom). f, Percentage of failures recorded in SCs in response to PF stimulation is significantly increased in α6^{Cre}-*Cacna1a* KO mice (white triangle, n = 12) compared to wild type (black diamond, n = 9) when the number of failures to the first stimulus is set to 80% (see SI for detailed description of methods) (for 2nd – 5th stimulus all P-values < 0.04).

Since the GC-PC pathway might be one of the cerebellar sites for formation and storage of procedural memories (Ito, 2002; Chapter 4), we studied the ability of α6^{Cre}-*Cacna1a* KO mice to adapt their vestibulo-ocular reflex (VOR). To our surprise, the decrease of the VOR amplitude in α6^{Cre}-*Cacna1a* KO mice following one session of *in-phase* visuovestibular training was comparable to that in controls (P = 0.9; Fig. 4a, b). However, when the animals were tested on the next day after staying overnight in the dark, the VOR gain values of α6^{Cre}-*Cacna1a* KO mice had returned to near-baseline, whereas wild type littermates largely consolidated their VOR adaptation (P = 0.02; Fig. 4b, c). To further test memory consolidation, we attempted to reverse the phase of the VOR by applying *in-phase* vestibular stimulation (5°) in combination with optokinetic stimuli of larger amplitudes

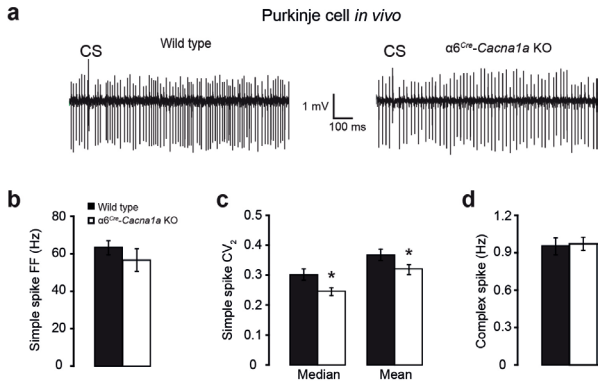

Figure 2. α6^{Cre}-*Cacna1a* KO mice show more regular Purkinje cell simple spike firing. a, Example traces of extracellularly recorded Purkinje cell activity from alert wild type (left) and α6^{Cre}-*Cacna1a* KO mice (right). Both traces show negative events (simple spikes) and a single positive event (complex spike; CS) of which the latter is consistently followed by a pause. **b**, Average simple spike firing frequency (FF) for wild type (n = 26) and α6^{Cre}-*Cacna1a* KO mice (n = 33) showed no significant difference. **c,** Regularity of simple spike firing as quantified by the median and mean coefficient of variance 2-value (CV2) (P = 0.02 and P = 0.01, respectively) indicates significantly more regular simple spike firing in α6^{Cre}-*Cacna1a* KO mice than in wild type littermates. **d,** Average complex spike firing frequency and coefficient of variance (CV) showed no difference between wild type and α6^{Cre}-*Cacna1a* KO mice.

(7.5 – 10°) during four consecutive days (Fig. 4d). Although these demanding stimuli consistently elicited a significant phase change in both wild type littermates and α6^{Cre}-*Cacna1a* KO mice on each day of the training (Fig. 4e), overnight consolidation only occurred in the wild types as indicated by the aberrant consolidation factor (P = 0.036 for mutant re wild type; Fig. 4f). Thus, although α6^{Cre}-*Cacna1a* KO mice are able to perform basic short-term motor learning tasks, they do show prominent impairments in overnight memory consoli-

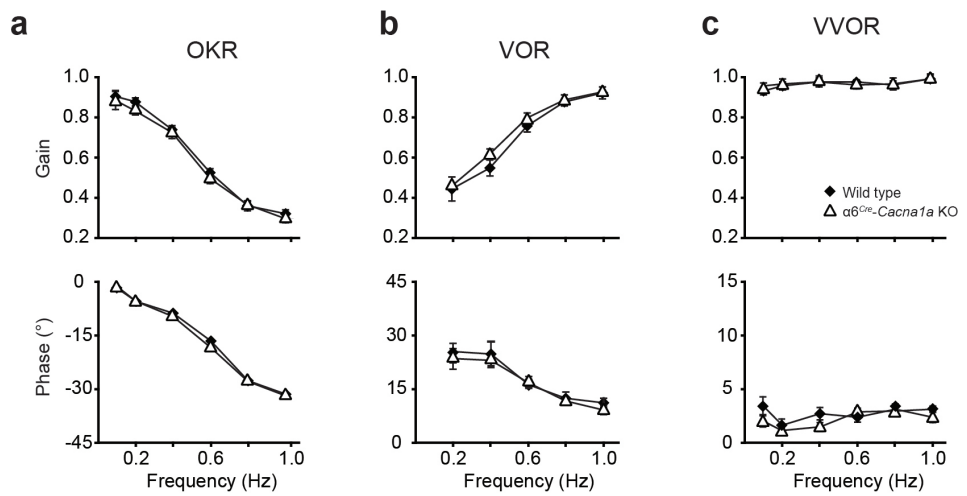

Figure 3. α6^{Cre}-*Cacna1a* KO mice show normal motor performance. Schematic representations and analysis of baseline compensatory eye movements. No significant differences were found in gain and phase values for the optokintic reflex (**a**, OKR), the vestibulo-ocular reflex (**b**, VOR) and the visually-enhanced VOR (**c**, VVOR) between wild type (black diamond, N = 13) and α6^{Cre}-*Cacna1a* KO mice (white triangle, N = 10).

dation of both gain and phase adaptation and as a consequence the ultimate outcome of their training is also affected in course of days.

Our findings show that the cerebellum requires a minimum amount of GCs to maintain basic motor performance but a larger number of GCs for consolidation of newly

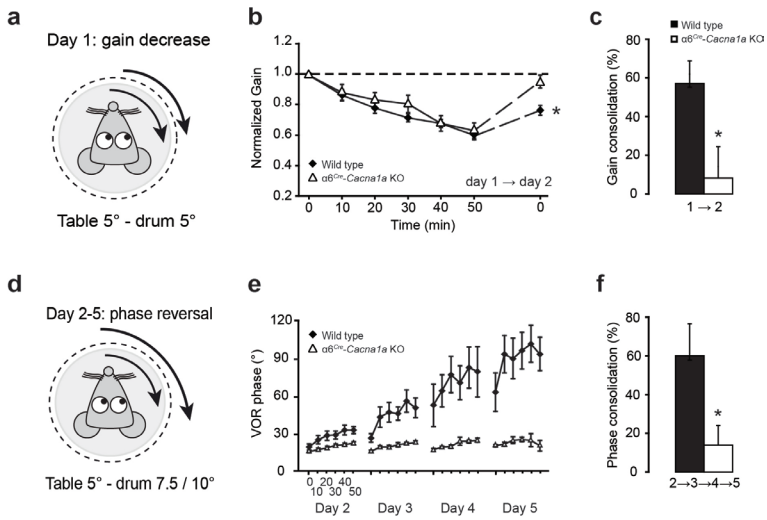

Figure 4. α6^{Cre}-*Cacna1a* KO mice show normal acquisition, but aberrant consolidation of VOR adaptation. a, Schematic representation of gain decrease training paradigm (day one: 5 × 10 min sinusoidal, *in phase* drum and table rotation at 0.6 Hz, both with an amplitude of 5°; day two: VOR gain measurement at 0.6 Hz). **b,** Normalized gain for VOR recorded with 10 min intervals during the one-hour training session show an equal decrease for wild type (black diamond, N = 8) and α6^{Cre}-*Cacna1a* KO mice (white triangle, N = 6), but absence of consolidation on the following day in α6^{Cre}-*Cacna1a* KO mice. **c,** Differences in consolidation (percentage change carried forward from the previous day) for gain decrease (day 1 to 2). The average consolidation is higher in wild type (black) than in α6^{Cre}-*Cacna1a* KO mice (white). **d,** Schematic representation of phase reversal training paradigm (from day two to day five: 5 × 10 min sinusoidal *in phase* drum and table rotation at 0.6 Hz, but with drum amplitudes of 7.5° (days 2 and 3) and 10° (days 4 and 5), while the table amplitude was 5°). **e,** VOR phase values of wild type (black diamond, N = 8) and α6^{Cre}-*Cacna1a* KO mice (white triangle, N = 6) show the inability to reverse the eye movements, as also indicated by the decreased consolidation (calculated by dividing the minimal gain or phase change carried onwards to day n+1 by the maximal change achieved during day n) in **f** (P = 0.036). Asterisks indicate significant differences.

acquired procedural memories. What could be the underlying mechanism of this group coding in consolidating long-term memory? Consolidation of procedural memory formation requires proper spatiotemporal patterning in the cerebellar cortical network (Wulff et al., 2009). Silencing the output of most, but not all GCs in a random fashion is likely to scatter the GC output to such an extent that the PC only receives GC input in a mosaic fashion. This reduction in spatial clustering of GC output is probably detrimental to the formation of appropriate spatiotemporal patterns (Wilms and Hausser, 2010). Furthermore, the scattering of GC output is also likely to affect the induction of long-term synaptic plasticity at PF-PC synapses, since these processes require a minimum number of simultaneously active PFs (Eilers et al., 1995). Indeed, we found that induction of LTD and even more so of LTP were affected at the PF-PC synapses in α6^{Cre}-*Cacna1a* KO mice ($P = 0.02$ and $P < 0.01$, respectively) (Supplementary Fig. 5). Even though the effect of aberrant LTD at the PF-PC synapse on procedural memory formation may be limited (Welsh et al., 2005; Chapter 4), LTP at the PF-PC synapse is probably essential for spatiotempotal pattern formation and consolidation of motor tasks (Chapter 4). On top of these direct deficits in PF-PC plasticity the putative reduction in feedforward inhibition due to the reduced PF input to the molecular layer interneurons most likely contributes to the aberrant regularity of the simple spike output in the α6^{Cre}-*Cacna1a* KO mice (Wulff et al., 2009; Chapter 4; Mittmann and Hausser, 2007). Together our results indicate that silencing most GCs will limit the integrative capacities of the remaining output: both effects are likely to synergistically disrupt the formation of appropriate spatiotemporal patterns and thereby consolidation of procedural memory formation.

In conclusion, our data reveal that the majority of cerebellar GCs are not recruited

to merely perform fundamental motor tasks, but to stabilize sophisticated memories. The overwhelming abundance of GCs, their high sensitivity for individual mossy fibre afferents and sparse coding in the granular layer (Marr, 1969; Isope and Barbour, 2002; Rothman et al, 2009) are all essential to encode and store the wide range of information presented to the cerebellar cortex. This specific design of the cerebellar cortex, which has been preserved throughout vertebrate phylogeny (Eccles, 1969) and is expanded in higher mammals such as non-human primates and human (Williams, 2000; Wetts and Herrup, 1983; Herculano-Houzel, 2009) warrants a memory storage capacity sufficient to last a life time.

References

Aller MI, Jones A, Merlo D, Paterlini M, Meyer AH, Amtmann U, Brickley S, Jolin HE, McKenzie AN, Monyer H, Farrant M, Wisden W (2003) Cerebellar granule cell Cre recombinase expression. Genesis 36:97-103.

Barmack NH, Yakhnitsa V (2008) Functions of interneurons in mouse cerebellum. J Neurosci 28:1140-1152.

Chadderton P, Margrie TW, Hausser M (2004) Integration of quanta in cerebellar granule cells during sensory processing. Nature 428:856-860.

D'Angelo E, De Filippi G, Rossi P, Taglietti V (1997) Synaptic activation of Ca^{2+} action potentials in immature rat cerebellar granule cells in situ. J Neurophysiol 78:1631-1642.

Daoudal G, Debanne D (2003) Long-term plasticity of intrinsic excitability: learning rules and mechanisms. Learn Mem 10:456-465.

De Zeeuw CI, Koekoek SKE, Van Alphen AM, C. L, F.E. H, Van der Steen J, Frens MA, Sun J, Goossens HHLM, Jaarsma D, Coesmans MPH, M.T. S, M.T.G. DJ, Galjart N (2004) Gain and phase control of compensatory eye movements by the vestibulo-cerebellar system. In: Handbook of Auditory Research (Highstein SM, Fay RR, Popper AN, eds). New York: Springer-Verlag.

Eccles JC (1969) The development of the cerebellum of vertebrates in relation to the control of movement. Naturwissenschaften 56:525-534.

Eilers J, Augustine GJ, Konnerth A (1995) Subthreshold synaptic Ca^{2+} signalling in fine dendrites and spines of cerebellar Purkinje neurons. Nature 373:155-158.

Herculano-Houzel S (2009) The human brain in numbers: a linearly scaled-up primate brain. Front Hum Neurosci 3:31.

Isope P, Barbour B (2002) Properties of unitary granule cell-Purkinje cell synapses in adult rat cerebellar slices. J Neurosci 22:9668-9678.

Ito M (2002) Historical review of the significance of the cerebellum and the role of Purkinje cells in motor learning. Ann N Y Acad Sci 978:273-288.

Jakab RL, Hamori J (1988) Quantitative morphology and synaptology of cerebellar glomeruli in the rat. Anat Embryol (Berl) 179:81-88.

Kim JC, Cook MN, Carey MR, Shen C, Regehr WG, Dymecki SM (2009) Linking genetically defined neurons to behavior through a broadly applicable silencing allele.

Neuron 63:305-315.
Marr D (1969) A theory of cerebellar cortex. J Physiol 202:437-470.
Mintz IM, Venema VJ, Swiderek KM, Lee TD, Bean BP, Adams ME (1992) P-type calcium channels blocked by the spider toxin omega-Aga-IVA. Nature 355:827-829.
Mittmann W, Hausser M (2007) Linking synaptic plasticity and spike output at excitatory and inhibitory synapses onto cerebellar Purkinje cells. J Neurosci 27:5559-5570.
Rothman JS, Cathala L, Steuber V, Silver RA (2009) Synaptic depression enables neuronal gain control. Nature 457:1015-1018.
Sidman RL, Green MC, Appel SH (1965) Catalog of the neurological mutants of the mouse. Cambridge, Mass.: Harvard University Press.
Silver RA (2010) Neuronal arithmetic. Nat Rev Neurosci 11:474-489.

Todorov B, van de Ven RC, Kaja S, Broos LA, Verbeek SJ, Plomp JJ, Ferrari MD, Frants RR, van den Maagdenberg AM (2006) Conditional inactivation of the Cacna1a gene in transgenic mice. Genesis 44:589-594.
Tymms MJ, Kola I (2001) Gene knockout protocols: Humana Press.
Wada N, Kishimoto Y, Watanabe D, Kano M, Hirano T, Funabiki K, Nakanishi S (2007) Conditioned eyeblink learning is formed and stored without cerebellar granule cell transmission. Proc Natl Acad Sci U S A 104:16690-16695.
Welsh JP, Yamaguchi H, Zeng XH, Kojo M, Nakada Y, Takagi A, Sugimori M, Llinas RR (2005) Normal motor learning during pharmacological prevention of Purkinje cell long-term depression. Proc Natl Acad Sci U S A 102:17166-17171.
Wetts R, Herrup K (1983) Direct correlation between Purkinje and granule cell number in the cerebella of lurcher chimeras and wild-type mice. Brain Res 312:41-47.
Williams RW (2000) Mapping genes that modulate brain development: a quantitative genetic approach. In: Mouse brain development (Goffinet A, Rakic P, eds), pp xiv, 339 p. Berlin ; New York: Springer.
Williams RW, Herrup K (1988) The control of neuron number. Annu Rev Neurosci 11:423-453.
Wilms CD, Hausser M (2010) Spatially clustered activation of cerebellar parallel fibers by sensory stimuli. In: FENS forum. Amsterdam.
Wulff P, Schonewille M, Renzi M, Viltono L, Sassoe-Pognetto M, Badura A, Gao Z, Hoebeek FE, van Dorp S, Wisden W, Farrant M, De Zeeuw CI (2009) Synaptic inhibition of Purkinje cells mediates consolidation of vestibulo-cerebellar motor learning. Nat Neurosci 12:1042-1049.

Supplementary figures and tables

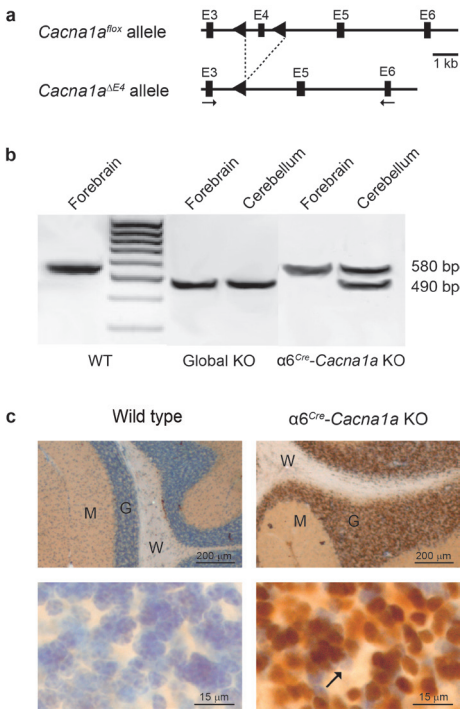

Supplementary Figure 1. The Cre-LoxP strategy to obtain granule cell –specific *Cacna1a* knock-out mice. a, Conditional knockout of *Cacna1a* gene in mice. Schematic representation of the genomic structure of the relevant part of the *Cacna1a*^{flox} allele; black boxes indicate exons (E), triangles indicate the relative position of the LoxP sites; arrows indicate the position of the exotic primers. **b,** RT-PCR of wild type cerebellar RNA amplified a 580 bp fragment. As a control, global KO of the *Cacna1a*^{flox} was induced by crossing with the conditional EIIA-driven Cre mice (EIIA^{Cre} mice(Lakso et al., 1996)), which resulted in 490 bp fragments that lack exon 4 in both forebrain and cerebellum. In α6^{Cre}-*Cacna1a* KO mice, RT-PCR of forebrain RNA amplified a wild type 580 bp fragments; both 580 and 490 bp fragments were found in the cerebellum, suggesting cell specific deletion of exon 4. **c,** Immunohistochemical staining using anti-Cre antibodies show GC-specific expression of Cre. Top: Cre is specifically expressed in the granule cell layer in α6^{Cre}-*Cacna1a* KO. M indicates molecular layer, G granule cell layer and W white matter. Bottom: Cre is expressed in most, but not all GCs. Arrow indicates an example of a Cre negative GC. Together these data indicate that we deleted exon 4 of the *Cacna1a* gene in most cerebellar GCs. See also **Supplementary Table 1**.

Supplementary Figure 2. Granule cells show normal intrinsic excitability and response to mossy fibre inputs. a, GC intrinsic excitability. Middle and right insets show responses to current injections in GCs for wild type and α6^{Cre}-*Cacna1a* KO mice. **b,** Mossy fibre – granule cell (MF-GC) input. Insets show typical responses to sub- and supra-action potential threshold MF stimulation in wild type and α6^{Cre}-*Cacna1a* KO mice. See also **Supplementary Table 2.**

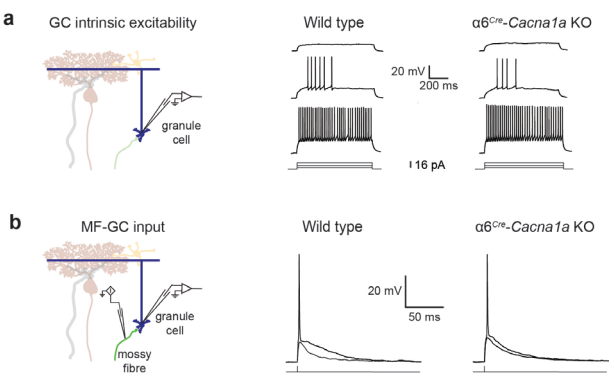

Supplementary Figure 3. Remaining granule cell output is sensitive to P/Q-type channel blocker and shows normal paired-pulse facilitation. a, EPSC ratio between the second and first response to double PF-stimuli with inter-stimulus intervals ranging between 25 – 300 ms reveal no significant difference between wild type and α6^{Cre}-*Cacna1a* KO mice. Insets: typical examples at 50 ms inter-stimulus interval. **b,** PF-PC EPSC amplitude of typical wild type (black diamond) and α6^{Cre}-*Cacna1a* KO PCs (white triangle) before (1) and after the application of ω-Conotoxin GVIA (N-type-specific Ca^{2+}-channel blocker) (2) and ω-Agatoxin IVA (P/Q-type Ca^{2+}-channel blocker) (3) to the recording chamber. Insets: PF-PC EPSCs at the indicated time points for wild type (top) and α6^{Cre}-*Cacna1a* KO mice (bottom). Note the differences between wild type and α6^{Cre}-*Cacna1a* KO mice in initial amplitude and absolute effects of the toxins. **c,** The average PF-PC EPSC component sensitive to the direct application of ω-Agatoxin IVA is significantly larger in wild type (black, n = 7) than in α6^{Cre}-*Cacna1a* KO mice (white, n = 5) (P < 0.001). **d,** The average PF-PC EPSC component sensitive to the application of ω-Conotoxin GVIA (left) is similar (P = 0.2), but the EPSC sensitive to additional application of ω-Agatoxin IVA (right) was significantly decreased (P = 0.003) in α6^{Cre}-*Cacna1a* KO (n = 4) compared to wild type (n = 8).

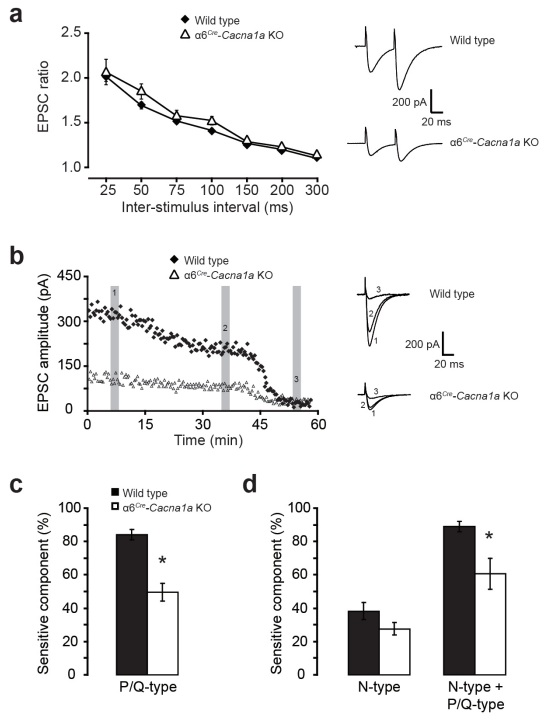

Supplementary Figure 4. Normal intrinsic excitability of Purkinje and stellate cells. a, PC intrinsic excitability. Top: Voltage responses were elicited from -65 mV injecting steps of current (intensities are indicated below the traces) in wild type and α6^{Cre}-*Cacna1a* KO. **c,** Average firing frequency is plotted against the injected current (wild type n = 11, α6^{Cre}-*Cacna1a* KO n = 13). Action potential kinetics are presented in Supplementary Table 3. **b,** SC intrinsic excitability. Voltage responses were elicited from -70 mV injecting steps of current (intensities are indicated below the traces) in wild-type and α6^{Cre}-*Cacna1a* KO. **d,** Average firing frequency is plotted against the injected current (wild type n = 14; α6^{Cre}-*Cacna1a* KO n = 12). Action potential kinetics are presented in Supplementary Table 4.

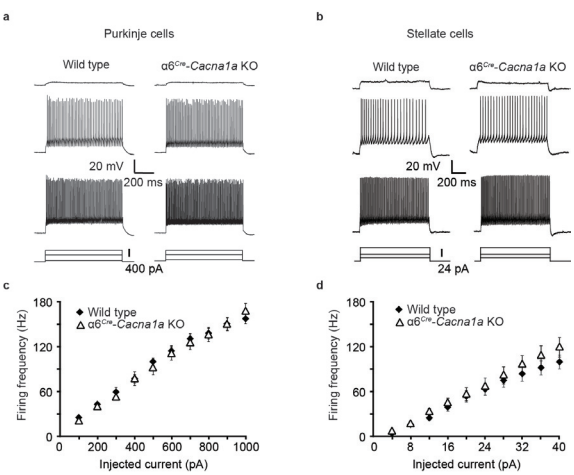

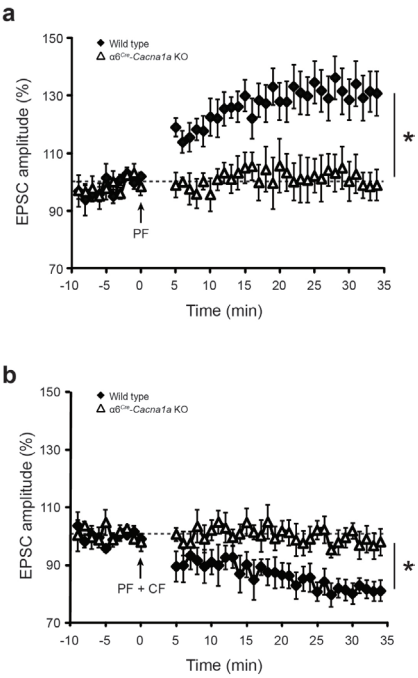

Supplementary Figure 5. Absent long-term synaptic plasticity at parallel fibre - Purkinje cell synapses. a, Long-term potentiation (LTP) was assessed by parallel fibre stimulation at 1 Hz for 5 min, which induced increased EPSC amplitudes in wild type PCs but not in α6^{Cre}-*Cacna1a* KO (wild type n = 8, α6^{Cre}-*Cacna1a* KO n = 6; P < 0.01). **b,** Long-term depression (LTD) was assessed by pairing parallel fibre and climbing fibre stimulation at 1 Hz for 5 min, which induced decreased EPSC amplitudes in wild type PCs but not in α6^{Cre}-*Cacna1a* KO (wild type n = 7, α6^{Cre}-*Cacna1a* KO n = 7, P = 0.02). Both experiments were done in presence of the $GABA_A$-receptor antagonist picrotoxin (100 µM).

Supplementary Table 1. Granule cell morphological characterization. Granule cell density and somatic area projections were quantified using electron-micrographs (wild type: WT; N = 5, n = 1070; α6^{Cre}-*Cacna1a* KO: KO; N = 5, n = 1011). The average number of dendrites and dendritic length were quantified using Golgi-Cox stained tissue (wild type: WT; N = 3, n = 300; α6^{Cre}-*Cacna1a* KO: KO; N = 3, n = 300).

GRANULE CELL MORPHOLOGY

	WT	KO	*P*-value
Granule cell number / 780 µm^2	14.98 ± 0.79	13.59 ± 0.55	0.19
Soma area (µm^2)	12.82 ± 0.57	13.89 ± 0.60	0.23
Soma area (µm^2)	3.85 ± 0.05	3.85 ± 0.05	0.75
Dendritic length (µm)	15.13 ± 0.39	17.91 ± 0.35	0.31

Supplementary Table 2. Parallel fibre-Purkinje cell synapse morphology. PF-PC synaptic morphology was quantified using electron-micrographs (wild type: WT; N = 5, n = 356; α6^{Cre}-*Cacna1a* KO: KO; N = 5, n = 354).

PARALLEL FIBRE-PURKINJE CELL MORPHOLOGY

	WT	KO	*P*-value
PF width (nm)	351 ± 32	363 ± 21	0.46
PC post synaptic density area (nm^2)	6513 ± 515	6414 ± 413	0.97
PC synaptic cleft length (nm)	309 ± 7	312 ± 17	0.43
PC spine head area (nm^2)	0.12 ± 0.01	0.13 ± 0.02	0.70

Supplementary Table 3. Granule cell electrophysiological properties. Top table: The passive properties of cerebellar GCs were investigated in voltage-clamp mode eliciting currents in response to -10 mV voltage steps delivered from the holding potential of -70 mV in both wild type (WT; n = 10) and $\alpha6^{Cre}$-*Cacna1a* KO (KO; n = 10). Middle table: GC intrinsic excitability. For each cell the input/output relationship was quantified as input current injections against number of action potentials elicited. This input/output relationship was fitted with a linear function (see SI for details). Spiking threshold indicates the minimum injected current needed to elicit an action potential. Spike properties are the kinetics quantification of the first action potentials activated by current injections (WT n = 10; KO n = 8). After-hyperpolarisation indicates the absolute amplitude of the undershoot relative to the resting membrane potential. Half-width indicates the width of the signal at 50% of the maximum amplitude. Bottom table: Granule cell responses to mossy fibre stimulation. Kinetics of excitatory postsynaptic potentials (EPSPs) and action potentials elicited by a single pulse mossy fibre stimulus for wild type (WT; n = 9 for EPSPs and n = 5 for action potentials) and $\alpha6^{Cre}$-*Cacna1a* KO (KO; n = 8 for EPSPs and n = 5 for action potentials).

PURKINJE CELLS

SPIKE PROPERTIES			
	WT	KO	*P*-value
Peak Amplitude (mV)	55.99 ± 2.07	53.29 ± 2.85	0.47
After hyperpolarization (mV)	8.10 ± 0.68	8.22 ± 0.71	0.95
Half-width (ms)	0.24 ± 0.01	0.25 ± 0.02	0.69

STELLATE CELLS

SPIKE PROPERTIES			
	WT	KO	*P*-value
Peak Amplitude (mV)	48.33 ± 2.09	52.48 ± 2.72	0.24
After hyperpolarization (mV)	10.96 ± 0.87	11.53 ± 1.03	0.68
Half-width (ms)	0.47 ± 0.01	0.51 ± 0.03	0.25

Supplementary Table 4. Purkinje and stellate cell action potential kinetics. Quantification of the first action potentials activated by current injections (see Fig. 1 in the main text and Supplementary Fig. 3). For Purkinje cells: wild type (WT); n = 11; $\alpha6^{Cre}$-*Cacna1a* KO (KO) n = 13; for stellate cells: wild type (WT); n = 14; $\alpha6^{Cre}$-*Cacna1a* KO (KO) n = 12. After-hyperpolarisation indicates the absolute amplitude of the undershoot relative to the resting membrane potential. Half-width indicates the width of the signal at 50% of the maximum amplitude.

PURKINJE CELLS

SPIKE PROPERTIES			
	WT	KO	*P*-value
Peak Amplitude (mV)	55.99 ± 2.07	53.29 ± 2.85	0.47
After hyperpolarization (mV)	8.10 ± 0.68	8.22 ± 0.71	0.95
Half-width (ms)	0.24 ± 0.01	0.25 ± 0.02	0.69

STELLATE CELLS

SPIKE PROPERTIES			
	WT	KO	*P*-value
Peak Amplitude (mV)	48.33 ± 2.09	52.48 ± 2.72	0.24
After hyperpolarization (mV)	10.96 ± 0.87	11.53 ± 1.03	0.68
Half-width (ms)	0.47 ± 0.01	0.51 ± 0.03	0.25

Supplementary Table 5. Purkinje cell spontaneous IPSCs. Spontaneous IPSC properties for wild type (WT) (300 events averaged per cell; n = 8) and $\alpha6^{Cre}$-*Cacna1a* KO (KO) (300 events averaged per cell; n = 8) Purkinje cells.

PURKINJE CELLS - spontaneous IPSCs

	WT	KO	*P*-value
Amplitude (pA)	94.53 ± 5.77	113.69 ± 11.46	0.16
Frequency (Hz)	13.14 ± 2.41	14.80 ± 2.97	0.67
Half-width (ms)	0.83 ± 0.08	0.94 ± 0.16	0.54
Rise Time (ms)	0.48 ± 0.03	0.56 ± 0.06	0.22
Decay Time (ms)	2.56 ± 0.19	2.71 ± 0.27	0.64

Generation of mutant mice

For the generation of GC-specific *Cacna1a* KO mice we crossed conditional *Cacna1a*^{flox} mice (Todorov et al., 2006) with GC-specific α6^{Cre} mice (Aller et al., 2003). For both mouse lines the F1-offspring was generated by crossing with C57BL/6. The *Cacna1a*^{flox} allele was genotyped by PCR of genomic DNA with primer pair P1: 5'-ACCTACAGTCTGCCAGGAG-3' and P2: 5'-TGAAGCCCAGACATCCTTGG-3'. The successful recombination and deletion of exon 4 were confirmed by PCR using primer set P3: 5'-AGTTTCTATTGGACAGTGCTGGT-3' and P4: 5'-TTGCTTAGCATGCACAGAGG-3'. The Cre transgene were genotyped using primer set P5 5'-ACTTAGCCTGGGGGTAACTAAACT-3' and P6: 5'-GGTATCTCTGACCAGAGTCATCCT-3'. All mice were genotyped at the age of ~p10. For all experiments we compared the results of mutants that were positive for Cre and homozygous for the *Cacna1a*^{flox} allele (α6^{Cre}-*Cacna1a* KO mice) to the pooled results of three wild type groups of which the results of both electrophysiological and behavioural experiments did not differ significantly (Cre-positive mice that harboured two wild type *Cacna1a* alleles, Cre-negative mice that are homozygous for the *Cacna1a*^{flox} allele and Cre-negative mice that harboured two wild type alleles, all p-values > 0.3). The researchers were blind to the genotype of the animals. For the various experiments we used littermates of 18 day - 6 month old. All experiments were performed in accordance with the guidelines for animal experiments of the respective universities and the Dutch national legislation.

RT-PCR

RNA was isolated from freshly dissected cerebellum and cortical regions of the cerebral frontal lobe (forebrain). For RT-PCR, first-strand cDNA was synthesized using random primers, and subsequent PCR was performed using *Cacna1a* specific primers P7: 5'-GATGACACGGAACCATAC-3' and P8: 5'-ATTGTAGAGGAGATCAGTCC-3', located in exon 3 and in exon 6, respectively.

Histology

Mice were anesthetized with an overdose of Nembutal (i.p.) and transcardially perfused with 4% paraformaldehyde. The tissue was subsequently embedded in gelatine and processed for immunohistochemistry. Sagittal sections of 40 μm thick were processed free-floating for immunohistochemistry. The rabbit anti-Cre (AB24608, Abcam, Cambridge, UK) primary antibody was diluted 1:1000 in TBS containing 1% normal horse serum. Biotinylated goat-anti-rabbit secondary antibody (1:200) was obtained from Vector Laboratories. The staining was visualized with the avidin-biotin-peroxidase complex method (ABC) (Vector Laboratories, CITY, USA) and diaminobenzidine (DAB, 0.05%) as the chromogen. For Golgi-Cox staining, a Rapid GolgiStain Kit (FD Neurotechnologies, Inc., Ellicott City, MD, USA) was used. Quantification of the GC dendritic length was done by measuring the distance between the exit of soma and the start of the claw-structure using an Olympus BH2 Microscope equipped with a motorized stage controlled by a computer running StereoInvestigator 4 software (MBF Bioscience, Williston, VT, USA).

Electron microscopy

Mice were anesthetized with an overdose of Nembutal (i.p.) and transcardially perfused with 4% paraformaldehyde and 0.5% glutaraldehyde in cacodylate buffer. Brains were removed, kept overnight in 4% paraformaldehyde, and cut into 80 µm thick coronal sections on a vibratome (Technical Products International, St. Louis, MO, USA). The vibratome sections were post-fixed in 1% osmium tetroxide, stained with 1% uranyl acetate, dehydrated and embedded in Araldite (Durcupan ACM, Fluka, Buchs, Switzerland). Ultrathin (50-70 nm) sections were cut using an ultramicrotome (Leica, Wetzlar, Germany), mounted on Formvar-coated copper grids and contrasted with 2% uranyl acetate and 1% lead citrate (Fluka). Sections of the mouse cerebellum containing granular and molecular layer were photographed using an electron microscope (Philips, Eindhoven, Netherlands). Electron micrographs were taken at magnifications of 2,600X for GC quantification and 25,000X for synaptic quantification (width of the parallel fibre terminal, length of the synaptic cleft, area of the postsynaptic density (PSD) and area of the PC dendritic spine head), and analyzed using MetaVue (Universal Imaging Corp., San Francisco, CA, USA). The parallel fibre width was quantified by measuring the distance between the middle of the synaptic structure and the opposing membrane. For the synaptic cleft, the length of the synaptic contact between the parallel fibre terminal and the PC spine was measured. The area of GCs soma, PSDs and spine heads were determined with the "Trace Region" function of the MetaVue program.

***In vitro* electrophysiology**

Mice were decapitated under isoflurane anaesthesia. Subsequently, the cerebellum was removed and transferred into ice-cold slicing medium containing (in mM): 240 Sucrose, 5 KCl, 1.25 Na_2HPO_4, 2 $MgSO_4$, 1 $CaCl_2$, 26 $NaHCO_3$ and 10 D-Glucose, bubbled with 95% O_2 and 5% CO_2. Parasagittal slices (200 or 250 µm thick) of the cerebellar vermis were cut using a vibratome (VT1000S, Leica) and afterwards kept in ACSF containing (in mM): 124 NaCl, 5 KCl, 1.25 Na_2HPO4, 2 $MgSO_4$, 2 $CaCl_2$, 26 $NaHCO_3$ and 20 D-Glucose, bubbled with 95% O_2 and 5% CO_2 for > 1 h before the experiments started. Patch-clamp experiments were performed at room temperature unless stated otherwise. Whole-cell patch-clamp recordings were performed using either an EPC-10 amplifier (HEKA Electronics, Lambrecht, Germany) or an Axopatch amplifier 700B (Molecular Devices, Union City, CA, USA). Recordings were excluded if series or input resistances (RS and RI, respectively) (assessed by -10 mV voltage steps following each test pulse) varied by > 15% over the course of the experiment.

Purkinje cell whole-cell recordings

PCs were visualized using an upright microscope (Axioskop 2 FS plus, Carl Zeiss, Jena, Germany) equipped with a 40X water immersed objective. Electrodes were filled with an intracellular solution containing (in mM): 124 K-Gluconate, 9 KCl, 10 KOH, 4 NaCl, 10 HEPES, 28.5 Sucrose, 4 Na_2ATP, 0.4 Na_3GTP (pH 7.25-7.35; osmolarity ~290). For extracellular stimulation, patch electrodes filled with ACSF were positioned to touch the surface of the slice at the most distal 1/3 of the molecular layer lateral to the recorded PCs to stimulate parallel fibres, and in the granular layer close to the recorded PC to stimulate

the climbing fibre. To assess the stimulus intensity - EPSC output (input-output) ratio consistently, only PCs with similar dendritic arborization (based on the width of molecular layer) were selected. To elicit paired-pulse facilitation, two consecutive stimuli with 8-10 μA stimulus intensity were given with 25 - 500 ms inter-stimulus intervals.

PF-PC EPSC fractions controlled by individual voltage-gated Ca^{2+}-channel subtypes were assessed using channel-type specific blockers. The N-type Ca^{2+}-channel blocker ω-Conotoxin GVIA (ω-CgTx) and the P/Q-type blocker ω-Agatoxin-IVA (ω-Aga-IVA) were applied to the bath after stable baseline EPSCs were obtained. Reductions of relative EPSCs were taken as functional indications after each blocker was applied. Both ω-CgTx and ω-Aga-IVA were obtained from Peptide Institute (Osaka, Japan). Stock solutions were prepared in ACSF in the presence of 1 mg/ml Cytochrome C to minimize nonspecific binding. Stock solutions (0.1 mM) were stored at -20°C and used within two weeks. ω-CgTx and ω-Aga-IVA stocks were diluted in ACSF supplemented with 0.1 mg/ml Cytochrome C, yielding final concentrations of 3 μM ω-CgTx and 0.2 μM ω-Aga-IVA.

PC intrinsic excitability was recorded in current-clamp mode at physiologically relevant temperatures (34 ± 1 °C). PCs that required > -800 pA to maintain the holding potential at -65 mV or started spiking at this holding potential were discarded. Current steps, ranging from 0 to 1000 pA in 100 pA increments, were injected to evoke action potential firing. The average spiking frequency measured over the entire current pulse was used to construct current-frequency plots. Action potential properties (peak amplitude, after-hyperpolarisation amplitude and half-width) were evaluated using the first action potential generated.

Long-term plasticity at the PF-PC synapse was assessed by either pairing PF and climbing fibre (CF) stimulation at 1 Hz for 5 minutes (PF-LTD protocol) or by PF stimulation alone at 1 Hz for 5 minutes (PF-LTP protocol). Test responses were evoked at a frequency of 0.05 Hz (2 stimuli; 50 ms inter-stimulus interval) with ~0.5 - 6 μA pulses. Holding potentials in the range of -65 to -70 mV were chosen to prevent spontaneous spiking activity. Picrotoxin (100 μM) (Sigma-Aldrich, Dordrecht, Netherlands) was added to the bath solution to isolate excitatory postsynaptic currents. Significance in plasticity was evaluated by performing a Student's t-test at the individual data points 20 min following the start of the tetanus.

Spontaneous IPSCs were examined at physiologically relevant temperatures (34 ± 1 °C) with internal solution containing (in mM): 150 CsCl, 15 CsOH, 1.5 $MgCl_2$, 0.5 EGTA, 10 HEPES, 4 Na_2ATP, 0.4 Na_3GTP (pH 7.25 – 7.35). PCs were voltage clamped at -70 mV in the presence of 10 μM NBQX (Tocris, Bristol, UK). IPSCs were analyzed using minianalysis software (RET synaptosoft, Decantur, USA).

Granule cell whole-cell recordings

Whole-cell patch-clamp recordings of GCs were made using borosilicate patch pipettes of 8-15 MΩ when filled with intracellular solution containing (in mM): 126 K-Gluconate, 1 $MgSO_4$, 4 NaCl, 5 HEPES, 0.05 $CaCl_2$, 0.1 BAPTA, 15 D-Glucose, 3 MgATP, 0.1

Na_3GTP (pH 7.25-7.35). Electrical stimulation of mossy fibres was performed with a patch pipette filled with ACSF. In current clamp mode, electrode capacitance was compensated electronically using the value matched during current transient cancellation in cell-attached configuration. Pipette offset was compensated electronically. GC passive properties were investigated in voltage-clamp mode by eliciting currents with a -10 mV voltage step relative to a resting potential of -70 mV. Cells with membrane capacitance of > 5 pF, RS > 30 MΩ and RI < 300 MΩ were discarded. GC intrinsic excitability was investigated in current-clamp mode, as described above for PCs, with depolarizing current steps of 2 pA starting from a holding potential of -80 mV. Synaptic activation of GCs was studied in current-clamp mode by increasing the stimulation intensity to the mossy fibre bundle so as to eventually reach the threshold for action potential firing

Paired Purkinje cell and granule cell recordings

PCs were voltage clamped at -65 to -70 mV with intracellular solution containing (in mM): 120 K-Gluconate, 9 KCl, 10 KOH, 3.48 $MgCl_2$, 4 NaCl, 10 HEPES, 4 Na_2ATP, 0.4 Na_3GTP 17.5 Sucrose and 10-20 µM Alexa 488 (pH 7.25-7.35). PC dendritic arborizations were visualized using epifluorescence and only PCs with a complete dendritic tree were selected. GCs were randomly selected in an area below the PC dendritic tree < 100 µm away from the PC soma. Whole-cell recordings of GCs were performed using intracellular solution containing (in mM): 126 K-Gluconate, 1 $MgSO_4$, 4 NaCl, 5 HEPES, 0.05 $CaCl_2$, 0.1 BAPTA, 15 D-Glucose, 3 MgATP, 0.1 Na_3GTP (pH 7.25 - 7.35). In our preparation, > 95% of the patched GCs were excitable. GCs were held at -60 mV with minimal current injection (-20 to 0 pA) in current-clamp mode. Trains of GC action potentials were evoked with a 50 ms square current pulse, of which the current intensity was adjusted in that the action potential train was maintained at a physiological relevant frequency (~200 Hz). Although no effort was made to differentiate between parallel fibre connections and ascending axon connections, it is likely that both connections were included in our experiment (c.f. (Isope and Barbour, 2002)). PC recordings with 15 to 30 repetitive GC stimulations were selected for offline analysis. The average unitary GC-PC EPSC response elicited by such high frequency spike train was usually > 5 pA, thus could be unambiguously depicted from baseline noise. Experiments were performed at 34 ± 1 ºC in the presence of 100 µM picrotoxin (Sigma-Aldrich) to block feed-forward inhibition from molecular layer interneurons.

Stellate cell whole-cell recordings

Visually-guided whole-cell patch-clamp recordings of SCs were performed using an EPC-10 amplifier (HEKA Electronics, Lambrecht, Germany). Patch electrodes were filled with an intracellular solution containing (in mM): 130 $CsMeSO_4$, 4 $MgCl_2$, 0.2 EGTA, 10 HEPES, 10 Na-Phosphocreatine, 1 QX-314, 4 Na_2ATP, 0.4 Na_3GTP (pH 7.25 - 7.35). For extracellular stimulation, patch electrodes filled with ACSF were positioned in the bath so that it touched the surface of the slice at the most distal 1/3 of the molecular layer. The stimulus intensity was adjusted so that the failure rate of eliciting PF-EPSCs with a single stimulus was ~80%. The failure rate following a train of five stimuli at 100 Hz was used as

a measure of the reliability of PF-SC synaptic transmission. SC intrinsic excitability was recorded in current-clamp mode at physiologically relevant temperatures (34 ± 1 °C) using an internal solution containing (in mM): 120 K-Gluconate, 9 KCl, 10 KOH, 3.48 $MgCl_2$, 4 NaCl, 10 HEPES, 4 Na_2ATP, 0.4 Na_3GTP and 17.5 Sucrose (pH 7.25 - 7.35). Current steps, ranging from 0 - 40 pA in 4 pA increments, were injected into SCs. The average spike frequency measured over the entire current pulse was used to construct current-frequency plots. Action potential properties (peak amplitude, after-hyperpolarisation amplitude and half-width) were evaluated with the use of the first action potential generated.

Extracellular Purkinje cell recordings in alert mice

The animals were prepared for chronic experiments under Isoflurane anesthesia (1.5 % in O_2) using procedures described previously (Hoebeek et al., 2005). In short, a dental acrylic (Simplex Rapid, Associate Dental Products, Swindon, UK) was implanted on the scull and a recording chamber was placed over a small hole (< 3 mm) in the occipital bone. During the experiments the animal was immobilized in a custom restrainer by bolting the head holder to a head fixation post. Extracellular activity was recorded with glass micropipettes that were advanced into the cerebellar cortex by a hydraulic microdrive (Trent Wells, TX, USA). The raw electrode signal was amplified, filtered, digitized and stored on disk for off-line analysis (Spike2, CED, Cambridge, UK). Single unit PC activity was identified by the presence of a brief pause in simple spike discharge after a complex spike and was carefully monitored during the course of a recording. Between recording sessions the brain was covered by ointment and the chamber was sealed using bone wax. Off-line analysis was performed in Matlab (Mathworks Inc., Natick, MA, USA). The simple spikes and complex spikes were detected and discriminated with custom software that clustered groups of spikes by means of a linear discriminant analysis on the first four principal components of the spike waveforms (Eggermont, 1990). Histograms of simple spikes triggered on the occurrence of a complex spike were made (bin width 1 ms) to verify that each isolated PC showed a clean climbing fibre pause (Simpson, 1996). Spontaneous activity of each PC was characterized by (1) the mean simple spike and complex spike firing rate; (2) the simple spike and complex spike coefficient of variance (standard deviation of interspike intervals (ISI)/ mean of ISI); (3) the climbing fibre pause duration(Goossens et al., 2001); (4) the coefficient of variation of adjacent intervals (CV2; mean value of $(2*(ISI_{n+1} - ISI_n))/(ISI_{n+1} + ISI_n)$)(Holt et al., 1996).

Compensatory eye movements

Mice were prepared for chronic, head-restrained recordings of compensatory eye movements as described previously (Wulff et al., 2009). In short, under isoflurane anaesthesia (~1.5% and O_2) a pedestal was constructed in parallel to the intracranial midline using Optibond prime and adhesive (Kerr, Bioggio, Switzerland) and Charisma (Haeraeus Kulzer, Armonk, NY, USA). After a recovery period (2-3 days) the mouse was restrained by means of the two nuts embedded in the pedestal. A cylindrical screen (diameter 63 cm) with a random-dotted pattern (each element 2°) surrounded the turntable (diameter 60 cm) on which the mouse was placed. Two table-fixed infrared emitters (maximum output 600 mW, dispersion

angle 7°, peak wavelength 880 nm) illuminated the eye during the recording, and a third emitter was connected to the camera and aligned horizontally with the camera's optical axis. This third emitter produced the tracked corneal reflection (CR). The eye movements were recorded using the eye-tracking device (ETL-200, ISCAN systems, Burlington, NA, USA). Calibrations were performed as described previously(Stahl et al., 2000). Gain and phase values of the eye movements were calculated using a custom-made Matlab routine (MathWorks Inc). Data were statistically analyzed using an ANOVA for repeated measures test.

Data analysis

All values are represented as mean ± s.e.m, P-values of < 0.05 were considered significant. Statistical analysis was done using Student's t-test, unless stated otherwise.

Supplementary references

Aller MI, Jones A, Merlo D, Paterlini M, Meyer AH, Amtmann U, Brickley S, Jolin HE, McKenzie AN, Monyer H, Farrant M, Wisden W (2003) Cerebellar granule cell Cre recombinase expression. Genesis 36:97-103.

Eggermont JJ (1990) The correlative brain : theory and experiment in neural interaction. Berlin Springer-Verlag.

Goossens J, Daniel H, Rancillac A, van der Steen J, Oberdick J, Crepel F, De Zeeuw CI, Frens MA (2001) Expression of protein kinase C inhibitor blocks cerebellar long-term depression without affecting Purkinje cell excitability in alert mice. J Neurosci 21:5813-5823.

Hoebeek FE, Stahl JS, van Alphen AM, Schonewille M, Luo C, Rutteman M, van den Maagdenberg AM, Molenaar PC, Goossens HH, Frens MA, De Zeeuw CI (2005) Increased noise level of purkinje cell activities minimizes impact of their modulation during sensorimotor control. Neuron 45:953-965.

Holt GR, Softky WR, Koch C, Douglas RJ (1996) Comparison of discharge variability in vitro and in vivo in cat visual cortex neurons. J Neurophysiol 75:1806-1814.

Isope P, Barbour B (2002) Properties of unitary granule cell-->Purkinje cell synapses in adult rat cerebellar slices. J Neurosci 22:9668-9678.

Lakso M, Pichel JG, Gorman JR, Sauer B, Okamoto Y, Lee E, Alt FW, Westphal H (1996) Efficient in vivo manipulation of mouse genomic sequences at the zygote stage. Proc Natl Acad Sci U S A 93:5860-5865.

Simpson JI, Wylie, D.R., and DeZeeuw, C.I. (1996) Climbing fiber signals and their consequences. In: Behavioral and brain sciences, pp 384-398. Cambridge, England: Cambridge University Press.

Stahl JS, van Alphen AM, De Zeeuw CI (2000) A comparison of video and magnetic search coil recordings of mouse eye movements. J Neurosci Methods 99:101-110.

Todorov B, van de Ven RC, Kaja S, Broos LA, Verbeek SJ, Plomp JJ, Ferrari MD, Frants RR, van den Maagdenberg AM (2006) Conditional inactivation of the *Cacna1a*

gene in transgenic mice. Genesis 44:589-594.
Wulff P, Schonewille M, Renzi M, Viltono L, Sassoe-Pognetto M, Badura A, Gao Z, Hoebeek FE, van Dorp S, Wisden W, Farrant M, De Zeeuw CI (2009) Synaptic inhibition of Purkinje cells mediates consolidation of vestibulo-cerebellar motor learning. Nat Neurosci 12:1042-1049.

Chapter 4

The role of synaptic plasticity at the PF-PC synapse in motor learning

Section 4.1

Re-evaluating the role of LTD in Cerebellar Motor Learning

Neuron 2011, 70, 43-50

Z. Gao, M. Schonewille, H.J. Boele, M.F. Vinueza Veloz, W.E. Amerika, A.A.M. Šimek, M.T. De Jeu, J.P. Steinberg, K. Takamiya, F.E. Hoebeek, D.J. Linden, R.L. Huganir, and C.I. De Zeeuw

Abstract

Long-term depression at parallel fiber-Purkinje cell synapses (PF-PC LTD) has been proposed to be required for cerebellar motor learning. To date, tests of this hypothesis have sought to interfere with receptors (mGluR1) and enzymes (PKC, PKG or CaMKII) necessary for induction of PF-PC LTD and then determine if cerebellar motor learning is impaired. Here, we tested three mutant mice that target the expression of PF-PC LTD by blocking internalization of AMPA receptors. Using three different cerebellar coordination tasks, adaptation of the vestibulo-ocular reflex, eyeblink conditioning, and locomotion learning on the Erasmus Ladder, we show that there is no motor learning impairment in these mutant mice that lack PF-PC LTD. These findings demonstrate that PF-PC LTD is not essential for cerebellar motor learning.

Introduction

Persistent use-dependent changes in synaptic function, including LTD and long-term potentiation (LTP), have been widely suggested to underlie learning. The theory of PF-PC LTD was originally based on models by Marr, later elaborated by Albus, which suggested that the cerebellar matrix consisting of the parallel fibers and orthogonally oriented climbing fibers is optimally designed for entraining and modifying Purkinje cell output (Marr, 1969; Albus, 1971). Recordings obtained by Ito and co-workers confirmed this concept by showing that combined activation of these two inputs resulted in a persistent depression of parallel fiber-evoked excitatory post-synaptic currents (EPSC) in Purkinje cells (Ito, 1982; Linden and Connor, 1995). Moreover, their findings indicated that *induction* of LTD during visuo-vestibular training could, in principle, persistently modify the gain and phase of the simple spike activity of the floccular Purkinje cells that drive the vestibulo-ocular reflex (VOR) (Nagao, 1989) (for underlying circuitry see Fig. 1A). The potential correlation between LTD *induction* and cerebellar motor learning was subsequently supported by series of studies in mouse mutants in which both processes were affected concomitantly (Aiba et al., 1994; Kim and Thompson, 1997; De Zeeuw et al., 1998; Feil et al., 2003; Koekkoek et al., 2003; Boyden et al., 2006; Hansel et al., 2006). For example, blockade of LTD *induction* by interfering with the mGluR1 / PKC, PKG or CaMKII pathways all resulted in impairment of VOR adaptation (Aiba et al., 1994; De Zeeuw et al., 1998; Feil et al., 2003; Hansel et al., 2006). Still, these studies were not conclusive as pharmacological blocking of LTD did not affect eyeblink conditioning (Welsh et al., 2005) and training without instructive signals from the climbing fibers partially allowed VOR adaptation (Ke et al., 2009). In principle the positive correlations found in the mouse mutants inwhich *induction* of LTD was affected could be attributed to the fact that the affected receptors and kinases mediate upstream signaling in a highly divergent fashion. Each kinase has many substrates, most of which are not involved in PF-PC LTD and could affect both baseline function of the cerebellar network and other forms of synaptic and non-synaptic plasticity in the cerebellum (Kano et al., 1996; Chen and Tonegawa, 1997; Hansel et al., 2006).

Here we investigated the role of PF-PC LTD in cerebellar motor learning by test-

ing three different mutant mice in which blockade of PF-PC LTD *expression* is achieved by targeting late events in the LTD signaling cascade, i.e. downstream at the level of the glutamate receptors and the related proteins that control their trafficking (Steinberg et al., 2006). The mutants are the PICK1 knockout (KO) mouse, the GluR2Δ7 knockin (KI) mouse, and the GluR2K882A KI mouse (Fig. 1A). The homozygous PICK1 KO mouse lacks PICK1, an essential intermediary between PKC activation and internalization of the AMPA receptor (Xia et al., 2000). The GluR2Δ7 KI mouse lacks the last seven amino acids of the carboxyl-terminal tail; this mutation eliminates the C-terminal type II PDZ ligand and disrupts the interaction of GluR2 with PICK1 and GRIP1/2 (Xia et al., 2000; Steinberg et al., 2006). Finally, and most specifically, the GluR2K882A KI mouse contains a mutated form of GluR2, which incorporates a single lysine mutation in the consensus recognition motif for PKC (S/T-X-K/R) and thereby prevents phosphorylation at S880 by PKC and internalization of the AMPA receptor while leaving the PDZ ligand and phosphorylation by other kinases functionally intact (Kemp and Pearson, 1990; Wang and Linden, 2000; Xia et al., 2000; Chung et al., 2003; Steinberg et al., 2006). Thus all three types of mutant mice lack *expression* of cerebellar LTD, while their upstream *induction* pathways are not directly affected (Steinberg et al., 2006). All three types of mutant mice were subjected to VOR adaptation, eyeblink conditioning, and locomotion learning on the Erasmus Ladder so as to cover a wide range of cerebellar learning behaviors (De Zeeuw et al., 1998; Koekkoek et al., 2003; Van Der Giessen et al., 2008).

Results

To determine whether the LTD-*expression*-deficient mutants are suitable for detecting specific phenotypes in vestibulo-cerebellar learning, we first ascertained whether they had gross deficits in their basic motor performance (Fig. 1B). Basic eye movement tests showed that both amplitude (gain) and timing (phase) of the optokinetic reflex (OKR), VOR in the dark, and visual VOR (VVOR) in the mutants were not significantly different from those in their wild type littermates, over a range of stimulus frequencies varying from 0.2 Hz to 1.0 Hz ($p > 0.4$ for all values; ANOVA for repeated measures; for n and p-values, see Tables S1, 2). These data were comparable to those obtained in the mutant mice in which the *induction* of LTD was impaired by blocking or deleting one of the kinases PKC, PKG or αCamKII (De Zeeuw et al., 1998; Feil et al., 2003; Hansel et al., 2006). Subsequently, we subjected the PICK1 KO, GluR2Δ7 KI, and GluR2K882A KI mice to various short-term adaptation tests including VOR gain-up and VOR gain-down training as well as OKR gain-up training (Fig. 1C). After being exposed for 50 min to different forms of visuo-vestibular training all mutants showed significant adaptation for all three protocols ($p < 0.005$ for all protocols, paired Student's t-test) and none of the mutants showed any sign of impairment compared to the adaptation levels in wild types ($p > 0.5$ for all parameters, ANOVA for repeated measures; for numerical details, see Tables S1 and S2). The outcomes of these tests stand in marked contrast to those of the LTD-*induction*-deficient kinase mutants (De Zeeuw et al., 1998; Feil et al., 2003; Boyden et al., 2006; Hansel et al., 2006), in which clear deficits of motor learning are found.

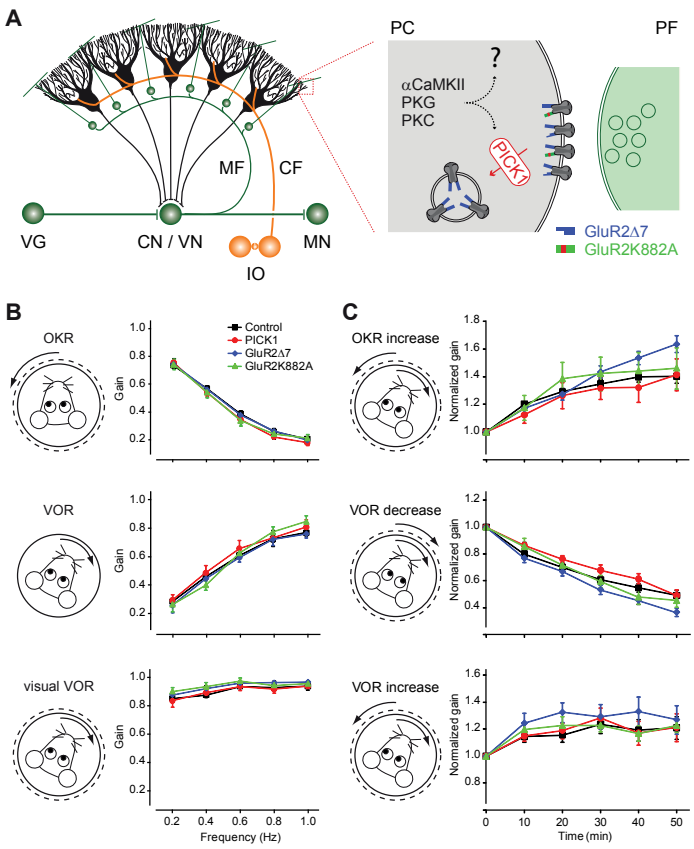

Figure 1 Cerebellar circuitry, basic motor performance and short-term motor learning. (A) The vestibulocerebellum receives excitatory input from the inferior olive (IO, orange) and vestibular ganglion cells (VG, green) and sends an inhibitory projection (black) back to the cerebellar and vestibular nuclei (CN/VN), and from there onwards to motor nuclei (MN). According to the Marr-Albus-Ito hypothesis the climbing fibers (CF) originating in the IO carry the error signal and the mossy fiber – parallel fiber system (MF-PF) relays motor activity signals. Inset shows how, after concomitant activity in CF and PF, AMPA receptors are internalized through interaction of PICK1 (red) with the C-terminal region of AMPA-type glutamate receptor subunit GluR2 (dark grey) resulting in long-term depression of the PF to Purkinje cell synapse (PF-PC LTD). In the mutant mice used herein, PF-PC LTD *expression* is blocked either by deletion of PICK1, a knockin in which GluR2 is replaced with a truncated form involving deletion of the last seven amino acids of GluR2 (GluRΔ7; blue), or a knockin harboring a point mutation in the PKC recognition motif of GluR2 (GluR2K882A; green). (B), Gain values of the PICK1 KO, GluRΔ7 KI, and GluR2K882A KI mutants during the optokinetic reflex (OKR), vestibulo-ocular reflex in the dark (VOR), and vestibulo-ocular reflex in the light (VVOR) are not significantly different from those of wild type controls (black). (C), Short-term visuo-vestibular, out-of-phase mismatch training resulted in significant ($p < 0.005$ for all groups) gain increases of PICK1 KO, GluRΔ7 KI, and GluR2K882A KI mutants during the OKR (top panel) and VOR (bottom panel). Short-term visuo-vestibular, in-phase mismatch training resulted in significant ($p < 0.001$ for all groups) gain decreases of PICK1 KO, GluRΔ7 KI, and GluR2K882A KI mutants during the VOR (middle panel). All these changes were not significantly different from those of wild type controls. For clarity of presentation the wild types are presented as a pooled group. For number of mice per group, see Table S1. The p-values for individual mutants versus all controls and versus littermates are listed in Table S2. Error bars denote SEM.

In theory, differences among the PICK1 KO, GluR2Δ7 KI, and GluR2K882A KI mutants and their wild type littermates could become apparent when they are subjected to a longer, more robust training paradigm (see also Blazquez et al., 2004; De Zeeuw and Yeo, 2005). To address this point, we also employed a six-day in-phase visuo-vestibular training paradigm, which results in very prominent gain and phase learning changes in wild types (Wulff et al., 2009), but less so in the LTD-*induction*-deficient kinase mutants (e.g. Van Alphen and De Zeeuw, 2002). With this long-term training, both VOR gain and VOR phase values of all PICK1 KO, GluRΔ7 KI, and GluR2K882A KI mutants are also adapted significantly ($p < 0.001$ for all mutants; ANOVA for repeated measures) and this form of adaptation also occurred at levels that were comparable to those of their wild type littermates ($p > 0.4$ for all comparisons; ANOVA; Fig. 2A).

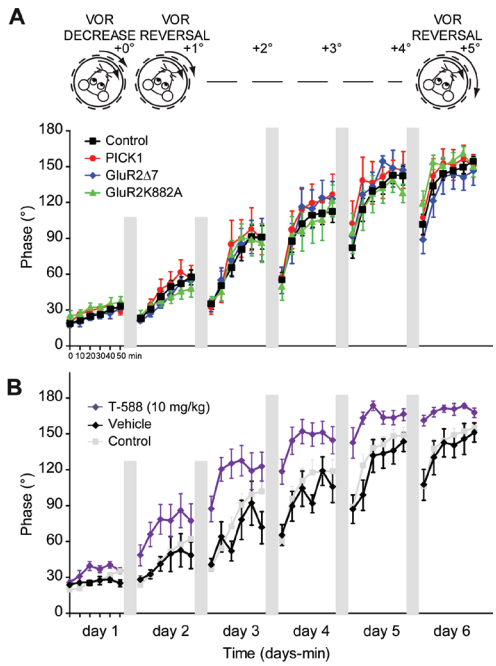

Figure 2 | Long-term VOR phase adaptation is normal. (A), Long-term visuo-vestibular in-phase mismatch training resulted in phase reversals of PICK1 KO (red), GluRΔ7 KI (blue), and GluR2K882A KI (green) mutants during the vestibulo-ocular reflex (VOR), but these reversals were not significantly different from those of wild type controls (black). For clarity of presentation the wild types are presented as a pooled group. Number of mice per group is listed in Suppl. Table S1, p-values in Suppl. Table S2. (B), VOR phase reversal in C57BL/6 mice injected with T-588 (purple, 10 mg/kg, i.p.) and subjected to the same visuo-vestibular mismatch training paradigm was significantly faster ($p < 0.003$ for day 3 to 5) compared to that of C57BL/6 mice injected with vehicle (black). Data from wild type control mice without injection (grey) are added for comparison. Error bars denote SEM.

One could argue that the PICK1 KO, GluRΔ7 KI, and GluR2K882A KI mice had sufficient time to develop compensatory mechanisms that bypass the requirement for LTD. To test this, we injected C57Bl/6 wild type mice with T-588 (10 mg/kg i.p.), a cognitive enhancer, shown to block LTD both *in vitro* and *in vivo* (Kimura et al., 2005; Welsh et al., 2005). In line with the data obtained in the PICK1 KO, GluRΔ7 KI, and GluR2K882A KI mice, the learning behavior was not impaired following injections with T-588. In fact, surprisingly, the injections resulted in a faster VOR phase reversal ($p < 0.003$ on days 3, 4 and 5; ANOVA for repeated measures; Fig. 2B) and higher gain values on day 6 ($p < 0.001$; ANOVA for repeated measures; data not shown). Thus, when we blocked LTD either chemically or by genetically targeting the late events in its signaling cascade, deficits in cerebellar motor learning could not be observed following three different types of short-term, visuo-vestibular training or an extremely strong and sensitive form of long-term, visuo-vestibular training.

To find out whether the absence of a phenotype in the LTD-*expression*-deficient mutants is specific for the vestibulo-cerebellum, or whether it can be extrapolated to other parts of the cerebellum, we subjected them to eyeblink conditioning tests using a tone and an airpuff as the conditioned and unconditioned stimulus, respectively. Eyeblink conditioning has previously been demonstrated to require mGluR1 (Aiba et al., 1994; Kishimoto et al., 2002) and PKC (Koekkoek et al, 2003), which are both necessary for the *induction* of LTD. Similar to that in controls, the percentage of conditioned responses (CRs) in the PICK1 KO, GluRΔ7 KI, and GluR2K882A KI mice increased significantly (all $p < 0.05$; t-test, between animals $p > 0.2$; ANOVA for repeated measures) (Fig. 3A; Table S1, 2). In addition, the timing and amplitude of the CRs in the PICK1 KO, GluRΔ7 KI and GluR2K882A KI mutants were indistinguishable from those in control mice (Fig. 3C; Table S1, 2). Moreover, the kinetics of the unconditioned eyelid responses in all three types of mutants did not differ significantly from control mice, suggesting that the performances of their eyelid responses were also normal (Fig. 3B). Subsequently, we subjected the LTD-*expression*-

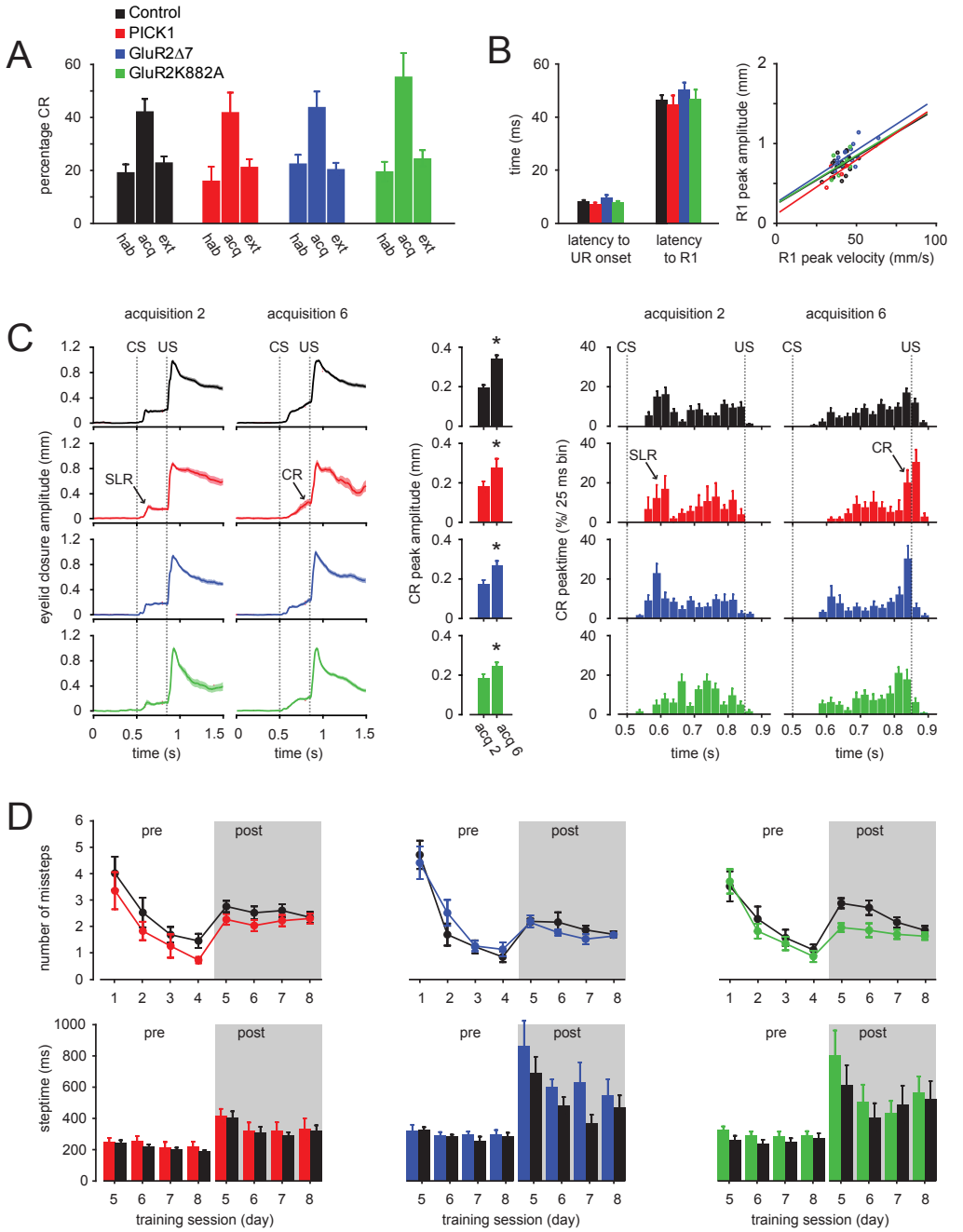

Figure 3 | Eyeblink conditioning and locomotion conditioning are not impaired. (A), Eyeblink conditioning increased the percentage of conditioned responses (CRs) significantly (all $p < 0.05$; habituation session vs. acquisition session 6) in PICK1 KO, GluRΔ7 KI, and GluR2K882A KI mutants as well as their littermate controls. (B), Kinetics of unconditioned responses (URs) are unaffected in all groups. Latency to UR onset, R1 during unconditioned stimulus only trials, and R1 peak amplitude vs. UR peak velocity (right) also did not differ between PICK1 KO, GluRΔ7 KI, GluR2K882A KI, and control mice. Each dot represents the mean value of one animal. (C), Amplitude (left three panels) and timing (right two panels) of CRs are normal in all three mutant mice compared to control mice. Left two panels, means of all eyeblink CR raw data traces for each group

in paired trials during training sessions 2 and 6. Middle panel, averaged CR amplitude for sessions 2 and 6. Right two panels, mean percentage of CR peak times (25 ms bin) for each group during training session 2 and 6. At the end of the training (session 6) in all groups the majority of CR peak times are clustered around US onset at 850 ms. Short-latency responses (SLRs), which occur frequently during mouse eyeblink conditioning, are indicated. CS onset is set at 500 ms, US onset at 850 ms, ISI = 350 ms, US duration = 30 ms. (D), Analysis of locomotion conditioning on the Erasmus Ladder revealed no significant differences in number of missteps and steptime between mutant and control mice. Both motor performance values (left panels without background) and motor learning values (right panels with gray transparent background) were not affected. During locomotion conditioning the US, i.e. a rising rung, occurs 250 ms after the onset of the conditioned stimulus (a 15 kHz tone). All mutants show an acquired change in steptime after (post) the conditioning stimulus compared to before (pre). This change is not different from that seen in littermate controls (Table S2). For number of mice per group, see Table S1. The p-values for individual mutants versus all controls and versus littermates are listed in Table S2. Error bars denote SEM.

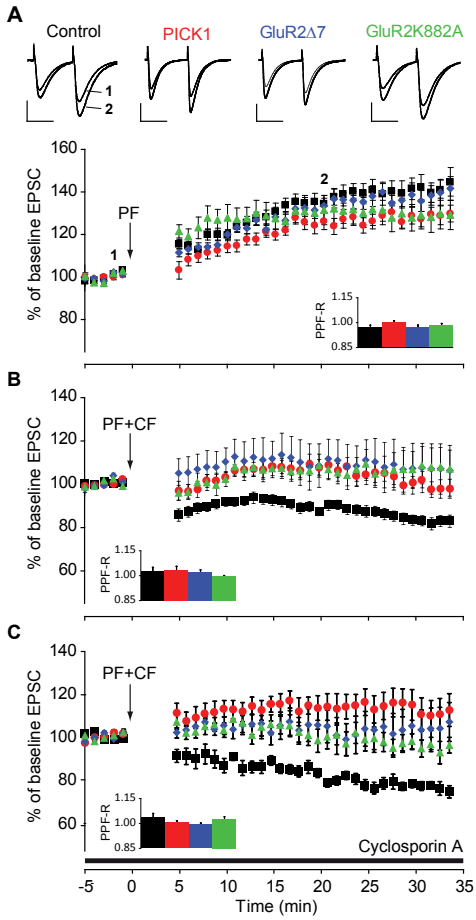

Figure 4 | Postsynaptic LTP is normal, whereas postsynaptic LTD is blocked. (A), EPSC amplitudes were significantly ($p < 0.005$ for all groups) increased following LTP induction (arrow) in PICK1 KO (red), GluRΔ7KI (blue), and GluR2K882A KI (green) mutants, but these increases were not significantly different from those in controls (black). (B), LTD induction in slices of 3 to 6 month old PICK1 KO, GluRΔ7 KI, and GluR2K882A KI mutants was significantly impaired compared to that of controls. (C), Even after application of the LTP blocker cyclosporin A, LTD induction did not occur in the mutants. Insets show that the ratio of paired pulse facilitation after induction of plasticity to that before induction (PPF-R) did not change in control, PICK KO, GluRΔ7 KI, and GluR2K882A KI mice, suggesting that plasticity occurred postsynaptically. For clarity of presentation the wild types are presented as a pooled group. Number of mice per group is listed in Table S1, p-values in Table S2. Scale bars: horizontal 30 ms, vertical 100 pA. Error bars denote SEM.

deficient mutants to locomotion conditioning tests on the Erasmus Ladder using a tone and a rising rung as the conditioned and unconditioned stimulus, respectively. Conditioning on the Erasmus Ladder has previously been demonstrated to require intact inferior olivary neurons and Purkinje cells (Van Der Giessen et al., 2008; Renier et al., 2010), the climbing fiber activity of which facilitates the *induction* of LTD (Marr, 1969; Albus, 1971). The PICK1 KO, GluR2Δ7 KI and GluR2K882A KI mutants demonstrated a normal basic performance in locomotion in that their baseline steptime and number of missteps were not significantly different from those in controls (Fig. 3D, pre panels, indicating pre-training; Table S1, 2). The introduction of a perturbation, preceded by a 15 kHz tone at a fixed time interval so as to condition their locomotion pattern, caused a significant increase in steptime in all groups (all $p < 0.01$, t-test; Fig. 3D, post panels (indicating post-training)). In all three types of mutants these changes were not significantly different from those in their controls (all $p > 0.14$, t-test; Table S1, 2).

Together, these data argue against the Marr-Albus-Ito hypothesis, which predicts

that PF-PC LTD is essential for cerebellar motor learning. However, certain questions must be addressed. First, do the PICK1 KO, GluRΔ7 KI, and GluR2K882A KI mutants show compensations that may rescue the behavioral phenotype even with LTD impaired? For example, changes in PF-PC LTP induction might partially compensate for impaired LTD induction (Lev-Ram et al., 2003; Coesmans et al., 2004; Schonewille et al., 2010). To address this possibility we investigated induction of postsynaptic LTP at the parallel fiber to Purkinje cell synapse in slices derived from mutant mice (Fig. 4A). No significant difference in LTP ($p > 0.2$; ANOVA for repeated measures) was found among the PICK1 KO, GluRΔ7 KI, and GluR2K882A KI mutants and wild type littermates. This suggests that the blockade of PF-PC LTD induction is not compensated by alterations in postsynaptic PF-PC LTP. Second, is LTD impaired in *adult* PICK1 KO, GluRΔ7 KI, and GluR2K882A KI mutants? To date, impaired LTD has only been shown in *young* PICK1 KO, GluRΔ7 KI, and GluR2K882A KI mutants (Steinberg et al., 2006), while all the behavioral experiments described herein have been performed in adults. We therefore assessed LTD in slices of 3 to 6 months old PICK1 KO, GluR2Δ7 KI, and GluR2K882A KI mutants. In these older mutants too, LTD was impaired compared to that of controls ($p < 0.04$ for all comparisons; ANOVA for repeated measures) (Fig. 4B; Table S2). Even when we repeated the LTD protocol in the presence of the postsynaptic LTP-blocker cyclosporin A, a calcineurin inhibitor (Belmeguenai and Hansel, 2005), LTD was not revealed ($p < 0.05$ for all comparisons; ANOVA for repeated measures) (Fig. 4C). Third, is there presynaptic compensation? Paired pulse facilitation was not affected in the mutant mice (data not shown; all $p > 0.10$; one-way ANOVA), arguing against compensation for the deletion through major presynaptic changes. The ratio of paired pulse facilitation before against after induction (PPF-R) did not differ significantly from 1 in any of the induction paradigms (all $p > 0.05$; One-Sample t-test), affirming the postsynaptic nature of the types of plasticity tested here. Finally, is LTD induction only required during motor learning in younger animals, while adult ones might depend on other forms of plasticity? To address this concern, we performed the same VOR and OKR adaptation tests in 4 to 6 weeks old mice. Similar to adults, these animals did not show any deficit in their motor learning capabilities ($p > 0.7$ for all comparisons) (Suppl. Fig. S1).

Discussion

Against our expectations, we did not find any deficit in various forms of cerebellar motor learning when we tested three different types of mutant mice that lack *expression* of cerebellar LTD. Together, these data argue against an essential role for LTD in cerebellar motor learning. Still, despite the absence of a compensatory change in PF-PC LTP induction or presynaptic PF plasticity, we cannot exclude the development of other compensatory mechanisms that might contribute to cerebellar motor learning in the three types of LTD-*expression*-deficient mutants tested here. These compensations could take the form of changes in basal electrophysiological function or use-dependent neuronal plasticity, or both. Perhaps, the cerebellar Purkinje cells and/or the neurons that feed into them are sufficiently enriched with various forms of plasticity such that deletion of PF-PC LTD alone

does not result in a behavioral deficit (Salin et al., 1996; D'Angelo et al., 1999; Jorntell and Ekerot, 2003). If the compensatory mechanisms indeed play a role, they may in fact operate rather fast, because even application of T-588, which blocks LTD by acutely reducing calcium release from intracellular stores, does not lead to deficits in cerebellar motor learning (current study; Welsh et al., 2005). However, the potential occurrence of compensatory mechanisms does not undermine the conclusion that the data presented here challenge the classical Marr-Albus-Ito hypothesis, because the ability to adjust the parallel fiber input to Purkinje cells was proposed to be the fundamental and essential requirement for motor learning (Marr, 1969; Albus, 1971). Our data demonstrate that motor learning can occur completely normally in the absence of PF-PC LTD, or at least in the absence of the form of PF-PC LTD that has been investigated intensely with a wide range of stimulus protocols over the past decades (Ito, 1982; Linden and Connor, 1995; De Zeeuw et al., 1998; Hansel et al., 2006).

Why can the general impairments in cerebellar motor learning that occur in the PKC, PKG and CaMKII mutants (De Zeeuw et al., 1998; Feil et al., 2003; Boyden et al., 2006; Hansel et al., 2006) not be compensated for? In these kinase mutants the blockades may, in contrast to those in the PICK1 KO, GluRΔ7 KI and GluR2K882A KI mutants, not only affect LTD at their parallel fiber synapses, but also other forms of cerebellar plasticity. For example, inhibition of PKC may affect the efficacy of GABA receptors at the molecular layer interneuron to Purkinje cell synapse by influencing their surface density and sensitivity to positive allosteric modulators and/or by modifying chloride conductance (Song and Messing, 2005), while inhibition of CaMKII may directly affect LTP at these GABAergic inputs (Kano et al., 1996). Interestingly, both plasticity at the parallel fiber to molecular layer interneuron synapse ánd that at the molecular layer interneuron to Purkinje cell synapse have, just like PF-PC LTD, been reported to depend on climbing fiber activity (Jörntell et al., 2010). Indeed, recent evidence demonstrates that loss of instructive climbing fiber signals results in impaired VOR adaptation (Ke et al., 2009), supporting the possibility that climbing fibers may play an important role here. Thus this disynaptic plasticity in the feed-forward inhibition onto Purkinje cells provides a possible answer to the emerging question what the role of the climbing fibers might be when climbing fiber induced PF-PC LTD is not essential. Similarly, Purkinje cells also display intrinsic plasticity (Belmeguenai et al., 2010), and protein kinases may well be required for persistent use-dependent modulation of one or more of the ion channels involved. Finally, the kinases might also play a role in presynaptic plasticity at the Purkinje cell to cerebellar nuclei neuron synapse (Pedroarena and Schwarz, 2003) and/or postsynaptic plasticity at the mossy fiber or climbing fiber collateral to cerebellar nuclei neuron synapse (Zhang and Linden, 2006; Pugh and Raman, 2008). Thus, combined deficits in plasticity at the parallel fiber to Purkinje cell synapse, the molecular layer interneuron to Purkinje cell synapse, the Purkinje cell to cerebellar nuclei neuron synapse, the collateral to cerebellar nuclei neuron synapse and/or in intrinsic plasticity of Purkinje cells provide interesting alternative explanations for the behavioral phenotypes observed in the Purkinje cell-specific PKC, PKG and CaMKII mutants (De Zeeuw et al., 1998; Feil et al., 2003; Hansel et al., 2006).

The mutations in the PICK1 KO, GluRΔ7 KI, and GluR2K882A KI mutants were

global, i.e. not cell-specific. Thus, it was remarkable that both cerebellar motor performance and motor learning were normal, despite the fact that the mutations affect multiple cell types in both the cerebellum and its supportive systems. The global character of the mutations even further strengthens the implications of the general absence of a necessary and sufficient correlation between our cell physiological and behavioral findings. One would expect more deficits in general, and it raises the possibility that the affected protein and receptors as well as the correlated cell physiological deficit in LTD can be readily compensated for in general. The same argument may hold for the specific concept that was put forward by the Marr-Albus-Ito hypothesis, i.e. the idea that climbing fiber activity during motor learning weakens the parallel fiber influence onto Purkinje cells and thereby reduces their output. As explained above, there may be different climbing fiber - driven mechanisms in place that can act simultaneously under normal conditions and that can compensate for each other's absence in particular mutant mice. For example, the climbing fibers might be able to both depress the parallel fiber to Purkinje cell synapse and potentiate the molecular layer interneuron to Purkinje cell synapse (Jörntell et al., 2010), which both could ultimately lead to a depression of Purkinje cell's simple spike activity. Thus, in principle a climbing fiber - driven reduction in simple spikes may still occur during learning in the PICK1 KO, GluRΔ7 KI, and GluR2K882A KI mutants, despite a blockade of LTD at the parallel fiber to Purkinje cell synapse. Such a combined action of different mechanisms might also explain why blocking the GABAergic input from the molecular layer interneurons onto the Purkinje cells still allows a substantial level of motor learning (Wulff et al., 2009); i.e. in that case PF-PC LTD may be enhanced to compensate. It might thus be useful to use the current LTD-*expression*-deficient mice in combination with others to identify the combination of plasticities that may be essential for cerebellar motor learning.

Experimental procedures

All experiments were conducted in accordance with The Dutch Ethical Committee for animal experiments.

Eye movement recordings. Mice aged 4-6 (young) or 12-30 (adult) wks were prepared for experiments under isoflurane anesthesia by placing a construct allowing immobilization on their skull. After 5 days of recovery mice were placed in a restrainer, which was fixed onto the centre of the turntable that was surrounded by a cylindrical screen. Baseline OKR and (V)VOR were evoked by rotating the screen and turntable, respectively. Short-term adaptation was evoked by drum and table rotation out-of-phase or in-phase with an amplitude of 5° at 0.6 Hz for 5 x 10 min. Long-term adaptation was induced by in-phase training with equal amplitude on day 1 (5° at 0.6 Hz, 5 x 10 min) and drum amplitude increasing by 1° each subsequent day. Gain (eye velocity / stimulus velocity) and phase (eye to stimulus in degrees) values were calculated offline. Chemical block of LTD was induced by intraperitoneal injections of 10.0 mg/kg T-588 (provided by Toyama, Japan), dissolved in sterile saline (1.0 mg/ml), heated to ~37° and injected 30 min prior to start of the experiment.

Eyeblink conditioning. Mice, aged 12-30 wks, were anesthetized, surgically prepared and investigated with the use of MDMT as described before (Koekkoek et al., 2003) (Neuras-

mus B.V., www.neurasmus.com). After a recovery period of 4 days mice were subjected to 2 habituation sessions, 6 training sessions, and 4 extinction sessions A training sessions consisted of 8 blocks, each consisting of 6 paired trials, 1 US only trail, and 1 CS only trial. For the US we used a mild corneal air puff (30 ms) and for the CS an auditory tone (inter stimulus interval 350 ms, CS and US co-terminate). Eyelid responses in paired trials were categorized into auditory startle response (latency to peak 5-50 ms), short-latency responses (latency to onset 50-70 ms and latency to peak ~115ms) or cerebellar conditioned responses (latency to onset 50-350 ms and latency to peak 360 ms). For CS only trials we used the same values, except that the latency to peak amplitude of the CR was smaller than 400 ms instead of 360 ms.

The Erasmus Ladder. Mice, aged 12-30 wks, were subjected to the Erasmus Ladder (Neurasmus B.V., www.neurasmus.com), which consists of two single opening black boxes and equipped with a bright white light. These shelters are connected by a ladder consisting of 37 double rungs placed 15 mm apart, with one in a descended position, alternating between left and right side, so as to create an alternating stepping pattern with 30 mm gaps. Mice were subjected to 4 motor performance sessions followed by 4 associative motor learning sessions, each consisting of 72 trials. On days 5-8, mice were trained to avoid an obstacle by presenting a tone (90 dB, 15 Hz tone; CS) 285 ms before a rung rises (12 mm; US) in the swing phase of their right paw. Steptime is defined as the time needed to place one of the front paws from one rung to the other; and missteps as the number of touches on the descended rungs. A decrease in post steptime (steptime directly after the CS) over the sessions, implying that mice learn to adjust their stepping pattern to the obstacle, is taken as a measure of associative motor learning.

Cell physiological recordings. Patch clamp experiments were performed as recently published (Schonewille et al., 2010). In short, sagittal slices of the cerebellar vermis (250 µm) from adult mice were made in ice-cold oxygenated 'slicing' solution containing (in mM): 2.5 KCl, 1 $CaCl_2$, 3 $MgCl_2$, 25 $NaHCO_3$, 1.25 NaH_2PO_4, 240 sucrose, and 25 D-glucose. Slices were kept at room temperature (23 ± 1°C) in oxygenated ACSF containing (in mM): 124 NaCl, 5 KCl, 1.25 Na_2HPO_4, 2 $MgSO_4$, 2 $CaCl_2$, 26 $NaHCO_3$, 20 D-glucose and 100 µM picrotoxin. Cyclosporin A (bath applied, 5 µM in 0.5% EtOH) was added where indicated. Whole-cell patch-clamp recordings were performed using an EPC-10 amplifier (HEKA, Lambrecht) and patch pipettes filled with (in mM): 120 K-Gluconate, 9 KCl, 10 KOH, 3.48 $MgCl_2$, 4 NaCl, 10 HEPES, 4 Na_2ATP, 0.4 Na_3GTP and 17.5 sucrose (at pH 7.25). PF-PC LTD was induced by pairing PF and CF stimulation at 1 Hz for 5 min and PF-PC LTP was induced by PF stimulation alone at 1 Hz for 5 min. Test responses (2 pulses of 500 µs (LTP) or 700 µs (LTD) at 50 ms interval) were evoked every 20 s in voltage clamp mode to prevent spontaneous spiking. In all experiments, cells were switched to current-clamp mode for tetanization.

Data analysis. All values are shown as mean ± SEM. All p-values were determined for mutants against pooled (values used here) and mutant-specific controls (see Table S2), using two-tailed Student's t-test, one-way ANOVA or ANOVA for repeated measures with a posthoc Tukey test to determine significance between the groups. A p-value < 0.05 was

considered statistically significant.

References

Aiba A, Kano M, Chen C, Stanton ME, Fox GD, Herrup K, Zwingman TA, Tonegawa S (1994) Deficient cerebellar long-term depression and impaired motor learning in mGluR1 mutant mice. Cell 79:377-388.

Albus JS (1971) A theory of cerebellar function. Math Biosci 10:25-61.

Belmeguenai A, Hansel C (2005) A role for protein phosphatases 1, 2A, and 2B in cerebellar long-term potentiation. J Neurosci 25:10768-10772.

Belmeguenai A, Hosy E, Bengtsson F, De Zeeuw CI, Pedroarena C, Jorntell H, Hansel C (2010) Intrinsic plasticity as a negative regulator of synaptic gain in cerebellar Purkinje cells. J Neurosci:In press.

Blazquez PM, Hirata Y, Highstein SM (2004) The vestibulo-ocular reflex as a model system for motor learning: what is the role of the cerebellum? Cerebellum 3:188-192.

Boyden ES, Katoh A, Pyle JL, Chatila TA, Tsien RW, Raymond JL (2006) Selective engagement of plasticity mechanisms for motor memory storage. Neuron 51:823-834.

Chen C, Tonegawa S (1997) Molecular genetic analysis of synaptic plasticity, activity-dependent neural development, learning, and memory in the mammalian brain. Annu Rev Neurosci 20:157-184.

Chung HJ, Steinberg JP, Huganir RL, Linden DJ (2003) Requirement of AMPA receptor GluR2 phosphorylation for cerebellar long-term depression. Science 300:1751-1755.

Coesmans M, Weber JT, De Zeeuw CI, Hansel C (2004) Bidirectional parallel fiber plasticity in the cerebellum under climbing fiber control. Neuron 44:691-700.

D'Angelo E, Rossi P, Armano S, Taglietti V (1999) Evidence for NMDA and mGlu receptor-dependent long-term potentiation of mossy fiber-granule cell transmission in rat cerebellum. J Neurophysiol 81:277-287.

De Zeeuw CI, Yeo CH (2005) Time and tide in cerebellar memory formation. Curr Opin Neurobiol 15:667-674.

De Zeeuw CI, Hansel C, Bian F, Koekkoek SK, van Alphen AM, Linden DJ, Oberdick J (1998) Expression of a protein kinase C inhibitor in Purkinje cells blocks cerebellar LTD and adaptation of the vestibulo-ocular reflex. Neuron 20:495-508.

Feil R, Hartmann J, Luo C, Wolfsgruber W, Schilling K, Feil S, Barski JJ, Meyer M, Konnerth A, De Zeeuw CI, Hofmann F (2003) Impairment of LTD and cerebellar learning by Purkinje cell-specific ablation of cGMP-dependent protein kinase I. J Cell Biol 163:295-302.

Hansel C, de Jeu M, Belmeguenai A, Houtman SH, Buitendijk GH, Andreev D, De Zeeuw CI, Elgersma Y (2006) alphaCaMKII Is essential for cerebellar LTD and motor learning. Neuron 51:835-843.

Ito M (1982) Cerebellar control of the vestibulo-ocular reflex--around the flocculus hypothesis. Annu Rev Neurosci 5:275-296.

Jorntell H, Ekerot CF (2003) Receptive field plasticity profoundly alters the cutaneous

parallel fiber synaptic input to cerebellar interneurons in vivo. J Neurosci 23:9620-9631.

Kano M, Kano M, Fukunaga K, Konnerth A (1996) Ca(2+)-induced rebound potentiation of gamma-aminobutyric acid-mediated currents requires activation of Ca2+/calmodulin-dependent kinase II. Proc Natl Acad Sci U S A 93:13351-13356.

Ke MC, Guo CC, Raymond JL (2009) Elimination of climbing fiber instructive signals during motor learning. Nat Neurosci 12:1171-1179.

Kemp BE, Pearson RB (1990) Protein kinase recognition sequence motifs. Trends in biochemical sciences 15:342-346.

Kim JJ, Thompson RF (1997) Cerebellar circuits and synaptic mechanisms involved in classical eyeblink conditioning. Trends Neurosci 20:177-181.

Kimura T, Sugimori M, Llinas RR (2005) Purkinje cell long-term depression is prevented by T-588, a neuroprotective compound that reduces cytosolic calcium release from intracellular stores. Proc Natl Acad Sci U S A 102:17160-17165.

Koekkoek SK, Hulscher HC, Dortland BR, Hensbroek RA, Elgersma Y, Ruigrok TJ, De Zeeuw CI (2003) Cerebellar LTD and learning-dependent timing of conditioned eyelid responses. Science 301:1736-1739.

Lev-Ram V, Mehta SB, Kleinfeld D, Tsien RY (2003) Reversing cerebellar long-term depression. Proc Natl Acad Sci U S A 100:15989-15993.

Linden DJ, Connor JA (1995) Long-term synaptic depression. Annu Rev Neurosci 18:319-357.

Marr D (1969) A theory of cerebellar cortex. J Physiol 202:437-470.

Nagao S (1989) Behavior of floccular Purkinje cells correlated with adaptation of vestibulo-ocular reflex in pigmented rabbits. Exp Brain Res 77:531-540.

Pugh JR, Raman IM (2008) Mechanisms of potentiation of mossy fiber EPSCs in the cerebellar nuclei by coincident synaptic excitation and inhibition. J Neurosci 28:10549-10560.

Salin PA, Malenka RC, Nicoll RA (1996) Cyclic AMP mediates a presynaptic form of LTP at cerebellar parallel fiber synapses. Neuron 16:797-803.

Schonewille M, Belmeguenai A, Koekkoek SK, Houtman SH, Boele HJ, van Beugen BJ, Gao Z, Badura A, Ohtsuki G, Amerika WE, Hosy E, Hoebeek FE, Elgersma Y, Hansel C, De Zeeuw CI (2010) Purkinje cell-specific knockout of the protein phosphatase PP2B impairs potentiation and cerebellar motor learning. Neuron 67:618-628.

Song M, Messing RO (2005) Protein kinase C regulation of GABAA receptors. Cell Mol Life Sci 62:119-127.

Steinberg JP, Takamiya K, Shen Y, Xia J, Rubio ME, Yu S, Jin W, Thomas GM, Linden DJ, Huganir RL (2006) Targeted in vivo mutations of the AMPA receptor subunit GluR2 and its interacting protein PICK1 eliminate cerebellar long-term depression. Neuron 49:845-860.

Van Alphen AM, De Zeeuw CI (2002) Cerebellar LTD facilitates but is not essential for long-term adaptation of the vestibulo-ocular reflex. Eur J Neurosci 16:486-490.

Wang YT, Linden DJ (2000) Expression of cerebellar long-term depression requires postsynaptic clathrin-mediated endocytosis. Neuron 25:635-647.

Welsh JP, Yamaguchi H, Zeng XH, Kojo M, Nakada Y, Takagi A, Sugimori M, Llinas RR (2005) Normal motor learning during pharmacological prevention of Purkinje cell long-term depression. Proc Natl Acad Sci U S A 102:17166-17171.

Wulff P, Schonewille M, Renzi M, Viltono L, Sassoe-Pognetto M, Badura A, Gao Z, Hoebeek FE, van Dorp S, Wisden W, Farrant M, De Zeeuw CI (2009) Synaptic inhibition of Purkinje cells mediates consolidation of vestibulo-cerebellar motor learning. Nat Neurosci.

Xia J, Chung HJ, Wihler C, Huganir RL, Linden DJ (2000) Cerebellar long-term depression requires PKC-regulated interactions between GluR2/3 and PDZ domain-containing proteins. Neuron 28:499-510.

Zhang W, Linden DJ (2006) Long-term depression at the mossy fiber-deep cerebellar nucleus synapse. J Neurosci 26:6935-6944.

Supplementary Materials

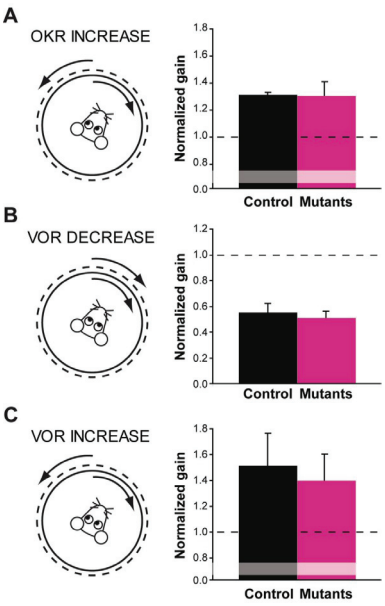

Figure S1. Young LTD-deficient mice show normal short-term adaptation. (A), Visuovestibular out-of-phase mismatch training (see Figure 2) did not result in significant differences (p = 0.88) in OKR gain increase of pooled PICK1 KO and GluR2Δ7 KI (pink) mutants (n=5) compared to pooled littermate controls (black, n=5). (B), VOR gain decreases as a result of visuovestibular in-phase mismatch training did not differ significantly (p = 0.75) between pooled PICK1 KO and GluR2Δ7 KI mutants and littermate controls. (C), Visuovestibular out-of-phase mismatch training did not result in significant differences (p = 0.71) between pooled mutant mice and littermate controls. For number of mice per group, see Suppl. Table.

Table S1. Number of PICK1, GluR2Δ7, GluR2K882A and littermate control mice, pooled and mutant-specific, used in all experiments.

					* littermates of		
	*Control**	*PICK1*	*GluR2Δ7*	*-K882A*	*PICK1*	*GluR2Δ7*	*-K882A*
Eye movements							
Performance							
OKR	23	10	12	11	11	7	5
VOR	23	9	12	11	11	7	5
VVOR	23	9	12	10	11	7	5
Adaptation							
OKR gain increase	23	11	13	10	10	10	3
VOR gain decrease	23	12	13	11	10	9	4
VOR gain increase	24	13	13	12	10	11	3
VOR phase reversal (day 6)	24	8	8	7	10	10	4
Eyeblink conditioning							
Motor performance	22	4	13	8	10	5	7
Motor learning	22	4	13	8	10	5	7
Erasmus Ladder							
Motor performance	19	4	5	8	8	5	6
Motor learning	19	4	5	8	8	5	6
Slice electrophysiology							
LTP	14	9	10	10	7	5	2
LTD	18	7	6	7	8	8	2
LTD+cyclosporin	9	9	8	8	3	4	2
PPF	36	18	20	20	15	16	5

Table S2. Significance levels for comparisons mutants to pooled and mutant-specific controls for all experiments.

	Grouped littermates vs.			*Mutant specific littermates vs.*		
	PICK1	*GluR2Δ7*	*-K882A*	*PICK1*	*GluR2Δ7*	*-K882A*
Compensatory Eye Movements						
Performance						
OKR gain	0.93	0.99	0.99	0.83	0.72	0.56
phase	1.00	0.80	0.75	0.24	0.45	0.21
VOR gain	0.87	1.00	0.95	0.73	0.93	0.30
phase	0.76	1.00	0.77	0.85	0.72	0.31
VVOR gain	1.00	0.52	0.48	0.26	0.16	0.99
phase	0.63	0.44	1.00	0.79	0.86	0.35
Adaptation						
OKR gain increase	0.96	0.69	0.93	0.26	0.74	0.71
VOR gain decrease	0.54	0.40	0.99	0.68	0.66	0.83
VOR gain increase	1.00	0.62	0.99	0.82	0.27	0.73
VOR phase reversal						
day 6 gain	0.81	0.79	0.99	0.60	0.42	0.33
phase	0.88	0.97	0.83	0.55	1.00	0.053
Eyeblink Conditioning						
Performance						
Latency to UR onset	0.17	0.25	0.63	0.14	0.16	0.61
Latency to R1	0.19	0.19	0.99	0.39	0.10	0.53
UR peak velocity	0.34	0.21	0.23	0.60	0.43	0.35
Learning						
CR acquisition	0.86	0.67	0.20	0.57	0.27	0.18
CR extinction	0.75	0.99	0.28	0.84	0.003	0.43
% CR on acq. session 6	0.96	0.74	0.15	0.74	0.20	0.18
CR ampl. acq. sesson 6	0.69	0.46	0.43	0.84	0.65	0.14
Erasmus Ladder						
Performance						
Steptime(session 1-4)	1.00	1.00	1.00	0.76	0.33	0.22
Missteps(session 1-8)	1.00	1.00	0.54	0.31	1.00	0.18
Missteps (session 1-4)	1.00	1.00	1.00	0.35	0.67	0.69
Missteps(session 5-8)	1.00	0.08	0.035	0.26	0.30	0.024
Learning						
Poststeptime(session 5-8)	1.00	0.20	0.58	0.75	0.14	0.65
Presteptime(session 5-8)	1.00	0.23	0.10	0.37	0.60	0.19
Slice Electrophysiology						
LTP	0.24	0.93	1.00	0.25	0.11	0.96
LTD	0.032	0.005	0.038	0.004	0.046	0.045
LTD+cyclosporin	0.001	0.041	0.032	0.063	0.054	0.034
PPF	0.91	1.00	0.97	0.89	0.99	0.21

$p < 0.05$ indicates control is significantly better than mutant
$p < 0.05$ indicates mutant is significantly better than control

Chapter 4
Section 4.2

Purkinje cell-specific knockout of the protein phosphatase PP2B impairs potentiation and cerebellar motor learning

Neuron. 2010 August 67, 618-28.

M. Schonewille, A. Belmeguenai, S.K. Koekkoek, S.H. Houtman, H.J. Boele, B.J. van Beugen, Z. Gao, A. Badura, G. Ohtsuki, W.E. Amerika, E. Hosy, F.E. Hoebeek, Y. Elgersma, C. Hansel and C.I. De Zeeuw

Abstract

Cerebellar motor learning is required to obtain procedural skills. Studies have provided supportive evidence for a potential role of kinase-mediated long-term depression (LTD) at the parallel fiber to Purkinje cell synapse in cerebellar learning. Recently, phosphatases have been implicated in the induction of potentiation of Purkinje cell activities in vitro, but it remains to be shown whether and how phosphatase-mediated potentiation contributes to motor learning. Here, we investigated its possible role by creating and testing a Purkinje cell specific knockout of calcium/calmodulin-activated protein-phosphatase-2B (L7-PP2B). The selective deletion of PP2B indeed abolished postsynaptic long-term potentiation in Purkinje cells and their ability to increase their excitability, whereas LTD was unaffected. The mutants showed impaired gain-decrease ánd gain-increase adaptation of their VOR as well as impaired acquisition of classical delay conditioning of their eyeblink response. Thus, our data indicate that PP2B may mediate indeed potentiation in Purkinje cells and contribute prominently to cerebellar motor learning.

Introduction

At excitatory synapses onto hippocampal or neocortical synapses, protein phosphatases are required for postsynaptic LTD induction, whereas kinases are required for postsynaptic LTP induction[1, 2]. In these regions protein phosphatase 1 (PP1), the activity state of which is indirectly controlled by calcium/calmodulin-activated protein phosphatase 2B (calcineurin or PP2B), has been suggested to act in concert with the α isoform of calcium/calmodulin-dependent kinase II (αCaMKII) to provide a molecular switch regulating the phosphorylation state of AMPA receptors[2, 3]. In contrast, at cerebellar PF synapses onto Purkinje cells LTD induction is PKCα- [4], cGKI- [5] and α/βCaMKII-dependent[6, 7], whereas LTP requires the activation of PP1, PP2A, and calcineurin[8]. Interestingly, changes in LTD and LTP induction can be associated with changes in intrinsic excitability in the hippocampus and cerebellum[9, 10], and calcineurin has indeed been associated differentially with changes in intrinsic excitability in pyramidal cells and Purkinje cells[11]. Thus, cerebellar Purkinje cells operate in general inversely to their hippocampal counterparts in that downstream kinase and phosphatase activity can push the balance towards LTD and LTP, respectively, even though the activity of these enzymes themselves can be regulated by proteins of the opposite category upstream[12, 13].

Over the past decades, attempts to determine the cellular mechanisms underlying cerebellar motor learning have focused virtually exclusively on the impact of LTD[14-17]. Genetic interference with kinase-mediated LTD induction and/or maintenance in Purkinje cells has been reported to be associated with impaired motor learning such as defects in VOR gain adaptation or eyeblink conditioning[5, 6, 15, 18, cf 19]. Some of these studies have encouraged scientists to hypothesize that LTD is specifically responsible for gain *increases* in VOR adaptation[20] and *acquisition* of conditioned eyeblink responses[16, 21] raising the possibility that potentiation might be responsible for gain-*decrease* VOR adaptations

and *extinction* of conditioned responses[20]. However, no transgenic mouse mutants have been created yet, which allow us to investigate specifically the possible contribution of potentiation in Purkinje cells. Since calcineurin is required for PF-PC LTP and increases in intrinsic excitability[8] , this protein forms an ideal molecular target to genetically manipulate potentiation in Purkinje cells, and to investigate for the first time a potential role of potentiation in cerebellar motor learning. Thus, here we created mutant mice (L7-PP2B), in which calcineurin activity is selectively impaired in Purkinje cells by crossing floxed CNB1 mice (regulatory subunit of calcineurin)[22] with a Purkinje cell specific (L7-) cre-line[23] (Figure 1A), and we subsequently investigated them at the cell physiological and behavioral level.

Results

L7-PP2B mice lack calcineurin but show normal histology

Immunocytochemical analysis of the L7-PP2B mice with antibodies directed against the

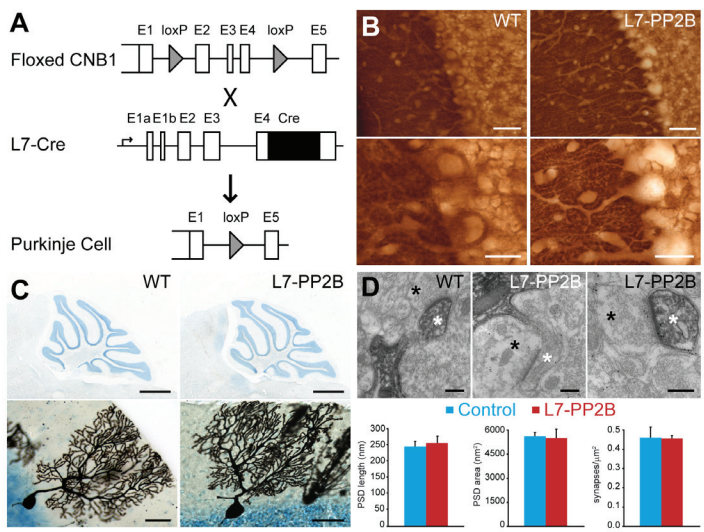

Figure 1. The L7-PP2B mutant: Creation and morphology. A, The L7-PP2B mutant mice were created by crossing a floxed calcineurin line with a L7-Cre line. B, Calcineurin (B subunit) stainings of the cerebellar cortex confirm the selective deletion of PP2B in Purkinje cells in L7-PP2B mice (n = 4); note the normal expression of PP2B in the parallel fibers of the molecular layer in which the unstained Purkinje cell dendrites stand out (right panels). C, Thionin (upper panel) and Golgi (lower panel) stainings of sagittal sections of the vermis showed no morphological or cyto-architectural differences between control (n = 4) and L7-PP2B mice (n = 4)($p > 0.49$; t-test). D, Electron micrographic quantification of parallel fiber contacts with calbindin stained Purkinje cell dendrites in the molecular layer revealed no significant differences between control (n = 3) and L7-PP2B mice (n = 3) in PSD length, PSD area, and density of synapses ($p > 0.26$ for all parameters; t-test). Scale bars indicate 50 µm (upper panels) and 25 µm (lower panels) in B, 1000 µm (upper panels) and 50 µm (lower panels) in C, and 200 nm (upper panels) in D. Black asterisks indicate parallel fiber terminals, and white asterisks indicate Purkinje cell spines in D.

CNB1 subunit showed that calcineurin is indeed specifically deleted in Purkinje cells (**Figure 1B**). Density analyses showed that PP2B staining intensity was significantly lower in Purkinje cell bodies and primary dendrites ($p = 0.003$ and 0.034, respectively; t-test), but not in granule cells or the neuropil of the molecular layer ($p > 0.6$ for both

parameters). Thionine and Golgi stainings revealed that the mutation did not affect the foliation of the cerebellar cortex or the cyto-architecture of Purkinje cells, respectively (**Figure 1C**). Moreover, electron microscopic examinations of calbindin-stained sections of the cerebellar cortex of L7-PP2B mice showed that the number and size of synaptic inputs from PFs onto Purkinje cells were not significantly different from those of littermate controls ($p > 0.26$ for all parameters, i.e. PSD length, PSD area, and density of synapses; t-test) (**Figure 1D**).

Moreover, the area covered by the Purkinje cell dendrites as well as the thickness of the different layers of the cerebellar cortex was also unaffected ($p > 0.49$ for both parameters; t-test).

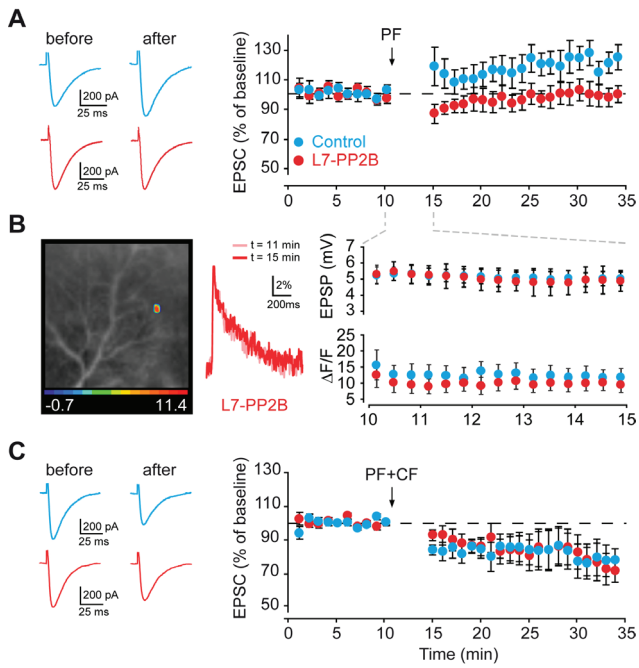

Figure 2. L7-PP2B mice show impaired parallel fiber – Purkinje cell potentiation. A, Induction of LTP at the parallel fiber to Purkinje cell synapse was significantly ($p < 0.03$; t-test) impaired in slices of adult L7-PP2B mice (8 cells from 5 mice) compared to those of controls (7 cells from 6 mice). B, Voltage responses (EPSP, average of 20 stimuli at 1 Hz) and changes in calcium transients (500 ms scans at 0.05 Hz) during the tetanus were not different (both $p > 0.5$; ANOVA for repeated measurements) between controls (n = 13 and 5, respectively) and L7-PP2B mice (n = 10 and 5). Left, sample image of parallel fiber stimulation induced Ca2+-signal. Middle, example trace of PF-stimulation elicited calcium transients (average of 3). C, Induction of LTD at the parallel fiber to Purkinje cell synapse was not affected ($p = 0.96$; t-test) (7 and 9 cells in 5 mutants and 5 controls, respectively). PF-PC LTP was induced by PF stimulation at 1 Hz for 5 min, while LTD was induced by paired PF and CF stimulation at 1 Hz for 5 min. Traces on the left side show EPSCs before (left) and after (right) induction of plasticity. See also Figure S1-2.

L7-PP2B mice show specific defects in parallel fiber to Purkinje cell plasticity

As predicted by our previous pharmacological *in vitro* studies in cerebellar rat tissue[8], our cell physiological examination of 10-24 week-old L7-PP2B mice indeed showed that LTP induction following parallel fiber stimulation alone was blocked ($p = 0.027$; t-test) (**Figure 2A**). In contrast, LTD induction following paired PF and climbing fiber (CF)

stimulation was unaffected in adult L7-PP2B mice (p = 0.96; t-test) (**Figure 2C**). In wild type littermates, both LTP and LTD were successfully induced (**Figures 2A and C**). The inability of L7-PP2B mutants to potentiate their parallel fiber input did not depend on the temperature, age or type of induction protocol, while it could be rescued by the addition of active PP2B (data not shown, see supplementary materials in the article). Moreover, EPSPs and intracellular calcium concentrations during the tetanus did not differ (**Figure 2B**), arguing against the possibility that these factors were responsible for the observed deletion of parallel fiber potentiation.

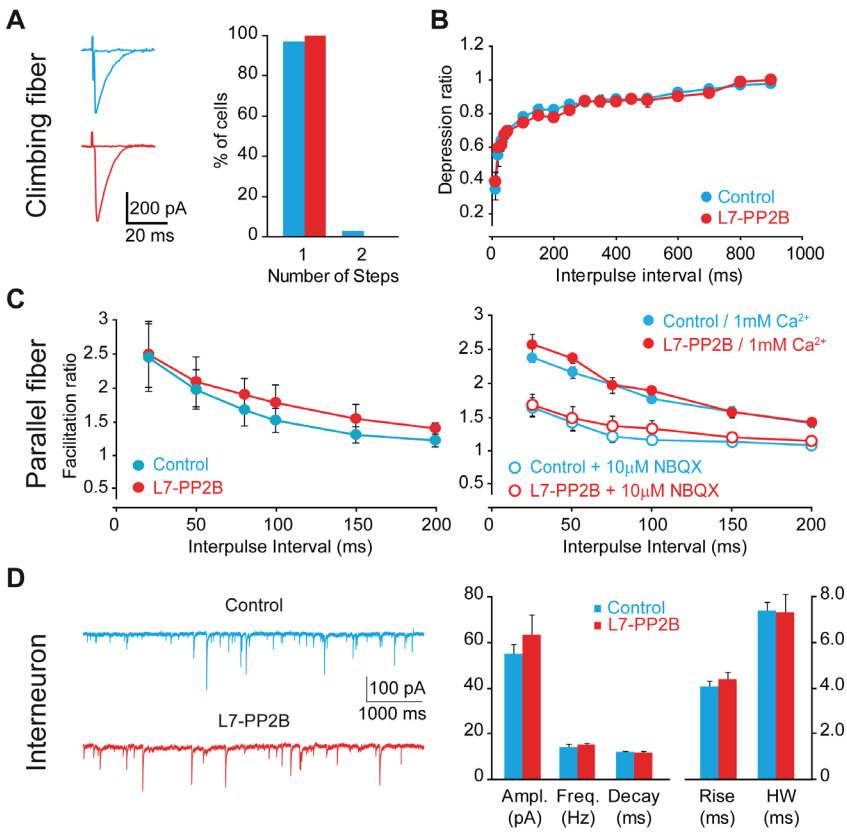

Figure 3. Climbing fiber elimination and basal state of excitatory and inhibitory input to Purkinje cells is unaffected in L7-PP2B mutant mice. A, All-or-none climbing fiber EPSCs were evoked at increasing stimulus intensities. Traces show EPSCs above and below threshold. Climbing fiber elimination is nearly complete in Purkinje cells of both controls and L7-PP2B mutants at 20 10 - 24 wks (33 cells from 12 control mice; 12 cells from 4 mutants). B and C, We did not detect differences in the paired-pulse depression (PPD) ratio at CF synapses (B) and the paired-pulse facilitation (PPF) ratio at PF synapses (C), respectively. PPF ratios were determined for the indicated stimulus intervals in both wild type (n = 8) and mutant mice (n = 5) and no differences are found (p = 0.163; ANOVA for repeated measurements). PPF ratios also did not differ in conditions of lower external calcium (p = 0.213; n = 6 vs. 6, control vs. L7-PP2B) or in the presence of NBQX (p = 0.314; n = 5 vs. 8). Insets show sample traces. D, Characterization of sIPSCs revealed no differences in frequency, amplitude, rise time, half width and decay time (all p > 0.34; n = 11 vs. 6, control vs. L7-PP2B; t-test). Sample traces on the left Error bars indicate SEM.

Climbing fiber elimination, paired-pulse ratios and inhibition are not affected in Purkinje cells of L7-PP2B mice

Since the presence or absence of CF activity is critical for the induction of depression and potentiation in Purkinje cells, respectively[24, 25], we also examined whether deletion

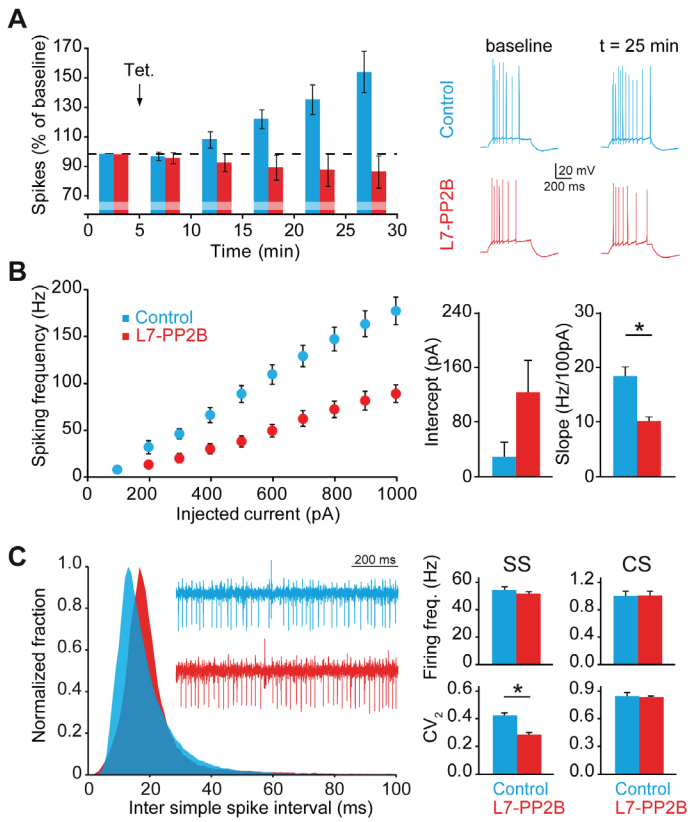

Figure 4. Intrinsic excitability and spiking activity in L7-PP2B mice. A, Following tetanization (150-300 pA at 5 Hz for 3 s) the spike rate evoked with 550 ms depolarizing current pulses of 100-200 pA increased in wild types (n = 9), but not in the L7-PP2B mutants (n = 16; p = 0.007; ANOVA for repeated measurements)(Figure 4A). Right, sample traces before and after induction. B, Basal intrinsic excitability is significantly lower in L7-PP2B mice (n = 7 vs. n = 10 for controls), quantified by slope (p = 0.002; t-test) and intercept with the x-axis (p = 0.07; t-test). C, Purkinje activity in vivo is characterized by a sharper inter-simple spike interval distribution (left) and concomitant higher regularity of spiking (i.e. CV2, p < 0.001), but the average frequencies of simple spikes and complex spikes were normal (both p > 0.5; t-test). Inset shows sample traces. See also Table S1.

of calcineurin in Purkinje cells directly affects the developmental elimination of surplus CF inputs, as previously observed for mutant mice lacking PKC[15] or αCaMKII activity[6]. CF elimination in adult L7-PP2B mice (10-24 weeks), however, appeared normal, and is therefore unlikely to have affected synaptic input patterns that could indirectly impair plasticity in Purkinje cells of L7-PP2B mice (**Figure 3A**). Likewise, we did not detect differences in the paired-pulse depression (PPD) ratio at CF synapses and the paired-pulse facilitation (PPF) ratio at PF synapses, respectively (**Figure 3B and C**). In fact, even in the presence of NBQX or lower extracellular calcium the PPF did not differ (**Figure 3C**). These findings suggest that the observed effects on plasticity were postsynaptic, but they don't allow us to conclude that presynaptic changes were completely absent. Finally, we found no differences in frequency, amplitude, rise/decay time and half width of spontaneous IPSCs in Purkinje cells (**Figure 3D**). Together, these data suggest that the basic synaptic transmission of both excitatory and inhibitory inputs to Purkinje cells is unaffected in L7-PP2B mice.

L7-PP2B mice show defects in intrinsic plasticity of Purkinje cells

In addition to synaptic parallel fiber potentiation, also non-synaptic Purkinje cell intrinsic excitability can be potentiated. This intrinsic potentiation could be readily induced in wild types, but not in the L7-PP2B mutants (p = 0.007; ANOVA for repeated measurements)

(**Figure 4A**). Notably, we also observed differences in baseline intrinsic excitability. Linear fits of the current-frequency curves showed that the slope of L7-PP2B mice is less steep ($p = 0.002$; t-test) (**Figure 4B**). This difference suggests that the cells are less excitable, which is confirmed by a lower maximum firing frequency ($p < 0.001$; t-test).

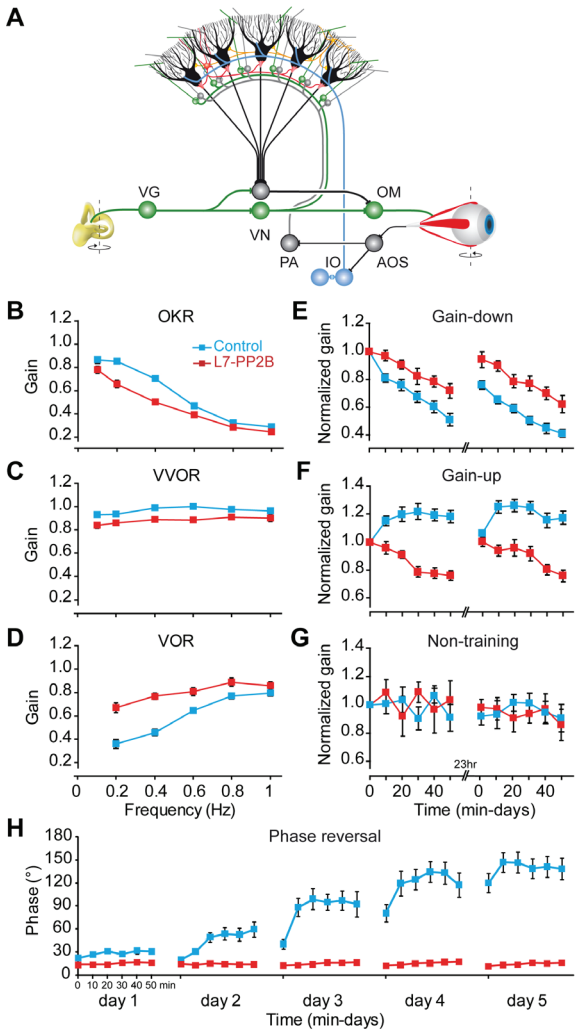

Figure 5. VOR adaptation is affected in L7-PP2B mice. A, Schematic drawing of the vestibulo-cerebellar system. Purkinje cells (black) in the flocculus of the vestibulo-cerebellum converge upon neurons in the vestibular nuclei (VN), through which they can influence the output of the oculomotor neurons (OM) that drive the eye movements. The Purkinje cells are innervated by two main inputs: they receive vestibular and eye movement signals through the mossy fiber - parallel fiber system (represented by green and grey inputs), and retinal slip signals through climbing fibers derived from the inferior olive (IO; blue). The parallel fibers, which all originate from the granule cells, innervate the dendritic trees of the Purkinje cells. VG, AOS and PA indicate vestibular ganglion cells, accessory optic system, and pontine areas, respectively. B, C and D, Motor performance during the optokinetic reflex (OKR), and the vestibulo-ocular reflex in the light (VVOR) and the dark (VOR) revealed moderate aberrations in L7-PP2B mice ($n = 15$) compared to controls ($n = 19$) (for OKR, VOR as well as VVOR $p < 0.001$; ANOVA for repeated measurements). E and F, Motor learning in L7-PP2B mice was severely affected; during two days of mismatch training so as to either decrease (E) or increase (F) their VOR gain the L7-PP2B mice ($n = 9$) learned significantly less than controls ($n = 10$) ($p < 0.0002$ and $p < 0.000001$ for gain-decrease and gain-increase paradigm, respectively; ANOVA for repeated measurements). Note that gain-increase training resulted in a decrease of the gain in the L7-PP2B mice. G, Without mismatch training stimuli as in E or F, no differences were observed ($p = 0.83$ on day 1 and $p = 0.90$ on day 2; ANOVA for repeated measurements). H, When the L7-PP2B mice ($n = 8$) were subjected during four consecutive days (days 2 to 5) to a mismatch training paradigm aimed at reversing the phase of their VOR, they learned significantly less ($p < 0.000001$; ANOVA for repeated measurements) than their controls ($n = 8$). On the day (day 1) preceding this reversal protocol the animals were subjected to the standard in-phase gain-decrease paradigm. Error bars indicate SEM. See also Figure S3-5.

A lack of PP2B affects regularity but not average firing frequency of simple spike activities in vivo

To test whether the deficits in PF-PC LTP and plasticity of intrinsic excitability affect Purkinje cell activity *in vivo* we performed extracellular recordings in awake mice (n = 25 vs. 30 for control vs. L7-PP2B). Firing frequencies of simple spikes and complex spikes were both normal ($p = 0.94$ and $p = 0.54$, respectively; t-test), but the inter-simple spike interval distribution was sharper with less high-frequency spiking and concomitant higher regularity in L7-PP2B mutants (**Figure 4C**). Thus, the changes in intrinsic excitability and potentiation in L7-PP2B mice correlate with a loss of high-frequency simple spike activity, but do not alter the average firing frequency of Purkinje cells. We therefore conclude that the deficits in potentiation in the L7-PP2B mice may selectively affect their spatiotemporal firing patterns of simple spike activities.

L7-PP2B mice show defects in adaptation of the vestibulo-ocular reflex

In the open field or during footprint analysis L7-PP2B mice did not show obvious signs of ataxia (data not shown, see supplementary materials in the article). To explore their specific capabilities for cerebellar motor learning, we first subjected the mice to compensatory eye movement tests, in particular VOR adaptation tests, which are controlled by the vestibulocerebellum[6, 15, 26] (**Figure 5**). Measurements of basic performance parameters including the gain (amplitude) and phase (timing) of the optokinetic reflex (OKR) and/or VOR showed overall that the motor performance of the L7-PP2B mutants was moderately, but significantly, affected **(Figures 5B-D, Figure S1A-C**). For OKR and VVOR the gain of L7-PP2B mutants were significantly lower than those of wild type littermates (both OKR and VVOR $p < 0.001$; ANOVA for repeated measurements) (**Figure 5B-C**), while their phase values were significantly lagging those of the wild types (OKR $p < 0.01$; VVOR $p < 0.001$; ANOVA for repeated measurements). In contrast, for VOR the gain of L7-PP2B mutants was significantly greater than that of wild type littermates ($p < 0.001$; ANOVA for repeated measurements) (**Figure 5D**), while their phase values were also significantly lagging those of the wild types ($p < 0.01$; ANOVA for repeated measurements) (**Figure S1**). The differences among mutants and wild types during OKR and VVOR were not caused by differences in vision itself, because the latencies of the eye movement responses to the onset of the optokinetic stimuli were unaffected in the mutants ($p = 0.55$, ANOVA for repeated measurements) (**Figure S2**).

A prominent phenotype of the L7-PP2B mice was observed when we subjected the animals to the mismatch learning paradigms. In a two-day visuo-vestibular training paradigm aimed at reducing the gain of the VOR, learning was significantly impaired in the mutants (**Figure 5E**) ($p < 0.0002$ for both days; ANOVA for repeated measurements). In the opposite training paradigm, which was aimed at increasing the gain, the gain values of the mutants even showed a decrease (**Figure 5F**; comparison among mutants and controls $p < 0.000001$ for both days, ANOVA for repeated measurements). Control experiments revealed that this decrease was not due to aspecific effects, because exposure to a normal, non-training paradigm for the same duration did not result in any decrease ($p = 0.83$ and $p = 0.90$ for day 1 and day 2, respectively, ANOVA for repeated measurements) (**Figure 5G**). Phase changes are minimal during these gain adaptation paradigms (**Figure S1D-F**),

but phase, like gain, can also be adapted. In this respect the ability of the mutants to learn was affected in such a profound way that they were completely unable to adapt their phase during a long-term 5-day phase reversal training paradigm (**Figure 5H)**. In contrast, wild type littermates were able to reverse their phase towards 180 degrees in five consecutive training sessions (5^{th} day, comparison among L7-PP2B mutants and wild type mice; $p < 0.000001$, ANOVA for repeated measurements). Thus, the Purkinje cell-specific PP2B knockout mice were moderately affected in the performance of their basic compensatory eye movements and markedly affected in all forms of VOR adaptation tested.

L7-PP2B mice show impaired eyeblink conditioning

Next, to find out whether the learning deficits in the L7-PP2B mutants are limited to abnormalities in VOR adaptation, which is controlled by the vestibulocerebellum, or whether they reflect a more global deficit in cerebellar motor learning, we also subjected them to a training paradigm that is controlled by a different region of the cerebellum: classical conditioning of eyeblink responses, which in mice is controlled by lobulus simplex in the hemisphere and lobule VI in the vermis[27] (for underlying circuitry see **Figure 6A**). The eyeblink responses of the mice were conditioned using a tone and an air-puff as the conditioned stimulus (CS) and unconditioned stimulus (US), respectively (Koekkoek et al., 2003). After 4 paired training sessions (T-1 to T-4), the L7-PP2B mutants showed significantly less conditioned responses than their wild type littermates (comparison between L7-PP2B mice and wild type littermates at T4: $p < 0.05$, t-test), while this difference was absent during the first training session (at T1: $p = 0.82$, t-test) (**Figures 6B and C**). In fact, the L7-PP2B mutant mice did not show any significant change in percentage of conditioned eyeblink responses over consecutive days of training (e.g. T4 versus T1, $p = 0.52$; one way within subjects ANOVA). The timing of the conditioned responses in the mutants was also affected in that the average peak latency of their CS-alone responses at T4 was significantly shorter ($p < 0.02$; t-test) than that of controls (**Figure 6C**; for peaks in paired trials, see also **Figure 6B**). In contrast, the kinetics of the unconditioned eyeblink responses in the L7-PP2B mutants were indistinguishable ($p > 0.4$ for onset, peak amplitude as well as velocity of UR; t-test) from those in controls (**Figure 6D**). Thus, our eyeblink tests showed that the L7-PP2B mice have a specific impairment in their conditioned responses rather than a general deficit in the motor component of all their eyeblink responses. Together with the VOR gain adaptation tests, we conclude that the L7-PP2B mutants have severe deficits in hallmark features of cerebellar learning functions: The fine-tuning of sensorimotor gains and the fast adaptation of motor output in response to changing behavioral needs.

Discussion

The current study is the first to specifically address the role of potentiation of Purkinje cell activities in cerebellar motor learning. Guided by the original ideas of Albus[28], and Ito[29], virtually all previous studies that were aimed at identifying the molecular and cellular mechanisms underlying cerebellar motor learning focused on depression for review see [16, 29]. These studies provided supportive evidence that kinases such as PKC[15], cGKI[5], CaMKIV[18]

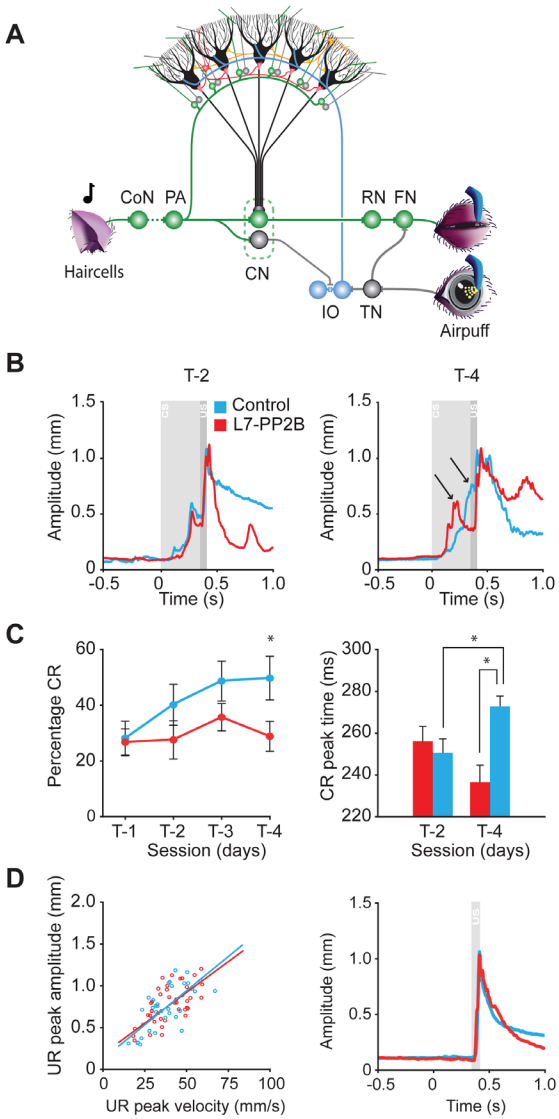

Figure 6. Eyeblink conditioning is impaired in L7-PP2B mutants. A, Neuro-anatomical circuitry involved in eyeblink conditioning. Purkinje cells in the cerebellar cortex form a central site where signal convergence of the unconditioned stimulus (US) and conditioned stimulus (CS) takes place. The US consists of a mild corneal air puff and the CS of an auditory tone. US signals reach the Purkinje cells via the inferior olive (IO) by climbing fibers, while mossy fiber projections from the pontine area (PA) relay the CS. Repeated paired presentation of the CS and US results in conditioned responses (CR), during which the eyelid closes in response to the tone. B, Representative traces of paired CS-US trials from an L7-PP2B knockout (red) and a littermate control (blue) during training sessions T2 and T4. CS onset occurs at time 0, while US follows 325 ms later. Note that the L7-PP2B knockout is not able to improve the timing of the CR (left arrow), whereas the control demonstrates a well-timed CR at T4 (right arrow). C, The percentage of CRs in L7-PP2B knockout mice (n = 9) does not significantly increase over the four training sessions ($p = 0.52$; t-test). Instead, the control littermates (n = 9) demonstrate a clear learning curve ($p < 0.01$; t-test) and at T4 they show significantly more CRs than L7-PP2B knockouts ($p < 0.05$). In addition, the quality of the CR does not improve in L7-PP2B knockout mice. Where controls demonstrate well timed CRs during training session 4 (e.g. T4 versus T2, $p < 0.001$; t-test), L7-PP2B knockout mice do not improve their timing (e.g. at T4 L7-PP2B versus controls, $p < 0.02$; t-test). D, Kinetics of the eyelid responses are not affected in L7-PP2B knockout mice. Onset, peak amplitude and velocity of the eyelid response to the air puff in the mutants do not differ from those of controls ($p > 0.4$ in all comparisons; t-test) indicating that kinetics of the eyelid are the same for both groups. Abbreviations: CN Cerebellar Nuclei; CoN Cochlear Nucleus; FN Facial Nucleus; RN Red nucleus; TN Trigeminal Nucleus. All error bars indicate SEM.

and α/βCaMKII[6, 7] are essential for both LTD at the parallel fiber to Purkinje cell synapse and motor learning. The idea has been put forward that gain-increase adaptations of the VOR may be mediated predominantly by LTD, while gain-decrease adaptations may result from potentiation of Purkinje cells[20]. Likewise, it has been suggested that LTD is required for the acquisition of well-timed conditioned responses[16, cf 19, 21], raising the possibility that the extinction is mediated by potentiation of Purkinje cells. This latter option is supported by the finding that the extinction process requires activation of the GABAergic input to the inferior olive[30], which in principle could reduce climbing fiber activities and thereby shift the balance at the Purkinje cell level from depression to potentiation[25]. Based on these hypotheses, one might have expected that L7-PP2B mice are specifically impaired in learning VOR gain decreases and in extinction of conditioned eyeblink responses. Instead, we observed, next to deficits in gain decreases, profound deficits in VOR gain increases and

a virtual absence of phase reversal learning, while the acquisition of conditioned eyeblink responses and their timing were also affected. In fact, the *acquisition* of the conditioning process was such prominently affected that there was no difference in the number of CRs between the last and the first training session making it impossible to estimate a potential contribution of Purkinje cell potentiation to *extinction*. By comparison the behavioral deficits of the potentiation-deficient L7-PP2B mice exceed those of the depression-deficient kinase mutants both during VOR adaptation and eyeblink conditioning[5, 6, 15, 21]. Moreover, a possible functional role for LTP at the parallel fiber to Purkinje cell synapse in our daily

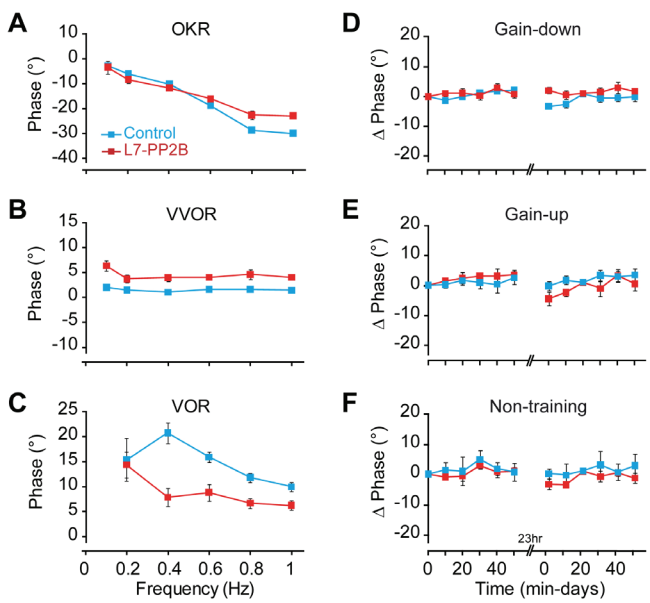

Figure S1. Phase data for compensatory eye movement experiments. A-C, The differences in VVOR and VOR gain, as depicted in Figure 5, are accompanied by differences in phase (OKR, $p = 0.010$; VVOR, $p < 0.001$; VOR, $p = 0.008$). D-F, All (non-) training sessions aimed at changing the gain have only minor effects on the phase. Absolute phase change (Δ phase) was significantly different between control and L7-PP2B mice on the second day of gain-down training ($p = 0.046$; for first day $p = 0.71$)(D), but not on either day for gain-up training (both $p > 0.24$) (E) or control non-training (both $p > 0.21$) (F). For number of animals used, see legends of Figure 5. Error bars indicate SEM.

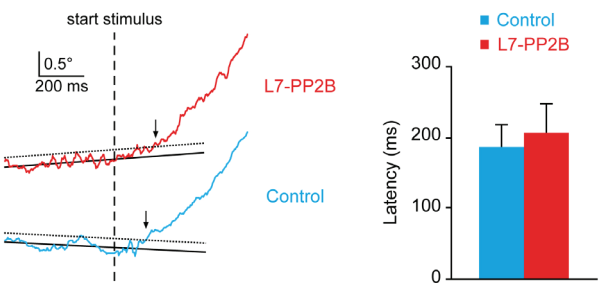

Figure S2. Latency data for OKR. The latency of the eye movement response to the optokinetic stimulus in the L7-PP2B mutants (n = 7) was not significantly different from that in the wild types (n = 7) ($p = 0.69$, t-test). Traces on the left show samples of individual animals. The moment of onset of the optokinetic response was determined by the crossing of the eye movement trace through the (dotted) line that was 2 SD above the average before the start of the stimulus (dashed line) for at least 10 ms.

motor behavior is further supported by the finding that natural cycles may influence this form of plasticity just like VOR adaptation itself[31]. Thus, Purkinje cell potentiation may not only have been neglected over the past decades, it may even be one of the most dominant players in cerebellar learning.

The approach of the current study has the advantage of simultaneously tackling the

two major forms of Purkinje cell potentiation, i.e. PF-PC LTP and PC intrinsic plasticity, in a single animal model and rendering prominent behavioral phenotypes. At the same time, it is not possible to determine to what extent both types of plasticity interact, and which of the two impaired types of potentiation in the L7-PP2B mice is more relevant for which parts of their behavioral phenotypes. Since both types can be induced at physiologically relevant temperatures in wild types, we expect both to contribute, but future studies will have to segregate the two.

Although the kinetics of the unconditioned eyeblink responses in the L7-PP2B mutants were unaffected and therefore unlikely to have contributed to their reduced level of conditioning, we cannot exclude the possibility that the moderate deficits in eye movement performance did contribute to the deficits in VOR adaptation. However, we recently investigated other Purkinje cell specific mutants with comparable performance deficits, and these mutants had no gain learning deficits[26]. Thus, a performance deficit does not necessarily induce a deficit in gain increase and/or gain decrease learning per se.

The robust behavioral phenotypes in our calcineurin-deficient mutants are in line with a recent adaptive-filter model of Porrill and Dean[32]. This model is based on the covariance learning rule, implicating a preponderance of silent PF synapse, which has been experimentally observed[33, 34]. Consequently, their model suggests that LTP is likely to initiate new motor learning, whereas LTD depresses synapses active in the pre-learning situation, a process controlled by the climbing fiber[35]. This way, the cerebellum optimizes the weight of each relevant PF to Purkinje cell synapse given their relative amount of signal and noise. Thus, PP2B-mediated LTP might set the appropriate weights at the PF to Purkinje cell synapses and together with related levels of intrinsic plasticity generate the appropriate spatiotemporal patterns of simple spike activities that are required for cerebellar motor learning. Such an operating scenario could be supported by various other pre- and postsynaptic forms of potentiation at the GABAergic molecular layer interneuron to Purkinje cell synapse[35, 36] allowing temporal pattern formation without affecting the average firing frequency[26]. By combining optimally learned levels of potentiated excitation and feed-forward inhibition Purkinje cells are probably equipped with a push-pull mechanism so as to convey and consolidate appropriately formed patterns of spikes and/or pauses that may be read out in the cerebellar nuclei provided that they occur coherently in ensembles of cells[26, 37-39]. We therefore suggest that potentiation in Purkinje cells complements other forms of cerebellar plasticity in controlling synaptic input strengths and excitability in a dynamic manner, and that the cerebellum uses these plasticity mechanisms to shape the spike activity patterns of the inhibitory Purkinje cell output required for motor learning.

References

1. Mulkey, R.M., Herron, C.E. & Malenka, R.C. An essential role for protein phosphatases in hippocampal long-term depression. *Science* **261**, 1051-5 (1993).
2. Lisman, J.E. & Zhabotinsky, A.M. A model of synaptic memory: a CaMKII/PP1 switch that potentiates transmission by organizing an AMPA receptor anchoring assembly. *Neuron* **31**, 191-201 (2001).

3. Malleret, G. et al. Inducible and reversible enhancement of learning, memory, and long-term potentiation by genetic inhibition of calcineurin. *Cell* **104**, 675-86. (2001).
4. Leitges, M., Kovac, J., Plomann, M. & Linden, D.J. A unique PDZ ligand in PKCalpha confers induction of cerebellar long-term synaptic depression. *Neuron* **44**, 585-94 (2004).
5. Feil, R. et al. Impairment of LTD and cerebellar learning by Purkinje cell-specific ablation of cGMP-dependent protein kinase I. *J Cell Biol* **163**, 295-302 (2003).
6. Hansel, C. et al. alphaCaMKII Is essential for cerebellar LTD and motor learning. *Neuron* **51**, 835-43 (2006).
7. van Woerden, G.M. et al. betaCaMKII controls the direction of plasticity at parallel fiber-Purkinje cell synapses. *Nat Neurosci* **12**, 823-5 (2009).
8. Belmeguenai, A. & Hansel, C. A role for protein phosphatases 1, 2A, and 2B in cerebellar long-term potentiation. *J Neurosci* **25**, 10768-72 (2005).
9. Armano, S., Rossi, P., Taglietti, V. & D'Angelo, E. Long-term potentiation of intrinsic excitability at the mossy fiber-granule cell synapse of rat cerebellum. *J Neurosci* **20**, 5208-16 (2000).
10. Lu, Y.M., Mansuy, I.M., Kandel, E.R. & Roder, J. Calcineurin-mediated LTD of GABAergic inhibition underlies the increased excitability of CA1 neurons associated with LTP. *Neuron* **26**, 197-205 (2000).
11. Misonou, H. et al. Regulation of ion channel localization and phosphorylation by neuronal activity. *Nat Neurosci* **7**, 711-8 (2004).
12. Eto, M., Bock, R., Brautigan, D.L. & Linden, D.J. Cerebellar long-term synaptic depression requires PKC-mediated activation of CPI-17, a myosin/moesin phosphatase inhibitor. *Neuron* **36**, 1145-58 (2002).
13. Launey, T., Endo, S., Sakai, R., Harano, J. & Ito, M. Protein phosphatase 2A inhibition induces cerebellar long-term depression and declustering of synaptic AMPA receptor. *Proc Natl Acad Sci U S A* **101**, 676-81 (2004).
14. Aiba, A. et al. Deficient cerebellar long-term depression and impaired motor learning in mGluR1 mutant mice. *Cell* **79**, 377-88 (1994).
15. De Zeeuw, C.I. et al. Expression of a protein kinase C inhibitor in Purkinje cells blocks cerebellar LTD and adaptation of the vestibulo-ocular reflex. *Neuron* **20**, 495-508 (1998).
16. De Zeeuw, C.I. & Yeo, C.H. Time and tide in cerebellar memory formation. *Curr Opin Neurobiol* **15**, 667-74 (2005).
17. Steuber, V. et al. Cerebellar LTD and pattern recognition by Purkinje cells. *Neuron* **54**, 121-36 (2007).
18. Boyden, E.S. et al. Selective engagement of plasticity mechanisms for motor memory storage. *Neuron* **51**, 823-34 (2006).
19. Welsh, J.P. et al. Normal motor learning during pharmacological prevention of Purkinje cell long-term depression. *Proc Natl Acad Sci U S A* **102**, 17166-71 (2005).
20. Boyden, E.S. & Raymond, J.L. Active reversal of motor memories reveals rules governing memory encoding. *Neuron* **39**, 1031-42 (2003).

21. Koekkoek, S.K. et al. Cerebellar LTD and learning-dependent timing of conditioned eyelid responses. *Science* **301**, 1736-9 (2003).
22. Zeng, H. et al. Forebrain-specific calcineurin knockout selectively impairs bidirectional synaptic plasticity and working/episodic-like memory. *Cell* **107**, 617-29 (2001).
23. Barski, J.J., Dethleffsen, K. & Meyer, M. Cre recombinase expression in cerebellar Purkinje cells. *Genesis* **28**, 93-8. (2000).
24. Lev-Ram, V., Wong, S.T., Storm, D.R. & Tsien, R.Y. A new form of cerebellar long-term potentiation is postsynaptic and depends on nitric oxide but not cAMP. *Proc Natl Acad Sci U S A* **99**, 8389-93 (2002).
25. Coesmans, M., Weber, J.T., De Zeeuw, C.I. & Hansel, C. Bidirectional parallel fiber plasticity in the cerebellum under climbing fiber control. *Neuron* **44**, 691-700 (2004).
26. Wulff, P. et al. Synaptic inhibition of Purkinje cells mediates consolidation of vestibulo-cerebellar motor learning. *Nat Neurosci* **12**, 1042-9 (2009).
27. Van Der Giessen, R.S. et al. Role of olivary electrical coupling in cerebellar motor learning. *Neuron* **58**, 599-612 (2008).
28. Albus, J.S. A theory of cerebellar function *Mathematical Biosciences* **10**, 25-61 (1971).
29. Ito, M. Cerebellar long-term depression: characterization, signal transduction, and functional roles. *Physiol Rev* **81**, 1143-95. (2001).
30. Medina, J.F., Nores, W.L. & Mauk, M.D. Inhibition of climbing fibres is a signal for the extinction of conditioned eyelid responses. *Nature* **416**, 330-3. (2002).
31. Andreescu, C.E. et al. Estradiol improves cerebellar memory formation by activating estrogen receptor beta. *J Neurosci* **27**, 10832-9 (2007).
32. Porrill, J. & Dean, P. Silent synapses, LTP, and the indirect parallel-fibre pathway: computational consequences of optimal cerebellar noise-processing. *PLoS Comput Biol* **4**, e1000085 (2008).
33. Chadderton, P., Margrie, T.W. & Hausser, M. Integration of quanta in cerebellar granule cells during sensory processing. *Nature* **428**, 856-60 (2004).
34. Isope, P. & Barbour, B. Properties of unitary granule cell-->Purkinje cell synapses in adult rat cerebellar slices. *J Neurosci* **22**, 9668-78 (2002).
35. Dean, P. & Porrill, J. Adaptive-filter Models of the Cerebellum: Computational Analysis. *Cerebellum* **7**, 567-71 (2008).
36. Jorntell, H. & Ekerot, C.F. Reciprocal bidirectional plasticity of parallel fiber receptive fields in cerebellar Purkinje cells and their afferent interneurons. *Neuron* **34**, 797-806. (2002).
37. Gauck, V. & Jaeger, D. The control of rate and timing of spikes in the deep cerebellar nuclei by inhibition. *J Neurosci* **20**, 3006-16 (2000).
38. De Zeeuw, C.I., Hoebeek, F.E. & Schonewille, M. Causes and consequences of oscillations in the cerebellar cortex. *Neuron* **58**, 655-8 (2008).
39. Telgkamp, P. & Raman, I.M. Depression of inhibitory synaptic transmission between Purkinje cells and neurons of the cerebellar nuclei. *J Neurosci* **22**, 8447-57 (2002).

Chapter 5

The role of synaptic inhibition at the MLI-PC synapse in motor learning

Nat Neurosci. 2009 Aug;12(8):1042-9.

Wulff P, Schonewille M, Renzi M, Viltono L, Sassoè-Pognetto M, Badura A, Gao Z, Hoebeek FE, van Dorp S, Wisden W, Farrant M, De Zeeuw CI.

Abstract

Although feedforward inhibition onto Purkinje cells was first documented 40 years ago, we understand little of how inhibitory interneurons contribute to cerebellar function in behaving animals. Using a mouse line (PC-Deltagamma2) in which GABA(A) receptor-mediated synaptic inhibition is selectively removed from Purkinje cells, we examined how feedforward inhibition from molecular layer interneurons regulates adaptation of the vestibulo-ocular reflex. Although impairment of baseline motor performance was relatively mild, the ability to adapt the phase of the vestibulo-ocular reflex and to consolidate gain adaptations was strongly compromised. Purkinje cells showed abnormal patterns of simple spikes, both during and in the absence of evoked compensatory eye movements. On the basis of modeling our experimental data, we propose that feedforward inhibition, by controlling the fine-scale patterns of Purkinje cell activity, enables the induction of plasticity in neurons of the cerebellar and vestibular nuclei.

Introduction

Feed-forward inhibitory microcircuits, in which interneurons and their target principal cells receive common excitatory input, enhance network performance in many brain regions[1,2]. In the hippocampus, feed-forward inhibition, by reducing the time window of synaptic integration, increases the precision of spike timing in CA1 pyramidal neurons[3], and plasticity of feed-forward inhibition is required to maintain the fidelity of information processing[4]. Inthe cerebellum, molecular layer interneurons (stellate and basket cells) control Purkinje cells by powerful feed-forward inhibition[5,6,7,8,9] (see Supplementary Fig. 1 in the online article). Additionally, subsets of Purkinje cells sparsely inhibit each other via axon collaterals[10]. Purkinje cells provide the only output of the cerebellar cortex and project to the cerebellar and vestibular nuclei. They fire complex spikes in response to climbing fiber activity[11], and simple spikes that reflect the integration of intrinsic pacemaker activity with excitatory and inhibitory synaptic inputs from parallel fibers and molecular layer interneurons[8,12,13,14,15].

Although feed-forward inhibition onto Purkinje cells was documented more than four decades ago[5], we still know little about how it contributes to cerebellar function in behaving animals. Fast synaptic inhibition at molecular layer interneuron to Purkinje cell synapses is mediated by α1β2/3γ2-type GABAA receptors[16]. The γ2 subunit is required to target the receptors to the postsynaptic membrane[17]. Thus, to investigate the role of GABAA receptor-mediated feedforward inhibition we selectively ablated the γ2 subunit, and thereby synaptic GABAA receptors, from Purkinje cells (PC-Δγ2 mice). The resulting changes in Purkinje cell simple spike activity and motor behaviour implicate molecular layer interneurons as essential regulators of cerebellar signal coding and memory formation.

Results

Purkinje cell-specific removal of synaptic GABAA receptors

To remove GABAA receptor-mediated feed-forward inhibition onto Purkinje cells, we selectively deleted the GABAA receptor γ2 subunit using the Cre/loxP-system (see Chapter 6 Methods). Cre recombinase, under the control of the L7 promoter, induced a Purkinje cell-specific deletion of the floxed γ2 subunit gene starting in the second postnatal week[16,18]. Ablation of synaptic GABAA receptors from Purkinje cells caused no anatomical alterations of the cerebellar circuitry (**Fig. 1**).

Patch-clamp recordings in acute slices of cerebellar vermis from adult animals showed spontaneous fast inhibitory postsynaptic currents (sIPSCs) at high frequency in all Purkinje cells (n = 21) from control mice (**Fig. 2a**), which could be blocked by the GABAA receptor antagonist SR-95531 (20μM; data not shown). By contrast, sIPSCs were absent from all Purkinje cells (n = 19) of PC-Δγ2 mice (**Fig. 2b**). In some PC-Δγ2 cells (12 of 19) occasional small, slow-rising currents remained. However, these produced on average less than 2% of the control synaptic charge (**Fig. 2**), and likely reflect spillover of synaptically released GABA onto extrasynaptic α and β subunit-containing receptors[19,20] (see Supplementary Fig. 2 in the online article). Consistent with a complete loss of synaptic GABAA receptors, recordings from PC-Δγ2 mice in the presence of TTX confirmed the absence of miniature IPSCs (mIPSCs) (**Fig. 2c,d**). The loss of synaptic GABAA receptors was restricted to Purkinje cells: mIPSCs in molecular layer interneurons were unaltered in PC-Δγ2 mice (see Supplementary Fig. 3 in the online aricle).

PC-Δγ2 mice show altered simple spike patterning

Feed-forward inhibition via molecular layer interneurons is rapidly (~ 1 ms) recruited by parallel fiber activation and curtails the parallel fiber-evoked excitatory postsynaptic potential (EPSP) in Purkinje cells[7,21]. To determine how absence of synaptic GABAA receptors affected Purkinje cells response to parallel fiber stimulation, we analyzed the temporal dispersion (jitter) of evoked Purkinje cell simple spikes (**Fig. 3a**). The jitter, quantified as the standard deviation of spike latency in a 10 ms window following stimulation (10V, 100μs), was strongly increased in PC-Δγ2 Purkinje cells (control: 0.81 ± 0.14 ms; PC-Δγ2: 1.80 ± 0.10 ms, $p < 0.0001$, n = 12 and 11, respectively). Acute blockade of GABAA receptors with SR-95531 significantly increased spike jitter in cells from control mice (to 1.45 ± 0.14 ms, $p = 0.0011$; see also Ref.7), but, as expected, had no effect in PC-Δγ2 cells (1.76 ± 0.10 ms, $p = 0.605$). We also determined the number of spikes evoked by parallel fiber stimulation (**Fig. 3a, lower panels**). On average, 0.60 ± 0.04 spikes were evoked in the 60 ms following each stimulus in control cells and 0.41 ± 0.05 spikes in PC-Δγ2 cells (n = 17 and 13, respectively; $p = 0.0069$). This smaller evoked response is consistent with a reduced parallel fiber excitatory input (see Supplementary Fig. 4 in the online article and Discussion). Consistent with the complete loss of GABAA receptor-mediated inhibition in PC-Δγ2 cells, SR-95531 increased the number of evoked spikes only in control cells (0.61 ± 0.05 to 0.76 ± 0.08, n = 11, $p = 0.0248$; PC-Δγ2 cells 0.41 ± 0.05 to 0.45 ± 0.06, n = 13, $p = 0.3199$). Thus, loss of molecular layer interneuronmediated feed-forward inhibition in PC-Δγ2 mice results in altered simple spike responses to parallel fiber inputs.

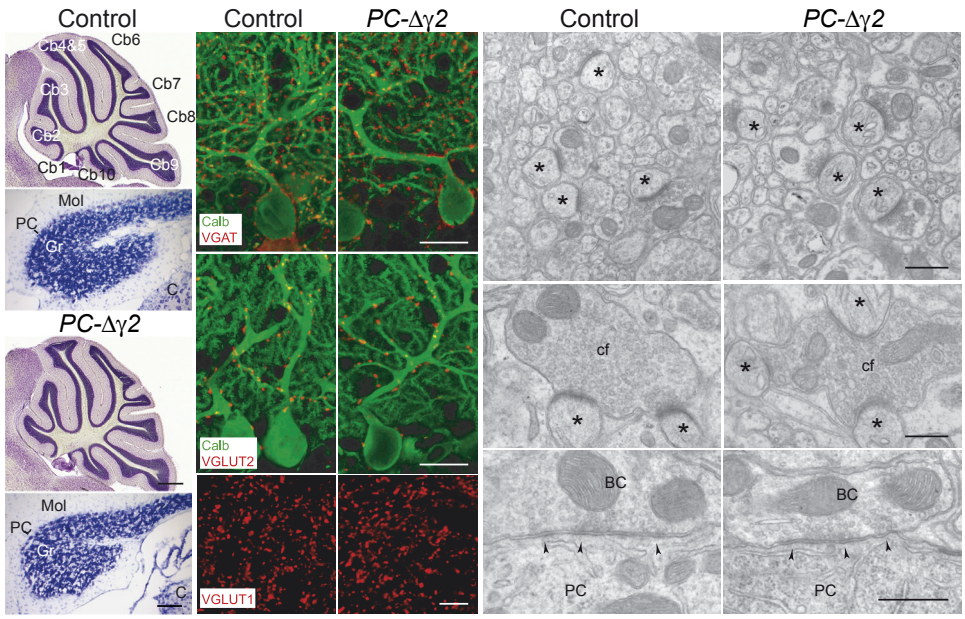

Figure 1. PC-Δγ2 mice show normal cerebellar morphology and synaptic organization. (a, b) Nissl stains of sections through vermis (sagittal) and flocculus (coronal) revealed no differences between control (a) and PC-Δγ2 (b) mice, and the number of Purkinje cells (24.5 ± 2.0 vs 23.9 ± 2.5 cells/1000μm; p = 0.75) and molecular layer interneurons (2.36 ± 0.19 vs 2.28 ± 0.18 cells/1000μm2; p = 0.53) were similar in both groups. Cb1-10, lobules 1-10; Mol, molecular layer; PC, Purkinje cell layer; Gr, granule cell layer, C, cochlear nucleus. (c-e) Immunofluorescence labelling in the flocculus showed no differences in the distribution of GABAergic terminals (vesicular γ-aminobutyric acid transporter; VGAT) (c), climbing fiber terminals (vesicular glutamate transporter 2; VGLUT2) (d) and parallel fiber terminals (VGLUT1) (e). Quantification of puncta per 1000 μm2 revealed no difference (p = 0.27, 0.62 and 0.68, respectively; n = 4). (f-h) Electron microscopy showed no obvious morphological changes of parallel and climbing fiber synapses. (f) Asymmetric synapses between parallel fibers and Purkinje cell spines (asterisks). The density of parallel fiber to Purkinje cell synapses was unchanged (33.0 vs 32.9 synapses/100 μm2 in PC-Δγ2 and control; see Chapter 6 Methods). (g) Asymmetric synapses made by climbing fibers (cf). (h) Symmetric synapses (arrowheads) made by basket cells (BC) onto the cell body of Purkinje cells (PC). Scale bars: (a and b) 250 μm and 50 μm; (c, d) 20 μm; (e) 5 μm; (f) 500 nm; (g) 360 nm; (h) 440 nm.

Purkinje cells in cerebellar slices from PC-Δγ2 mice showed a significant increase in simple spike firing regularity compared with controls (**Fig. 3b**). The mean firing rate at room temperature was not different between groups (control 12.3 ± 1.6 vs PC-Δγ2 13.7 ± 0.6 Hz, n = 26 and 9; p = 0.062, Mann-Whitney U-test), but the coefficient of variation (CV; SD/mean) of the inter-spike interval (ISI) was reduced in PC-Δγ2 mice (0.20 ± 0.03 in control vs 0.10 ± 0.01 in PC-Δγ2; p = 0.018, Mann-Whitney U-test). The coefficient of variation of adjacent intervals (CV2; mean value of 2 |ISIn+1 − ISIn| / (ISIn+1 + ISIn); a measure for the regularity of firing on small timescales[22]) also differed. CV2 was 0.19 ± 0.02 in control vs 0.10 ± 0.01 in PC-Δγ2 mice (p = 0.018; Mann-Whitney U-test). Blockade of GABAA receptors with SR-95531 in control Purkinje cells decreased the CV of the ISI (0.20 ± 0.04 vs 0.13 ± 0.02 in SR-95531; p = 0.024, n = 8) to a value comparable to that found in PC-Δγ2 mice (see also Refs. [12,15,23]). As expected, SR-95531 failed to alter the CV of the ISI in cells from PC-Δγ2 mice (0.13 ± 0.02 vs 0.13 ± 0.04, n = 3). Importantly, similar results were obtained at nearphysiological temperature (34-35°C), with no change in mean rate (51.3 ± 9.1 in control vs 50.0 ± 3.5 Hz in PC-Δγ2, n = 9 and 7; p = 0.61; Mann-Whitney U-test), but a significant decrease in the CV (0.14 ± 0.01 in control vs 0.06

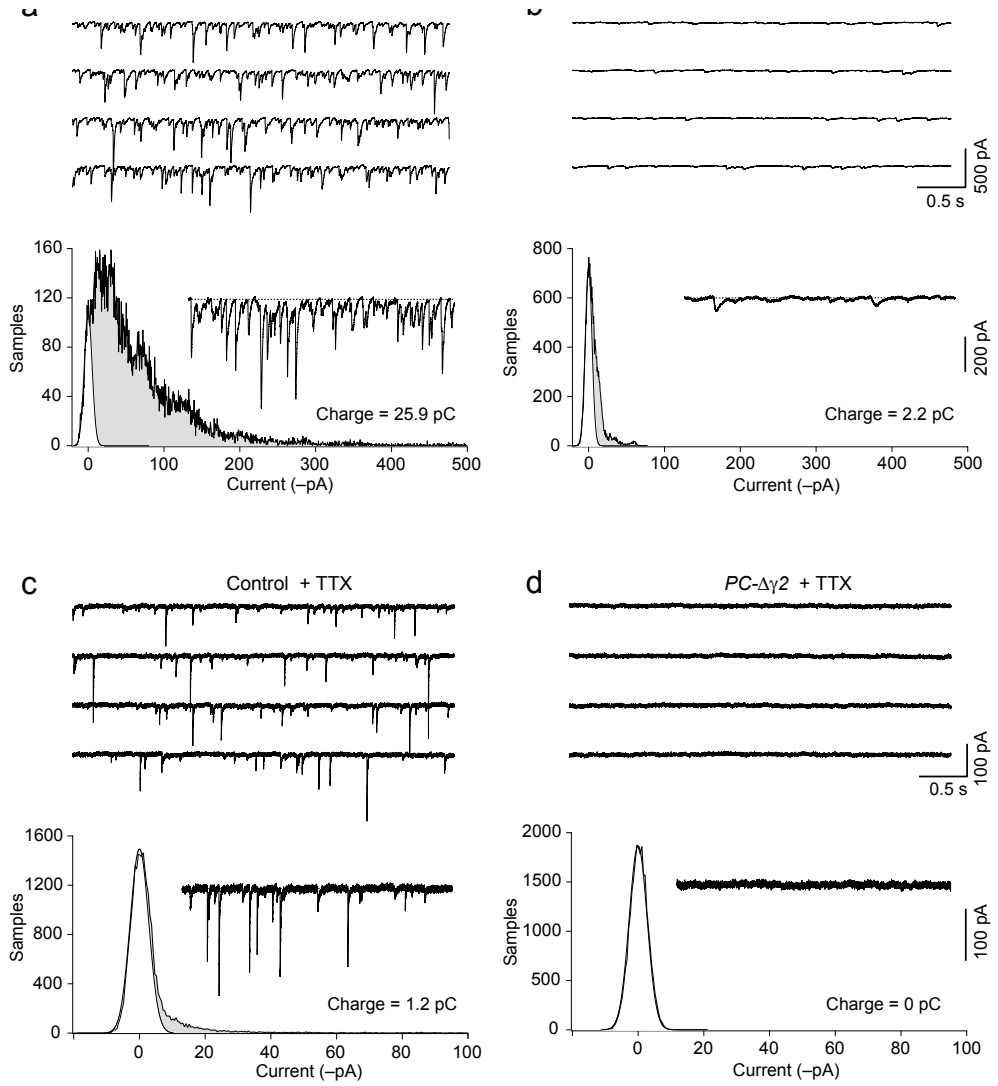

Figure 2. Loss of fast synaptic inhibition from Purkinje cells in PC-Δγ2 mice. (a) Representative contiguous segments of whole-cell recording (−70 mV) from a Purkinje cell of a control mouse. Ionotropic glutamate receptors were blocked with CNQX and d-AP5. Lower panel shows quantification of mean synaptic charge in a different Purkinje cell, with a 2.5 s record of sIPSCs and corresponding all-point amplitude histogram. The left-hand peak (most positive current values), corresponding to the baseline current noise, is fitted with a single-sided Gaussian (white). The peak of the histogram is taken as the zero current value (dotted line in inset). The filled grey area corresponds to all sample points other than those within the baseline noise, and thus represents the current produced by phasic synaptic events. In this cell, the mean synaptic charge was 25.9 pC. (b) Corresponding data from two PC-Δγ2 mice. sIPSCs were seen in all cells from control mice but in none from PC-Δγ2 mice. Slow SR-95531-sensitive currents were seen in ~60% of PC-Δγ2 cells. For the cell shown in the lower panel, phasic charge transfer was 2.2 pC. On average, the charge transfer was reduced from 59.8 ± 18.4 pC in control (n = 8) to 1.0 ± 0.5 pC in PC-Δγ2 cells (n = 15; p < 0.0002; Mann-Whitney U-test). (c) and (d) Corresponding data recorded in the presence of TTX. Note the different scaling of the current record and the abscissa of the all-point histogram and the complete absence of mIPSCs in PC-Δγ2 cells.

± 0.01 in PC-Δγ2; p = 0.001; Mann-Whitney U-test) and CV2 (0.15 ± 0.02 vs 0.06 ± 0.01; p = 0.0099).

Finally, we examined whether loss of inhibition onto Purkinje cells modified long-

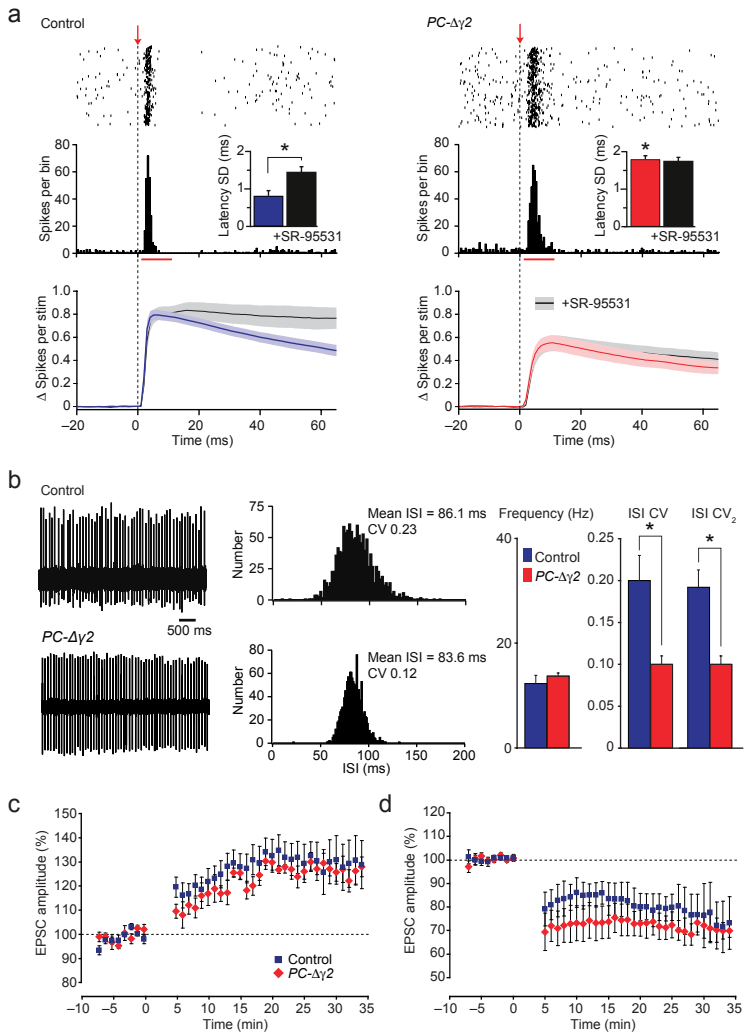

Figure 3. PC-Δγ2 mice display altered parallel fiber-evoked and spontaneous simple spike firing in vitro and unaltered parallel fiber-Purkinje cell LTP and LTD. (a) Simple spikes evoked by parallel fiber activation. Upper and middle panels are raster plots (400 sweeps at 0.5Hz) and corresponding PSTHs (0.5 ms bin-width). Arrows and dashed lines denote stimulation. Insets show SD of spike latency in a 10 ms window (red bars; 12 control, 11 PC-Δγ2 cells). Here, and throughout, error bars denote s.e.m. Jitter was greater in PC-Δγ2 (red) than in control (blue) cells (* $p < 0.0001$). SR-95531 increased jitter in control (* $p = 0.0011$) but not in PC-Δγ2 cells ($p = 0.605$). Lower panels show global averages of baseline-corrected cumulative spike probability (see Chapter 6 Methods). Shaded areas denote s.e.m.; 17 control, 13 PC-Δγ2 cells. Stimulation evoked fewer spikes in PC-Δγ2 cells (averaged between 0 and 60ms, $p = 0.0069$). SR-95531 (40 μM; black line, grey shading) increased spikes in control ($n = 11$; $p = 0.0248$) but not in PC-Δγ2 cells ($n = 13$; $p = 0.3199$). (b) Representative simple spikes (room temperature) and corresponding ISI histograms. Right panels show pooled data (26 control, 9 PC-Δγ2 cells). Mean firing rate was not significantly different. However, the CV and CV2 of ISIs differed significantly (* $p < 0.05$) (see text for details). (c) Pooled data showing parallel fiber-Purkinje cell LTP in control ($n = 7$, blue) and PC-Δγ2 cells ($n = 4$, red); EPSC amplitude was similarly increased in the strains (both $p < 0.005$; control vs PC-Δγ2 $p = 0.257$). (d) Parallel fiber-Purkinje cell LTD was similar in PC-Δγ2 ($n = 5$) and control ($n = 4$) cells (both $p < 0.05$; control vs PC-Δγ2 $p = 0.624$).

term plasticity at parallel fiber to Purkinje cell synapses. Neither parallel fiber LTD nor LTP (see Chapter 6 Methods) were significantly impaired in PC-Δγ2 mice compared with controls ($p = 0.624$ and $p = 0.257$, respectively) (**Fig. 3c,d**).

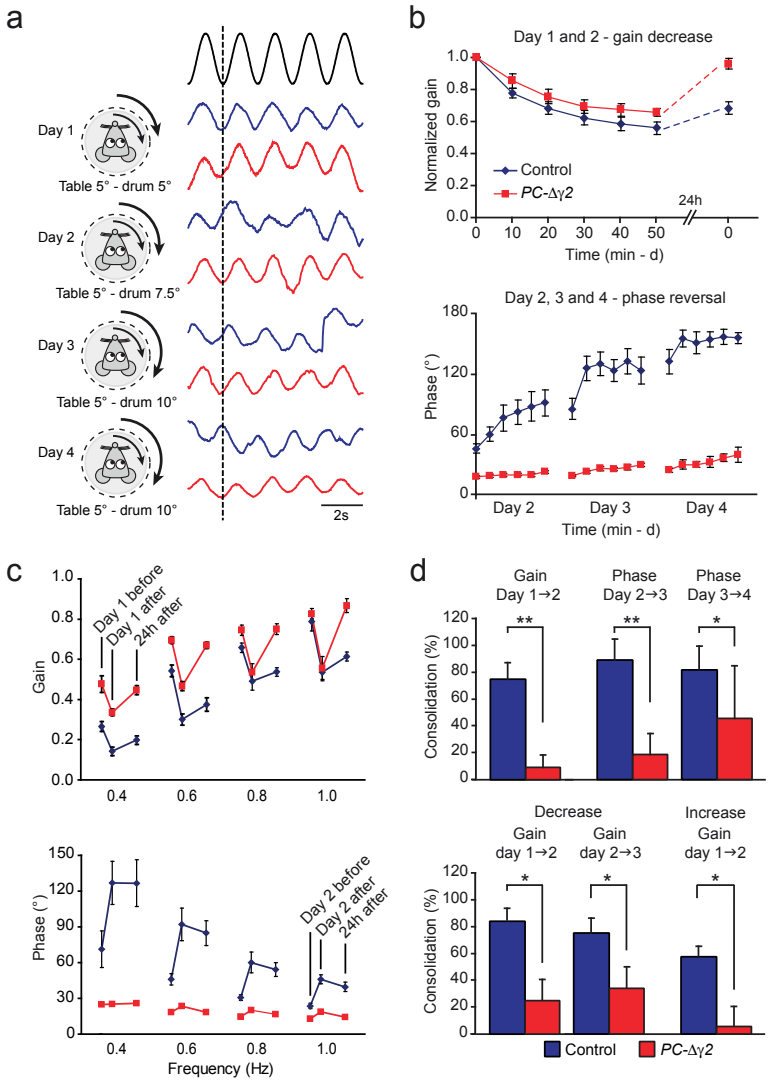

Figure 4. Motor learning is severely affected in PC-Δγ2 mice. (a) Illustration of drum and table rotation during the training paradigm. Traces show sinusoidal drum rotation (black) and examples of eye movement (control, blue; PC-Δγ2, red). Gain and phase parameters were evaluated 5 times at 10 min intervals. (b) On day 1 PC-Δγ2 and control mice showed similar gain reduction ($p = 0.11$), but the first test on day 2 revealed clear differences ($p = 0.001$) (upper panel). During phase reversal training, control mice learned better than PC-Δγ2 mice (day 4 $p < 0.00001$) (lower panel). (c) Differences in gain consolidation and phase reversal occurred over a wide range frequencies. "Day x before" and "Day x after" indicate values before and after training on day "x"; "24hr after" indicates the value on the next day, just before a new measurement. (d) Upper panel: differences in consolidation (percentage change carried forward from the previous day) for gain decrease (day 1 to 2) and phase reversal (day 2 to 3 and day 3 to 4). Lower panel: differences in gain consolidation were also seen with constant in phase drum and table rotation (gain decrease; two histograms on the left), and with constant out of phase drum and table rotation (gain increase; histogram on the right). For the lower panel in (d) data are from 5 control and 6 PC-Δγ2 mice, for all other panels, data are from 10 control and 9 PC-Δγ2 mice. Error bars denote s.e.m.; * and ** $p < 0.05$ and 0.01.

PC-Δγ2 mice display little impairment in motor performance

PC-Δγ2 mice showed no obvious neurological abnormality[16]. To assess cerebellar performance we analyzed compensatory eye movements in male PC-Δγ2 mice (n = 9) and lit-

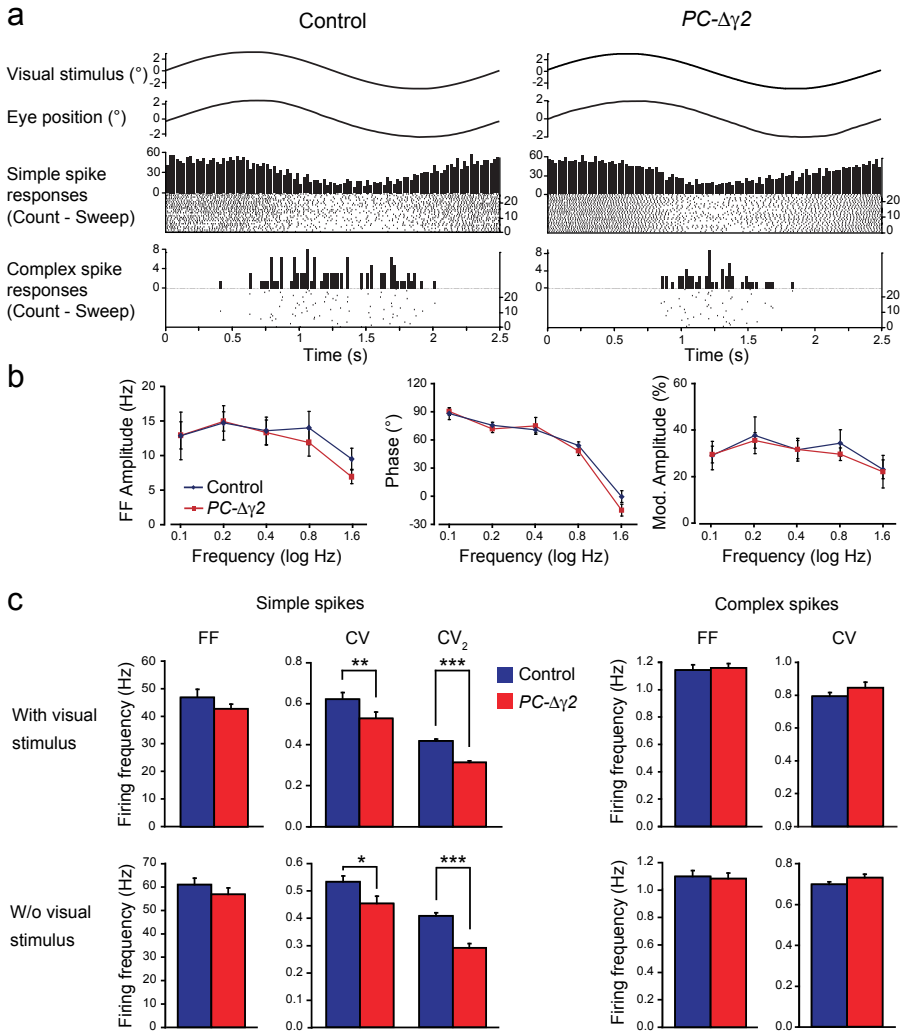

Figure 5. Temporal patterns of simple spike activities of floccular Purkinje cells are specifically affected in PC-Δγ2 mice, both during compensatory eye movement behaviour and during spontaneous behaviour. (a) Representative single unit activity recorded from Purkinje cells in the flocculus of a control and a PC-Δγ2 mouse during fixed velocity (8°/s, 0.2 Hz) OKR stimulation. The visual stimulus and eye position are shown together with histograms of simple spike and complex spike frequencies and corresponding raster plots. (b) Firing frequency, phase relative to stimulus and amplitude of modulation (see Chapter 6 Methods) of floccular simple spike activities during optokinetic stimulation (8°/s, 0.1 - 1.6 Hz) were not significantly different among PC-Δγ2 and control mice. (c) Although average firing frequency of simple and complex spike activity did not differ between PC-Δγ2 and control mice, the coefficient of variation (CV) of simple spikes in PC-Δγ2 mice was significantly reduced in recordings both with and without visual stimuli ($p = 0.008$ and $p = 0.022$, respectively). Also, CV2 values of simple spikes were significantly lower than those of controls in both conditions. Error bars denote s.e.m., * denotes $p < 0.05$, ** $p < 0.01$ and *** $p < 0.0001$.

termate controls (n = 8). Mice were exposed to whole-field visual stimuli to determine the amplitude (gain) and timing (phase) of their optokinetic reflex (OKR) and/or tested with turntable stimulation to investigate the same parameters for the vestibulo-ocular reflex in the dark (VOR) and light (visual VOR or VVOR). During OKR, PC-Δγ2 mice showed a relatively small, but significant, deficit, evident as a reduction in gain and a lag in phase

compared to controls (p = 0.018 and p = 0.012, respectively; two-way repeated-measures ANOVA) (see Supplementary Fig. 5a in the online article). During VOR the gain values

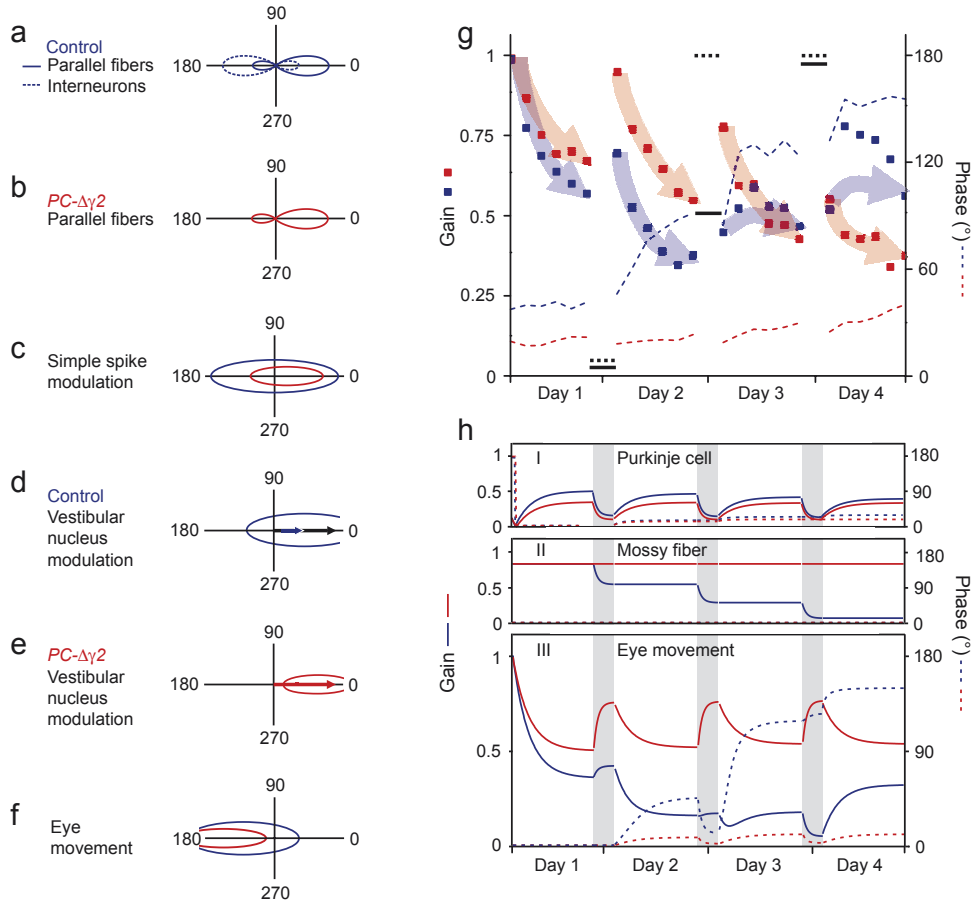

Figure 6. Interpretation of VOR adaptation data using a 'distributed memory' model. (a) Modelled activation of parallel fibers and interneurons plotted in polar coordinates. Most parallel fibers modulate in phase with ipsilateral head movement (0°), while a fraction responds to input from the contralateral horizontal canal (180°). Interneurons are modeled similarly, but with opposite sign representing their inhibitory nature. (b) Same as (a), but for PC-Δγ2 mice lacking inhibition. (c) Maximum simple spike modulation attainable by appropriate depression and potentiation of excitatory and inhibitory inputs shown in (a) and (b) for control (blue) and PC-Δγ2 (red) mice (based on linear input summation). (d) Modulation of target vestibular nucleus neurons attainable by linear summation of mossy fiber inputs (blue arrow, in phase with head movement) and Purkinje cell inputs (panel (c), blue curve) in control mice. The black arrow represents the efficacy of mossy fiber input prior to training. (e) Same as (d), but for PC-Δγ2 mice, where the efficacy of plasticity at the mossy fiber synapses is presumably impaired. (f) Limited simple spike modulation and mossy fiber plasticity restrain eye movements in PC-Δγ2 mice (red curve) as compared to control mice (blue curve). The control curve also covers the area of VOR phase reversal, from out-of-phase with head movement (180° in this figure) to in-phase (0°). (g) Experimental data; squares represent VOR gain and dashed lines represent VOR phase relative to the head (shifted by 180°, for ease of illustration) (see also Fig. 4). For each session, after initial adaptation, the learned Purkinje cell signal determines the new 'desired' phase and gain state for the vestibular nucleus neurons (dashed and solid black bars, respectively). The superimposed blue (control) and red (PC-Δγ2) arrows indicate the direction of change. (h) Simulation of the training paradigm shown in g. During training, Purkinje cells rapidly approach their target modulation (I), reflecting short-term VOR adaptation. Purkinje cell-guided plasticity of mossy fiber input to vestibular nuclei (II) allows control mice to gradually adapt the phase of their VOR during prolonged training (III). In PC-Δγ2 mice, loss of vestibular nucleus consolidation impairs phase adaptation. For simplicity, adaptation in the vestibular nuclei and partial extinction of cortical memory were simulated to occur between training sessions (grey bars).

and phase leads of PC-Δγ2 mice were larger and smaller, respectively, than those of controls ($p = 0.012$ and $p = 0.030$; two-way repeated-measures ANOVA) (see Supplementary Fig. 5b in the online article). By contrast, no significant differences were observed during VVOR ($p = 0.43$ and $p = 0.63$, for gain and phase values, respectively) (see Supplementary Fig. 5c in the online article). Thus, PC-Δγ2 mice show small, but significant, abnormalities in motor performance when visual and vestibular systems are investigated separately, but not when they operate together, as under natural conditions or during visuo-vestibular training.

PC-Δγ2 mice show marked deficits in learning and consolidation

Loss of inhibition onto Purkinje cells had more profound effects on cerebellar motor learning. We studied gain and phase learning by applying a protocol aimed at reducing the gain of the VOR on day 1 (5 × 10 min sinusoidal, in phase drum and table rotation at 0.6 Hz, both with an amplitude of 5°) and subsequently shifting its phase on days 2, 3 and 4 (5 × 10 min sinusoidal in phase drum and table rotation at 0.6 Hz, but with drum amplitudes of 7.5° on day 2 and 10° on days 3 and 4, while the table amplitude remained 5°). Animals were kept in the dark between the recording days. Gain-decrease learning of PC-Δγ2 ($n = 9$) and control mice ($n = 10$) on day 1 was similar ($p = 0.11$; two-way repeated-measures ANOVA) (**Fig. 4a,b**). However, when the measurements were resumed the next day, the degree of gain reduction carried forward from the previous day's learning was significantly smaller in PC-Δγ2 mice than in controls ($p = 0.001$) (**Fig. 4b, upper panel**). This consolidation deficit was apparent at a wide range of frequencies (**Fig. 4c, upper panel**). To exclude non-specific effects (habituation during gain-decrease learning) we tested PC-Δγ2 and control mice in non-adapting VOR paradigms; importantly, mice of both genotypes showed no significant decreases in VOR over consecutive days (last gain value of session 1 vs first value of session 2; $p = 0.610$ for controls and 0.551 for PC-Δγ2 mice) (see Supplementary Fig. 6 in the online article).

Deficits in gain consolidation were also seen when the drum rotation amplitude was kept constant (3 × 10 min of sinusoidal in phase drum and table rotation at 0.6 Hz, both with an amplitude of 5°) (Fig. 4d, lower panel). Here too, the initial level of learning was not significantly affected (PC-Δγ2 mice vs controls; $p = 0.61$; $n = 6$ and 5, respectively), whereas the level of consolidation was significantly reduced (gain day 1→ 2, $p = 0.034$; gain day 2→ 3, $p = 0.046$). Moreover, gain consolidation deficits in PC-Δγ2 mice did not depend on the direction of learning. With a gain-increase paradigm (5 × 10 min sinusoidal out of phase drum and table rotation at 1.0 Hz, both with an amplitude of 1.6°) no significant consolidation was present in the PC-Δγ2 mice (gain day 1→ 2, $p = 0.744$, $n = 6$; One-Sample t-test). By contrast, consolidation in controls was present and was significantly stronger than in PC-Δγ2 mice ($p = 0.002$) (**Fig. 4d, lower panel**). Notably, the level of gain increase learning in PC-Δγ2 mice was not significantly different from that in controls ($p = 0.800$). Thus, deficits in consolidation of learned gain changes, during both gain decrease and increase training paradigms, were not due to differences in baseline performance.

The adaptation paradigm provided on days 2, 3 and 4 immediately revealed signifi-

cant deficits in phase learning in PC-Δγ2 mice, starting 10 - 20 min after the initiation of visuo-vestibular training (e.g. at 20 min p = 0.009) (**Fig. 4b, lower panel**). These deficits in phase change acquisition were followed by clear differences in consolidation (e.g. from day 2 to day 3 p = 0.0008) (Fig. 4d, upper panel). Phase adaptation deficits also occurred at a wide range of frequencies (Fig. 4c, lower panel) and were not caused by visual problems in PC-Δγ2 mice, as eye movement recordings during the adaptation sessions showed that PC-Δγ2 mice were capable of full phase reversal (see Supplementary Fig. 7 in the online article). In short, PC-Δγ2 mice showed a relatively normal capacity for acquisition during gain-decrease and gain-increase motor learning, but a profound deficit in acquisition during phase adaptation learning and a general deficit in consolidation of gain and phase adaptation.

Abnormal temporal patterns of Purkinje cell simple spikes

Since the flocculus controls adaptation of compensatory eye movements[24,25,26] and Purkinje cells provide the sole output of the cerebellar cortex (see Supplementary Fig. 1 in the online article), we analyzed floccular Purkinje cell activity during optokinetic stimulation (**Fig. 5a**). Single units of Purkinje cells that responded optimally to stimulation around the vertical axis were identified by creating tuning curves of their complex spike responses and by identifying a clean climbing fiber pause[26,27]. The average climbing fiber pause in PC-Δγ2 mice and controls was 15.3 ± 0.8 and 18.6 ± 1.3 ms, respectively (55 and 60 PC-Δγ2 and control cells, respectively; p = 0.029). The average simple spike firing frequency, phase relative-to-stimulus and modulation amplitude, were similar in PC-Δγ2 and control mice (**Fig. 5b**). However, as predicted by the in vitro recordings, the regularity of Purkinje cell firing was affected. For floccular simple spike activities, the CV of the ISIs was significantly reduced during visual stimulation in PC-Δγ2 mice (p = 0.008; PC-Δγ2: n = 55, controls: n = 60) (**Fig. 5c**). This difference reflected specific changes in temporal patterning, as CV2 was significantly lower in PC-Δγ2 mice (p < 0.0001) (**Fig. 5c**; see also Supplementary Fig. 8 in the online article).

If these differences in Purkinje cell firing patterns contribute to consolidation deficits in PC-Δγ2 mice, we would also expect to find them outside periods of optokinetic stimulation. Indeed, both CV and CV2 of ISIs were significantly reduced in the absence of stimulation (p = 0.022 and p < 0.0001, respectively; PC-Δγ2: n = 41, controls: n = 43) (**Fig. 5c**). By contrast, the patterns of complex spike activities of Purkinje cells did not differ between PC-Δγ2 and control mice (**Fig. 5a,c**; see also Supplementary Fig. 9 in the online article). Also the antiphasic modulation of complex and simple spikes was unchanged (**Fig. 5a**), arguing against a critical involvement of molecular layer interneurons in this phenomenon[8].

Model and simulations

We interpreted the experimental data from the 4-day gain decrease - phase adaptation routine using a 'distributed memory' model (**Fig. 6**). Short-term adaptation is assumed to take place in the cerebellar cortex, and is expressed as adaptation of the phase and gain of modulation of Purkinje cell simple spikes, which in turn modulate the activity of target neu-

rons in the vestibular nucleus; this process underlies the rapid VOR gain adaptation observed in both PC- Δγ2 and control mice. On a longer timescale, the learned Purkinje cell activity guides plasticity at the target neurons in the vestibular nuclei[28,29], the polarity of which is presumably regulated by the precise timing of simple spikes relative to input from mossy fiber collaterals[30]. Simultaneously, a partial extinction of the previously learned changes at the level of the Purkinje cells takes place[31]. The memory is thus partially transferred to the target nuclei, potentially underlying long-term consolidation[29,32]. After several days of training, this form of 'systems-consolidation' ensures that the cerebellar cortex is no longer responsible for the expression of the learned behavior, but mainly regulates the precise timing (phase). In PC- Δγ2 mice, the altered temporal patterns of Purkinje cell simple spikes could impair the induction of plasticity in the nuclei and thus consolidation.

Given this working hypothesis, we examined whether deficits in VOR gain consolidation and phase adaptation in PC-Δγ2 mice could be replicated in a conceptual model of the idealized VOR circuit (Supplementary Material online). We modeled the modulation of Purkinje cell simple spike firing during head movement as resulting from linear summation of sinusoidal excitatory (parallel fiber) and inhibitory (interneuron) inputs[6]. We assumed the gain and phase of such modulation to be regulated through bidirectional plasticity of the inputs[33]. Purkinje cells and mossy fiber collaterals modulate, by linear summation of their activity, the firing of cells in the vestibular nuclei, which in turn control eye movement. Panels a-f in **Fig. 6** depict an overview of the gains and phases of sinusoidal modulation that can be attained by the elements in the simulation, drawn as positions in a polar plot in which 0° represents modulation in phase with head movement (increased activation during ipsilateral head velocity). The order of the panels follows the signal flow through the vestibulo-cerebellar system from the modeled activation of parallel fibers and interneurons (**Fig. 6a,b**), to the simple spike modulation attainable by appropriate depression and potentiation of these excitatory and inhibitory inputs (**Fig. 6c**), to the modulation of target vestibular nucleus neurons (**Fig. 6d,e**), and ultimately the resulting limits on eye movement (**Fig. 6f**). Due to the absence of inhibition in *PC-Δγ2* mice, the simple spike activation required for adequate modulation of the vestibular nucleus is out of range of the normal plasticity mechanisms in the cerebellar cortex (**Fig. 6c**). In addition, impaired plasticity of the inputs to the vestibular nucleus (**Fig. 6e**) both abolishes consolidation and excludes the possibility of extreme phase adaptations (**Fig. 6f**).

Data from four training sessions, each followed by an overnight period (**Fig. 6g**), were simulated using the upper bounds on sinusoidal modulation as depicted in panels a-f. Adaptation of modulation (**Fig. 6h I and II**) was simulated as an exponential decay from thestart position in the polar plot (defined by the initial gain and phase) towards a new position determined by the experimental paradigm (black horizontal bars in Fig. 6g). As detailed in the Supplementary Material, simulation parameters were chosen to mimic the rate of adaptation observed experimentally. Under these conditions, both control and *PC-Δγ2* Purkinje cells rapidly reached the required modulation during short-term VOR adaptation (**Fig. 6h I**). However, impairments in both VOR gain consolidation and phase adaptation, can be generated if we assume disrupted plasticity in the vestibular nucleus is caused by

poor timing of simples pikes. (**Figs. 3, 5, 6h**).

Discussion

Signal coding and plasticity in cerebellar learning

Although inhibitory interneurons in the molecular layer of the cerebellum have been studied extensively[5,6,7,8], their behavioural relevance has remained enigmatic. Here, we show that these interneurons shape the temporal patterns of Purkinje cell simple spikes and suggest that this process could be essential for plasticity and consolidation in the cerebellar and vestibular nuclei.

Floccular Purkinje cells control the adaptation of compensatory eye movements by modulating the activity of vestibular nucleus neurons (see Supplementary Fig. 1 in the online article). To adapt the VOR, two things should happen within the framework of a 'distributed memory' model. First, Purkinje cells should 'learn' the correct simple spike modulation and express it at sufficient gain in order to modulate the vestibular nuclei. Second, the input from the direct vestibular pathway to the vestibular nuclei should be suppressed, as it only allows modulation in phase with ipsilateral head movement. The first of these processes is thought to reflect complementary inhibitory and excitatory actions, with plasticity at parallel fiber to Purkinje cell and parallel fiber to interneuron synapses, both under climbing fiber control[13,24,25]. The second is thought to occur through plasticity at mossy fiber to vestibular nuclei synapses[25,28]. In *PC-Δγ2* mice the temporal fidelity of Purkinje cell firing is disrupted and consolidation of learned VOR adaptations is severely compromised (**Figs. 4 and 6g**). As induction of various forms of plasticity in the vestibular and cerebellar nuclei could depend on the precise timing of inhibitory and excitatory input from Purkinje cells and mossy fiber collaterals (Supplementary online Material), disruption of this timing would impair transfer of plasticity to the nuclei and thus 'systems consolidation'.

Simple spike trains in Purkinje cells show significantly more temporal patterns than expected from random activation, and these patterns are influenced by natural stimuli[22]. Both the electrical coupling among interneurons and the sagittal orientation of their axons[34,35] (see Supplementary Fig. 1 in the online article) will enhance the effects of feedforward inhibition by promoting common firing patterns in ensembles of Purkinje cells within individual zones, known to project to the same nucleus[26]. The activity patterns of individual Purkinje cells in an ensemble might thus interact with each other and/or with those of mossy fiber and/or climbing fiber collaterals to facilitate the induction of plasticity in the cerebellar and vestibular nuclei[25,28,36,37]. We therefore propose that the vestibular nuclei are the locus for consolidation (see also Ref. [29,32]). Alternatively, both initial learning and consolidation could occur in the cerebellar cortex and the consolidation signal could be preserved in the average simple spike frequency of a particular Purkinje cell. In fact, changes in simple spike frequencies in the flocculus of monkeys are sufficient to drive changes in eye velocity during trial-by-trial motor learning[38]. To determine the extent to which spatiotemporal patterns of simple spikes contribute to consolidation, and whether this consolidation occurs in the nuclei, future experiments will require simultaneous multiunit recording from ensembles of Purkinje cells and cerebellar or vestibular nuclei neurons during learning.

Previous studies have identified long-term changes at the parallel fiber to Purkinje cell synapse as a potential plasticity mechanism during cerebellar learning, and some mouse lines with disrupted LTD induction at this synapse indeed show impaired motor learning[39,40,41]. However, neither parallel fiber LTD nor LTP were impaired in *PC-Δγ2* mice. Notably, the motor learning deficits in *PC-Δγ2* mice differed from those seen in mouse lines in which LTD was impaired by blocking PKC, PKG, or alpha-CaMKII activity in Purkinje cells. Furthermore, in the latter mouse lines acute learning was affected more severely than in *PC-Δγ2* mice, whereas learning over multiple days of training was less affected[39,40,41,42].

GABAergic interneurons in the cerebellar cortex have ample possibilities to induce and express plasticity at both the synaptic input and output level[1,9,13,43,44,45]. Simultaneous induction of LTP at molecular layer interneuron and parallel fiber to Purkinje cell synapses is required for associative fear conditioning[9]. In this scenario, the potentiation of GABAergic synapses may balance the LTP of excitatory inputs in a form of scaling to preserve coincidence detection of parallel fiber inputs[7,9]. Loss of this scaling mechanism in *PC-Δγ2* mice might contribute to the observed phenotype.

Inhibition is essential for spike patterning and learning

Although *PC-Δγ2* mice showed marked deficits in cerebellar motor learning, baseline motor performance was only moderately affected. Despite the lack of synaptic GABAA receptors on *PC-Δγ2* Purkinje cells we found their average simple spike frequency to be normal. This could reflect enhancement of another inhibitory input (e.g. GABAB receptors) and/or reduced parallel fiber excitatory input. Whereas GABAB receptor-mediated inhibition of *PC-Δγ2* Purkinje cells was unchanged (see Supplementary Fig. 10 in the online article), we found a significant decrease in AMPA receptormediated EPSC charge transfer after parallel fiber stimulation (see Supplementary Fig. 4 in the online article). This might allow Purkinje cells to maintain their excitability in a normal operational range in the absence of fast inhibition. By contrast, the loss of temporal fidelity in Purkinje cell responses to parallel fiber stimulation and the increase in simple spike regularity in *PC-Δγ2* mice, were comparable to the changes seen after acute pharmacological blockade of GABAA receptors[7,12] (**Figs. 3 and 5**). The cerebellum may thus compensate for the loss of certain functions of molecular layer interneurons, but these interneurons are essential for the temporal control of Purkinje cell activity and for both phase adaptation learning and consolidation of gain adaptations.

Purkinje cell collaterals

By deleting synaptic GABAA receptors from Purkinje cells in *PC-Δγ2* mice we also disrupted any inhibition mediated by recurrent collaterals of Purkinje cell axons[10,46]. However, as GABAergic terminals from basket and stellate cells onto Purkinje cells vastly outnumber those from recurrent collaterals, and as Purkinje-Purkinje contacts in mice appear restricted to young animals[46], the phenotype we observe is most likely caused by the loss of inhibition from molecular layer interneurons. Although it has been proposed that Purkinje cell axon collaterals contribute to fast cerebellar oscillations in adult rats[47], such oscillations have not been recorded in wild-type mice[10].

General functional implications

Studies on learning and memory have focused largely on the role of plasticity at excitatory synapses onto projecting neurons. However, GABAergic interneurons also express plasticity, which increases the computational capacity of their microcircuit[1,2,9]. Here we examined the role of fast synaptic inhibition in cerebellar motor learning using genetic dissection of the circuit and suggest that feed-forward inhibition is essential for specific aspects of procedural learning. Can our findings be extrapolated to other brain regions? Feed-forward inhibition is a common motif throughout the CNS. In the amygdala it mediates extinction learning of conditioned fear responses[48]. In cortical circuits some interneuron types may serve functions similar to those we have identified in the cerebellum. For example, feed-forward inhibitory interneurons in the hippocampus may promote the temporal fidelity of synaptic integration and action potential generation in pyramidal cells necessary for encoding declarative memories[2,3]. Thus, feedforward inhibition might be an operational necessity for memory formation in different brain circuits.

References

1. Smith SL, Otis TS. Pattern-dependent, simultaneous plasticity differentially transforms the inputoutput relationship of a feedforward circuit. *Proceedings of the National Academy of Sciences of the United States of America* 2005;102:14901–14906.
2. Kullmann DM, Lamsa KP. Long-term synaptic plasticity in hippocampal interneurons. *Nature reviews* 2007;8:687–699.
3. Pouille, F.; Scanziani, M. *Science.* Vol. 293. New York, N.Y: 2001. Enforcement of temporal fidelity in pyramidal cells by somatic feed-forward inhibition; p. 1159-1163.
4. Lamsa K, Heeroma JH, Kullmann DM. Hebbian LTP in feed-forward inhibitory interneurons and the temporal fidelity of input discrimination. *Nature neuroscience* 2005;8:916–924.
5. Eccles, JC.; Ito, M.; Szentagothai, J. The cerebellum as a neuronal machine. springer; 1967.
6. Miyashita Y, Nagao S. Contribution of cerebellar intracortical inhibition to Purkinje cell response during vestibulo-ocular reflex of alert rabbits. *The Journal of physiology* 1984;351:251–262.
7. Mittmann W, Koch U, Hausser M. Feed-forward inhibition shapes the spike output of cerebellar Purkinje cells. *The Journal of physiology* 2005;563:369–378.
8. Barmack NH, Yakhnitsa V. Functions of interneurons in mouse cerebellum. *J Neurosci* 2008;28:1140–1152.
9. Scelfo B, Sacchetti B, Strata P. Learning-related long-term potentiation of inhibitory synapses in the cerebellar cortex. *Proceedings of the National Academy of Sciences of the United States of America* 2008;105:769–774.
10. Orduz D, Llano I. Recurrent axon collaterals underlie facilitating synapses between cerebellar Purkinje cells. *Proceedings of the National Academy of Sciences of the United States of America* 2007;104:17831–17836.
11. Davie JT, Clark BA, Hausser M. The origin of the complex spike in cerebellar Purkinje cells. *J Neurosci* 2008;28:7599–7609.
12. Hausser M, Clark BA. Tonic synaptic inhibition modulates neuronal output pattern and spatiotemporal synaptic integration. *Neuron* 1997;19:665–678.

13. Jorntell H, Ekerot CF. Reciprocal bidirectional plasticity of parallel fiber receptive fields in cerebellar Purkinje cells and their afferent interneurons. *Neuron* 2002;34:797–806.
14. Santamaria F, Tripp PG, Bower JM. Feedforward inhibition controls the spread of granule cellinduced Purkinje cell activity in the cerebellar cortex. *Journal of neurophysiology* 2007;97:248–263.
15. Raman IM, Bean BP. Resurgent sodium current and action potential formation in dissociated cerebellar Purkinje neurons. *J Neurosci* 1997;17:4517–4526.
16. Wulff P, et al. From synapse to behavior: rapid modulation of defined neuronal types with engineered GABAA receptors. Nature neuroscience 2007;10:923–929.
17. Schweizer C, et al. The gamma 2 subunit of GABA(A) receptors is required for maintenance of receptors at mature synapses. *Molecular and cellular neurosciences* 2003;24:442–450.
18. Barski JJ, Dethleffsen K, Meyer M. Cre recombinase expression in cerebellar Purkinje cells. *Genesis* 2000;28:93–98.
19. Brickley SG, Cull-Candy SG, Farrant M. Single-channel properties of synaptic and extrasynaptic GABAA receptors suggest differential targeting of receptor subtypes. *J Neurosci* 1999;19:2960–2973.
20. Lorez M, Benke D, Luscher B, Mohler H, Benson JA. Single-channel properties of neuronal GABAA receptors from mice lacking the gamma2 subunit. *The Journal of physiology* 2000;527(Pt 1):11–31.
21. Brunel N, Hakim V, Isope P, Nadal JP, Barbour B. Optimal information storage and the distribution of synaptic weights: perceptron versus Purkinje cell. *Neuron* 2004;43:745–757.
22. Shin SL, et al. Regular patterns in cerebellar Purkinje cell simple spike trains. *PLoS ONE* 2007;2:e485.
23. Walter JT, Alvina K, Womack MD, Chevez C, Khodakhah K. Decreases in the precision of Purkinje cell pacemaking cause cerebellar dysfunction and ataxia. *Nature neuroscience* 2006;9:389–397.
24. Ito M. Cerebellar flocculus hypothesis [letter]. *Nature* 1993;363:24–25.
25. Lisberger SG. Cerebellar LTD: A molecular mechanism of behavioral learning? *Cell* 1998;92:701–704.
26. Schonewille M, et al. Zonal organization of the mouse flocculus: physiology, input, and output. *The Journal of comparative neurology* 2006;497:670–682.
27. Hoebeek FE, et al. Increased noise level of purkinje cell activities minimizes impact of Their modulation during sensorimotor control. *Neuron* 2005;45:953–965.
28. Gittis AH, du Lac S. Intrinsic and synaptic plasticity in the vestibular system. *Current opinion in neurobiology* 2006;16:385–390.
29. Kassardjian CD, et al. The site of a motor memory shifts with consolidation. *J Neurosci* 2005;25:7979–7985.
30. Medina JF, Mauk MD. Computer simulation of cerebellar information processing. *Nature* neuroscience 2000;3(Suppl):1205–1211.
31. Medina JF, Nores WL, Mauk MD. Inhibition of climbing fibres is a signal for the extinction of conditioned eyelid responses. *Nature* 2002;416:330–333.
32. Shutoh F, Ohki M, Kitazawa H, Itohara S, Nagao S. Memory trace of motor learning shifts transsynaptically from cerebellar cortex to nuclei for consolidation. *Neuroscience* 2006;139:767–777.
33. Coesmans M, Weber JT, De Zeeuw CI, Hansel C. Bidirectional parallel fiber plasticity in the cerebellum under climbing fiber control. *Neuron* 2004;44:691–700.

34. Mann-Metzer P, Yarom Y. Electrotonic coupling interacts with intrinsic properties to generate synchronized activity in cerebellar networks of inhibitory interneurons. *J Neurosci* 1999;19:3298–3306.
35. Van Der Giessen RS, Maxeiner S, French PJ, Willecke K, De Zeeuw CI. Spatiotemporal Distribution of Connexin45 in the olivocerebellar system. *The Journal of comparative neurology* 2006;495:173–184.
36. Steuber V, et al. Cerebellar LTD and pattern recognition by Purkinje cells. *Neuron* 2007;54:121–136.
37. Blazquez PM, Hirata Y, Highstein SM. Chronic changes in inputs to dorsal Y neurons accompany VOR motor learning. *Journal of neurophysiology* 2006;95:1812–1825.
38. Medina JF, Lisberger SG. Links from complex spikes to local plasticity and motor learning in the cerebellum of awake-behaving monkeys. *Nature neuroscience* 2008;11:1185–1192.
39. De Zeeuw CI, et al. Expression of a protein kinase C inhibitor in Purkinje cells blocks cerebellar LTD and adaptation of the vestibulo-ocular reflex. *Neuron* 1998;20:495–508.
40. Feil R, et al. Impairment of LTD and cerebellar learning by Purkinje cell-specific ablation of cGMPdependent protein kinase I. *J Cell Biol* 2003;163:295–302.
41. Hansel C, et al. alphaCaMKII Is essential for cerebellar LTD and motor learning. *Neuron* 2006;51:835–843.
42. Boyden ES, et al. Selective engagement of plasticity mechanisms for motor memory storage. *Neuron* 2006;51:823–834.
43. Kano M, Rexhausen U, Dreessen J, Konnerth A. Synaptic excitation produces a long-lasting rebound potentiation of inhibitory synaptic signals in cerebellar Purkinje cells. *Nature* 1992;356:601–604.
44. Duguid IC, Smart TG. Retrograde activation of presynaptic NMDA receptors enhances GABA release at cerebellar interneuron-Purkinje cell synapses. *Nature neuroscience* 2004;7:525–533.
45. Mittmann W, Hausser M. Linking synaptic plasticity and spike output at excitatory and inhibitory synapses onto cerebellar Purkinje cells. *J Neurosci* 2007;27:5559–5570.
46. Watt AJ, et al. Traveling waves in developing cerebellar cortex mediated by asymmetrical Purkinje cell connectivity. *Nature neuroscience* 2009;12:463–473.
47. de Solages C, et al. High-frequency organization and synchrony of activity in the purkinje cell layerof the cerebellum. *Neuron* 2008;58:775–788.
48. Likhtik E, Popa D, Apergis-Schoute J, Fidacaro GA, Pare D. Amygdala intercalated neurons are required for expression of fear extinction. *Nature* 2008;454:642–645.

Chapter 6

The role of CaMKII in plasticity at the excitatory and inhibitory cerebellar synapses

Section 6.1

βCaMKII controls the direction of plasticity at parallel fiber – Purkinje cell synapses

Nature Neurosci. 2009 July;12(7):823-5

Geeske M. van Woerden, Freek E. Hoebeek, Zhenyu Gao, Raghavendra Y. Nagaraja, Casper C. Hoogenraad, Steven A. Kushner, Christian Hansel, Chris I. De Zeeuw and Ype Elgersma

Abstract

Here we show that βCaMKII, the predominant CaMKII isoform of the cerebellum, plays an essential role in controlling the direction of plasticity at the parallel fiber–Purkinje cell synapse: a protocol that induces synaptic depression in wild–type mice, results in synaptic potentiation in βCaMKII knock–out mice, and *vice versa.* These findings provide us with unique experimental insight into the mechanisms that transduce graded calcium signals into either synaptic depression or potentiation.

The ability to strengthen and weaken synaptic connections is essential for memory formation. According to the Bienenstock, Cooper, and Munro model of synaptic plasticity, the magnitude and direction of synaptic weight changes is not only affected by the temporal pattern of calcium influx, but also by the ability of the synapse to change the modification threshold for synaptic depression and potentiation (Bienenstock et al., 1982). However, the precise mechanisms by which a synapse controls the direction of synaptic weight change are still poorly understood.

Calcium–calmodulin dependent kinase type II (CaMKII) plays an essential role in transducing neuronal calcium signals. The CaMKII holoenzyme is a heteromeric protein complex, composed of a cell–type dependent ratio of αCaMKII to βCaMKII isoforms. In the adult hippocampus and neocortex, aCaMKII is the predominant isoform (Erondu and Kennedy, 1985), where its quantity and autophosphorylation status determine the amplitude and induction threshold of long–term potentiation (LTP) (Silva et al., 1992; Giese et al., 1998; Elgersma et al., 2002). In contrast, αCaMKII is required for long–term depression (LTD), but not LTP, at cerebellar parallel fiber–Purkinje cell synapses (Hansel et al., 2006). Notably, although βCaMKII is the most prominent cerebellar isoform (Erondu and Kennedy, 1985), the function of βCaMKII at this synapse is unknown. In addition, although *in vitro* studies show that changes in the α– to βCaMKII ratio have opposing effects on unitary synaptic strength (Thiagarajan et al., 2002), it is unknown to what extent changes in the subunit ratio would affect synaptic plasticity *in vivo*.

To elucidate the role of βCaMKII in synaptic plasticity, we generated a βCaMKII knock–out mouse by inserting the neomycin resistance gene in the βCaMKII regulatory domain at exon 11 (Supplementary Fig. 1). *In situ* hybridization and semi–quantitative RT–PCR analysis of these mice showed loss of full–length βCaMKII mRNA (**Fig. 1** and **Supplementary Fig. 2**). In addition, immunostaining and Western blot analysis revealed a total loss of βCaMKII immunoreactivity and no presence of a truncated βCaMKII protein in these mutants (**Fig. 1c**,**e**). The loss of bCaMKII did not cause up–regulation of βCaMKII mRNA or protein (**Fig. 1b** and **Supplementary Fig. 2**). Consequently, total CaMKII activity was significantly reduced, in particular in the cerebellum where βCaMKII is the predominant CaMKII isoform (reduction of 51% ($P<0.0001$) for Ca^{2+}/CaM–dependent activity and 41% ($P<0.005$) for Ca^{2+}/CaM–independent activity; **Supplementary Fig. 1b**), altogether suggesting a successful knock–out of the *βCaMKII* gene.

Even though adult *βCaMKII*$^{-/-}$ mice showed no differences in survival (measured

from weaning till 8 months of age) or general health, they showed pronounced ataxia (**Supplementary Movie 1**), and a severe deficit on the accelerating rotarod test and balance beam test **(Fig. 1g**, **Supplementary Fig. 3**). Ataxia commonly arises from cerebellar dysfunction, and is often observed in mutants with immature or degenerated Purkinje cells. However, Thionin staining of brain slices from adult mice revealed no gross differences in overall brain development between wild–type mice and *βCaMKII*$^{-/-}$ mutants at the light microscopy level (**Fig. 1a**). Moreover, Purkinje cells of *βCaMKII*$^{-/-}$ mutants did not show significant changes in the complexity of dendritic branching, and the density of spines, nor in Purkinje cell spine maturity (spine neck length and head width), indicating that the loss of βCaMKII does not affect gross brain development or the maturation of Purkinje cells *in vivo* (**Fig. 1f**, **Supplementary Fig. 4**).

Purkinje cells are the sole output of the cerebellar cortex, and plasticity at the parallel fiber–Purkinje cell synapse is generally believed to be required for cerebellar motor learning. To investigate the role of βCaMKII in parallel fiber–Purkinje cell plasticity, we performed *in vitro* whole–cell recordings of Purkinje cells from adult wild–type and *βCaMKII*$^{-/-}$ mice. The ability to induce LTD was tested by paired parallel fiber and climbing fiber stimulation at 1Hz for 5 minutes (Coesmans et al., 2004; Tanaka et al., 2007). This stimulation protocol indeed resulted in significant LTD in wild–type mice (83 ± 5%; $P < 0.01$), but failed to induce LTD in *βCaMKII*$^{-/-}$ mice. In fact, it resulted in significant LTP (112 ± 3%; $P< 0.01$) in these mutants (**Fig. 2a**), similar to what has been reported previously for *αCaMKII*$^{-/-}$ mice (Hansel et al., 2006). These results suggest that a critical amount of both αCaMKII and βCaMKII is required for the induction of cerebellar LTD.

We next tested the role of βCaMKII in cerebellar LTP, by applying the same parallel fiber stimulus, but now in the absence of climbing fiber stimulation (Lev-Ram et al., 2002). This postsynaptic form of LTP requires lower calcium transients than LTD induction (Lev-Ram et al., 2002; Coesmans et al., 2004). Using this protocol, we indeed obtained significant LTP in wild–type Purkinje cells (120 ± 3%; $P< 0.001$), but surprisingly *βCaMKII*$^{-/-}$ Purkinje cells now showed robust LTD (84 ± 4%; $P< 0.01$; **Fig. 2b**). To our knowledge, this is the first report of a genetic or pharmacological manipulation that bidirectionally inverts the polarity of changes in synaptic strength.

Even though the plasticity induced by the protocols described above is known to be expressed postsynaptically (Lev-Ram et al., 2002; Coesmans et al., 2004; Belmeguenai and Hansel, 2005; Kakegawa and Yuzaki, 2005), the observed changes in synaptic plasticity could potentially result from additional presynaptic changes. However, *βCaMKII*$^{-/-}$ mutants showed no difference in basal excitatory synaptic transmission and the Purkinje cells showed innervation by a single climbing fiber (**Supplementary Fig. 5**, **6**), suggesting that the bidirectional inversion of parallel fiber–Purkinje cell plasticity is indeed caused by changes in postsynaptic plasticity.

To better understand how the loss of βCaMKII can result in a bidirectional inversion of plasticity at the parallel fiber–Purkinje cell synapse, we propose the following plasticity rules that collectively provide a model which fully accounts for the observed data: First, the synaptic depression and potentiation pathways are independent competing processes driven

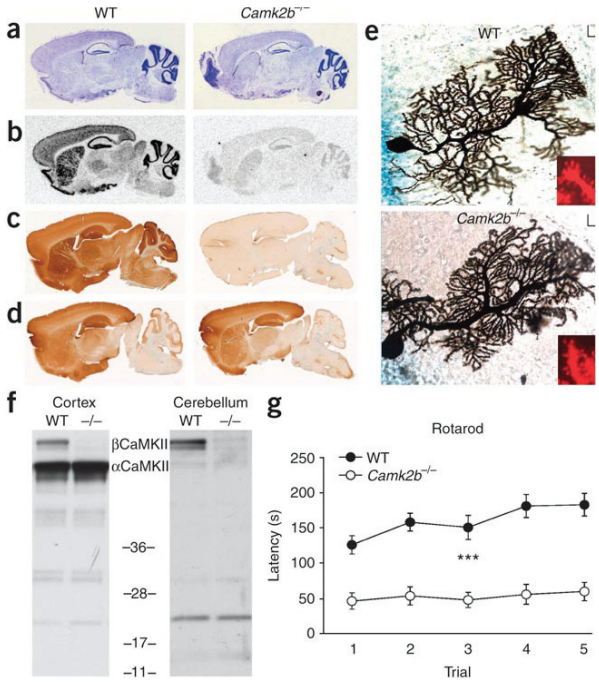

Fig. 1. Basal characterization of the *βCaMKII*$^{-/-}$ mutant

a, Thionin staining shows no apparent morphological changes in βCaMKII$^{-/-}$ brains. **b**, *In situ* analysis shows decreased levels of 3' UTR βCaMKII mRNA in *βCaMKII*$^{-/-}$ mutant mice, indicating a successful gene disruption. **c**,**d**, Immunocytochemistry using α– and βCaMKII–isoform specific antibodies, shows complete loss of βCaMKII immunoreactivity in *βCaMKII*$^{-/-}$ brains (**c**) which is not compensated by up–regulation of αCaMKII immunoreactivity (**d**). **e**, Western blot analysis of wild–type and mutant cortex and cerebellum using a N–terminal pan–CaMKII antibody revels no truncated βCaMKII product in *βCaMKII*$^{-/-}$ mutants. **f**, Analysis of Purkinje cell morphology using Golgi–Cox staining and diOlistic labeling (inlay), showed no differences in arborization and spine density, neck length and width (see for quantification **Supplementary Fig. 4**). **g**, Motor performance assessed by an accelerating rotarod. *βCaMKII*$^{-/-}$ mice (n=16) stay on the rod significantly shorter than wild–type littermates (n=16) and do not increase their performance upon training (effect of genotype: $P<0.005$; interaction training x genotype $P<0.05$; Repeated measures ANOVA). Depicted is the latency until the mice fell from the rod.

by kinases and phosphatases, respectively (Lev-Ram et al., 2002; Coesmans et al., 2004; Belmeguenai and Hansel, 2005), each regulated by a distinct sensitivity for calcium. LTP is generated when phosphatase activity outweighs kinase activity, and LTD is generated when kinase activity outweighs phosphatase activity (schematically depicted in **Fig. 2c**, **Supplementary Fig. 7**). Second, since LTP induction is not affected by deleting the αCaMKII gene (Hansel et al., 2006), nor by inhibition of CaMKII kinase activity(Kakegawa and Yuzaki, 2005), we assume that the basic molecular mechanism driving the synaptic potentiation pathway is entirely independent of CaMKII kinase activity. In contrast, activity of both αCaMKII and βCaMKII is contributing to the synaptic depression pathway (**Fig. 2c**, **Supplementary Fig. 7**). Hence, loss of either αCaMKII or βCaMKII selectively decreases the depression driving force, and patterns of stimulation that normally produce LTD, will therefore yield LTP in the *αCaMKII*$^{-/-}$ mutant (Hansel et al., 2006) or *βCaMKII*$^{-/-}$ mutant (**Fig. 2a**). Consequently, we predicted that blocking the opposing potentiation pathway, by inhibiting calcium sensitive phosphatase PP2B (calcineurin) activity (Belmeguenai and Hansel, 2005), should restore LTD induction in the *βCaMKII*$^{-/-}$ mutant. Indeed, the presence of cyclosporin A during an LTD inducing protocol, yielded a significant induction of LTD in the *βCaMKII*$^{-/-}$ mutant (**Fig. 2d**). This indicates that the PP2B–driven synaptic potentiation pathway is in direct competition with the CaMKII–driven synaptic depression pathway, and that loss of bCaMKII activity can be compensated by inactivating PP2B activity.

Although the aforementioned plasticity rules readily explain the shift from LTD to LTP as seen in the *αCaMKII*$^{-/-}$(Hansel et al., 2006) and *βCaMKII*$^{-/-}$ mutants, they are not sufficient to explain why an LTP inducing protocol results in LTD in *βCaMKII*$^{-/-}$ mutants. An inversion of the plasticity curve as observed in the *βCaMKII*$^{-/-}$ mutant, can be achieved only if the depression driving force in *βCaMKII*$^{-/-}$ mutants is shifted to the left (indicated in

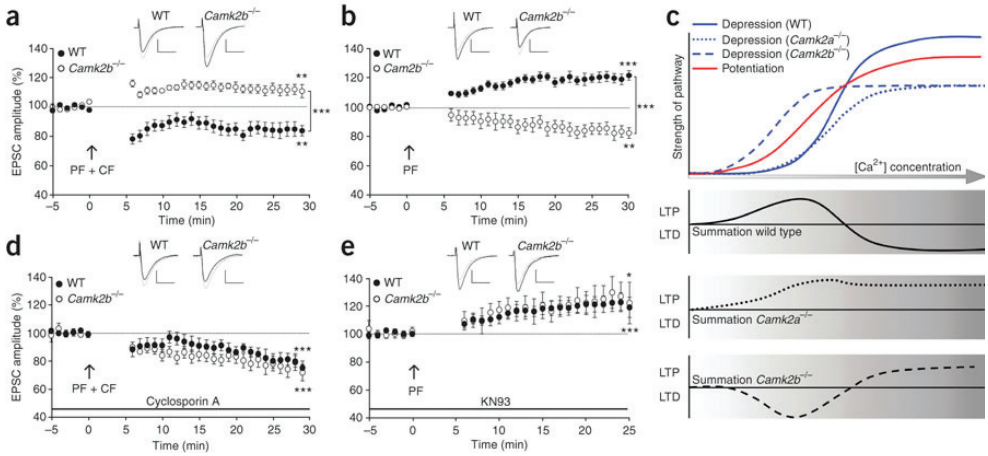

Fig. 2 Bidirectional inversion of plasticity at the parallel fiber–Purkinje cell synapse. a, Paired parallel fiber and climbing fiber stimulation yields LTD in wild–type (n=12) cells but LTP in *βCaMKII*$^{-/-}$ (n=11) cells. **b**, Parallel fiber stimulation only, results in LTP in wild–type (n=11) cells but yields LTD in *βCaMKII*$^{-/-}$ (n=13) cells. **c**, Schematic model, visualizing how changes in the CaMKII driven depression pathway (top) can result in the different plasticity curves as observed in wild–type, *αCaMKII*$^{-/-}$ and *βCaMKII*$^{-/-}$ mice (bottom). The model illustrates that a reduced strength of the kinase driven depression pathway ('down–shift'), combined with a reduced threshold for calcium activation ('left–shift') results in an inversion of the plasticity curve in *βCaMKII*$^{-/-}$ mice. **d**, LTD is rescued in *βCaMKII*$^{-/-}$slices in the presence of PP2B inhibitor Cyclosporin A (wild–type: n=6; *βCaMKII*$^{-/-}$: n=13). **e**, LTP is rescued in *βCaMKII*$^{-/-}$slices using the CaMKII inhibitor KN93 (wild–type: n=12; bCaMKII$^{-/-}$: n=7). Insets show representative traces before (solid line) and after (dashed line) tetanization (scale bars 100pA/10ms). Error bars represent SEM. Asterisks with brackets indicate statistical significance between wild–type and mutant slices (Student's *t*–test over last 5 min). Asterisks without brackets indicate significant difference from baseline (paired *t*–test). **P*<0.05; ***P*<0.01; ****P*<0.005.

Fig. 2c), reflecting a lower threshold for activation of this pathway. As αCaMKII is a major driver of the depression pathway (Hansel et al., 2006), this model would predict that activation of αCaMKII is facilitated in the *βCaMKII*$^{-/-}$ mutant, leading to precocious induction of the LTD pathway under low calcium conditions. If this is true, a strong but counter–intuitive prediction can be made: the presence of a CaMKII inhibitor under LTP inducing conditions should rescue the LTP deficits in the *βCaMKII*$^{-/-}$ mutant (**Fig. 2c**, **Supplementary Fig. 7**). This was indeed the case: addition of the CaMKII inhibitor KN93 restored LTP in *βCaMKII*$^{-/-}$slices to wild–type levels (**Fig. 2e**). These results confirm that the induction of the LTD pathway under low calcium conditions in the *βCaMKII*$^{-/-}$ mutant is indeed caused by the inadvertent activation of aCaMKII.

What could be the cause of the reduced threshold of αCaMKII activation in *βCaMKII*$^{-/-}$ mutants? Notably, the reduced threshold for αCaMKII activation is not caused by increased expression of αCaMKII (**Fig. 1**, **Supplementary Fig. 8**). In addition, there is not a strong increase in basal levels of autonomously activated αCaMKII, as the reduction of calcium–dependent activity was not significantly different from the reduction of calcium–independent activity (*P*= 0.5), and no increase in T286P–αCaMKII was observed (**Supplementary Fig.1, 8**). Moreover, the competitive KN93 inhibitor, which rescued the LTP deficit, cannot inhibit αCaMKII if it is already in the autonomously active state, arguing strongly against high basal levels of autonomously active αCaMKII in *βCaMKII*$^{-/-}$ mutants.

A more likely explanation comes from the biochemical differences between αCaMKII and βCaMKII. βCaMKII contains an additional domain which enables βCaMKII to cluster the entire CaMKII holoenzyme to F–actin(Shen et al., 1998; Shen and Meyer, 1999; Okamoto et al., 2007). Since all cerebellar αCaMKII is associated with βCaMKII in wild–type mice (**Supplementary Fig. 8**), the loss of βCaMKII will cause a loss of αCaMKII clustering to F–actin, potentially increasing the availability of CaMKII holoenzymes(Shen et al., 1998; Shen and Meyer, 1999). In addition, elegant *in vitro* experiments showed that translocation to the PSD is 4 times shorter for αCaMKII homo–oligomers as compared to mixed αCaMKII/βCaMKII hetero–oligomers, and even 24 times shorter as compared to βCaMKII homo–oligomers (Shen and Meyer, 1999). Such a substantial reduction in the translocation rate of CaMKII holoenzymes could well explain the reduced threshold for CaMKII activation in the *βCaMKII*$^{-/-}$ mutants.

Taken together, we show that βCaMKII is not an essential gene for overall brain development or Purkinje cell maturation, but rather plays an essential role in motor coordination and cerebellar plasticity. Although we cannot rule out that these defects are potentially caused by developmental changes, the observation that we can rescue both the LTD and LTP deficits by pharmacology, suggest a direct role of βCaMKII in regulating bidirectional synaptic plasticity at the parallel fiber–Purkinje cell synapse. Specifically, we show that parallel fiber–Purkinje cell plasticity is regulated by a balanced and integrated coordination of kinase and phosphatase activity, and that βCaMKII modulates the polarity of synaptic plasticity by two functionally distinct roles. Like αCaMKII (Hansel et al., 2006), βCaMKII activity is required for driving the synaptic depression pathway under high calcium conditions. However under low calcium conditions, βCaMKII prevents activation of this pathway. Overall, these findings provide us with a unique insight in the molecular mechanisms governing the rules for bidirectional synaptic plasticity.

References

Belmeguenai A, Hansel C (2005) A role for protein phosphatases 1, 2A, and 2B in cerebellar long-term potentiation. J Neurosci 25:10768-10772.

Bienenstock EL, Cooper LN, Munro PW (1982) Theory for the development of neuron selectivity: orientation specificity and binocular interaction in visual cortex. J Neurosci 2:32-48.

Coesmans M, Weber JT, De Zeeuw CI, Hansel C (2004) Bidirectional parallel fiber plasticity in the cerebellum under climbing fiber control. Neuron 44:691-700.

Elgersma Y, Fedorov NB, Ikonen S, Choi ES, Elgersma M, Carvalho OM, Giese KP, Silva AJ (2002) Inhibitory autophosphorylation of CaMKII controls PSD association, plasticity, and learning. Neuron 36:493-505.

Erondu NE, Kennedy MB (1985) Regional distribution of type II Ca2+/calmodulin-dependent protein kinase in rat brain. J Neurosci 5:3270-3277.

Giese KP, Fedorov NB, Filipkowski RK, Silva AJ (1998) Autophosphorylation at Thr286 of the α calcium-calmodulin kinase II in LTP and learning. Science 279:870-873.

Hansel C, de Jeu M, Belmeguenai A, Houtman SH, Buitendijk GH, Andreev D, De Zeeuw

CI, Elgersma Y (2006) alphaCaMKII Is essential for cerebellar LTD and motor learning. Neuron 51:835-843.

Kakegawa W, Yuzaki M (2005) A mechanism underlying AMPA receptor trafficking during cerebellar long-term potentiation. Proc Natl Acad Sci U S A 102:17846-17851.

Lev-Ram V, Wong ST, Storm DR, Tsien RY (2002) A new form of cerebellar long-term potentiation is postsynaptic and depends on nitric oxide but not cAMP. Proc Natl Acad Sci U S A 99:8389-8393.

Okamoto K, Narayanan R, Lee SH, Murata K, Hayashi Y (2007) The role of CaMKII as an F-actin-bundling protein crucial for maintenance of dendritic spine structure. Proc Natl Acad Sci U S A 104:6418-6423.

Shen K, Meyer T (1999) Dynamic control of CaMKII translocation and localization in hippocampal neurons by NMDA receptor stimulation. Science 284:162-166.

Shen K, Teruel MN, Subramanian K, Meyer T (1998) CaMKIIbeta functions as an F-actin targeting module that localizes CaMKIIalpha/beta heterooligomers to dendritic spines. Neuron 21:593-606.

Silva AJ, Stevens CF, Tonegawa S, Wang Y (1992) Deficient hippocampal long-term potentiation in alpha-calcium- calmodulin kinase II mutant mice. Science 257:201-206.

Tanaka K, Khiroug L, Santamaria F, Doi T, Ogasawara H, Ellis-Davies GC, Kawato M, Augustine GJ (2007) Ca2+ requirements for cerebellar long-term synaptic depression: role for a postsynaptic leaky integrator. Neuron 54:787-800.

Thiagarajan TC, Piedras-Renteria ES, Tsien RW (2002) alpha- and betaCaMKII. Inverse regulation by neuronal activity and opposing effects on synaptic strength. Neuron 36:1103-1114.

Supplementary figures and legends

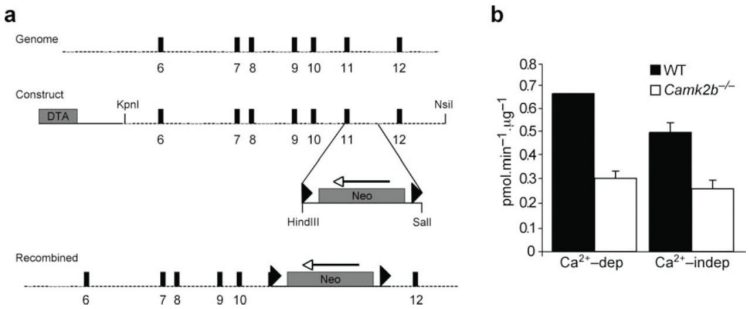

Supplementary Fig 1. Generation of the *Camk2b*$^{-/-}$ mutant mice.

a, Strategy to generate the *Camk2b*$^{-/-}$ mutant mice. (Top) Wild-type *Camk2b* locus with the location of exons 6-12 depicted as black boxes. (Middle) Targeting construct used for generation of *Camk2b*$^{-/-}$ mutant mice with the gene encoding the Diphteria Toxin A chain (DTA) outside the homologous recombination sites and the Neomycin resistance gene (NEO) inserted in exon 11. Shown are the restriction sites used for insertion of the *NEO* gene and the NsiI site used to linearize the targeting construct. (Bottom) Mutant *Camk2b* locus after homologous recombination. **b**, Ca^{2+}-dependent and Ca^{2+}-independent CaMKII activity are significantly ($P<0.0001$;$P<0.005$ respectively) reduced in the cerebellum of *Camk2b*$^{-/-}$ mutant mice (n=5) as compared to wild-type mice (n=5).

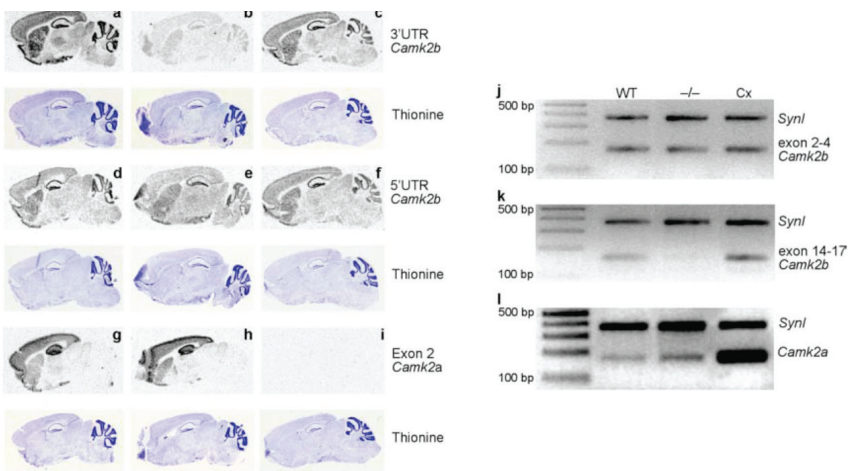

Supplementary Fig. 2. *In situ* hybridization and RT-PCR analysis of *Camk2b* and *Camk2a* mRNA in mutant and wild-type mice.

a-I, *In situ* hybridization of *Camk2a* and *Camk2b* mRNA in wild-type (left panels), *Camk2b*$^{-/-}$ (middle panels), and *Camk2a*$^{-/-}$ mice (right panels). Thionin staining (blue stained slices) was performed after the *in situ* hybridization to investigate brain morphology. **a-f**, *In situ* hybridization shows that *Camk2b* mRNA is highly abundant in cerebellum, cortex, hippocampus and striatum of wild-type mice. *Camk2b*$^{-/-}$ mutant mice show decreased levels of 3' UTR *Camk2b* mRNA **(b)** but normal levels of 5' UTR *Camk2b* mRNA in *Camk2b*$^{-/-}$ mice **(e)**, suggesting a successful truncation of the gene. **g-i**, *Camk2a* mRNA level is not affected in *Camk2b*$^{-/-}$ mutant mice. **j-l**, semi-quantitative RT-PCR analysis shows normal *Camk2a* mRNA levels but strongly reduced 3' (exon 14-17) *Camk2b* mRNA levels in the cerebellum of *Camk2b*$^{-/-}$ mutant mice. PCR primers were directed against exon 2-4 **(j)** and exon 14-17 **(k)** of *Camk2b* (which are up- or downstream of the inserted *NEO* gene, respectively) and directed against exon 2-5 of the *Camk2a* gene **(i).** As a quantitative control, primers against *Synapsin I* mRNA were included. The 'Cx' lane is a RT-PCR on the same amount of mRNA (0.3 µg) derived from wild-type cortical tissue. To assure that the PCR conditions were in the linear range, a serial dilution was performed on all samples (not shown).

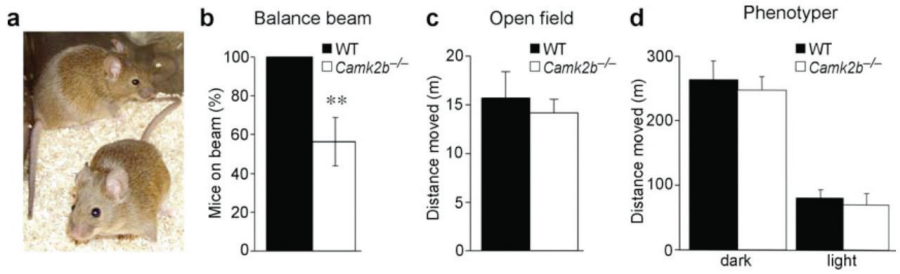

Supplementary Fig. 3. Assessment of general locomotion deficits of *Camk2b*$^{-/-}$ mutant mice.

a, *Camk2b*$^{-/-}$ mutants (front) are viable and healthy. The mouse in the back is a littermate wild-type mouse (age 4 months). But despite their healthy appearance, *Camk2b*$^{-/-}$ mutants show signs of cerebellar ataxia (see **Supplementary Movie**). **b**, Balance beam test. Indicated is the number of mice that were able to stay on a 1.5 cm thick square beam. All wild-type mice (n=16) were able to stay on the beam for 60 sec, whereas only 9/16 of the *Camk2b*$^{-/-}$ mutant mice could stay on the beam for one minute ($P<0.01$, paired t-test). Error bars are standard errors of the mean taken from binomial distribution. **c**,**d**, The balance beam and rotarod deficits are not caused by a lack of desire to move, as *Camk2b*$^{-/-}$ mice move a similar distance as wild-type mice in the open-field **(b)** (n=5/5; $P=0.6$) and in an home cage-like environment (Phenotyper, Noldus Information Technology, The Netherlands) **(c)** (n=12/12; $P=0.7$ during dark phase, $P=0.6$ during light phase). Error bars represent standard error of the mean.

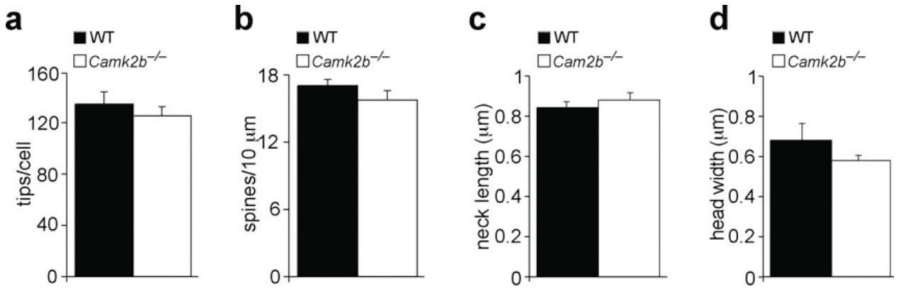

Supplementary Fig. 4. Assessment of cerebellar Purkinje cell morphology in *Camk2b*$^{-/-}$ mutant mice.

Quantification of the arborization (**a**) and number of spines (**b**) of Golgi-Cox stained Purkinje cells showed no significant differences between wild-type mice and mutants ($P=0.4$ and $P=0.2$, respectively). Arborization was determined by counting the number of tips per Purkinje cell and the number of spines per 10 mm dendrite. Quantification of the neck length (**c**) and head width (**d**) of Purkinje cell spines using diOlistic labeling also showed no significant differences (n=3/3; $P=0.5$ and $P=0.3$, respectively). Error bars represent standard error of the mean.

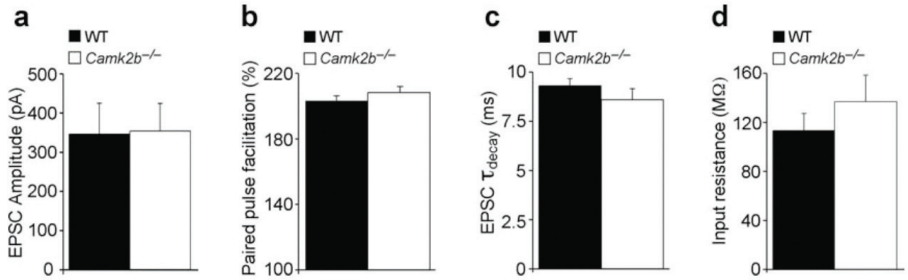

Supplementary Fig. 5. Parallel fiber-Purkinje cell transmission and basal properties of Purkinje cells are not significantly different in *Camk2b*$^{-/-}$ mutant mice.

a, *Camk2b*$^{-/-}$ Purkinje cells show a normal PF-EPSC amplitude ($P=0.9$; n=11 WT, n=9 *Camk2b*$^{-/-}$ mutants). **b**, *Camk2b*$^{-/-}$ Purkinje cells show normal paired pulse facilitation (50 ms inter-stimulus interval) ($P=0.3$; n=13 WT, n=13 *Camk2b*$^{-/-}$ mutants). **c**, *Camk2b*$^{-/-}$ Purkinje cells show normal t_{decay} (single-exponential fit) of the PF-EPSC ($P=0.3$; n=13 WT, n=10 *Camk2b*$^{-/-}$ mutants). **d**, *Camk2b*$^{-/-}$ Purkinje cells show normal average input resistance (calculated by a 10 mV hyperpolarizing voltage step; see supplementary methods) ($P=0.4$; n=9 WT, n=7 *Camk2b*$^{-/-}$ mutants). Error bars represent standard error of the mean.

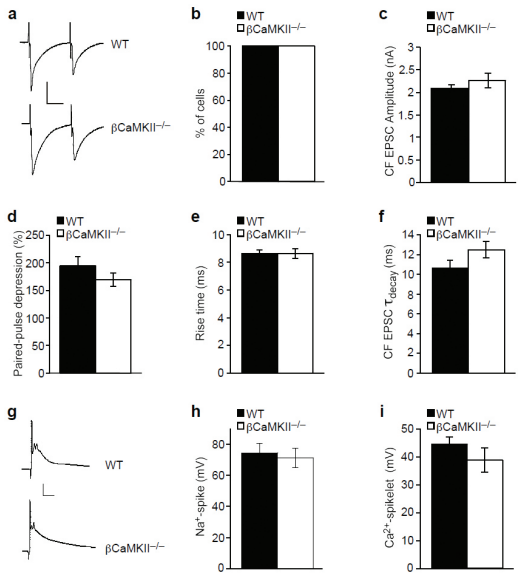

Supplementary Fig. 6. Climbing fiber-Purkinje cell synaptic transmission is normal in *Camk2b*$^{-/-}$ mutant mice.

a, Average trace of six double CF-EPSCs for wild-type (upper) and *Camk2b*$^{-/-}$ (lower) cells. Horizontal scale bar indicates 20 ms; vertical indicates 1 nA. **b**, All recorded Purkinje cells of both wild-type (n=10) and *Camk2b*$^{-/-}$ (n=13) mice showed absence of multiple climbing fiber innervation. Shown is the percentage of Purkinje cells with mono-climbing fiber innervation. **c**, *Camk2b*$^{-/-}$ Purkinje cells show normal CF-EPSC amplitudes (P=0.6; n=10 WT, n=13 *Camk2b*$^{-/-}$). **d**, *Camk2b*$^{-/-}$ Purkinje cells show normal paired-pulse depression of the CF-EPSCs at an inter-stimulus interval of 50 ms (P=0.2; n=10 WT, n=13 *Camk2b*$^{-/-}$). **e**, *Camk2b*$^{-/-}$ Purkinje cells show normal 10-90% rise times of the first CF-EPSC (P=1.0; n=10 WT, n=13 *Camk2b*$^{-/-}$). **f**, *Camk2b*$^{-/-}$ Purkinje cells show normal t_{decay} (single-exponential fit) of the first CF-EPSC (P=0.2; n=10 WT, n=13 *Camk2b*$^{-/-}$). **g**, Average trace of 20 CF-EPSPs for wild type (upper) and *Camk2b*$^{-/-}$ (lower). Horizontal scale bar indicates 20 ms; vertical indicates 20 mV **h**, *Camk2b*$^{-/-}$ Purkinje cells show normal amplitudes of Na^+-spikes in CF-EPSPs (P=0.7; n=7 WT, n=7 *Camk2b*$^{-/-}$). **i**, *Camk2b*$^{-/-}$ Purkinje cells show normal amplitudes of the first Ca^{2+}-spikelet in CF-EPSPs (P=0.3; n= 7 WT, n=7 *Camk2b*$^{-/-}$). Error bars represent standard error of the mean.

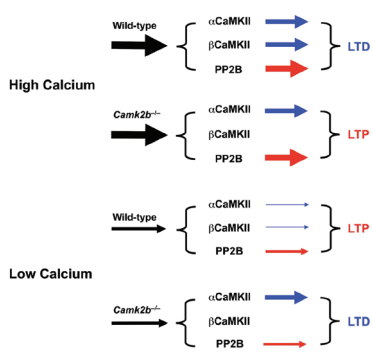

Supplementary Fig. 7. Role of CaMKII and PP2B in parallel fiber-Purkinje cell plasticity.

Simplified model depicting the role of αCaMKII, bCaMKII and phosphatase PP2B in LTP and LTD at the parallel fiber-Purkinje cell synapse. In wild-type Purkinje cells high calcium influx (top) activates the phosphatase PP2B driven synaptic potentiation pathway. In addition, it results in maximal induction of the CaMKII driven synaptic depression pathway, which effectively out-competes PP2B, leading to a net LTD. In contrast, in the absence of bCaMKII the synaptic depression pathway (which requires CaMKII *and* bCaMKII activity) is no longer able to out-compete PP2B, resulting in net LTP. Low calcium influx (bottom) only moderately activates PP2B, but as there is no or insignificant activation of CaMKII, the net result is LTP. In *Camk2b*$^{-/-}$ Purkinje cells, low calcium influx results in precocious activation of αCaMKII, which is sufficient to out-compete PP2B, resulting in net LTD.

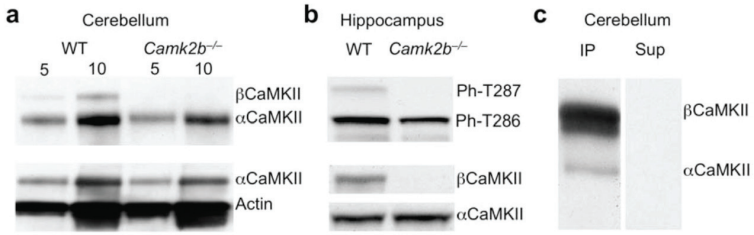

Supplementary Fig. 8. Neither αCaMKII protein level nor its autophosphoryation is increased in *Camk2b*$^{-/-}$ mutants.

a, Expression of αCaMKII protein is not increased in the cerebellum. If anything, there is a slight reduction at the protein level. Shown are Western blots of cerebellar lysates of 2 wild-type mice and 2 mutants; with 5 mg and 10 mg loaded of each sample. Blots were probed with a specific αCaMKII (Chemicon; clone 6G9) or bCaMKII (Zymed; clone CB-b1) antibody. **b**, The amount of Ph-T286-αCaMKII is not changed in the hippocampus of *Camk2b*$^{-/-}$ mutants. Ph-T286-αCaMKII could not be detected in the cerebellum, which is likely due to the 60-fold lower concentration of αCaMKII in cerebellar lysates (not shown). **c**, Immunoprecipitation using a bCaMKII-specific antibody, reveals that all αCaMKII is asscoiated with bCaMKII in the cerebellum of wild-type mice. IP: immunoprecipitated fraction; Sup: supernatant fraction after immunoprecipitation.

Supplementary Materials and Methods

Generation of Camk2b mutant mice

The *Camk2b* knock-out targeting construct was generated as follows. The *Camk2b* genomic sequence (ENSMUSG00000057897) was obtained from a public database (Ensembl) and used to design the primers for the targeting constructs. PCR fragments encompassing exon 6-11 (5.3 Kb; exon denotation according to ENSMUST00000019133) using:

5' primer: 5'-GGTACCTGAGGAAGGTGCCAGCTCTGTCCC-3' and 3' primer: 5'–TTATCGATTCTCCTGTCTGTGCATCATAGAGG-3' and exon 11-13 (6 Kb) using: 5' primer: 5'-GCGGCCGCCTGTTAAAGGAATGGTTCTC-3' and 3' primer: 5'-ATG-CATCTAAAAGGCAGGCAGGATGATCTGC-3' were amplified using High Fidelity Taq Polymerase (Roche) on ES cell genomic DNA and cloned on either site of a PGK-Neomycin selection cassette. All exons were sequenced to verify that no mutations were introduced accidentally. For counter selection, a gene encoding Diphtheria toxin chain A (DTA) was inserted at the 5' of the targeting construct. The targeting construct was linearized and electroporated into E14 ES cells (derived from 129P2 mice). Cells were cultured in BRL cell conditioned medium in the presence of Leukemia inhibitory factor (LIF). After selection with G418 (200 μg/ml), targeted clones were identified by PCR (long-range PCR from Neomycin resistance gene to the region flanking the targeted sequence). A clone with normal karyotype was injected into blastocysts of C57Bl/6 mice. Male chimeras were crossed with female C57Bl/6 mice (Harlan). The resulting F1 heterozygous mice (in the 129P2-C57Bl/6 background) were used to generate F2 homozygous mutants and wild-type littermate controls. These mice were used for all the behavioral and electrophysiological experiments. The experimenter was blind for the genotype, but homozygous mice were easily recognizable by the ataxic gait. Therefore, data was also analyzed by a second person blind to the genotype. Mice were housed on a 12 hours light/dark cycle with food and water available *ad libitum* and used between 2 and 6 months of age for all experiments described (including electrophysiology). All animal procedures were approved by a Dutch Ethical Committee (DEC).

Molecular analysis of mutants

In situ hybridization. Whole brains were quickly isolated and frozen on dry ice. Sagittal slices (14μm) were cut using Cryostat (Jung CM 300, Leica. Instruments, Nussloch, Germany) and thaw-mounted on slides (Superfrost®Plus, Menzel-Glaser, Germany). In situ hybridization was performed as described previously(Wisden et al., 1988). Probes used were antisense to the 5' UTR of *Camk2b*: 5'-GGCCATGGCGGTGGCGATCGGGCTCG-GCGTGCGCTCGGC-3', antisense to the 3'UTR of *Camk2b*: 5'-GGTACCTACAGAC-TAACACGGTCGGCATGGGCACATTCACG-3' and antisense to exon 2 of *Camk2a*: 5'-GCTGCATACTCATGGCCGGTACAGAGCTTGACACAGCGTCGGAC-3'. Afterwards slices were stained with thionin.

RT-PCR. RNA was isolated from cerebellum and cortex, by homogenization in TRIzol® Reagent (Invitrogen). A semi-quantitative RT-PCR (verified by serial dilutions) was performed using Superscript™III Reverse transcriptase (Invitrogen) and RNAsin (Promega). Expression of the *Camk2b* mRNA in the heterozygous and homozygous *Camk2b* mutant

mice, was analyzed separately up- and downstream of the Neomycin cassette by detection of exon 2-4 of *Camk2b*, using 5' primer 5'-CGACGCTGTGTCAAGCTCTGTAC-3' and 3' primer: 5'-GAAGCCCTCTTCAGAGATGC-3' and detection of exon 14-17 of *Camk2b*, using 5' primer: 5'-GAAAGCAGATGGAGTCAAG-3' and 3' primer: 5'-GTTGTGTTG-GTGCTGTCG-3'. The expression of *Camk2a* mRNA was analyzed by detection of exon 2-5 of *Camk2a*, using 5' primer: 5'-GCGCAGGTGTGTGAAGGTGC-3' and 3' primer: 5'-CACAATGTCTTCAAACAGTTCC-3'. A control PCR was performed with pimers against exon 5-8 of *Synapsin I* using 5' primer: 5'-TGCCCAGATGGTTCGACTAC-3' and 3' primer: 5'-TGTCAGACATGGCAATCTGC-3'.

Western blot and immunoprecipitations. Lysates for westernblot were prepared by quick dissection of the brain and by homogenization of the brain tissue in lysis buffer (10mM TRIS-HCl 6.8, 2.5% SDS, 2mM EDTA) and protease and phosphatase inhibitor cocktails (Sigma). The concentration of the lysates was adjusted to 1 mg/ml. 10 µg was used for Western blot analysis, unless otherwise specified. Western blots in Fig. 1 were probed with antibodies directed against the N-terminal CaMKII (H-300, 1:500; Santa-Cruz). Western-blots shown in Supplementary Fig. 8 were probed with aCaMKII (clone 6G9; 1:1000; Chemicon), bCaMKII (clone CB-b1; 1:10000; Zymed), Ph-T286/T87 CaMKII antibody (1:5000; #06-881, Upstate Cell Signaling Solutions) or actin (clone C4; 1:10.000; Chemicon). Bands were visualized using Enhanced Chemo Luminescence (Pierce). For immunoprecipitations P2 synaptosomes were solubilized in a final buffer containing 25mM Hepes, 150mM NaCl, 1%. Triton and diluted to a final concentration to 2.5 mg/ml protein. For the immunoprecipitation we used 1 ml of homogenate (2.5 mg) and added 10 mg bCaMKII antibody (Zymed, clone CB-b1).

Kinase activity. Ca^{2+}-dependent and Ca^{2+}-independent activity were determined in fresh cerebellar lysates, using Autocamtide 2 as a substrate (CaMKII assay kit from Upstate cell signaling solutions, Boiling Springs, USA). Each assay was tested for linearity (serial dilution of lysates), and data was normalized to a wild-type (Ca^{2+}-dependent) control, which was present at each run.

Immunocytochemistry. Brains from adult mice were fixed with 4% paraformaldehyde by transcardial perfusion. Immunocytochemistry was performed on free-floating 40 µm thick frozen sections employing a standard avidin-biotin-immunoperoxidase complex method (ABC, Vector Laboratories, USA) with bCaMKII (Zymed), aCaMKII (Chemicon) or Calbindin (Sigma) as the primary antibody and diaminobenzidine (0.05%) as the chromogen(Hansel et al., 2006).

Morphological analysis: For dendritic arborization measurements we used Golgi-Cox staining on unfixed cerebelli using the FD Rapid GolgiStain Kit (FD NeuroTechnologies Inc., USA), according to the manufacturers' instructions. Sagittal sections, 100 µm thick, were cut on a microtome with cryostat adaptations. Purkinje cell counting and selection for further detailed analysis was done by an observer who was blind to the genotype. The tips of the outer branches were manually counted using a 40X objective and were used as a measure for dendritic branching. A calibration grid was used to count the number of spines per 10 µm dendrite, using a 100X objective. For the spine analysis, brains from adult mice were fixed with 4% paraformaldehyde by transcardial perfusion. To examine dendritic

spine number and morphology, 200 mm cerebellar sections were subjected to 'diOlistic' labeling(Gan et al., 2000). Tungsten particles (1.7 mm; Bio-Rad, Hercules, CA) coated with 1,1'-dioctadecyl-3,3,3',3'-tetramethylindocarbocyanine perchlorate crystals (DiI; Invitrogen, Eugene, OR) were propelled into fixed tissue with biolistic Helios gene gun (Bio-Rad) through a membrane filter with a 3 μm pore size (Falcon 3092; BD Biosciences, Franklin Lakes, NJ). Sections were postfixed in 4% paraformaldehyde overnight and then mounted for confocal microscopy. A Zeiss LSM510 confocal microscope, with a Zeiss 63x objective was used to obtain an image series of sections at 0.5 μm intervals. All imaging and analysis was performed in blinded manner. For quantification n=6 cells per genotype were identified (number of mice: WT (3); *Camk2b*$^{-/-}$ (3)), and protrusions were measured as described previously(Hoogenraad et al., 2007). Morphometric analysis and quantification were performed using MetaMorph software (Universal Imaging Corporation, West Chester, PA) by investigators who were blind to genotype and experimental manipulation.

Behavioral analysis

Balance beam. Mice were placed on a 1.5 cm wide square beam, which was elevated 30 cm, and were allowed to stay on the beam for a maximum of 60 seconds. *Accelerating Rotarod.* Motor coordination on the accelerating (4–40 rpm, in 5 minutes) rotarod (model 7650, Ugo Basile Biological Research Apparatus, Varese, Italy) was measured in 5 trials with 1 hour inter trial interval. The indicated time is the time spent on the rotarod, or time until the mouse made 3 consecutive rotations on the rotarod. *Open field.* Mice we placed in a dimly–lit open field (120 cm diameter), and the total distance moved was recorded for 5 minutes (SMART software, Panlab, Barcelona, Spain). *Phenotyper.* Mice were placed in the Phenotyper (Noldus Information Technology, Wageningen, The Netherlands) for 24 hours, and the total distance moved was determined. The phenotyper is a home-cage like environment, with a camera in the top-lid.

Electrophysiology

Sagittal slices of the cerebellar vermis (200-250 μm) of 16-22 week old mice, were made using a Vibratome (Leica VT1000S, Leica, Nussloch, Germany) and afterwards kept for >2 hours in ACSF (containing (in mM): 124 NaCl, 5 KCl, 1.25 Na_2HPO_4, 2 $MgSO_4$, 2 $CaCl_2$, 26 $NaHCO_3$, and 10 D-glucose aerated with 95% O_2 and 5% CO_2) before the recordings started. All drugs were purchased from Sigma. Experiments were performed at room temperature and in the presence of bath-applied 100 mM picrotoxin to block $GABA_A$-receptors. KN-93 (1 μM) and Cyclosporin A (5 μM dissolved in 0.5% EtOH) were added where indicated to block kinase and phosphatase activity, respectively(Belmeguenai and Hansel, 2005). Purkinje cells were visualized using an upright microscope (Axioskop 2 FS *plus*, Carl Zeiss, Jena, Germany) equipped with a 40X water immersed objective. Whole-cell patch-clamp recordings were performed using an EPC-10 amplifier (HEKA Electronics, Lambrecht, Germany). For long-term plasticity recordings, electrodes were filled with a solution containing (in mM): 9 KCl, 10 KOH, 120 K-gluconate, 3.48 $MgCl_2$, 10 HEPES, 4 NaCl, 4 Na_2ATP, 0.4 Na_3GTP and 17.5 sucrose (pH 7.25, osmolarity ~290 osm). Currents were filtered at 3 kHz and digitized at 8 kHz. For extracellular stimulation, glass pipettes

were filled with external saline. Long-term plasticity at the parallel fiber – Purkinje cell synapse was assessed by either pairing parallel fiber and climbing fiber stimulation at 1 Hz for 5 minutes (PF-LTD protocol) or by parallel fiber stimulation alone at 1 Hz for 5 minutes (PF-LTP protocol). Test responses were evoked at a frequency of 0.05 Hz (2 stimuli; 50 ms inter-stimulus interval) with ~0.5-6 μA pulses that were applied for 500 (LTP) or 700 μs (LTD). Holding potentials in the range of -60 to -75 mV were chosen to prevent spontaneous spike activity. In all experiments, cells were switched to current-clamp mode for tetanization. Recordings were excluded if R_S or R_I varied by >15% over the course of the experiment. Paired-pulse facilitation was tested using double test pulses with 50 ms inter-stimulus interval. EPSC kinetics were recorded using Cs^{2+}-based intracellular recordings (containing (in mM) 115 $CsMeSO_4$, 20 TEA-Cl, 10 HEPES, 2.5 $MgCl_2$, 4 Na_2ATP, 0.4 Na_3GTP, 10 Na_2-Phosphocreatine, 0.6 EGTA, pH 7.25-7.30, osmolarity ~290 osm) while 50-80% online R_S-compensation (residual R_S < 10 MΩ) was applied. For climbing fiber-mediated EPSC recordings Purkinje cells were voltage-clamped at -10 mV and 5 mM QX-314 were added to the internal medium to prevent spiking activity. During these recordings we checked for multiple climbing fiber innervation by gradually increasing the stimulus intensity[2].

Statistical analysis

Statistical analysis was performed using StatView (SAS institute, USA). For behavioral analysis (more than one measurement per group) we used a repeated measurements ANOVA, followed by a *post hoc* Fisher's PLSD analysis whenever it was appropriate. For comparison of two groups (one measurement each) we used a Student's *t*-test. Differences in LTD/LTP between wild-type mice and mutants were assessed by running a two-sample Student's *t*-test on the average values of the 5 last minutes of the recording (as indicated in the graphs). To assess whether significant LTP/LTD was obtained within a group, we used a paired *t*-test, in which we compared for each animal the average baseline value with the average value of the last 5 minutes of the recording (as indicated in the graphs). For climbing fiber-mediated EPSC analysis we averaged 6 responses per cell and used a single-exponential fit to calculate the decay time constant, 10-90% rise time and amplitude. Twenty climbing fiber-mediated EPSCs were averaged to calculate the absolute amplitude of the Na^+-spike and the first Ca^{2+}-spikelet.

Supplementary References

Belmeguenai A, Hansel C (2005) A role for protein phosphatases 1, 2A, and 2B in cerebellar long-term potentiation. J Neurosci 25:10768-10772.

Gan WB, Grutzendler J, Wong WT, Wong RO, Lichtman JW (2000) Multicolor "DiOlistic" labeling of the nervous system using lipophilic dye combinations. Neuron 27:219-225.

Hansel C, de Jeu M, Belmeguenai A, Houtman SH, Buitendijk GH, Andreev D, De Zeeuw CI, Elgersma Y (2006) alphaCaMKII Is essential for cerebellar LTD and motor learning. Neuron 51:835-843.

Hoogenraad CC, Feliu-Mojer MI, Spangler SA, Milstein AD, Dunah AW, Hung AY, Sheng M (2007) Liprinalpha1 degradation by calcium/calmodulin-dependent protein kinase II regulates LAR receptor tyrosine phosphatase distribution and dendrite de-

velopment. Dev Cell 12:587-602.
Wisden W, Morris BJ, Darlison MG, Hunt SP, Barnard EA (1988) Distinct GABAA receptor alpha subunit mRNAs show differential patterns of expression in bovine brain. Neuron 1:937-947.

Chapter 6
Section 6.2

Interactions between specific CaMKII subtypes and $GABA_B$-receptors control long-term potentiation at inhibitory synapses

Submitted

Zhenyu Gao, Geeske M. van Woerden, Ype Elgersma, Chris I. De Zeeuw and Freek E. Hoebeek

Abstract

Calcium/Calmodulin-dependent kinase type II (CaMKII) is essential for various forms of synaptic plasticity. The predominant α- and βCaMKII isoforms have been shown to individually contribute to plasticity at excitatory synapses, but nothing is known about their functional difference at inhibitory synapses. Using both α- and βCaMKII knockout mice we demonstrate that in the absence of either α- or βCaMKII the induction of inhibitory long-term potentiation (iLTP) at stellate cell – Purkinje cell synapses by repetitive climbing fiber stimulation is blocked. Moreover, the blockade of the competing protein phosphatase 2B pathway revived iLTP in *Camk2b*$^{-/-}$ mice, but not in *Camk2a*$^{-/-}$ mice, which suggests that αCaMKII embodies the main enzymatic power of the CaMKII holo-enzyme. When we co-activated the inhibitory interneurons during the climbing fiber stimulation iLTP was suppressed in wt by $GABA_B$-receptor activation, but in *Camk2b*$^{-/-}$ mutants iLTP was rescued. The essential molecular substrate for this rescue of iLTP in *Camk2b*$^{-/-}$ mice was not protein kinase A but inositol-tri-phosphate-controlled calcium release from internal stores. Together our results suggest distinct roles of α- and βCaMKII isoforms in controlling iLTP and thereby redefine the molecular pathway of inhibitory synaptic plasticity.

Introduction

Calcium/Calmodulin-dependent Kinase type II (CaMKII) is one of the most densely expressed proteins in the central nervous system (Erondu and Kennedy, 1985). The intracellular signalling pathways that are controlled by CaMKII have been shown to be important for memory formation by controlling synaptic plasticity (Silva et al., 1992a; Silva et al., 1992b; Colbran and Brown, 2004; Wayman et al., 2008). The CaMKII holoenzyme has been shown to be essential for pre- and postsynaptic mechanisms at both excitatory and inhibitory synapses in hippocampal, amygdalar, cortical and cerebellar neurons (Castillo et al., 2011), indicating the importance of this molecule for proper neuronal functioning.

Alpha- and βCaMKII subunits are the predominant isoforms of CaMKII holo-enzyme in the brain (Miller and Kennedy, 1985). Although these two isoforms are predominantly homologous, βCaMKII contains an additional actin binding domain and has a higher calcium sensitivity compared to αCaMKII (Shen et al., 1998; Brocke et al., 1999; Thiagarajan et al., 2002; Fink et al., 2003; Cho et al., 2007). Recent studies revealed that in neurons that express both α- and βCaMKII, indeed each isoform has a distinct function in controlling synaptic plasticity at excitatory synapses. For instance, the deletion of αCaMKII from cerebellar Purkinje cells results in disrupted long-term depression (LTD), whereas the deletion of βCaMKII from these neurons results in a bidirectional reversal of LTD and long-term potentiation (LTP) (Hansel et al., 2006; van Woerden et al., 2009).

The molecular mechanisms that control long-term plasticity at excitatory synapses show considerable overlap with those for inhibitory long-term plasticity (REF). Also at inhibitory synapses the effects of CaMKII are competed by protein phosphatases: in Purkinje cells CaMKII results in LTP at inhibitory synapses (iLTP) and is rivalled by

activation of protein phosphatase 2B (calcineurin) (Kano et al., 1996; Kawaguchi and Hirano, 2002). However, up to now, it remains to be elucidated whether α- and βCaMKII serve distinct functions in controlling inhibitory plasticity. In order to do so, we studied the molecular mechanism of synaptic plasticity of inhibitory stellate cell – Purkinje cell (SC-PC) synapses in both αCaMKII knockout mice (*Camk2a*$^{-/-}$) and βCaMKII knockout mice (*Camk2b*$^{-/-}$). Our results suggest distinct roles of α- and βCaMKII isoforms in controlling iLTP.

Material and methods

Animals

Camk2a$^{-/-}$ mice were generated as previously described (Elgersma et al., 2002). For the *Camk2b*$^{-/-}$ we used exon 2 knock-out mice, which showed complete loss of βCaMKII expression and ataxia, as described previously for the *Camk2b* exon11 knock-out mice (van Woerden et al., 2009). Homozygous mice and wt littermates (both genders) ranging from postnatal day (P) 17 to 21 old were used in the experiments. Animals were maintained at 22 ± 2 °C with 12 hrs dark and light cycle and were provided with food and water ad libitum. All studies were performed in accordance with the guidelines of the Erasmus Medical Center and the Dutch national legislation.

Slice preparation for electrophysiology

Camk2a$^{-/-}$ and *Camk2b*$^{-/-}$ mice and WT littermates were decapitated under isoflurane anesthesia. Subsequently, the cerebellum was removed and transferred into ice-cold slicing medium that contains (in mM): 240 Sucrose, 5 KCl, 1.25 Na_2HPO_4, 2 $MgSO_4$, 1 $CaCl_2$, 26 $NaHCO_3$ and 10 D-Glucose, bubbled with 95% O_2 and 5% CO_2. Parasagittal slices (250 μm thick) of the cerebellar vermis were cut using a vibratome (VT1000S, Leica) and kept in ACSF containing (in mM): 124 NaCl, 5 KCl, 1.25 Na_2HPO_4, 2 $MgSO_4$, 2 $CaCl_2$, 26 $NaHCO_3$ and 20 D-Glucose, bubbled with 95% O_2 and 5% CO_2 for > 1 h at 34 ± 1 ºC before the experiments started.

Whole-cell electrophysiology

Experiments were performed with a constant flow of oxygenated ACSF (1.5-2.0 ml/min). Purkinje cells were visualized using an upright microscope (Axioskop 2 FS plus, Carl Zeiss, Germany) equipped with a 40X water immersion objective. Patch-clamp recordings were performed using an EPC-10 double amplifier (HEKA electronics, Lambrecht, Germany). All recordings were performed at 34 ± 1 ºC.

Whole cell current clamp recordings of Purkinje cells were performed using borosilicate pipettes (R_{pip} = 2 - 4 mΩ) filled with intracellular solution containing (in mM): 130 K-Gluconate, 10 KOH, 3.48 $MgCl_2$, 4 NaCl, 10 HEPES, 4 Na_2ATP, 0.4 Na_3GTP and 17.5 sucrose (pH 7.25, osmolarity 295). Stellate cell - Purkinje cell (SC-PC) synapses were

stimulated as previously described (Mittmann and Hausser, 2007). In short, an additional patching pipette filled with ACSF was located at the outer 1/3 of cerebellar molecular layer and >200 µm lateral from Purkinje cell dendrites to avoid stimulating parallel fiber-Purkinje cell synapses. Our conditions resulted in a reversal potential for IPSPs of -75 to -78 mV. IPSPs were completely blocked by bath applied picrotoxin or SR95531, confirming their pure GABAergic nature. Evoked IPSPs from SC-PC synapses appeared to be all or none, suggesting direct stimulations at stellate cell somata. To avoid intrinsically generated action potentials, Purkinje cells were kept at -60 to -65 mV with hyperpolarizing currents. Under these conditions, SC-PC IPSPs were inward potentials ranging from -0.2 to -3 mV. Climbing fibers (CF) were stimulated with a patch electrode filled with external solution located in the granule cell layer. To induce LTP of IPSPs (iLTP), a physiological relevant tetanus of 5 CF stimuli at 10 Hz was applied every 2 s for 3 min. For paired stellate cell-climbing fiber stimulation, each CF stimulus was coincided with two stellate cell stimuli at 20 Hz. The holding currents and input resistances of Purkinje cells were constantly monitored, and cells with >15% shift of these parameters were excluded from analysis.

Purkinje cell spontaneous IPSCs and rebound potentiation

Purkinje cells were voltage clamped at -60 mV using intracellular solution containing (in mM): 150 CsCl, 15 CsOH, 1.5 $MgCl_2$, 0.5 EGTA, 10 HEPES, 4 Na_2ATP and 0.4 Na_3GTP (pH 7.3; osmolarity 300). Ten µM NBQX were supplemented in the ACSF to avoid contamination with spontaneous EPSCs. Spontaneous IPSCs were analyzed using Minianalysis (Synaptosoft, Decatur, USA). To analyze IPSC kinetics, unitary IPSCs of 50-100 pA were selected to avoid interference of noise or insufficient voltage clamp. Traces were scaled, averaged and fit using a single decay time constant. Series and input resistances were monitored every 3 min, and recordings were terminated if series or input resistances changed >15%.

Pharmacology

Baclofen (2 µM), cyclosporin A (5 µM), KN-93 (2 µM), SCH50911 (10 µM), KT 5720 (0.2 µM) and thapsigargin (10 µM) were obtained from Tocris. Other chemicals were obtained from Sigma unless stated elsewhere.

Results

To elucidate how α- and βCaMKII isoforms mediate inhibitory synaptic plasticity, we investigated iLTP at SC-PC synapses in both *Camk2a*$^{-/-}$ and *Camk2b*$^{-/-}$ mice. We first studied the induction rules for iLTP at SC-PC synapses. Physiologically relevant climbing fiber (CF) stimulation of five CF bursts at 10 Hz, repeated every 2 s for 3 min (Fig. 1 A, inset), robustly increased the SC-IPSP amplitude in wild type (wt) Purkinje cells (138.8 ± 5.8% and 141.2 ± 7.5% relative to baseline for *Camk2a* and *Camk2b* wt littermates, respectively; Fig. 1 A,B). This potentiation occurred without inducing any change in the paired pulse

ratio of two consecutive IPSPs, which indicates that the site of plasticity was postsynaptic (Student's t–test of averages after the stimulus protocol: all p-values > 0.5). In accordance to other stimulus protocols (Kano et al., 1992; Kawaguchi and Hirano, 2000) iLTP was fully blocked in wt by application of the global CaMKII blocker KN-93 (106.7 ± 2.0% and 103.5 ± 2.2%, respectively; Fig. 1 A,B). Likewise, this CF stimulus protocol failed to induce iLTP in both *Camk2a*$^{-/-}$ and *Camk2b*$^{-/-}$ mice when KN-93 was not applied (108.8 ± 3.4% and 106.4 ± 2.5%, respectively), despite the normal spontaneous IPSC activity (Table 1). The lack of iLTP in both mutants is unlikely to originate from aberrant responses to CF stimulation, since none of the response parameters, e.g., the Na^+-spike, Ca^{2+}-spike and Ca^{2+}-plateau amplitudes appeared different in *Camk2a*$^{-/-}$ and *Camk2b*$^{-/-}$ (all p-values > 0.2). Moreover, replacement of the CF stimulation by depolarizing voltage steps (Kano et al., 1992) resulted in similarly impaired iLTP of spontaneous IPSC amplitudes in both *Camk2a*$^{-/-}$ and *Camk2b*$^{-/-}$ mice (Fig. 1 C,D). Together these results indicate that both α- and βCaMKII are essential for proper post-synaptic iLTP at inhibitory synapses.

Following direct post-synaptic depolarization or CF activity the intracellular calcium concentration in Purkinje cells rises and activates not only α- and βCaMKII, but also protein phosphatase 2B (PP2B), which counteracts the effects of CaMKII activation (Kawaguchi and Hirano, 2002; Belmeguenai and Hansel, 2005; van Woerden et al., 2009). In order to test whether the residual CaMKII activity in *Camk2a*$^{-/-}$ and *Camk2b*$^{-/-}$ mutants is outcompeted by PP2B activity we next applied the specific PP2B blocker cyclosporin A. Although in *Camk2a*$^{-/-}$ the inhibition of PP2B did not reveal iLTP (95.8 ± 4.9%) in response to the CF stimulus protocol, in *Camk2b*$^{-/-}$ the same conditions indeed revived iLTP (129.3 ± 5.9% re 128.8 ± 5.2% for wt) (Fig. 2 A,B). Thus, the residual αCaMKII activity in *Camk2b*$^{-/-}$ is potent enough to induce iLTP when the suppressing PP2B cascade is blocked, but the residual βCaMKII in *Camk2a*$^{-/-}$ is not.

The suppressing effect of PP2B on CaMKII-mediated iLTP in wt Purkinje cells has been shown to be triggered by activation of postsynaptic $GABA_B$-receptors (Kawaguchi and Hirano, 2000; Kawaguchi and Hirano, 2002). To investigate how α- and βCaMKII are individually involved in this $GABA_B$-mediated suppression of iLTP, we next adapted our CF tetanus protocol by adding SC burst stimuli of 20 Hz, which has been shown to trigger postsynaptic $GABA_B$-receptor activation (Kawaguchi and Hirano, 2000) (Fig. 2 C, inset). This combined stimulus protocol indeed suppressed the induction of iLTP in both wt groups (103.6 ± 5.2% and 102.5 ± 3.7% for *Camk2a* and *Camk2b* littermates, respectively; Fig. 2 C,D) without changing the paired pulse ratio (Student's t–test of averages after the stimulus protocol: all p-values > 0.7). In *Camk2a*$^{-/-}$ this suppression protocol resulted in a similar lack of iLTP (97.8 ± 4.1%; Fig. 2 C), whereas in *Camk2b*$^{-/-}$ the same conditions rescued iLTP (132.2 ± 4.8%; Fig. 2 D). Given that this surprisingly robust iLTP in *Camk2b*$^{-/-}$ following the suppression protocol was blocked by the application of KN-93 (103.0 ± 5.4%; Fig. 2D), it is likely that in *Camk2b*$^{-/-}$ mutants $GABA_B$-receptor activation results in the activation of residual CaMKII and hence iLTP. If so, then the blockade of $GABA_B$-receptor activation during the paired CF and SC stimulation should not only reinstate iLTP in wt, but also cancel the rescue of iLTP in *Camk2b*$^{-/-}$. Indeed, in the presence of the $GABA_B$-inhibitor SCH 50911, the suppression protocol reinstated iLTP in wt (133.3 ± 8.4%) and did not

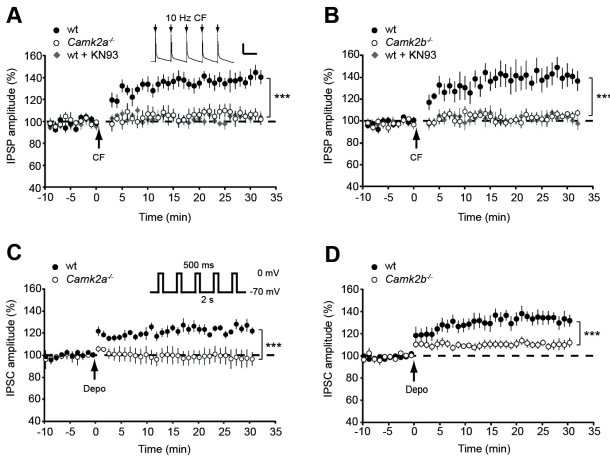

Figure 1. Aberrant iLTP at stellate cell-Purkinje cell synapses in α and βCaMKII knockout mice. (A) Five pulses, 10 Hz climbing fiber (CF) stimulation (inset; scale bars 20 mV/ 100 ms) repeated every 2 s for 3 min yields iLTP in wild–type (wt, n=10) Purkinje cells but not in *Camk2a*$^{-/-}$ Purkinje cells (n=9) or in wt Purkinje cells in the presence of KN-93 (wt + KN93, n=6). (B) CF stimulation yields iLTP in wt Purkinje cells (n=8) but not in *Camk2b*$^{-/-}$ Purkinje cells (n=8) or in wt Purkinje cells when KN-93 was present (wt + KN93, n=5). (C) Inset shows schematic drawing of rebound potentiation experiment. Rebound potentiation in Purkinje cells was induced by five 500 ms depolarization pulses to 0 mV at 0.5 Hz; IPSC amplitudes were compared before and after tetanus. Impaired rebound potentiation in *Camk2a*$^{-/-}$ mice (wt, n=7; *Camk2a*$^{-/-}$, n=6). (D) Impaired rebound potentiation in Camk2b$^{-/-}$ mice (wt, n=8; Camk2b$^{-/-}$, n=9). Error bars represent SEM. Asterisks with brackets indicate statistical significance between wt and knockout mice (Student's t–test of averages over last 5 min). **P<0.01; ***P<0.005.

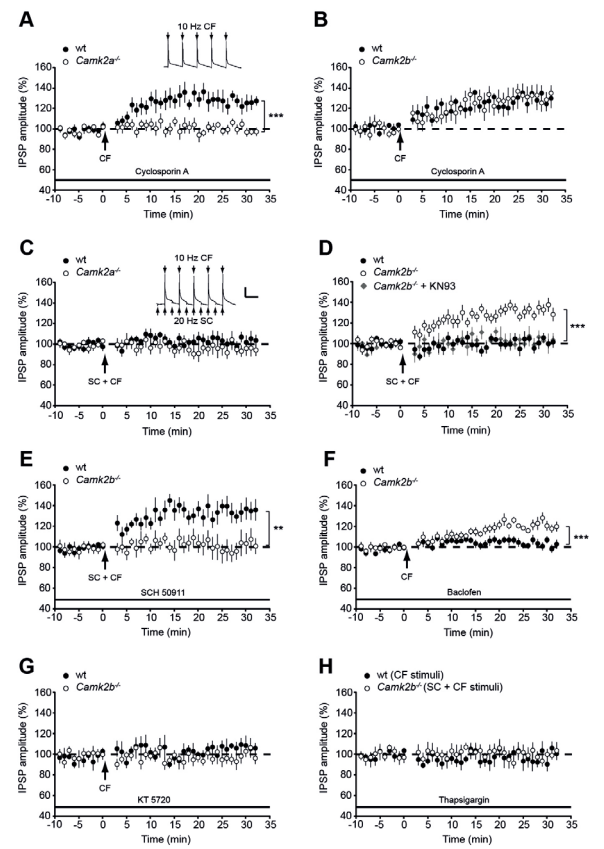

Figure 2. Block of PP2B reveals iLTP and block of IP_3 disrupts rescue of iLTP in *Camk2b*$^{-/-}$. (A) CF stimulation yields iLTP in wt Purkinje cells (n=7) in the presence of 5 μM PP2B inhibitor cyclosporin A, but not in *Camk2a*$^{-/-}$ Purkinje cells (n=10). (B) CF stimulation yields iLTP in wt Purkinje cells (n=6) in the presence of 5 μM PP2B inhibitor cyclosporin A, as well as in *Camk2b*$^{-/-}$ Purkinje cells (n=8). (C) Paired stellate cell (SC; 20 Hz) and climbing fiber (CF; 5 pulses, 10 Hz) stimulation every 2 s for 3 min (inset; scale bars 20 mV/ 100 ms) yields no change in IPSP amplitude in both wt (n=10) and *Camk2a*$^{-/-}$ (n=8) Purkinje cells. (D) Paired SC - CF stimulation yields no change in IPSP amplitude in wt Purkinje cells (n=10) and in *Camk2b*$^{-/-}$ Purkinje cells when KN93 is present (*Camk2b*$^{-/-}$ + KN93, n=5). In the absence of KN-93 the paired SC-CF stimulation significantly facilitates iLTP in *Camk2b*$^{-/-}$ Purkinje cells (n=13). (E) Inhibition of $GABA_B$-receptor activation with SCH 50911 rescues iLTP in wt Purkinje cells (n=9), but inhibits iLTP in *Camk2b*$^{-/-}$ Purkinje cells (n=7) following paired SC - CF stimulation. (F) Activation of $GABA_B$ receptors with baclofen inhibits iLTP in wt Purkinje cells (n=10), but facilitates iLTP in *Camk2b*$^{-/-}$ cells (n=8) following CF stimulation. (G) Inhibition of PKA with KT 5720 suppresses iLTP in wt Purkinje cells (n=5), but does not rescue iLTP in *Camk2b*$^{-/-}$ Purkinje cells (n=6) following CF stimulation. (H) Inhibition of Ca^{2+}-release from internal Ca^{2+}-store with thapsigargin abolishes the facilitation of iLTP in *Camk2b*$^{-/-}$ Purkinje cells (n=7) following paired SC - CF stimulation, as well as iLTP in wt Purkinje cells (n=6) following CF stimulation. Error bars represent SEM. Asterisks with brackets indicate statistical significance between wt and knockout mice (Student's t–test of averages over last 5 min). **P<0.01; ***P<0.005.

induce iLTP in *Camk2b*$^{-/-}$ (101.7 ± 8.9%; Fig. 2 E). Conversely, the replacement of SC stimulation by the $GABA_B$-receptors agonist baclofen suppressed the induction of iLTP in wt (101.5 ± 2.7%) and rescued the iLTP in *Camk2b*$^{-/-}$ (121.0 ± 4.1%; Fig. 2 F). Together these experiments unequivocally show that in wt $GABA_B$-receptor activation suppresses iLTP, but in *Camk2b*$^{-/-}$ $GABA_B$-receptor activation facilitates sufficient residual CaMKII activity to rescue iLTP.

How can $GABA_B$-receptor activation inhibit iLTP in wt, while it facilitates iLTP in *Camk2b*$^{-/-}$? We hypothesized that two counteracting pathways are controlled by $GABA_B$-receptor activation in Purkinje cells: one pathway that inhibits CaMKII-mediated iLTP (Kawaguchi and Hirano, 2002) and another one that enables CaMKII-mediated iLTP (Shen et al., 1998; Xu et al., 2008) (Fig. 3 A). To test this working hypothesis, we first assessed whether $GABA_B$-mediated inhibition of protein kinase A (PKA), which is critical for the suppression of iLTP in wt (Kawaguchi and Hirano, 2002), also mediated the rescue of iLTP in *Camk2b*$^{-/-}$. However, the presence of the PKA blocker KT5720 did not result in a rescue of iLTP in *Camk2b*$^{-/-}$ following the CF stimulus (Fig. 2 G). These results indicate that $GABA_B$-receptor activation facilitates iLTP in *Camk2b*$^{-/-}$ by a separate pathway that is PKA-independent. Previous studies showed that $GABA_B$-receptor activation boosts the levels of inositol-tri-phosphate (IP_3), which induces calcium release from internal stores and facilitates iLTP (Komatsu, 1996; Yamauchi, 2005). To test whether this $GABA_B$-IP_3 pathway drives the rescue of iLTP in *Camk2b*$^{-/-}$ following the suppression protocol, we applied thapsigargin, which depletes intracellular calcium stores. Indeed, in the presence of thapsigargin, the suppression protocol failed to rescue iLTP in *Camk2b*$^{-/-}$ and the CF protocol failed to induce iLTP in wt (Fig. 2 H). Together these results validated our working hypothesis that $GABA_B$-receptor activation suppresses CaMKII-mediated iLTP in wt in a PKA-dependent manner, but rescues CaMKII-mediated iLTP in *Camk2b*$^{-/-}$ by triggering calcium release from internal stores. Thus, the specific composition of CaMKII holoenzyme, i.e., both α- and βCaMKII or only αCaMKII, determines the dominant effect of $GABA_B$-receptor activation on CaMKII-mediated iLTP: facilitation or suppression.

Discussion

The principle finding that emerges from the current study is that although both α- and βCaMKII are essential for the proper induction of iLTP at SC-PC synapses, each isoform has a distinct function. Our data describes two lines of evidence for this finding. First, when the competing PP2B is blocked, only the residual αCaMKII in *Camk2b*$^{-/-}$ is able to drive iLTP following CF stimulation. Apparently, the residual βCaMKII in *Camk2a*$^{-/-}$ lacks the enzymatic power to initiate iLTP. Second, whereas coactivation of the presynaptic stellate cells during the CF stimulation suppresses iLTP in wt by $GABA_B$-receptor activation, this protocol is essential for iLTP induction in *Camk2b*$^{-/-}$. Our results reveal the opposing effects following coincident presynaptic activity at the SC-PC synapses in the presence or absence of βCaMKII.

Several studies confirmed the involvement of the CaMKII holoenzyme in synaptic plasticity at inhibitory synapses in the hippocampus, amygdala, cerebral cortex

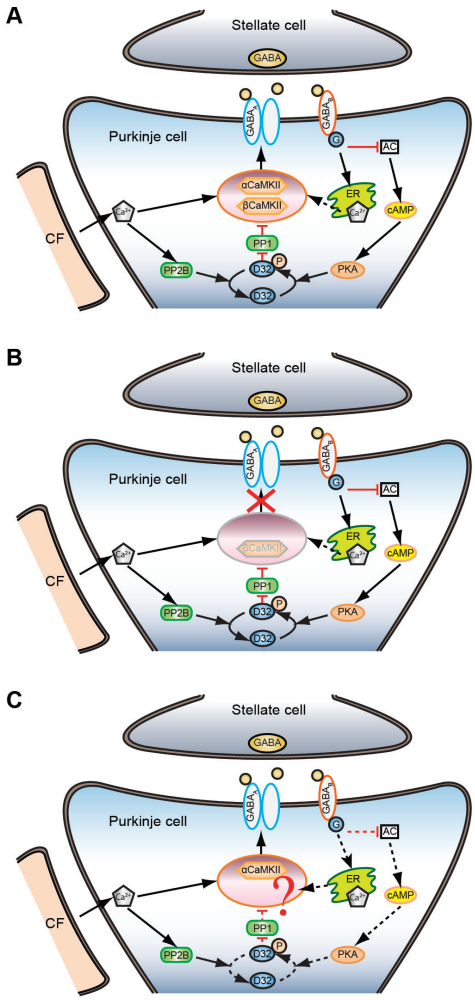

Figure 3. Cascades of CaMKII and $GABA_B$-receptor mediated iLTP in *Camk2a*$^{-/-}$ and *Camk2b*$^{-/-}$ mice. (A) Schematic representation of the CaMKII mediated iLTP induction cascade and $GABA_B$-receptor mediated inhibition of iLTP in wt Purkinje cell. The model is proposed based on previous studies (Kano et al., 1996; Kawaguchi and Hirano, 2002) and the current data. Cascades are simplified for the clarity of illustration. Black arrows indicate activation cascades, red bars indicate inhibitory cascades. Note that the calcium release from internal stores upon $GABA_B$-receptor activation is outcompeted by the suppressing PKA-PP1 pathway (dashed arrow). AC, adenylyl cyclase; D32, DARPP-32. (B) Schematic representation of the CaMKII mediated iLTP induction cascade and $GABA_B$-receptor mediated inhibition of iLTP in *Camk2a*$^{-/-}$ Purkinje cells. Genetic deletion of αCaMKII minimizes the CaMKII enzymatic activity (shadow representation of CaMKII holoenzyme) and disrupts iLTP induction (red cross). (C) Schematic representation of the CaMKII mediated iLTP induction cascade and $GABA_B$-receptor mediated inhibition of iLTP in *Camk2b*$^{-/-}$ Purkinje cells. Genetic deletion of βCaMKII revealed a rescue of iLTP by $GABA_B$-receptor activation. The underlining mechanisms of this rescue remains to be shown.

	#	FF (Hz)	Amp (pA)	Rise (ms)	Decay (ms)	Width (ms)
wt	12	18.4 ± 1.7	62.8 ± 4.0	1.28 ± 0.1	15.1 ± 1.1	2.8 ± 0.2
Camk2a$^{-/-}$	10	18.5 ± 0.8	65.1 ± 7.6	1.31 ± 0.1	13.7 ± 1.0	3.0 ± 0.2
t-test		0.97	0.79	0.79	0.35	0.38
wt	13	19.2 ± 2.8	66.3 ± 3.0	1.0 ± 0.1	13.7 ± 0.9	2.6 ± 0.2
Camk2b$^{-/-}$	12	19.0 ± 2.8	64.4 ± 2.5	1.0 ± 0.1	13.2 ± 0.6	2.6 ± 0.1
t-test		0.97	0.64	0.63	0.61	0.97

Table 1. Normal spontaneous IPSC properties in *Camk2a*$^{-/-}$ and *Camk2b*$^{-/-}$ mice. Spontaneous (s)IPSCs appeared normal between wt and *Camk2a*$^{-/-}$ Purkinje cells as well as between wt and *Camk2b*$^{-/-}$ Purkinje cells. Table: quantification of IPSC frequency (FF), amplitude (Amp), and kinetics (10-90% rise time, decay time constant and width at 50% of the maximal amplitude) of IPSCs.

and cerebellum (as reviewed by(Castillo et al., 2011)), but it has not yet been possible to decipher the individual contributions of α- and βCaMKII to iLTP in any of these structures. Given the overlap of molecular components between the signalling pathways that control synaptic plasticity at both excitatory and inhibitory synapses (Collingridge et al., 2004), one would predict distinct roles of α- and βCaMKII in iLTP much alike those recently described for excitatory synapses (Cho et al., 2007; van Woerden et al., 2009). Indeed, we found that in *Camk2b*$^{-/-}$ Purkinje cells both the $GABA_B$-induced IP_3-mediated release of calcium from internal stores and CF-mediated calcium influx were essential to elicit iLTP (Fig. 3). Although these results seem in accordance with the predicted lower calcium sensitivity of αCaMKII than in wt or in *Camk2a*$^{-/-}$ Purkinje cells (Brocke et al., 1999), the fact that the similar stimulus protocol suppresses iLTP in Purkinje cells when βCaMKII molecules are present argues against a dominant role of the enhanced calcium sensitivity of βCaMKII. In contrast, our data suggest that the actin-binding domain of βCaMKII may act as a differentiator: in *Camk2b*$^{-/-}$ mutants the residual αCaMKII is not confined to the actin and thereby could be more readily activated by local calcium sources like intracellular calcium stores (Finch and Augustine, 1998). This hypothesis should be tested by future experiments that take into account that IP_3-mediated release of calcium from internal stores is essential for iLTP induction in wt Purkinje cells and cortical neurons (Komatsu, 1996).

The induction rules for plasticity of inhibitory synapses at cerebellar SC-PC synapses are opposite from those in hippocampal CA1 tissue: coincident pre- and postsynaptic activity results through $GABA_B$-receptor activation in the suppression of iLTP in the former synapse (Kawaguchi and Hirano, 2000) (Fig. 2), whereas this cascade is essential for iLTP in the latter synapse (Xu et al., 2008). Our data shows that genetic ablation of βCaMKII reverts the iLTP induction rules at cerebellar SC-PC synapses to hippocampal CA1-like rules, in that coincident presynaptic activity is essential for the induction of iLTP in *Camk2b*$^{-/-}$. This surprising finding at this inhibitory synapse shows a remarkable coherence with the inversion of induction rules of long-term plasticity at excitatory parallel fiber – Purkinje cell synapses (van Woerden et al., 2009). Here also the lack of βCaMKII reversed the induction rules for LTP and LTD highlighting the overlap in molecular pathways of inhibitory and excitatory plasticity (Collingridge et al., 2004). Moreover, recent evidence indicates that local calcium concentrations control the selective translocation of αCaMKII molecules to either excitatory or inhibitory synapses in hippocampal tissue (Marsden et al., 2010), physically merging the molecular pathways that control plasticity at both types of synapses. Current studies promote a central role of βCaMKII in coordinating the translocation of CaMKII holoenzyme complexes in both excitatory (van Woerden et al., 2009) and inhibitory synapses in cerebellar Purkinje cells.

References

Belmeguenai A, Hansel C (2005) A role for protein phosphatases 1, 2A, and 2B in cerebellar long-term potentiation. J Neurosci 25:10768-10772.

Brocke L, Chiang LW, Wagner PD, Schulman H (1999) Functional implications of the subunit composition of neuronal CaM kinase II. J Biol Chem 274:22713-22722.

Castillo PE, Chiu CQ, Carroll RC (2011) Long-term plasticity at inhibitory synapses. Curr Opin Neurobiol.

Cho MH, Cao X, Wang D, Tsien JZ (2007) Dentate gyrus-specific manipulation of beta-Ca2+/calmodulin-dependent kinase II disrupts memory consolidation. Proc Natl Acad Sci U S A 104:16317-16322.

Colbran RJ, Brown AM (2004) Calcium/calmodulin-dependent protein kinase II and synaptic plasticity. Curr Opin Neurobiol 14:318-327.

Collingridge GL, Isaac JT, Wang YT (2004) Receptor trafficking and synaptic plasticity. Nat Rev Neurosci 5:952-962.

Elgersma Y, Fedorov NB, Ikonen S, Choi ES, Elgersma M, Carvalho OM, Giese KP, Silva AJ (2002) Inhibitory autophosphorylation of CaMKII controls PSD association, plasticity, and learning. Neuron 36:493-505.

Erondu NE, Kennedy MB (1985) Regional distribution of type II Ca2+/calmodulin-dependent protein kinase in rat brain. J Neurosci 5:3270-3277.

Finch EA, Augustine GJ (1998) Local calcium signalling by inositol-1,4,5-trisphosphate in Purkinje cell dendrites. Nature 396:753-756.

Fink CC, Bayer KU, Myers JW, Ferrell JE, Jr., Schulman H, Meyer T (2003) Selective regulation of neurite extension and synapse formation by the beta but not the alpha isoform of CaMKII. Neuron 39:283-297.

Hansel C, de Jeu M, Belmeguenai A, Houtman SH, Buitendijk GH, Andreev D, De Zeeuw CI, Elgersma Y (2006) alphaCaMKII Is essential for cerebellar LTD and motor learning. Neuron 51:835-843.

Kano M, Fukunaga K, Konnerth A (1996) Ca(2+)-induced rebound potentiation of gamma-aminobutyric acid-mediated currents requires activation of Ca2+/calmodulin-dependent kinase II. Proc Natl Acad Sci U S A 93:13351-13356.

Kano M, Rexhausen U, Dreessen J, Konnerth A (1992) Synaptic excitation produces a long-lasting rebound potentiation of inhibitory synaptic signals in cerebellar Purkinje cells. Nature 356:601-604.

Kawaguchi S, Hirano T (2000) Suppression of inhibitory synaptic potentiation by presynaptic activity through postsynaptic GABA(B) receptors in a Purkinje neuron. Neuron 27:339-347.

Kawaguchi SY, Hirano T (2002) Signaling cascade regulating long-term potentiation of GABA(A) receptor responsiveness in cerebellar Purkinje neurons. J Neurosci 22:3969-3976.

Komatsu Y (1996) GABAB receptors, monoamine receptors, and postsynaptic inositol trisphosphate-induced Ca2+ release are involved in the induction of long-term potentiation at visual cortical inhibitory synapses. J Neurosci 16:6342-6352.

Marsden KC, Shemesh A, Bayer KU, Carroll RC (2010) Selective translocation of Ca2+/calmodulin protein kinase IIalpha (CaMKIIalpha) to inhibitory synapses. Proc Natl Acad Sci U S A 107:20559-20564.

Miller SG, Kennedy MB (1985) Distinct forebrain and cerebellar isozymes of type II Ca2+/calmodulin-dependent protein kinase associate differently with the postsynaptic density fraction. J Biol Chem 260:9039-9046.

Mittmann W, Hausser M (2007) Linking synaptic plasticity and spike output at excitatory

and inhibitory synapses onto cerebellar Purkinje cells. J Neurosci 27:5559-5570.

Shen K, Teruel MN, Subramanian K, Meyer T (1998) CaMKIIbeta functions as an F-actin targeting module that localizes CaMKIIalpha/beta heterooligomers to dendritic spines. Neuron 21:593-606.

Silva AJ, Paylor R, Wehner JM, Tonegawa S (1992a) Impaired spatial learning in alpha-calcium-calmodulin kinase II mutant mice. Science 257:206-211.

Silva AJ, Stevens CF, Tonegawa S, Wang Y (1992b) Deficient hippocampal long-term potentiation in alpha-calcium-calmodulin kinase II mutant mice. Science 257:201-206.

Thiagarajan TC, Piedras-Renteria ES, Tsien RW (2002) alpha- and betaCaMKII. Inverse regulation by neuronal activity and opposing effects on synaptic strength. Neuron 36:1103-1114.

van Woerden GM, Hoebeek FE, Gao Z, Nagaraja RY, Hoogenraad CC, Kushner SA, Hansel C, De Zeeuw CI, Elgersma Y (2009) betaCaMKII controls the direction of plasticity at parallel fiber-Purkinje cell synapses. Nat Neurosci 12:823-825.

Wayman GA, Lee YS, Tokumitsu H, Silva AJ, Soderling TR (2008) Calmodulin-kinases: modulators of neuronal development and plasticity. Neuron 59:914-931.

Xu C, Zhao MX, Poo MM, Zhang XH (2008) GABA(B) receptor activation mediates frequency-dependent plasticity of developing GABAergic synapses. Nat Neurosci 11:1410-1418.

Yamauchi T (2005) Neuronal Ca^{2+}/Calmodulin-dependent protein kinase II - Discovery, progress in a quarter of a century, and perspective: Implication for learning and memory. Biol Pharm Bull 28:1342-1354.

Chapter 7

Effects of enhanced granule cell-Purkinje cell transmission and Purkinje cell excitability in *Cacna1a*^{S218L} mutants Rescued by SK-channel activators

Submitted

Zhenyu Gao, Boyan Todorov, Curtis F. Barrett, Stijn van Dorp, Michel D. Ferrari, Arn M.J.M. van den Maagdenberg, Chris I. De Zeeuw and Freek E. Hoebeek

Abstract

Mutations in the *CACNA1A* gene are associated with neurological disorders, such as ataxia, hemiplegic migraine, and epilepsy. These mutations can be categorized by their effects on Ca^{2+}-channel function and/or expression as loss- or gain-of-function mutations. Whereas recent evidence demonstrates that loss-of-function mutations decrease the regularity of cerebellar Purkinje cell activity and thereby induce cerebellar ataxia, it is unknown how gain-of-function mutations induce ataxia. Here, we show that the synaptic transmission between granule cells and Purkinje cells is enhanced in gain-of-function *Cacna1a*^{S218L} knock-in mice, while relatively many of their individual parallel fiber varicosities contact multiple Purkinje cell spines. In addition, *Cacna1a*^{S218L} Purkinje cells show hyperexcitable somatic action potentials and Ca^{2+}-burst firing, which deregulates their spontaneous firing pattern and can be counteracted by Ca^{2+}-activated K^+-channel activators. Our findings illustrate the underlying mechanisms of ataxia induced by a gain-of-function mutation, which are surprisingly similar to those in loss-of-function *Cacna1a* mutants. This commonality reveals the existence of a narrow window for optimal Ca^{2+}-homeostasis: sufficiently decreased and increased Ca^{2+}-influx can induce ataxia.

Introduction

Since the entry of Ca^{2+}-ions via voltage-gated Ca^{2+}-channels (VGCCs) controls crucial processes in mammalian neurons, such as neurotransmitter release, synaptic plasticity, and membrane excitability, mutations that affect VGCC functioning are likely to have severe effects (as reviewed by [1]). Indeed, mutations in the *CACNA1A* gene, which codes for the α_{1A}-subunit of $Ca_V2.1$ (P/Q-type) VGCCs, are associated with various neurological disorders, including ataxia, hemiplegic migraine, and epilepsy [2,3].

Mutations in $Ca_V2.1$-channels can be divided in gain- and loss-of-function mutations, depending on whether a mutation increases or decreases channel function/expression, respectively. Recent studies suggest a clear division in phenotypes induced by loss-of-function and gain-of-function mutations. Gain-of-function mutations in the *CACNA1A* gene are linked to familial hemiplegic migraine type 1 (FHM1) [3,4], whereas hereditary forms of ataxia induced by mutations in the *CACNA1A* gene, like episodic ataxia type 2 [3], are due to loss-of-function mutations. Studies of natural mouse mutants bearing mutations in the orthologous mouse *Cacna1a* gene, such as tottering, leaner, and rolling Nagoya mice [5,6], revealed that loss-of-function mutations consistently induce altered connectivity and transmission at the parallel fiber-Purkinje cell (PF-PC) synapse, as well as irregular Purkinje cell activity [7,8,9,10,11]. These aberrations have been shown to disturb the information processing in the cerebellar cortex [7] and therefore are considered true hallmarks of cerebellar ataxia.

Although it is clear that inadequate Ca^{2+}-influx, as found in loss-of-function *Cacna1a* mutants, can induce both developmental and electrophysiological aberrations that

eventually lead to ataxia, it remains to be elucidated why FHM1 patients with, for instance, the S218L mutation in the *Cacna1a* gene, which enhances the $Ca_V2.1$-mediated Ca^{2+}-influx, are ataxic [12]. In order to reveal how mutations that induce such a gain-of-function of $Ca_V2.1$-channels, we performed detailed morphological and electrophysiological analysis of *Cacna1a*^{S218L} knock-in mice [13]. Our results show that the synaptic connectivity is altered and the synaptic transmission between granule cells and Purkinje cells is enhanced and that Purkinje cells show distinct signs of hyperexcitability, which together induce irregular Purkinje cell firing both *in vitro* and *in vivo*. In addition, the irregular spiking and the ataxic motor performance can be counteracted by the activation of Ca^{2+}-dependent K^+-channels. Thus, our data reveal not only key cerebellar hallmarks of ataxia in the *Cacna1a*^{S218L} gain-of-function mouse mutant that resemble those seen in loss-of-function *Cacna1a* mutants, but also reveal a striking similarity in potential therapeutic pathways.

Results

Normal cerebellar structure but altered connectivity at *Cacna1a*^{S218L} PF-PC synapses

Given the widespread and dense expression of the *Cacna1a* gene in the rodent cerebellum [5,14], we first quantified to what extent the gross morphology of the cerebellum is affected by the S218L mutation. Parasagittal slices taken from 2-month old *Cacna1a*^{S218L} mice showed a normal cerebellar structure with no change in the foliation or organization of molecular, Purkinje cell, and granular layers (Figures 1A-D). In addition, neither the estimated volume of the cerebellum nor the number of Purkinje cells of *Cacna1a*^{S218L} mutants was significantly different from wild type (WT) mice (Table S1). Still, we could not rule out that the S218L mutation affects synaptic morphology, as ultrastructural aberrations of PF-PC synapses have been a consistent finding in loss-of-function *Cacna1a* mutants [9]. Therefore, we performed a detailed morphological study of the PF-PC synapse using electron microscopy and found that in both WT (Figure 1E) and *Cacna1a*^{S218L} (Figure 1F) tissue, PF-PC synapses appeared as asymmetrical contacts with loosely clustered spherical synaptic vesicles in PF varicosities and clear postsynaptic density structures in Purkinje cell spines. Both the density and dimensions of PF-PC cell synapses in *Cacna1a*^{S218L} mutants were not significantly different from WT animals (Table S1), but we did observe single PF varicosities contacting multiple Purkinje cell spines more frequently in *Cacna1a*^{S218L} mutants ($p < 0.001$) (Figures 1G, 1H and Table S2). As far as could be seen from our 2D-analyses there were no varicosities that contacted two spines that were unequivocally from the same cell. To further clarify whether the difference in connectivity originates from abnormal numbers of PF varicosities or Purkinje cell spines we quantified the number of PF varicosities and Purkinje cell spines independent of contact ratios using Golgi-Cox stained tissue. No significant differences were found in the density of both the PF varicosities and Purkinje cell spines (Table S1). Thus, these results show that although there are no significant differences either in gross morphology of the cerebellar cortex of *Cacna1a*^{S218L} mutants or in the densities of synaptic components in PF-PC synapses, the chance of single PF varicosities contacting multiple Purkinje cell spines was increased.

Increased synaptic transmission at *Cacna1a*^{S218L} PF-PC synapses

Given the altered synaptic connectivity between PFs and Purkinje cell spines, we first measured the synaptic transmission at the PF-PC synapse, by recording excitatory postsynaptic currents (EPSCs) in Purkinje cells in response to PF stimulation at geometrically determined locations in the molecular layer (c.f. Material and methods). Parallel fiber EPSCs were elicited in Purkinje cells that were voltage-clamped at -70 mV The stimulus electrode was placed in the most distal 1/3 of molecular layer adjacent to the Purkinje cell at similar distance in parasagittal slices, so that PF-EPSCs with 2 µA stimulus intensity did not exceed 20 pA. Systematically increasing the stimulus intensity with 2 µA increment yielded essentially linear input - output curves for both *Cacna1a*^{S218L} and WT synapses; however, at stimulus intensity > 8 µA EPSCs were significantly larger in *Cacna1a*^{S218L} than in WT Purkinje cells (all p-values < 0.05) (Figure 2A). In fact, at the maximum stimulus intensity tested (i.e., 20 µA), the PF-EPSCs in *Cacna1a*^{S218L} mutants were ~30% larger than in WT, whereas the kinetics of the PF-EPSCs showed no significant differences between *Cacna1a*^{S218L} and WT (p = 0.2 for 10 - 90% rise time value and p = 0.3 for decay time constant (τ_{decay})) (Figure S1A). To study the synaptic transmission efficacy at the level of single granule cell to Purkinje cell synapses, we performed simultaneous, dual-patch clamp recordings of granule cells and Purkinje cells. Such paired whole-cell recordings showed that the chances of obtaining detectable synaptic connections (characterized by observing EPSCs in Purkinje cells in response to action potentials from single granule cells) appeared normal in *Cacna1a*^{S218L} mutants (p = 0.63) (Figure 2B), whereas the average amplitude of granule cell-Purkinje cell EPSCs was increased. In fact, in *Cacna1a*^{S218L} Purkinje cells the maximum EPSC amplitude elicited by a physiologically relevant [15,16,17] 50 ms long 200 Hz train of action potentials in a single granule cell was on average ~90% increased (p < 0.01) compared to WT (c.f. Material and methods) (Figure 2B). Thus, both the stimulation of a PF bundle and activation of a single granule cell resulted in increased Purkinje cell responses, which indicates that in addition

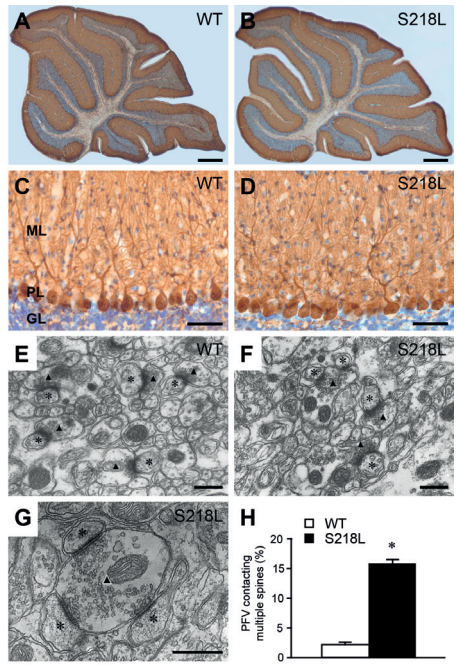

Figure 1. No change in gross cerebellar structure, but increased connectivity at PF-PC synapses in *Cacna1a*^{S218L} mice

(A, B) Overview of anti-calbindin D-28k and Nissl-stained mid-sagittal cerebellar sections from WT and *Cacna1a*^{S218L} animals (scale bars: 500 µm). (C, D) High magnification of anti-calbindin and Nissl stained Purkinje cells in WT and Cacna1a^{S218L} cerebellum (scale bars: 50 µm). ML, PL and GL indicate molecular layer, Purkinje cell layer and granule cell layer, respectively. (E, F) Electron micrographs of distal PF-PC synapses, triangles indicate the parallel fiber varicosity, asterisks indicate Purkinje cell spines (scale bars: 0.3 µm). (G) Multiple synaptic contacts between a single parallel fiber varicosity and three Purkinje cell dendritic spines (scale bar: 0.3 µm). (H) Percentages of parallel fiber varicosities that contact multiple Purkinje cell spines in WT (n = 4) and *Cacna1a*^{S218L} mutants (n = 4). Asterisks indicate significant difference (p-values indicated in the results section). See also Table S1 and S2.

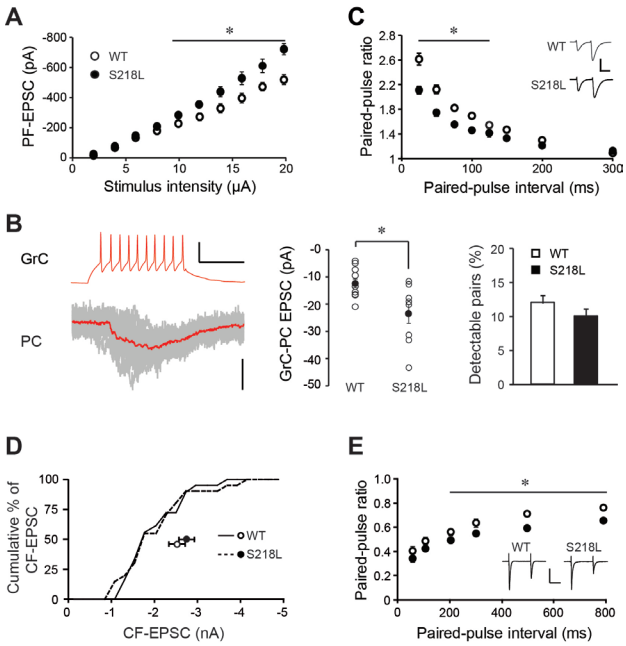

Figure 2. Increased synaptic transmission at PF-PC, but not CF-PC synapses

(A) Mean PF-EPSC amplitudes of WT (open circles, n = 8) and *Cacna1a*^{S218L} (solid circles, n = 10) Purkinje cells in response to increasing stimulus intensities. (B) Left: representative traces of a connected granule cell (GrC) and Purkinje cell (PC) pair from WT animal. Note that a train of action potentials in the granule cell (scale bars: vertical 50 mV, horizontal 25 ms) induces post synaptic responses in the Purkinje cell (scale bar: 10 pA). Red trace indicates the averaged response of 10 repetitive sweeps (gray traces) of GrC-PC EPSC. Middle: summary of maximum EPSC amplitudes in response to the granule cell train stimulusfrom 9 WT and 8 *Cacna1a*^{S218L} dual granule cell-Purkinje cell whole-cell recordings. Right: Percentage of pairs with detectable EPSC responses among all successful double recordings. (C) Paired-pulse ratios (second EPSC amplitude/first EPSC amplitude) of PF-EPSCs with various paired stimulation intervals (25-300 ms) from WT (open circles, n = 8) and *Cacna1a*^{S218L} (solid circles, n = 8) Purkinje cells. Insets show single PF-EPSC traces evoked by double PF stimulations with 50 ms inter-stimulus interval from WT and *Cacna1a*^{S218L} Purkinje cells (scale bars: vertical 200 pA, horizontal 20 ms). (D) Symbols indicate average CF-EPSC amplitudes from WT (n = 21) and *Cacna1a*^{S218L} (n = 20) Purkinje cells recorded at membrane potentials 20 mV below the reversal potential (see Material and Methods). Lines indicate the cumulative chart of CF-EPSC amplitude distributions of WT (continuous line) and Cacna1a^{S218L} (dashed line) Purkinje cells. (E) Paired-pulse ratios (second EPSC / first EPSC) of CF-EPSC with various stimulation intervals (50 - 800 ms) from WT (n = 11) and *Cacna1a*^{S218L} (n = 10) Purkinje cells. Insets show single CF-EPSC traces evoked by double CF stimulations with 200 ms inter-stimulus interval from WT and *Cacna1a*^{S218L} Purkinje cells (scale bars: vertical 500 pA, horizontal 100 ms). Asterisk indicates significant difference (p-value indicated in the results section). See also Figure S1 and S2.

to the morphological alterations, the synaptic efficacy is also increased in *Cacna1a*^{S218L} mutants.

To investigate a possible presynaptic origin of the increased synaptic transmission at the PF-PC synapse in *Cacna1a*^{S218L} mutants we first recorded the paired-pulse facilitation between two successive PF-EPSCs elicited by stimulation in the molecular layer, which reflects the increased efficacy of vesicle release due to residual free Ca^{2+}-ions in the PF terminal. At inter-stimulus intervals of 25–100 ms the paired-pulse facilitation in *Cacna1a*^{S218L} was significantly smaller than in WT (all p-values < 0.001) (Figure 2C). Second, we applied channel-specific Ca^{2+}-channel blockers to study the effects of the S218L mutation on neurotransmitter release mediated by $Ca_V2.2$ (N-type) and $Ca_V2.1$ (P/Q-type) VGCCs, which together mediate the bulk of neurotransmitter release from PFs. The contribution of N-type channels was measured by bath application of the N-type specific blocker ω-Conotoxin GVIA (ω-CgTx). We found that N-type channels have a smaller contribution to PF-EPSC amplitude in *Cacna1a*^{S218L} mutants (p = 0.004) (Figures S2A and S2B). Subsequent bath-application of the P/Q-type specific blocker ω-Agatoxin IVA (ω-Aga-IVA) further reduced the PF-EPSC amplitude in both WT and *Cacna1a*^{S218L} mutants to equal residual currents (p = 0.8). The residual currents were similar to when ω-Aga-IVA was applied without ω-CgTx in the bath (p = 0.7). Thus, although the effect of blocking P/Q-type-mediated presynaptic Ca^{2+}-influx on PF-PC synaptic transmission is

not increased in *Cacna1a*^{S218L} mutants, we observed a possibly compensatory decrease in the percentage of N-type-mediated neurotransmitter release. Together these data indicate that the S218L mutation altered the efficacy of neurotransmitter release efficacy from PFs, which together with altered synaptic connectivity is likely to enhance the input that Purkinje cells receive from granule cells.

Decreased paired-pulse depression at *Cacna1a*^{S218L} climbing fiber – Purkinje cell synapses

$Ca_V2.1$-VGCCs also mediate the transmission at the climbing fiber – Purkinje cell (CF-PC) synapse [18]. Therefore, we recorded the Purkinje cell response to CF activation in *Cacna1a*^{S218L} mutants and found typical all-or-none responses with amplitudes and rise time values similar to those in WT littermates (all p-values > 0.2) but faster τ_{decay} (p = 0.02) (Figure S1B). In order to clarify whether the S218L mutation altered the release probability at the climbing fiber synapse, we compared the response to double CF stimulations with inter-stimulus intervals ranging from 50 - 800 ms in the presence of 2 mM γ-DGG, a low affinity glutamate antagonist that competes with glutamate and thereby dampens glutamate receptor saturation at this synapse so as to allow caul quantification of the dynamics of the transmitter release at the CF terminals [19]. Such stimuli revealed smaller paired-pulse ratios of CF-EPSCs in *Cacna1a*^{S218L} mutants at intervals longer than 200 ms (p-values < 0.05) (Figure 2E). To study the contribution of P/Q- and other types of voltage-gated calcium channels to the release of glutamate from climbing fiber terminals we sequentially applied ω-CgTx and ω-Aga-IVA (Figure S2C, D). These recordings revealed that neither N- nor P/Q-type mediated neurotransmitter release from *Cacna1a*^{S218L} climbing fiber terminals, nor the residual EPSC component were affected (all p-values > 0.5). Together, these data show that the S218L mutation affects the CF-PC synaptic transmission, but without disrupting the typical all-or-none response, which is warranted by the saturated release probability at this synapse [8].

Figure 3. Negative shift of current-voltage relationships of whole-cell Ca^{2+}-currents in acutely dissociated *Cacna1a*^{S218L} Purkinje cells

(A) Current-voltage relationship of Ca^{2+}-current in acutely dissociated WT (n = 10) and *Cacna1a*^{S218L} (n = 10) Purkinje cells. Mean current densities were plotted against depolarizing voltages. Insets show representative traces of Ca^{2+}-currents in WT and *Cacna1a*^{S218L} Purkinje cells evoked by 50 ms depolarizing pulses to -40, -30 and -20 mV (holding potential = -70 mV; scale bars: vertical 75 pA/pF, horizontal 20 ms). (B) Normalized Ca^{2+}-conductance at different depolarizing voltages in WT (n = 10) and *Cacna1a*^{S218L} (n = 10) Purkinje cells. Solid curves indicate Boltzmann fits and dashed lines indicate corresponding voltages of half-maximum conductance (p-values indicated in the results section). See also Figure S3.

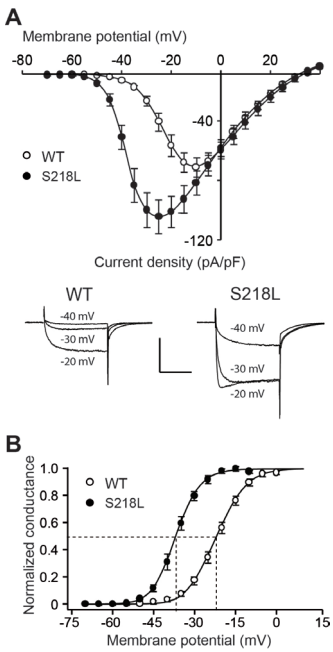

Altered Ca^{2+}-influx in Cacna1a^{S218L} Purkinje cells

Aside from altered synaptic inputs, *Cacna1a*^{S218L} Purkinje cells are likely to be affected intrinsically, as 90% of their high-voltage activated Ca^{2+}-influx is mediated by $Ca_V2.1$-

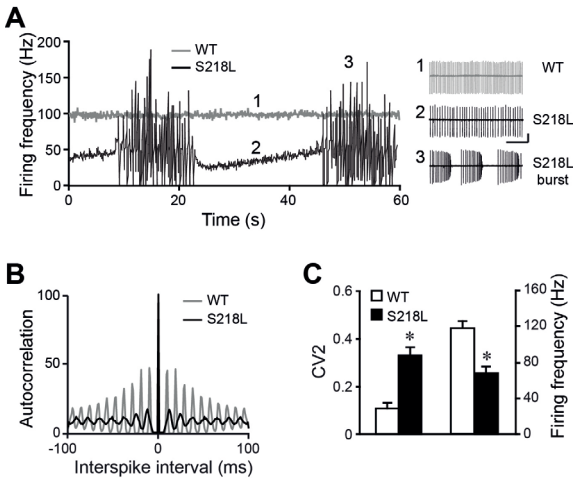

Figure 4. Irregular pacemaking activity of *Cacna-1a*^{S218L} Purkinje cells

(A) Moving averages (bin width 100 ms) of the firing frequency of intrinsic Purkinje cell activity in WT (grey line) and *Cacna1a*^{S218L} (black line) Purkinje cells. Left arrow indicate the time point of representative traces of continuous firing pattern in WT and *Cacna1a*^{S218L} shown in the top and middle insets and right arrow indicates *Cacna1a*^{S218L} burst pattern shown in the lower inset (scale bar: vertical 50 pA; horizontal 200 ms). (B) Representative autocorrelograms of interspike intervals from intrinsic WT (grey line) and *Cacna1a*^{S218L} (black line) Purkinje cell activity. (C) Mean second coefficient of variance (CV2) and firing frequency of spontaneous Purkinje cell activity from WT (n = 15) and *Cacna1a*^{S218L} (n = 15). Asterisks indicate significant differences (p-values indicated in the results section). See also Figure S4.

channels [10,20] and, moreover, the $Ca_V2.1$-channel activation curve in cerebellar *Cacna1a*^{S218L} granule cells where shown to have a clear negative shift [13,21]. In order to clarify to what extent $Ca_V2.1$-mediated Ca^{2+}-influx in Purkinje cells is changed by the S218L mutation we recorded the whole-cell Ca^{2+}-current density in acutely dissociated Purkinje cell somata from p16-p21 *Cacna1a*^{S218L} mice and wild type littermates. In WT we recorded an inward Ca^{2+}-current in response to depolarizing voltage steps from -44 ± 2 mV, which peaked (-67.3 ± 6.3 pA/pF) at -10 mV (Figure 3A). In contrast, *Cacna1a*^{S218L} mutant $Ca_V2.1$-channels in Purkinje cells were activated at a more negative membrane potential of -56 ± 2 mV ($p < 0.001$ compared to WT) and peaked (-103.5 ± 12.1 pA/pF) at -25 mV. To quantify the effect of the mutation on voltage-dependent activation, we determined the normalized whole-cell conductance at each voltage and fitted the data to a Boltzmann function, revealing a significant negative-shift in $V_{1/2}$ of the *Cacna1a*^{S218L} neurons relative to WT neurons (-36.4 ± 1.2 mV vs. -21.2 ± 1.5 mV; $p < 0.001$) (Figure 3B). The potency of this shift can be appreciated by considering the larger current density in *Cacna1a*^{S218L} neurons upon relatively mild depolarization (e.g., at –30 mV currents through *Cacna1a*^{S218L} channels are 5 times greater than WT). In addition, we recorded Ca^{2+}-currents of Purkinje cells in neonatal cerebellar slices (at p5-p6). These recordings showed a similar negative voltage shift in *Cacna1a*^{S218L} Purkinje cells ($p < 0.001$) (Figure S3), confirming the persistence of this direct effect of the S218L mutation throughout the development of *Cacna1a*^{S218L} mutants. Together these findings indicate that $Ca_V2.1$ VGCCs in *Cacna1a*^{S218L} Purkinje cells respond more readily and robustly to minor depolarization of the membrane potential.

Irregular spontaneous spiking patterns in *Cacna1a*^{S218L} Purkinje cells

The extent of the negative shift in the $Ca_V2.1$ activation curve predicts a severe effect of the S218L mutation on intrinsic pacemaking activity of Purkinje cells (see also [11]). Therefore, we recorded in loose cell-attached mode the spontaneous activity patterns of Purkinje cells in acutely prepared cerebellar slices in the presence of blockers for all synaptic transmission. Under these conditions, the Purkinje cell spiking activity appeared continuous and regular

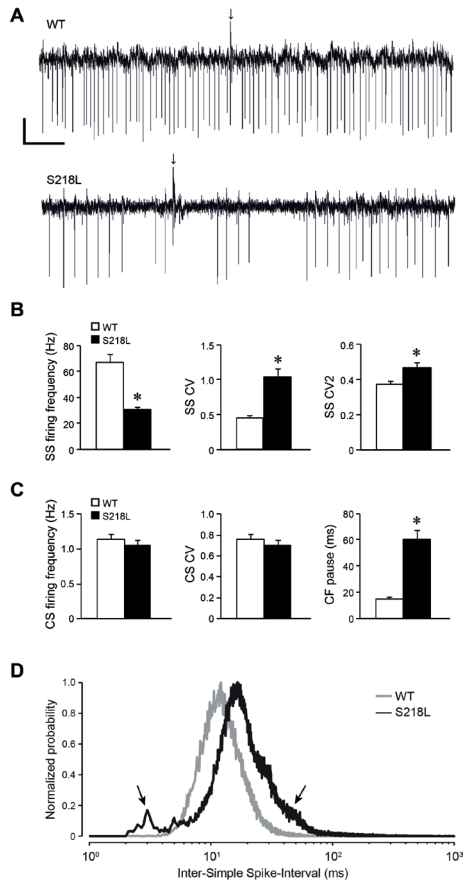

Figure 5. Irregular Purkinje cell firing in alert *Cacna1a*^{S218L} mutant mice

(A) Typical extracellular recordings of single unit Purkinje cell activity in wild type (WT; Top) and *Cacna1a*^{S218L} (S218L; Bottom) (Scale bars: vertical 400 μV, horizontal 100 ms). Arrows indicate complex spikes and all negative going events are simple spikes. (B) Left: average simple spike (SS) firing frequency (FF). Middle: SS coefficient of variation (CV). Right: SS second coefficient of variation (CV2) for WT (white; n = 14) and S218L (black; n = 25). (C) Accompanying average complex spike (CS) FF, CS CV, and length of climbing fiber (CF) pause. (D) Normalized probability distribution of all inter-simple spike-intervals pooled from all recordings of WT (grey line) and S218L (black line). Note that the burst activity of simple spikes in *Cacna1a*^{S218L} is illustrated by the peak at short inter-simple spike-intervals (left arrow) and the long pauses in simple spike activity are illustrated by the long tail in long inter simple spike intervals range (right arrow). Asterisks indicate significant differences (p-values indicated in the results section). See also Figure S5.

in all 15 recorded WT cells, but in only 1 out of 15 recorded *Cacna1a*^{S218L} Purkinje cells: the bulk of *Cacna1a*^{S218L} Purkinje cells showed an intermittent firing pattern (Figure 4A) in which periods of continuous firing (27.8 ± 6.1 s) were interrupted by bursting activity (35.3 ± 9.5 s). As a result, both the regularity and the average firing frequency of *Cacna1a*^{S218L} Purkinje cell activity were significantly different in that the second coefficient of variance (CV2) (c.f. Material and methods) was also higher and the average firing frequency was lower ($p = 0.003$ and $p < 0.001$, respectively) (Figures 4B and 4C). In addition, similar disruptions of Purkinje cell activities were observed both in the absence of blockers for all synaptic transmission and in ACSF containing a lower K^+-concentration (3.2 mM) (Figure S4), which together underline the persistent effects of the S218L mutation on Purkinje cell intrinsic pacemaking activity.

Disrupted Purkinje cell firing in alert *Cacna1a*^{S218L} mice

To study the combined effects of the altered synaptic inputs and the irregular pacemaking activity in *Cacna1a*^{S218L} mutants on the output of the cerebellar cortex we next performed *in vivo* extracellular recordings of Purkinje cell activity in alert mice. *Cacna1a*^{S218L} Purkinje cells showed qualitatively normal simple and complex spikes waveforms (Figure 5A). However, the average simple spike firing frequency was significantly lower ($p < 0.001$) (Figure 5B). A more detailed quantification of the simple spike firing patterns revealed severe irregularity in *Cacna1a*^{S218L} Purkinje cells by the occurrence of long pauses and occasional burst firing (Figures 5A and S5). In fact, both the average irregularity calculated over the whole recording (CV) as well as the irregularity calculated on a spike-to-spike basis (CV2) were significantly increased in *Cacna1a*^{S218L} Purkinje cells (p-values < 0.02) (c.f.

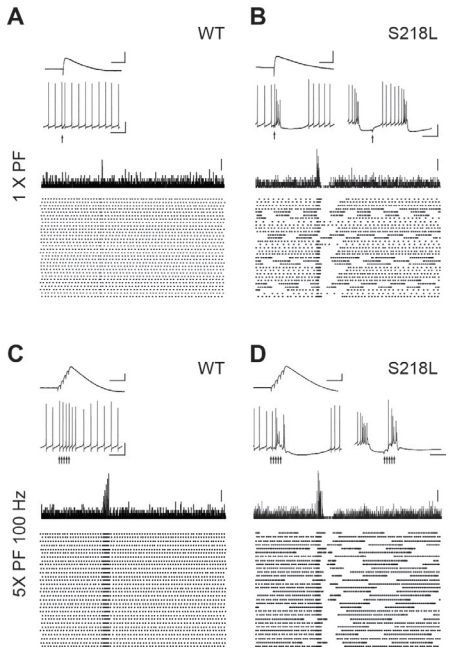

Figure 6. PF-stimulation induces Ca^{2+}-spikes in *Cacna1a*^{S218L} Purkinje cells

(A) Top: Representative traces of 2 mV PF-EPSP (top inset, scale bars: vertical 2 mV, horizontal 50 ms) and typical Purkinje cell spiking pattern in response to PF stimuli (bottom inset, scale bars: vertical 20 mV, horizontal 50 ms). Vertical arrow indicates time of stimulus. Bottom: Histogram of spike counts and accompanying raster plot of 30 repeats of single PF stimulus (scale bar: 4 spike counts). (B) Similar to (A) for a typical *Cacna1a*^{S218L} Purkinje cell that showed intermittent continuous and bursting episodes. Bottom insets show representative responses to single PF stimulus while the neuron fired continuously (left) or burst-like (right) prior to the stimulus. Note that when the *Cacna1a*^{S218L} Purkinje cell fired continuously, single PF-EPSP induced a burst; whereas when the Purkinje cell fired bursts the PF-EPSP depolarized the membrane potential to reset the burst-pause-burst cycle. (C, D) similar to (A, B) but now for a 100 Hz train of 5 PF-stimuli. (C) WT Purkinje cells respond with an action potential to each individual PF stimulus in the train (bottom inset). Scale bars: for PF-EPSP, vertical 4 mV, horizontal 50 ms; for action potential, vertical 20 mV, horizontal 50 ms; for histogram: 4 spike counts. (D) *Cacna1a*^{S218L} Purkinje cells always responded with a burst to the PF train stimulus, regardless of the pre-stimulus firing pattern.

Material and methods) (Figure 5B). Moreover, the pause in the simple spike activity after each complex spikes was 4-fold longer in *Cacna1a*^{S218L} Purkinje cells ($p < 0.001$). Remarkably, pauses in the simple spike firing with a length similar to CF pauses often occurred without a preceding complex spike (Figures 5A and 5D). In contrast to this disrupted simple spike firing pattern, both the firing frequency and the regularity of complex spikes was not affected in *Cacna1a*^{S218L} Purkinje cells (p-values > 0.4) (Figure 5C). Thus, increased PF-PC synaptic transmission and the irregular pacemaking activity are manifested in severely deregulated simple spike firing patterns in *Cacna1a*^{S218L} mutants.

Parallel fiber output elicits burst-like activity in *Cacna1a*^{S218L} Purkinje cells

In order to further reveal how the PF-PC synaptic input contributes to disrupting the simple spike firing in *Cacna1a*^{S218L} Purkinje cells, we next studied the effects of PF input on spontaneous Purkinje cell activity *in vitro*. To do so, we first adjusted the PF stimulation to elicit PF-EPSPs of 2 mV (c.f. Material and methods) in both groups, by which we canceled any influence of differences in PF input strength (c.f. Figure 2). Under these conditions, all Purkinje cells fired spontaneously, and a single PF-EPSP stimulus consistently resulted in one well-timed action potential in all 12 WT Purkinje cells, but elicited a burst and pause sequence in 12 out of 13 *Cacna1a*^{S218L} Purkinje cells (Figures 6A and 6B). The average burst and pause sequence consisted of 6.4 ± 1.3 action potentials and a 186.6 ± 25.6 ms long pause. In *Cacna1a*^{S218L} Purkinje cells that fired a burst or was pausing after a burst, the PF stimulus seemed to reset the burst-like firing state (Figure 6B). This difference in response pattern to PF stimuli between WT and *Cacna1a*^{S218L} Purkinje cells persisted when we applied a 100 Hz stimulus train of 5 pulses [22] (Figures 6C and 6D). All WT cells responded to each PF-EPSP in the train with a well-timed action potential, whereas in the

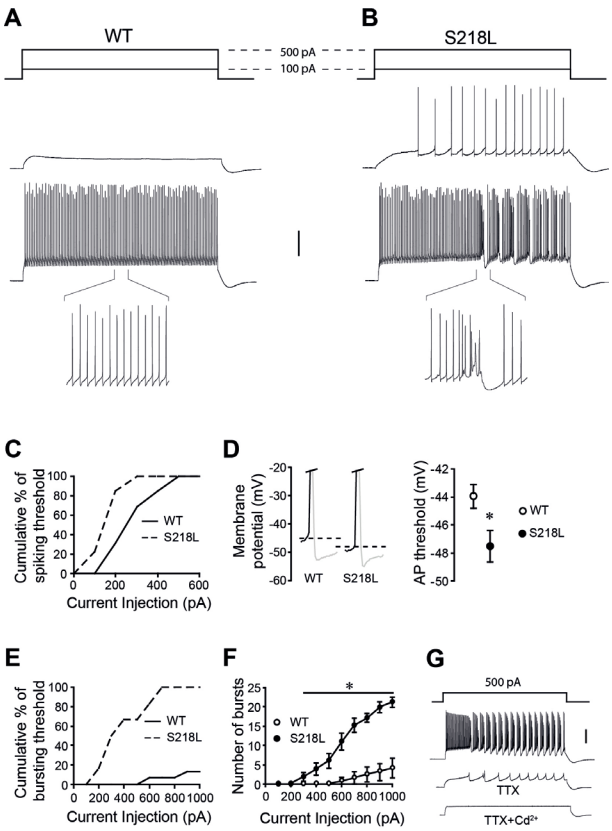

Figure 7. Hyperexcitable action potentials and Ca^{2+}-spikes in *Cacna1a*^{S218L} Purkinje cells

(A, B) Samples of Purkinje cell responses to 1500 ms depolarizing current pulses ranging from 100 – 1000 pA in WT and *Cacna1a*^{S218L} (Scale bar: 20 mV). Bottom: Purkinje cell responses of 150 ms represent regular Na^+-spikes in WT and Ca^{2+}-spikes in *Cacna1a*^{S218L}. (C) Cumulative percentage of spiking thresholds plotted against the injected currents in WT (n = 13) and *Cacna1a*^{S218L} (n = 13) Purkinje cells. (D) Left: Representative examples of action potentials from WT and *Cacna1a*^{S218L} Purkinje cells; Right: mean action potential (AP) threshold in WT (n = 13) and *Cacna1a*^{S218L} (n = 13) Purkinje cells. (E) Cumulative percentage of Purkinje cells firing bursts during the 1500 ms current injections. (F) Mean number of bursts in response to current injections of 100 - 1000 pA in WT (n = 13) and *Cacna1a*^{S218L} (n = 13) Purkinje cells. (G) Top: Sample of *Cacna1a*^{S218L} Purkinje cell responses to 1500 ms long current injections of 500 pA depolarizing current; Middle: after application of 1 µM TTX; Bottom: after co-application of 1 µM TTX and 100 µM Cd^{2+} (scale bar: 20 mV). Asterisks indicate significant differences (p-values indicated in the results section). See also Table S3.

Cacna1a^{S218L} Purkinje cells the train stimuli consistently induced bursts, regardless of the preceding activity patterns. Thus, an excitatory synaptic input with normal amplitudes elicits burst-like firing in *Cacna1a*^{S218L} Purkinje cells, which together with increased PF-PC synaptic transmission, is likely to mediate the disrupted simple spike firing *in vivo*.

Hyperexcitability of action potential and burst activity by somatic current injections in *Cacna1a*^{S218L} Purkinje cells

To determine the origin of the altered excitability in *Cacna1a*^{S218L} Purkinje cells, we tested the responses to somatic current injections ranging from 100 – 1000 pA relative to the holding current (c.f. Material and methods) (Figures 7A and 7B). Starting at the lowest current injection tested, *Cacna1a*^{S218L} Purkinje cells fired action potentials, whereas WT Purkinje cells remained silent ($p < 0.005$) (Figure 7C). Analysis on the kinetics of *Cacna1a*^{S218L} Purkinje cell action potentials showed a more negative initiation threshold ($p < 0.001$) and resting membrane potential, but the action potential rise time, amplitude and decay time kinetics as well as the basic membrane properties of the cells were normal (Figure 7D and Figure 11E; Table S3). Again, like with the PF stimulation, burst-like firing could be readily elicited by direct current injection in *Cacna1a*^{S218L} Purkinje cell somata, whereas such activity was observed only in 2 out of 15 WT neurons and only in response to current injections of ≥ 600 pA ($p < 0.001$) (Figures 7E and 7F). Since previous studies identified

Figure 8. Dendritic Ca^{2+}-spikes and enhanced backpropagation of somatic action potentials in *Cacna1a*^{S218L} Purkinje cell dendrites

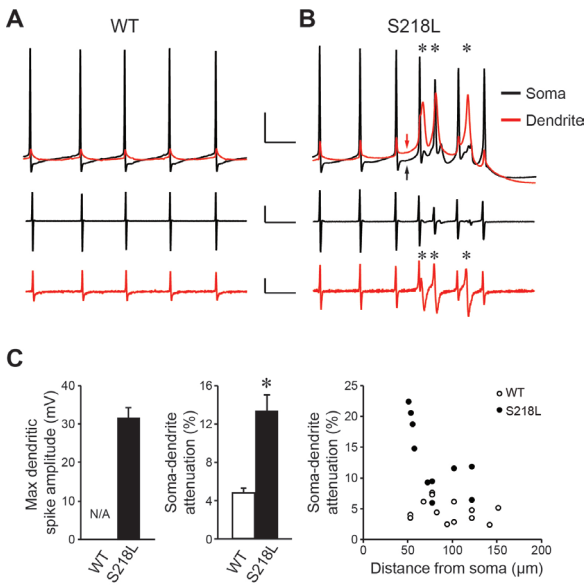

Simultaneous recordings of spontaneous spiking activity from Purkinje cell somata and dendrites. (A) Stable level of somatic action potential firing in the WT Purkinje cells causes poor back propagation of membrane depolarization into the dendrite (top, scale bars: vertical 20 mV, horizontal 10 ms). The accompanying derivatives (dV/dt) show equal time scales in the somatic (black) and dendritic (red) waveforms (scale bars: somata: vertical 300 mV/ms, horizontal 10 ms; dendrites: vertical 30 mV/ms, horizontal 10 ms). (B) Somatic and dendritic membrane potentials during spontaneous burst firing in *Cacna1a*^{S218L} Purkinje cells (top, scale bars: vertical 20 mV, horizontal 10 ms). A rise of dendritic membrane potential (red arrow) precedes the burst firing that is composed of somatic action potentials and dendritic Ca^{2+}-spikes. Dendritically generated Ca^{2+}-spikes can be recognized from their distinct kinetics compared with backpropagated somatic action potentials (indicated by asterisks). Both the rise and decay time of Ca^{2+}-spikes are slower than the backpropagated somatic action potentials (see main text for quantification; scale bars: somata (black): vertical 300 mV/ms, horizontal 10 ms; dendrites (red): vertical 30 mV/ms, horizontal 10 ms). (C) Summary of the maximum amplitudes of Ca^{2+} spikes in the *Cacna1a*^{S218L} Purkinje cell dendrites (n = 10). No dendritic Ca^{2+} spike was observed from WT Purkinje cells (left). The level of attenuation (indicated as the ratio of dendritic and somatic spike amplitudes) of somatic action potential backpropagation was smaller in *Cacna1a*^{S218L} Purkinje cells as shown in the averaged attenuation (middle) and attenuation from individual neurons (right) (WT (n = 13) and *Cacna1a*^{S218L} (n = 10).

similar burst-like activity in Purkinje cells as dendritic Ca^{2+}-spikes [6,23], we repeated the current injection experiment in *Cacna1a*^{S218L} Purkinje cells in the presence of the Na^{+}-channel blocker tetrotodoxin (TTX), which abolishes the fast somatic action potentials,

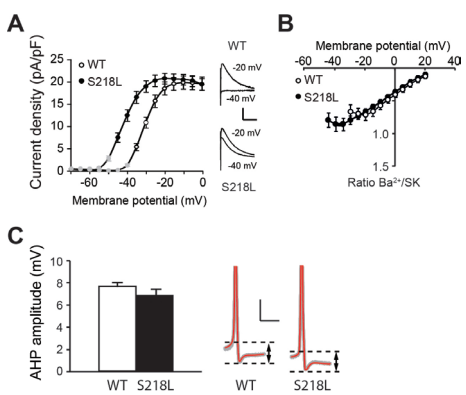

Figure 9. Concurrent left shift of SK-channel activation

(A) Voltage-current relationship of SK-currents in WT (n = 18) and *Cacna1a*^{S218L} (n = 20) Purkinje cells. Peak tail current densities were plotted against depolarizing voltages. Insets show representative traces of tail currents in WT and *Cacna1a*^{S218L} Purkinje cells evoked by 50 ms depolarizing pulses to -40 and -20 mV (holding potential = -70 mV; scale bars: vertical 10 pA/pF, horizontal 20 ms). (B) Ratio of Ba^{2+}- and SK-currents at various voltages in WT (n = 9) and *Cacna1a*^{S218L} (n = 8) Purkinje cells. (C) Mean afterhyperpolarization (AHP) amplitude in WT (n = 13) and *Cacna1a*^{S218L} (n = 13) Purkinje cells in acute cerebellar slices. Representative examples of the AHP amplitude (indicated by dashed lines and arrows) in 10 action potentials (grey) from a single WT and a single *Cacna1a*^{S218L} Purkinje cell and their average (red) (scale bars: vertical 10 mV, horizontal 2 ms). Note that action potentials have been clipped for clarity of representation.

but not the slow spikes. Co-application of $CdCl_2$, a non-specific Ca^{2+}-channel blocker, completely abolished the remaining slow spikes, confirming that *Cacna1a*^{S218L} Purkinje cells fire Ca^{2+}-spikes (Figure 7G). Thus, these data suggested that the S218L mutation induces a reduction in the initiation threshold of both action potentials and dendritic Ca^{2+}-spikes in *Cacna1a*^{S218L} Purkinje cells.

Cacna1a^{S218L} mutation induces dendritic calcium spikes and enhances backpropagation of somatic action potentials

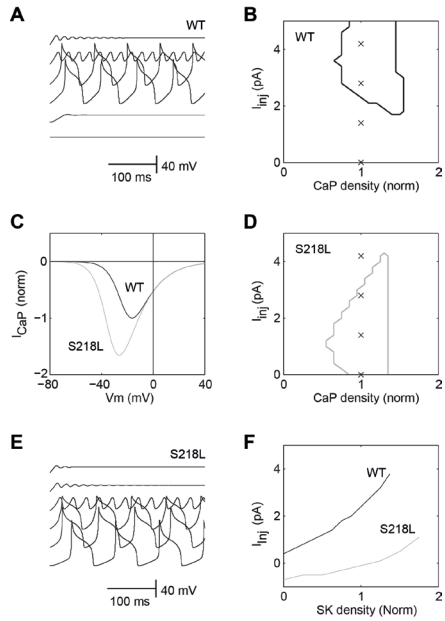

Figure 10. Simulated regulation of dendritic Ca^{2+}-spiking

Model of an isolated piece of Purkinje cell dendrite to simulate Ca^{2+} spike generation. The model contained five active membrane conductances, of which the upstroke and repolarization of a spike where facilitated by a P/Q-type calcium current and a B-type potassium current, respectively. (A) Development of the membrane potential (V_m) in response to current injections (I_{inj}) of 0, 1.4, 2.8, 4.2, 8.0 and 12.8 pA, from bottom to top. Traces were separated by 40 mV intervals for clarity of display. The model generated calcium spikes for a finite range of I_{inj}. (B) The bounded area indicates combinations of I_{inj} and CaP channel density that were suited for generating sustained calcium spiking in the model. The crosses correspond to the first four traces in (A). (C) Simulated steady-state Ca^{2+}-current I_{ss} through the model CaP-channel as a function of V_m, for WT (black) and Cacna1a^{S218L} (grey). The mutation was simulated by shifting the half-maximum activation value ($V_{1/2}$) of the CaP-channel by 12 mV in the hyperpolarizing direction. (D) The bounded area indicates the combinations of I_{inj} and CaP-channel density that were suited for generating sustained Ca^{2+} spiking with mutant CaP-cahnnels. (E) Membrane potential in response to current injections as in (A), for the *Cacna1a*^{S218L} model. (F) Regulation of the onset of spiking. The solid curves show the current injection $I_{inj,\ onset}$ at which sustained spiking starts for WT (black) and *Cacna1a*^{S218L} (grey), as a function of the SK-channel density. The *Cacna1a*^{S218L} model had a lower threshold for firing Ca^{2+}-spikes as compared to the WT model, while for both models the threshold could be modulated by changing the SK-current density.

To investigate the effect of a hyperpolarizing shift in Ca^{2+}-channel activation on Ca^{2+}-spiking in *Cacna1a*^{S218L} Purkinje cell dendrites, we performed simultaneous patch clamp recordings from both the Purkinje cell soma and dendrite. In WT Purkinje cells the spontaneous action potential firing did not elicit any burst like activity and both the somatic and dendritic recordings showed stable waveforms during spontaneous activity as well as in response to current injections (Figure 8A). In accordance with previous findings [24] the action potentials generated from the soma were heavily attenuated in the dendrite, and thus had little influence on the dendritic waveforms. In fact, even direct current injections of up to 1000 pA in the dendrite did not elicit any dendritic Ca^{2+}-spikes in WT Purkinje cells (data not shown). In contrast, all of the 10 recorded *Cacna1a*^{S218L} Purkinje cells frequently showed spontaneous bursting activity that consistently started with an elevation of the dendritic membrane potential (5.2 ± 1.3 mV relative to the membrane potential during the previous interspike-interval; c.f. Material and methods) that preceded the initiation of somatic bursting activity (Figure 8B). During the bursting activity, the dendritic electrode recorded both the dendritic spikes as well as the backpropagated somatic spikes (Figure 8B). Although the dendritic amplitude of the somatic action potential firing was related to the distance between the soma and the dendritic recording electrode, our results show that the backpropagation of somatic spikes was enhanced in the *Cacna1a*^{S218L} Purkinje cells (Figure 8C). The dendritic spikes and backpropagated action potentials were separated by amplitude,

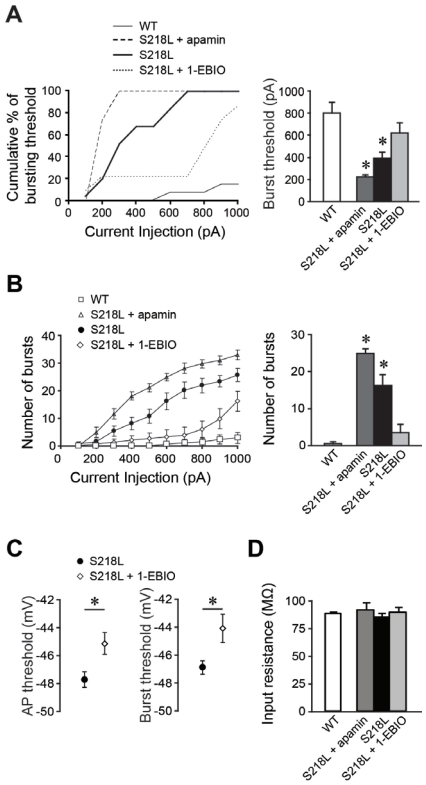

Figure 11. SK-channel activator 1-EBIO increases the threshold for Ca^{2+}-spike activity in *Cacna1a*^{S218L} mice.

(A) Left: Cumulative percentage of bursting thresholds plotted against the injected currents in Cacna1a^{S218L} Purkinje cells with 0.5 nM apamin (n = 7) or in *Cacna1a*^{S218L} Purkinje cells with 10 µM 1-EBIO in the bath (n = 8). For comparison the WT and *Cacna1a*^{S218L} Purkinje cell data are represented again (as in Figure 7). Right: Averaged bursting threshold for the four groups represented in left panel. Note that the WT values did not differ significantly from the S218L + 1-EBIO group. (B) Left: Similar groups as in (A) but now representing the mean number of bursts in response to 1500 ms current injections of 100 - 1000 pA. Right: The average number of bursts at 600 pA of current injection. Note that application of apamin increases the bursting activity, whereas 1-EBIO rescues the bursting activity. (C) Average action potential threshold (Left) and Ca^{2+} burst threshold (Right) in *Cacna1a*^{S218L} cells with and without 1-EBIO. (D) The average input resistances recorded at 34 ± 1°C of all cells presented in (A, B and C). Asterisks indicate significant differences.

rise time and decay time: The maximal amplitude of the dendritic spikes during a single burst was 31.5 ± 2.7 mV relative to the spiking threshold, which surpasses the dendritic amplitude of the backpropagated action potentials when recorded as proximal as ~50 µm (Figure 8C). The rise (1.46 ± 0.15 ms) and decay time (1.92 ± 0.1 ms) of these dendritic events is significantly longer than from backpropagated somatic events (0.29 ± 0.04 ms and 0.21 ± 0.01 ms; both $p < 0.001$). Moreover, towards the end of the bursts the dendritic events preceded the somatic events (Figure 8B). These results indicate that the S218L mutation promotes both dendritic depolarization and backpropagation of somatic

Figure 12. SK-channel activator 1-EBIO reduces irregular simple spike firing and shortens CF pause in alert *Cacna1a*^{S218L} mice

(A) Top: average complex spike (CS) firing frequency (FF) (Left), CS coefficient of variation (CV) and climbing fiber (CF) pause for WT (white; n = 14), WT + 1-EBIO (light grey; n = 13), *Cacna1a*^{S218L} (black; n = 25), and *Cacna1a*^{S218L} + 1-EBIO (dark grey; n = 21). Bottom: Accompanying average simple spike (SS) FF, SS CV, and SS CV2. (B) Normalized probability distribution of all inter – simple spike – intervals pooled from all recordings of *Cacna1a*^{S218L} (thin) and *Cacna1a*^{S218L} + 1-EBIO (bold). Note the absence of bursting simple spike activity in the presence of 1-EBIO (indicated by arrow). Inset shows a zoom in on the normalized probability of long (50 – 300 ms) inter – simple spike – intervals for *Cacna1a*^{S218L} (thin), *Cacna1a*^{S218L} + 1-EBIO (bold) and WT (gray) (for clarity reasons constructed using a 1 ms bin size). Note the significant reduction of long simple spike pause in the presence of 1-EBIO. Asterisks indicate significant differences (p-values indicated in results section).

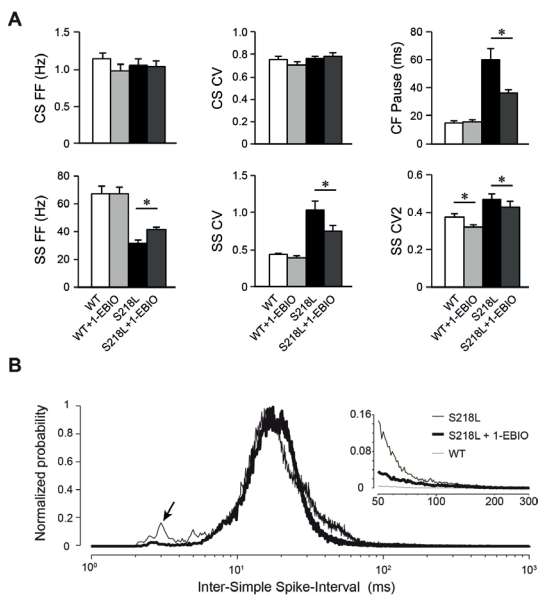

action potentials, which together frequently trigger dendritic Ca^{2+}-spike firing.

Involvement of Ca^{2+}-activated K^+-channels in modulating dendritic Ca^{2+}-spike activity in *Cacna1a*^{S218L} Purkinje cells

As indicated by various studies [11,25,26], the balance between $Ca_V2.1$ and Ca^{2+}-dependent K^+-channels is crucial for proper Purkinje cell functioning. To study the possible effects of the negative shift in activation of $Ca_V2.1$-channels on Ca^{2+}-dependent K^+-channels, we recorded the tail currents in response to Ca^{2+}-influx at various holding potentials in dissociated Purkinje cells. Under our conditions (c.f. Material and methods), the tail currents are known to be indicative of small-conductance Ca^{2+}-dependent K^+-channels, e.g., SK-channels [27]. The activation curve of these SK-currents showed a significant

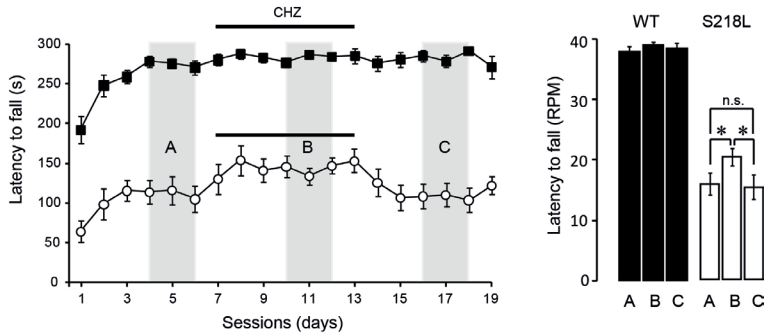

Figure 13. Oral administration of CHZ improves motor performance in *Cacna1a*^{S218L} mice.

The performance of *Cacna1a*^{S218L} mice (n = 9) and WT littermates (n = 14) were evaluated using an accelerating rotarod on daily bases. CHZ was applied for 7 days (black bar) after a stable score was achieved for three days. The performance was scored before, during and after CHZ treatment by comparison of the latency to fall in time (left) and rotations per minute (RPM; right). Three days were averaged during each period as indicated by grey bars, e.g., A, B and C, respectively. CHZ administration improved the motor performance, in that the latency to fall was significantly increased in *Cacna1a*^{S218L} mice but not their WT littermates. Asterisks indicate significant difference.

left-shift in *Cacna1a*^{S218L} Purkinje cells relative to WT Purkinje cells ($V_{1/2}$ in *Cacna1a*^{S218L} -41.9 ± 0.1 mV vs. WT -30.6 ± 0.6 mV; $p < 0.001$) (Figure 9A). The maximal amplitude of these SK-currents in Cacna1a^{S218L} Purkinje cells are similar to those in WT ($p = 0.69$). The extend of adaptation of SK-currents in Cacna1a^{S218L} Purkinje cells becomes apparent from the ratio between Ca_V- and SK-currents (see Material and methods): at all membrane potentials that evoked > 5 pA/pF current density for both Ca_V- and SK-currents in WT Purkinje cells, the ratio was not significantly different (all p-values > 0.15) (Figure 9B). In addition, the ratio between Ca_V- and SK-current densities remains within normal limits at membrane potentials more hyperpolarized than -35 mV, e.g., potentials at which only in Cacna1a^{S218L} Purkinje cells $Ca_V2.1$ are activated. Similarly, in cerebellar slices we found no difference in the amplitude of the afterhyperpolarization (AHP), which is known to be mediated by SK-currents, relative to the action potential threshold ($p = 0.26$) (Figure 9C). These results indicate that in *Cacna1a*^{S218L} Purkinje cells the SK-channels activate at more negative membrane potentials in response to the left shift of the $Ca_V2.1$ activation without apparent compensatory properties.

Given that SK-channel functions have been shown to be the critical modulator of Purkinje cell burst firing [26,28], we next studied the possible effects of left shift in Ca_V-channel activation and concurrent shift in SK-channel activation on dendritic Ca^{2+}-spiking and the impacts of modulating SK channel function in regulating Purkinje cell burst firing. We first modeled an isolated piece of a Purkinje cell dendrite with active membrane currents that control dendritic excitability to generate Ca^{2+}-spikes (see Material and methods for details). The upstroke and repolarization of the Ca^{2+}-spike were facilitated by a high-voltage-activated Ca^{2+}-current (CaP) and a high-affinity Ca^{2+}-activated potassium current (SK), respectively. In addition, the model contained a low-threshold calcium current (CaT), a persistent potassium current (KM) and the BK-type Ca^{2+}-activated potassium current. The model generated Ca^{2+}-spikes upon increasing external current injection I_{inj} (Figure 10A), for a range of CaP channel densities (Figure 10B) and shifting the activation of the CaP channel (Figure 10C) indeed increased the excitability of the model, up to a point where a CaP-generated upstroke was generated even when no external current was injected (Figures 10D and 10E). The threshold for Ca^{2+}-spike generation could be modulated by changing the SK current density in that decreasing the SK channel density did not reduce the excitability, but increasing SK channel density effectively elevated the threshold that elicit Ca^{2+}-spikes (Figure 10F). In contrast, the CaP-BK balance proved irrelevant for the threshold for spike generation. Taken together, the model shows that dendritic Ca^{2+}-spike firing indeed could be modulated by increasing the SK current density.

In order to test the computational predictions of the effects of SK-channel modulation on the occurrence of dendritic Ca^{2+}-spikes in *Cacna1a*^{S218L} Purkinje cells, we studied the effects of both SK-channel blockers and activators. We first applied a SK-channel blocker to cerebellar slices of the gain-of-function *Cacna1a*^{S218L} mutants. Bath-application of various concentrations of apamin (0.5 nM - 1 mM) did not restore the disrupted spiking pattern in *Cacna1a*^{S218L} Purkinje cells. Instead, similar to the effect of apamin to WT Purkinje cells, application of apamin (shown 0.5 - 1 nM apamin) to *Cacna1a*^{S218L} Purkinje cells induced continuous burst firing of Na^+-spikes and decreased threshold of dendritic Ca^{2+}-spikes (Figures 11A and 11B). In contrast, bath-application of the SK-activator 1-EBIO (10 μM) restored the thresholds of both Na^+- and Ca^{2+}-spiking as well as the number of bursts in *Cacna1a*^{S218L} Purkinje cells to near WT levels without changing the input resistance (all p-values > 0.3) (Figures 11C and 11D). Thus, the enhanced SK-channel function following application of 1-EBIO (as indicated by the increase threshold of Na^+- and Ca^{2+}-spikes) counteracts the effects of the S218L mutation on Purkinje cell spiking *in vitro*.

In vivo application of SK-activators increased regularity of Purkinje cell firing and improved motor performance

To further test the effectiveness of 1-EBIO in normalizing *Cacna1a*^{S218L} Purkinje cell firing, we applied this drug *in vivo*. Following the application of 1-EBIO to the craniotomy (c.f. Material and methods) extracellularly recorded activity patterns of *Cacna1a*^{S218L} Purkinje cells reverted towards WT levels: both the CV- and CV2-values decreased, the average firing frequency increased and the climbing fiber pause reduced (all p-values < 0.02) (Figure 12A). Most strikingly, 1-EBIO almost completely eliminated the burst-like

activity as well as the long spontaneous pauses in the simple spike firing, and thereby greatly improved the regularity of simple spike firing (Figure 12B). Moreover, 1-EBIO also induced a change in WT Purkinje cell firing, in that the average CV2-value reduced significantly ($p < 0.03$) (Figure 12A). Thus, our data show that enhancing SK-currents counteracts the disruptive effect of the S218L gain-of-function mutation on $Ca_V2.1$-currents.

The positive effects of enhancing SK-currents in *Cacna1a*^{S218L} Purkinje cells prompted us to test whether the motor behavior would also improve by application of SK-activators, as recently shown for loss-of-function *Cacna1a* mutants [29]. In order to do so, we trained the animals on the accelerating rotarod until a stable score was reached (Figure 13). In *Cacna1a*^{S218L} this baseline score was 111 ± 15 s and for wild type 275 ± 6 s ($p < 0.001$). During the next 7 consecutive days we supplied the mice with Chlorzoxazone (CHZ), a FDA-approved drug that has been indicated to enhance SK-currents, in their drinking water (c.f. Material and methods) [29]. Whereas in wild type CHZ did not affect their near maximal rotarod score, in *Cacna1a*^{S218L} we found a significant increase in the maximal rotation speed (Figure 13) ($p = 0.02$). After we stopped the supply of CHZ the scores of the *Cacna1a*^{S218L} mutants returned to baseline values, whereas in wild type mice no change was observed. Together these data show that application of a SK-channel activator reduces both the irregularity of Purkinje cell firing in *Cacna1a*^{S218L} mutants as well as the ataxic motor performance.

Discussion

Previous studies have provided clear evidence as to how cerebellar ataxia comes about in loss-of-function *Cacna1a* mutants, but as of yet it remained unclear how gain-of-function mutations in the same gene can induce ataxia. Here we show that mice that harbor the S218L gain-of-function mutation in the *Cacna1a* gene [13] exhibit typical cerebellar hallmarks of ataxia, such as altered connectivity and transmission at the PF-PC synapse as well as irregular Purkinje cell pacemaking activity and disrupted simple spike firing. Moreover, our results reveal that the irregular firing of Purkinje cells in alert *Cacna1a*^{S218L} mutants is based upon hyperexcitability; somatic current injections trigger action potentials and dendritic Ca^{2+}-bursts more readily and PF stimulation also results in Ca^{2+}-spikes. Finally, our study reveals that not only the Ca^{2+}-spikes in *Cacna1a*^{S218L} Purkinje cells, which are enabled by a left-shift in the activation curve of $Ca_V2.1$-channels, and the burst-pause sequences in simple spike firing can be counteracted by increasing the SK-channel function, but also the ataxic motor behavior of *Cacna1a*^{S218L} mutants is relieved by a similar approach. Below we will discuss the impact of these findings for cerebellar functioning in general and we will address the analogy with phenotypes of loss-of-function *Cacna1a* mutants.

Origins of increased synaptic transmission between granule cells and Purkinje cells in *Cacna1a*^{S218L} mice

Instead of showing compensational signs of decreased activity such as a decreased number of PF-PC synapses, PF varicosities or Purkinje cell spines, our results demonstrated that the S218L gain-of-function *Cacna1a* mutation increased the percentage of PF varicosities that

contact multiple Purkinje cell spines. This alteration in connectivity between granule cells and Purkinje cells was counterintuitive, since the same increase was found in various loss-of-function *Cacna1a* mutants and was suggested to be a likely candidate to compensate for the partial loss of synaptic transmission at this synapse [9,30,31]. Since we did not observe any Purkinje cell spine contacting with multiple PF varicosities in the *Cacna1a*^{S218L} mutants, the normal density of PF-PC synaptic components may be due to some PF varicosities contacting no Purkinje cell spine. In principle such varicosities may also contact spines of multiple Purkinje cells, molecular layer interneurons or Golgi cell dendrites, and further detailed experiments are needed to elucidate how the offset in Ca^{2+}-homeostasis affects the distribution of such synaptic connections in both loss- and gain-of-function mutations.

Apart from the altered morphology, the granule cell – Purkinje cell synaptic connection is strengthened by the S218L mutation, in that both the stimulation of a bundle of granule cell axons and the activation of a single granule cell elicit a larger response in *Cacna1a*^{S218L} Purkinje cells. Although our experiments were not designed to unravel to what extend the release probability at granule cell – Purkinje cell synapses is increased in *Cacna1a*^{S218L} mice, our findings are in parallel with those of a recent study that reported on the continuously facilitated $Ca_V2.1$-channels and enhanced Ca^{2+}-influx in *Cacna1a*^{S218L} granule cell terminals [32]. In summary these recent and our current findings indicate that the release of glutamate is presumably increased at *Cacna1a*^{S218L} granule cell – Purkinje cell synapses.

In contrast to the differences in PF-PC contacts, we found that the synaptic transmission at the CF-PC synapse is relatively unaffected in *Cacna1a*^{S218L} mutants. Although a substantial portion of neurotransmitter release from climbing fibers is mediated by $Ca_V2.1$-channels we only found a reduced release in response to the second stimulation at longer intervals ($\geq$ 200 ms). As both loss-of-function *Cacna1a* mutants and the gain-of-function *Cacna1a*^{S218L} mutant show a normal initial CF-EPSC amplitude [8,33], our data support the possibility that synaptic transmission at the CF-PC synapse is less vulnerable to Ca^{2+}-channelopathies than PF-PC synapses; this difference may be due to the saturated release probability of transmitter release at the CF-PC synapse [8,34]. Our *in vivo* data further support this idea in that both the frequency and regularity of complex spikes remained intact in *Cacna1a*^{S218L} Purkinje cells. Although we cannot rule out the possible effect of decreased τ_{decay} of CF-EPSCs, it seems reasonable to state that the S218L mutation affects the CF input less than the PF input.

The *Cacna1a*^{S218L} mutation induces Purkinje cell hyperexcitability and irregular pacemaking activity

The current results show that, as in other cell types (including cerebellar granule neurons [13], and transfected cortical neurons [21]), in Purkinje cells the S218L mutation causes a negative shift in activation of $Ca_V2.1$-currents, which probably leads to Purkinje cell hyperexcitability and irregular pacemaking activity. These phenomena could be explained by various factors. First, *Cacna1a*^{S218L} $Ca_V2.1$-channels are activated at membrane potentials (~-56 mV in dissociated somata and -48 mV in p5/p6 Purkinje cells) close to

the initiation threshold of Na^+-dependent action potentials [23,35,36]. As the lower action potential threshold was partially rescued by blockage of VGCCs (Figure S6), the $Ca_V2.1$-channels are the most likely candidate for the hyperexcitability of action potential firing. Second, $Ca_V2.1$ channels in *Cacna1a*^{S218L} Purkinje cells are prone to be active more during spontaneous action potential firing and thus could readily initiate Ca^{2+}-spikes, as indicated by the frequent burst-pause sequences in spontaneous pacemaking activity. At this point, however, we cannot rule out the possibility that the S218L mutation also induces secondary effects on various Na^+- and K^+-channels, which in turn could also have a direct impact on action potential firing in Purkinje cells (see also [35]). Third, our simultaneous somatic and dendritic whole cell patch clamp recordings during spontaneous activity show that depolarization of the dendritic membrane triggers the burst-firing in *Cacna1a*^{S218L} Purkinje cells. This bursting activity can also be elicited by minor current injections to both soma and dendrite of *Cacna1a*^{S218L} Purkinje cells, but not in wild type Purkinje cells. Moreover, when we project the increased PF-EPSC amplitude on the intrinsic hyperexcitability of *Cacna1a*^{S218L} Purkinje cells, it becomes clear that the PF-input further disrupts the irregular pacemaking activity, which together form a solid basis for the irregular simple spike firing found in alert *Cacna1a*^{S218L} mice.

Still, we cannot exclude a contribution of disrupted feed-forward inhibition by the molecular layer interneuron - Purkinje cell input to the irregular Purkinje cell firing pattern [37,38]. One possible effects of the S218L mutation on this prominent inhibitory input to Purkinje cells is that the release of GABA is enhanced, since it was found to be decreased in various loss-of-function mutants [39]. However, it was recently found that in the cerebral cortex the comparable R192Q gain-of-function mutation in the *Cacna1a* gene did not affect inhibitory transmission whereas it did enhance excitatory transmission [40]. We found no difference in the *in vitro* Purkinje cell activity with or without inhibitory neurotransmission and thus it appears likely that the enhanced granule cell input to Purkinje cells and the hyperexcitable intrinsic pacemaking activity together are the main cause for the disrupted Purkinje cell output in *Cacna1a*^{S218L} mice.

Ataxia in gain- and loss-of-function *Cacna1a* mutants

The current study reveals striking similarities in the effects of *Cacna1a*^{S218L} gain-of-function mutants with those described in ataxic loss-of-function *Cacna1a* mutants. Clearly, PF-PC synapses and Purkinje cells are both sensitive to increases and decreases in $Ca_V2.1$-currents. However, the type of disturbance of Purkinje cell pacemaking activity that these shifts in $Ca_V2.1$-currents induce differs between *Cacna1a*^{S218L} gain-of-function mutants and loss-of-function mutants. Whereas the hyperexcitability of *Cacna1a*^{S218L} Purkinje cells results in frequent spontaneous or PF-induced burst (e.g., Ca^{2+}-spike) firing, ataxic tottering, leaner and ducky mice show a highly irregular pacemaking activity in Purkinje cells, but no spontaneous Ca^{2+}-spikes [11,35]. Still, both types of abnormalities are equally detrimental for information processing in the cerebellar cortex and both gain-of-function and loss-of-function *Cacna1a* mutants are ataxic [7,13].

A recent study showed that both irregular Purkinje cell pacemaking activity and

ataxic motor behavior in loss-of-function *Cacna1a* mutants were rescued by SK-channel activators [11]. Similarly, but counter intuitively, the same SK-activator also improved the regularity of Purkinje cell firing and motor performance in gain-of-function *Cacna1a*^{S218L} mutants. Although both in loss-of-function and gain-of-function *Cacna1a* mutants direct evidence for a misbalanced Ca_V-SK ratio in loss-of-function *Cacna1a* mutants is not available([11] and this study), it appears that enhancing the SK-channel function reduces the effects of the decreased and increased $Ca_V2.1$-mediated current. Application of SK-channel activating drugs like 1-EBIO and CHZ improves the regularity of Purkinje cell pacemaking activity in loss-of-function mutants whereas these drugs reduce the burst firing in gain-of-function mutants. Therefore, the present study further widens the avenue of therapeutical applications for SK-channel activators in treating ataxia in *CACNA1A*-mutated patients (see also [29]). Interestingly enough, 4-AP, a voltage gated K^+-channel inhibitor, also restores the precision of Purkinje cell pacemaking activity by broadening the action potentials and increasing the AHP amplitude in tottering Purkinje cells [41]. These data suggest that in loss-of-function mutants, other drugs that promote AHP are functional in restoring regular Purkinje cell firing and hint that perhaps in gain-of-function mutants substances that reduce the bursting threshold and/or hyperexcitability could also reduce the irregularity of Purkinje cell firing and thereby reduce ataxic motor performance like we found for 1-EBIO and CHZ.

Granting the irregular *Cacna1a*^{S218L} Purkinje cell firing pattern, we should also consider potential additional downstream effects of the S218L mutation. For instance, as shown for ataxic loss-of-function mutants, irregular Purkinje cell firing may result in a further loss of information since the propagation reliability of Purkinje cell axons drops off at intra-burst frequencies (e.g., > 280 Hz) [42,43]. Moreover, it is known that (semi-) chronic alterations of the Purkinje cell firing patterns can lead to severe morphological aberrations of their axon terminals [44,45,46] and thereby mediate irregular activity of cerebellar nuclei neurons, as was recently shown for the loss-of-function *Cacna1a* mutant tottering [47]. Our results thus predict that the firing patterns of *Cacna1a*^{S218L} cerebellar nuclei neurons are similarly disturbed as in loss-of-function *Cacna1a* mutants, and that their activities should be carefully addressed in exploring the potential therapeutical power of SK-channel activators.

Material and Methods

Animals

Cacna1a^{S218L} mice were generated as previously described [13]. Homozygous *Cacna1a*^{S218L} mice and WT littermates (both genders) ranging from postnatal day (p) 5 to three-month-old were used in the experiments. Animals were maintained at 22 ± 2 °C with 12 hrs dark and light cycle and were provided with food and water ad libitum. All studies were performed with experimenters blind to the genotype and in accordance with the guidelines of the respective universities and national legislation.

Immunohistochemistry

Two-month-old *Cacna1a*^{S218L} mice and WT littermates were anaesthetized with Nembutal (50 mg/kg, i.p.) and perfused transcardially with 50 ml phosphate-buffered saline (PBS) (pH 7.4) containing 4% paraformaldehyde. The cerebellum was carefully removed and post-fixed in fresh fixative for 2 hrs at room temperature. Sixty-µm thick parasagittal sections were sliced with a cryotome (Leica, Wetzlar, Germany), collected in 0.1 M PB and rinsed in 50 mM PB. Free-floating slices were blocked with 10% normal horse serum (NHS) and 0.5% Triton-X100 for 1 hr and incubated with rabbit anti-calbindin D-28K antibody (1:10.000, Sigma-aldrich, Zwijndrecht, Netherlands), diluted in PBS with 2% NHS and 0.5% Triton-X100 for 72 hrs. Subsequently, slices were incubated with biotinylated goat-anti-rabbit secondary antibody (1:200; Vector Laboratories, Burlingame, CA, USA) for 1.5 hrs and followed by 1.5 hrs incubation with avidin-biotinylated horseradish peroxidase complex (ABC-HRP, Vector Laboratories). Sections were rinsed in 0.1 M phosphate buffer and visualized with 0.05% 3, 3-diaminobenzidine tetrahydrochloride. After rinsing in 0.1 M PBS, slices were mounted and counterstained using Nissl staining. For a subset of mice (n = 3 for each genotype) we applied a fast Golgi-Cox staining method as described before [48]. Spine numbers per 10 µm of dendritic length and varicosities along parallel fibers [49] were quantified using MetaVue (Universal Imaging Corp., San Francisco, CA, USA).

Electron microscopy

Four two-month-old *Cacna1a*^{S218L} mice and four WT littermates were anaesthetized with Nembutal (50 mg/kg, i.p.) and perfused transcardially with 50 ml 0.12 M phosphate buffer (pH 7.4) containing 4% paraformaldehyde and 0.2% glutaraldehyde. Next, cerebella were cut into 80 to 100 µm sections using a vibratome (Technical Products International, St. Louis, MO, USA) and collected in 0.12 M phosphate buffer. Sections were post-fixed in 1% osmium tetroxide, stained with 1% uranyl acetate, dehydrated and embedded in Araldite (Durcupan ACM, Fluka, Germany). Ultrathin (50-70 nm) sections were cut using a ultramicrotome (Leica), mounted on Formvar-coated copper grids, contrasted with 2% uranyl acetate and 1% lead citrate (Fluka), and analyzed using a CM100 electron microscope (Philips, Eindhoven, The Netherlands). Electron micrographs were collected with a CCD-camera (Megaview II, Olympus Soft Imaging System, Munster, Germany) and analyzed with AnalySIS (Olympus Soft Imaging System) and MetaVue (Universal Imaging Corp., San Francisco, CA, USA) image processing software. To estimate the average numbers of Purkinje parallel fiber-Purkinje cell synapses, 25 images of the most distal 1/3 of the molecular layer were collected per animal at 13,500X. PF-PC synapses were recognized as asymmetrical contacts with loosely clustered spherical synaptic vesicles in PF varicosities and clear postsynaptic density structures in Purkinje cell spines. CF-PC synapses were identified by their more proximal location and high number of tightly compacted vesicles. The morphology of PF varicosities and Purkinje cell spines was analyzed at 19,000X. To verify the percentage of PF varicosities that contact multiple Purkinje cell spines, 1000 synaptic contacts per genotype were quantified. To quantify the dimensions of the PF varicosity and dendritic spine > 50 structures per animal were used. The Purkinje cell spine length was calculated by measuring the distance between the tip of the spine head and

the base of the spine neck. Electron micrograph analysis was performed by averaging per animal and then by genotype. Data are represented as mean ± S.E.M.

Slice preparation for electrophysiology

Cacna1a^{S218L} mutants and WT littermates of various ages were decapitated under isoflurane anesthesia. Subsequently, the cerebellum was removed and transferred into ice-cold slicing medium that contains (in mM): 240 Sucrose, 5 KCl, 1.25 Na_2HPO_4, 2 $MgSO_4$, 1 $CaCl_2$, 26 $NaHCO_3$ and 10 D-Glucose, bubbled with 95% O_2 and 5% CO_2. Parasagittal slices (200 or 250 μm thick) of the cerebellar vermis were cut using a vibratome (VT1000S, Leica) and kept in ACSF containing (in mM): 124 NaCl, 5 KCl, 1.25 Na_2HPO_4, 2 $MgSO_4$, 2 $CaCl_2$, 26 $NaHCO_3$ and 20 D-Glucose, bubbled with 95% O_2 and 5% CO_2 for > 1 h at 34 ºC before the experiments started.

Whole-cell electrophysiology

Experiments were performed with a constant flow of oxygenated ACSF (1.5-2.0 ml/min). Purkinje cells were visualized using an upright microscope (Axioskop 2 FS plus, Carl Zeiss, Jena, Germany) equipped with a 40X water immersion objective. Patch-clamp recordings were performed using an EPC-10 double amplifier (HEKA electronics, Lambrecht, Germany). Voltage-clamp recordings were performed at room temperature whereas current clamp and loose cell-attached recordings were performed at 34 ± 1 ºC. All *in vitro* experiments are performed in the presence of picrotoxin (100 μM) except for the recording of spontaneous Purkinje cell activity presented in Figure S4. Blockers of other neurotransmitters were applied where indicated.

Parallel fiber response

Four two- to three-month-old *Cacna1a*^{S218L} mutants and five WT littermates were used to record Purkinje cell responses to PF stimulation. The resistances of borosilicate patch pipettes ranged from 2.8 - 3.5 MΩ when filled with intracellular solution containing (in mM): 70 Cs-Methalsulfonate, 80 CsCl, 2 $MgCl_2$, 1 EGTA, 10 HEPES, 4 Na_2ATP and 0.4 Na_3GTP (pH 7.3). Membrane potentials were clamped at -70 mV with holding currents ranging from -100 to -200 pA. A voltage step of -10 mV was applied following each stimulus to monitor series and input resistances. Cells were discarded if the input resistance was < 150 MΩ or when series and/or input resistance shifted more than 15% during the recording. To evoke PF-mediated excitatory postsynaptic currents (PF-EPSCs), patch pipettes filled with ACSF were placed in the most distal 1/3 of molecular layer adjacent to the patched Purkinje cells at the same distance and orientation. To assess the stimulus intensity - EPSC output (input-output) ratio consistently, only Purkinje cells with similar dendritic arborization (based on the width of molecular layer) were selected. To elicit paired-pulse facilitation, two consecutive stimuli with 8-10 μA stimulus intensity were given with 25 - 500 ms inter-stimulus intervals. PF-EPSC kinetics were characterized by calculating the 10 - 90% rise time and τ_{decay} using a single exponential fit (IGOR pro, Wavemetrics, Inc., Portland, OR) to averaged (4-6 subsequent) PF-EPSCs recorded in response to stimuli of 10 μA.

Paired Purkinje cell and granule cell recordings

P21-30 *Cacna1a*^{S218L} mutants (n = 10) and WT littermates (n = 12) were used for paired whole-cell recording. Purkinje cells were voltage clamped at -65 to -70 mV with intracellular solution containing (in mM): 120 K-Gluconate, 9 KCl, 10 KOH, 3.48 $MgCl_2$, 4 NaCl, 10 HEPES, 4 Na_2ATP, 0.4 Na_3GTP 17.5 sucrose and 10-20 µM Alexa 488 (pH 7.25). Purkinje cell dendritic arborizations were visualized using epifluorescence to select Purkinje cells with complete dendritic tree. Following the visualization of Purkinje cells, granule cells below the Purkinje cell dendrite tree and < 100 µm away for soma were randomly selected. Whole-cell recordings of granule cells were performed using intracellular solution containing (in mM): 126 K-Gluconate, 1 $MgSO_4$, 4 NaCl, 0.1 BAPTA, 0.05 $CaCl_2$, 5 HEPES, 3 MgATP, 0.1 Na_3GTP and 15 D-Glucose (pH 7.2). In our preparation, > 95% patched granule cells were excitable. Granule cells were held at -60 mV with minimal current injection (-20 to 0 pA) in current clamp mode. Trains of granule cell action potentials were evoked with a 50 ms square current pulse, of which the current intensity was adjusted in that the action potential train was maintained at a physiological relevant frequency (~ 200Hz). Although no effort was made to differentiate between parallel fiber connections and ascending axon connections, it is likely both connections were included in our experiment (see also [50]). Purkinje cell recordings with 15 to 30 repetitive granule cell stimulations were selected for offline analysis. The EPSC amplitude at a single granule cell-Purkinje cell synapse elicited by such high frequency spike train was usually > 5 pA, thus could be unambiguously depicted from baseline noise. Experiments were performed at 34 ± 1 ºC.

Climbing fiber response

Eight *Cacna1a*^{S218L} mutants and eight WT littermates ranging from p16 - p21 were used to quantify Cf-PC synaptic transmission [51]. To avoid contamination of CF-EPSC by Na^+-spikes, we included 5 mM QX-314 in the Cs^+-based intracellular solution. To standardize the driving force, we continuously clamped the membrane potential at -20 mV from the reversal potential (~0 mV). This also implicated that the elicited currents are well within the limits of our amplifiers; at resting membrane potentials (~-65 mV) the currents elicited by climbing fiber activation often saturate the amplifier. Only cells with low initial series resistance of 8 - 12 MΩ and series resistance compensated for > 70% were included in the study. Reversal potentials were measured before and after experiments and cells were excluded if reversal potential shifted > 3 mV. Stimulation electrodes were placed in the granule cell layer surrounding the Purkinje cell somata. We checked for Purkinje cells innervated by multiple climbing fibers by gradually increasing the stimulus intensity while recording CF-EPSCs. Purkinje cells that responded with a stepwise increase of CF-EPSC amplitude were considered to be innervated by multiple climbing fibers [52] and were excluded from further analysis. Paired-pulse depression was measured using two stimulation pulses with inter-stimulus intervals ranging from 50 - 800 ms. For paired-pulse depression measurement, a low affinity, competitive AMPA receptor antagonist 2 mM γDGG was added into ACSF to prevent receptor saturation [18]. The γ-DGG molecules compete with the glutamate and thereby reduce the CF-EPSC amplitude. However, the paired-pulse ratio is still proportional to the glutamate released from the presynaptic

terminal. CF-EPSC kinetics where characterized by calculating the 10 - 90% rise time and the single-exponential τ_{decay} to averaged (4 - 6 consecutive) CF-EPSCs with Igor Pro (Wavemetrics, Inc., Portland, OR).

Estimation of VGCC subtypes that contribute to neurotransmitter release at PF-PC and CF-PC synapse

N-type blocker ω-Conotoxin-GVIA (ω-CgTx) and P/Q-type blocker ω-Agatoxin-IVA (ω-Aga-IVA) (Peptide Institute, Osaka, Japan) were applied to the bath after stable baseline EPSCs were obtained. Reductions of relative EPSCs were taken as functional indications after each blocker was applied. Stock solutions were prepared in ACSF in the presence of 1 mg/ml Cytochrome C to minimize nonspecific binding. Stock solutions (0.1 mM concentrations) were stored at -20°C and used within two weeks. ω-CgTx and ω-Aga-IVA stocks were diluted in ACSF supplemented with 0.1 mg/ml Cytochrome C, yielding final concentrations of 3 μM ω-CgTx and 0.2 μM ω-Aga-IVA.

Ca^{2+}-current and Ca^{2+}-dependent K^+-current in dissociated Purkinje cells

Purkinje cells were isolated enzymatically from p16 to p21 mouse cerebellum using a protocol adapted from [53]. 250 or 300 μm thick coronal slices were incubated in dissociation solution containing (in mM): 69 Na_2SO_4, 30 K_2SO_4, 5 $MgCl_2$, 25 $NaHCO_3$, 10 D-Glucose, supplemented with 3 mg/ml protease XXIII, bubbled with 95% O_2 and 5% CO_2 at 32 °C for 7 min. After incubation, slices were washed three times with warm dissociation solution containing 1 mg/ml trypsin inhibitor and 1 mg/ml BSA, and subsequently washed in Tyrode's solution containing (in mM): 150 NaCl, 4 KCl, 2 $CaCl_2$, 2 $MgCl_2$, 10 HEPES and 10 D-Glucose, at room temperature. Slices were triturated in Tyrode's solution with fire polished Pasteur pipettes to liberate individual neurons. Neurons were suspended and mounted on Poly-D-Lysine/Laminin coated coverslips (BD Biosciences, Bedford, USA) for further experiments. Purkinje cells were identified by their large diameter and pear-shaped soma. To insure an adequate voltage clamp, only Purkinje cells that lost most of the primary dendrites were selected. Whole-cell Ca^{2+}-currents were recorded in dissociated Purkinje cells from *Cacna1a*^{S218L} and WT animals using an intracellular solution containing (in mM): 100 Cs-Methalsulfonate, 2 $MgCl_2$, 20 TEA, 10 EGTA, 5 QX-314, 10 HEPES, 10 Na-Phosphocreatine, 4 Na_2ATP and 0.4 Na_3GTP (pH 7.3). Additionally, 1 μM TTX and 2.5 mM 4-AP were added in the ACSF to block voltage-gated Na^+- and K^+-currents. The series resistance was compensated for > 70% and leak and capacitive currents were subtracted by the -P/4 method. Cells were discarded when the holding current at -70 mV exceeded -100 pA. Ca^{2+}-currents were obtained by 50 ms depolarizing pulses to various membrane potentials ranging between -70 mV and +40 mV at 5 mV increments. Current-voltage (I-V) curves were obtained only from cells with a voltage error of < 5 mV and without any signs of inadequate voltage-clamp as measured by notch-like current discontinuities and slow components in the decay of capacitance currents (in response to hyperpolarizing pulses). The current density was calculated by dividing the current amplitude by the cells capacitance. We consider currents > 3 SD from the average holding current detectable. To estimate the Ca^{2+}-dependent K^+-channels, whole-cell currents were measured with intracellular solution

containing (in mM): 120 K-Gluconate, 9 KCl, 10 KOH, 3.48 $MgCl_2$, 4 NaCl, 10 HEPES, 4 Na_2ATP, 0.4 Na_3GTP and 17.5 sucrose (pH 7.25). One μM TTX, 2.5 mM 4-AP and 1 mM TEA were added into ACSF to block voltage gated Na^+ and most of voltage-gated K^+- and BK-channels [27,53]. To estimate the remaining Ca^{2+}-dependent K^+-channels, we adopted a protocol used previously to isolate SK-mediated tail currents in Purkinje cells [27]. Ca^{2+}-influx were obtained by 50 ms depolarizing pulses to various membrane potentials ranging between -70 mV and +20 mV and adjusted back to holding potential. A positive tail current after depolarizing pulse were measured as indication of Ca^{2+}-dependent K^+ channels. To estimate the ratio between Ca_V- and SK-conductances in individual Purkinje cell, Ca^{2+}-dependent K^+-currents were first measured in Tyrode's solution supplemented with 2.5 mM 4-AP, 1 mM TEA and 1 μM TTX (pH 7.25). After a stable I-V curve was obtained, the extracellular solution was replaced by the second extracellular solution containing (in mM): 165 TEA-Cl, 2 $BaCl_2$, 10 HEPES, 2.5 4-AP and 0.001 TTX (pH 7.25) to isolate the Ba^{2+}-current. I-V curves were constructed from data obtained after a stable Ba^{2+}-current was achieved. SK- and Ba^{2+}-current densities of < 5 pA/pF were excluded to avoid inaccurate analysis of the ratio between these currents for each Purkinje cell.

Purkinje cell spontaneous activity and current clamp recording

The Purkinje cell spiking activity was recorded in loose cell-attached configuration with patch pipettes (diameter 2-3 μm) filled with ACSF at 34 ± 1°C. Eight two- to three-month-old *Cacna1a*^{S218L} mutants and 10 WT littermates were used in this experiment. Spontaneous activity was observed as fast current deflections of -100 to -200 pA. Analysis of the regularity of spiking and the frequency was performed with MATLAB Matlab (Mathworks, Natick MA, USA) and Excel (Microsoft) using the first 5,000 spikes recorded from each cell. The regularity of firing was calculated using the second coefficient of variance (CV2) of interspike intervals (ISI), to quantify the instantaneous regularity of firing ($CV2 = 2|ISI_{n+1} - ISI_n|/(ISI_{n+1}+ISI_n)$) [54]. Autocorrelograms of ISIs were generated using a 1 ms bin width as previously described [7] using custom-written Matlab routines.

For current clamp experiments, an intracellular solution containing (in mM): 120 K-Gluconate, 9 KCl, 10 KOH, 3.48 $MgCl_2$, 4 NaCl, 10 HEPES, 4 Na_2ATP, 0.4 Na_3GTP and 17.5 sucrose (pH 7.25) was used. Purkinje cells from eight two- to three-month old *Cacna1a*^{S218L} and eight WT animals were held at -65 to -70 mV using -400 to -500 pA current injection to avoid spontaneous spiking activity at 34 ± 1 °C. To study the effects of PF input on Purkinje cell spiking patterns, holding current injections were cancelled to allow spontaneous firing. For current injection experiments, after obtaining stable holding potentials, spiking patterns were elicited by injection of depolarizing currents ranging from 100-1000 pA (relative to the holding current). Simultaneous recordings from Purkinje cell somata and dendrite were performed in a set of experiment. Both somatic and dendritic recordings were obtained in current clamp with either no holding current injections or -400 to -500 pA somatic current injection to keep Purkinje cell at -65 mV. Dendritic spikes were characterized by their distinct dV/dt from backpropagation potentials (Figure 8B) and the spiking thresholds were set when dV/dt exceeds 5 mV/ms.

Extracellular recordings *in vivo*

Extracellular recordings of Purkinje cell activity patterns were performed as described previously [55]. In short, mice (WT n = 4, *Cacna1a*^{S218L} n = 5) were immobilized using head-fixed pedestals over the frontal, medial and temporal bones constructed of dental acrylic and stainless steel screws of 1 mm diameter equipped with custom-made connectors that were located in the frontal, medial and temporal bones. Craniotomies (~2 mm in diameter) were placed in the occipital bone overlying (para)vermal regions. In order to prevent *Cacna1a*^{S218L} mice from seizing [13] it was essential to let the mice wake up slowly in the restrainer by means of reducing the 1.5% isoflurane anesthesia (in O_2) in a slow fashion. The recovery from this anesthesia was monitored by electro-encephalograms (EEG) that was recorded from the motor and sensory cortices. To prevent any possible contamination from the anesthesia, the extracellular recordings were started > 1 hour after standard fast fourier transform analysis of the EEG signals indicated a full recovery (see also [56]). Extracellular recordings were performed using borosilicate glass pipettes filled with 0.5 M NaCl of 4-8 MΩ, which were advanced into the cerebellum using a hydraulic manipulator (Trent wells, Austin, Texas, USA). Only single-unit Purkinje cell recordings (qualified as such by the presence of a clear climbing fiber pause following each complex spike [57]) of > 60 s were analyzed using principal component waveform analysis [58]. For each recording we analyzed the firing frequency, coefficient of variance (CV = stdev (ISI) / mean (ISI)) and the minimal climbing fiber pause. In addition, for simple spikes we calculated the mean CV2 value as a measure for irregularity on a spike-to-spike basis (temporal coding) [54]. Recordings were subsequently amplified, filtered, and digitized using a CyberAmp (Axon Instrument, Inc., Union City, CA, USA) and CED1401 (CED, Cambridge, UK), and were stored for off-line analysis using custom-written Matlab (Mathworks) routines. Inter spike interval distributions were constructed using a 0.1 ms bin size, unless stated otherwise. The normalization of the distribution was performed by dividing by the maximal probability.

Behavioral analysis

Motor coordination on the accelerating (4–40 rpm, in 5 minutes) rotarod (model 7650, Ugo Basile Biological Research Apparatus, Varese, Italy) was measured every day in 2 trials with 1 hour inter trial interval. The indicated time is the time spent on the rotarod, or time until the mouse made 3 consecutive rotations on the rotarod.

CHZ (Sigma) was orally administrated by adding it to their drinking water as previously described [29]. In short, the 15 mM CHZ solution was prepared fresh every day in the water supplemented with 0.1% hydroxypropyl-β-cyclodextrin (Tocris Bioscience) and 10% sucrose. pH was adjusted with 1 M NaOH till CHZ just dissolved completely. Mice drank on average 5.5 ml/d in our experiments, resulted in an estimated plasma concentration of ~30 μM [29]. The weight of the animals and the extent of their water intake were monitored throughout the experiment and no significant change was found.

Computational modeling

Mechanisms of dendritic calcium spikes were simulated in a single-compartment model of an isolated piece of Purkinje cell dendrite, using the NEURON environment (For details see supplemental experimental procedures).

Statistics

Statistical comparison between *Cacna1a*^{S218L} mutants and WT littermates was performed using paired or unpaired two-tailed Student's t-test or two-way ANOVA, with $P < 0.05$ defining a significant difference. Summarized data are represented as mean ± S.E.M.

References

1. Catterall WA, Dib-Hajj S, Meisler MH, Pietrobon D (2008) Inherited neuronal ion channelopathies: new windows on complex neurological diseases. J Neurosci 28: 11768-11777.
2. Jouvenceau A, Eunson LH, Spauschus A, Ramesh V, Zuberi SM, et al. (2001) Human epilepsy associated with dysfunction of the brain P/Q-type calcium channel. Lancet 358: 801-807.
3. Ophoff RA, Terwindt GM, Vergouwe MN, van Eijk R, Oefner PJ, et al. (1996) Familial hemiplegic migraine and episodic ataxia type-2 are caused by mutations in the Ca2+ channel gene CACNL1A4. Cell 87: 543-552.
4. van den Maagdenberg AM, Haan J, Terwindt GM, Ferrari MD (2007) Migraine: gene mutations and functional consequences. Curr Opin Neurol 20: 299-305.
5. Fletcher CF, Lutz CM, O'Sullivan TN, Shaughnessy JD, Jr., Hawkes R, et al. (1996) Absence epilepsy in tottering mutant mice is associated with calcium channel defects. Cell 87: 607-617.
6. Mori Y, Wakamori M, Oda S, Fletcher CF, Sekiguchi N, et al. (2000) Reduced voltage sensitivity of activation of P/Q-type Ca2+ channels is associated with the ataxic mouse mutation rolling Nagoya (tg(rol)). J Neurosci 20: 5654-5662.
7. Hoebeek FE, Stahl JS, van Alphen AM, Schonewille M, Luo C, et al. (2005) Increased noise level of purkinje cell activities minimizes impact of their modulation during sensorimotor control. Neuron 45: 953-965.
8. Matsushita K, Wakamori M, Rhyu IJ, Arii T, Oda S, et al. (2002) Bidirectional alterations in cerebellar synaptic transmission of tottering and rolling Ca2+ channel mutant mice. J Neurosci 22: 4388-4398.
9. Rhyu IJ, Abbott LC, Walker DB, Sotelo C (1999) An ultrastructural study of granule cell/Purkinje cell synapses in tottering (tg/tg), leaner (tg(la)/tg(la)) and compound heterozygous tottering/leaner (tg/tg(la)) mice. Neuroscience 90: 717-728.
10. Wakamori M, Yamazaki K, Matsunodaira H, Teramoto T, Tanaka I, et al. (1998) Single tottering mutations responsible for the neuropathic phenotype of the P-type calcium channel. J Biol Chem 273: 34857-34867.
11. Walter JT, Alvina K, Womack MD, Chevez C, Khodakhah K (2006) Decreases in the

precision of Purkinje cell pacemaking cause cerebellar dysfunction and ataxia. Nat Neurosci 9: 389-397.
12. Kors EE, Terwindt GM, Vermeulen FL, Fitzsimons RB, Jardine PE, et al. (2001) Delayed cerebral edema and fatal coma after minor head trauma: role of the *CACNA1A* calcium channel subunit gene and relationship with familial hemiplegic migraine. Ann Neurol 49: 753-760.
13. van den Maagdenberg AM, Pizzorusso T, Kaja S, Terpolilli N, Shapovalova M, et al. (2010) High cortical spreading depression susceptibility and migraine-associated symptoms in Ca(v)2.1 S218L mice. Ann Neurol 67: 85-98.
14. Kulik A, Nakadate K, Hagiwara A, Fukazawa Y, Lujan R, et al. (2004) Immunocytochemical localization of the alpha 1A subunit of the P/Q-type calcium channel in the rat cerebellum. Eur J Neurosci 19: 2169-2178.
15. Barmack NH, Yakhnitsa V (2008) Functions of interneurons in mouse cerebellum. J Neurosci 28: 1140-1152.
16. Chadderton P, Margrie TW, Hausser M (2004) Integration of quanta in cerebellar granule cells during sensory processing. Nature 428: 856-860.
17. Ruigrok TJ, Hensbroek RA, Simpson JI (2011) Spontaneous activity signatures of morphologically identified interneurons in the vestibulocerebellum. J Neurosci 31: 712-724.
18. Regehr WG, Mintz IM (1994) Participation of multiple calcium channel types in transmission at single climbing fiber to Purkinje cell synapses. Neuron 12: 605-613.
19. Wadiche JI, Jahr CE (2001) Multivesicular release at climbing fiber-Purkinje cell synapses. Neuron 32: 301-313.
20. Mintz IM, Venema VJ, Swiderek KM, Lee TD, Bean BP, et al. (1992) P-type calcium channels blocked by the spider toxin omega-Aga-IVA. Nature 355: 827-829.
21. Tottene A, Pivotto F, Fellin T, Cesetti T, van den Maagdenberg AM, et al. (2005) Specific kinetic alterations of human CaV2.1 calcium channels produced by mutation S218L causing familial hemiplegic migraine and delayed cerebral edema and coma after minor head trauma. J Biol Chem 280: 17678-17686.
22. Jorntell H, Ekerot CF (2006) Properties of somatosensory synaptic integration in cerebellar granule cells *in vivo*. J Neurosci 26: 11786-11797.
23. Llinas R, Sugimori M (1980) Electrophysiological properties of *in vitro* Purkinje cell somata in mammalian cerebellar slices. J Physiol 305: 171-195.
24. Stuart G, Hausser M (1994) Initiation and spread of sodium action potentials in cerebellar Purkinje cells. Neuron 13: 703-712.
25. Edgerton JR, Reinhart PH (2003) Distinct contributions of small and large conductance Ca2+-activated K+ channels to rat Purkinje neuron function. J Physiol 548: 53-69.
26. Womack MD, Khodakhah K (2003) Somatic and dendritic small-conductance calcium-activated potassium channels regulate the output of cerebellar purkinje neurons. J Neurosci 23: 2600-2607.
27. Cingolani LA, Gymnopoulos M, Boccaccio A, Stocker M, Pedarzani P (2002) Developmental regulation of small-conductance Ca2+-activated K+ channel expression and function in rat Purkinje neurons. J Neurosci 22: 4456-4467.

28. Womack MD, Chevez C, Khodakhah K (2004) Calcium-activated potassium channels are selectively coupled to P/Q-type calcium channels in cerebellar Purkinje neurons. J Neurosci 24: 8818-8822.
29. Alvina K, Khodakhah K (2010) KCa channels as therapeutic targets in episodic ataxia type-2. J Neurosci 30: 7249-7257.
30. Miyazaki T, Hashimoto K, Shin HS, Kano M, Watanabe M (2004) P/Q-type Ca2+ channel alpha1A regulates synaptic competition on developing cerebellar Purkinje cells. J Neurosci 24: 1734-1743.
31. Rhyu IJ, Oda S, Uhm CS, Kim H, Suh YS, et al. (1999) Morphologic investigation of rolling mouse Nagoya (tg(rol)/tg(rol)) cerebellar Purkinje cells: an ataxic mutant, revisited. Neurosci Lett 266: 49-52.
32. Adams PJ, Rungta RL, Garcia E, van den Maagdenberg AM, MacVicar BA, et al. (2010) Contribution of calcium-dependent facilitation to synaptic plasticity revealed by migraine mutations in the P/Q-type calcium channel. Proc Natl Acad Sci U S A 107: 18694-18699.
33. Liu S, Friel DD (2008) Impact of the leaner P/Q-type Ca2+ channel mutation on excitatory synaptic transmission in cerebellar Purkinje cells. J Physiol 586: 4501-4515.
34. Konnerth A, Llano I, Armstrong CM (1990) Synaptic currents in cerebellar Purkinje cells. Proc Natl Acad Sci U S A 87: 2662-2665.
35. Ovsepian SV, Friel DD (2008) The leaner P/Q-type calcium channel mutation renders cerebellar Purkinje neurons hyper-excitable and eliminates Ca2+-Na+ spike bursts. Eur J Neurosci 27: 93-103.
36. Raman IM, Bean BP (1997) Resurgent sodium current and action potential formation in dissociated cerebellar Purkinje neurons. J Neurosci 17: 4517-4526.
37. M, Clark BA (1997) Tonic synaptic inhibition modulates neuronal output pattern and spatiotemporal synaptic integration. Neuron 19: 665-678.
38. Mittmann W, Hausser M (2007) Linking synaptic plasticity and spike output at excitatory and inhibitory synapses onto cerebellar Purkinje cells. J Neurosci 27: 5559-5570.
39. Lonchamp E, Dupont JL, Doussau F, Shin HS, Poulain B, et al. (2009) Deletion of Cav2.1(alpha1(A)) subunit of Ca2+-channels impairs synaptic GABA and glutamate release in the mouse cerebellar cortex in cultured slices. Eur J Neurosci 30: 2293-2307.
40. Tottene A, Conti R, Fabbro A, Vecchia D, Shapovalova M, et al. (2009) Enhanced excitatory transmission at cortical synapses as the basis for facilitated spreading depression in Ca(v)2.1 knockin migraine mice. Neuron 61: 762-773.
41. Alvina K, Khodakhah K (2010) The therapeutic mode of action of 4-aminopyridine in cerebellar ataxia. J Neurosci 30: 7258-7268.
42. Khaliq ZM, Raman IM (2005) Axonal propagation of simple and complex spikes in cerebellar Purkinje neurons. J Neurosci 25: 454-463.
43. Monsivais P, Clark BA, Roth A, Hausser M (2005) Determinants of action potential propagation in cerebellar Purkinje cell axons. J Neurosci 25: 464-472.
44. Desclin JC, Colin F (1980) The olivocerebellar system. II. Some ultrastructural correlates of inferior olive destruction in the rat. Brain Res 187: 29-46.

45. Rossi F, Cantino D, Strata P (1987) Morphology of Purkinje cell axon terminals in intracerebellar nuclei following inferior olive lesion. Neuroscience 22: 99-112.
46. Strata P, Montarolo PG (1982) Functional aspects of the inferior olive. Arch Ital Biol 120: 321-329.
47. Hoebeek FE, Khosrovani S, Witter L, De Zeeuw CI (2008) Purkinje cell input to cerebellar nuclei in tottering: ultrastructure and physiology. Cerebellum 7: 547-558.
48. Glaser EM, Van der Loos H (1981) Analysis of thick brain sections by obverse-reverse computer microscopy: application of a new, high clarity Golgi-Nissl stain. J Neurosci Methods 4: 117-125.
49. Huang CM, Wang L, Huang RH (2006) Cerebellar granule cell: ascending axon and parallel fiber. Eur J Neurosci 23: 1731-1737.
50. Isope P, Barbour B (2002) Properties of unitary granule cell-->Purkinje cell synapses in adult rat cerebellar slices. J Neurosci 22: 9668-9678.
51. Llano I, Marty A, Armstrong CM, Konnerth A (1991) Synaptic- and agonist-induced excitatory currents of Purkinje cells in rat cerebellar slices. J Physiol 434: 183-213.
52. Hansel C, de Jeu M, Belmeguenai A, Houtman SH, Buitendijk GH, et al. (2006) alphaCaMKII Is essential for cerebellar LTD and motor learning. Neuron 51: 835-843.
53. Raman IM, Bean BP (1999) Ionic currents underlying spontaneous action potentials in isolated cerebellar Purkinje neurons. J Neurosci 19: 1663-1674.
54. Holt GR, Softky WR, Koch C, Douglas RJ (1996) Comparison of discharge variability *in vitro* and *in vivo* in cat visual cortex neurons. J Neurophysiol 75: 1806-1814.
55. Wulff P, Schonewille M, Renzi M, Viltono L, Sassoe-Pognetto M, et al. (2009) Synaptic inhibition of Purkinje cells mediates consolidation of vestibulo-cerebellar motor learning. Nat Neurosci 12: 1042-1049.
56. Hoebeek FE, Witter L, Ruigrok TJ, De Zeeuw CI (2010) Differential olivo-cerebellar cortical control of rebound activity in the cerebellar nuclei. Proc Natl Acad Sci U S A 107: 8410-8415.
57. Wylie DR, De Zeeuw CI, Simpson JI (1995) Temporal relations of the complex spike activity of Purkinje cell pairs in the vestibulocerebellum of rabbits. J Neurosci 15: 2875-2887.
58. Eggermont JJ (1990) The correlative brain; Braitenberg V, editor. New York: Springer Verlag.

Supplementary information

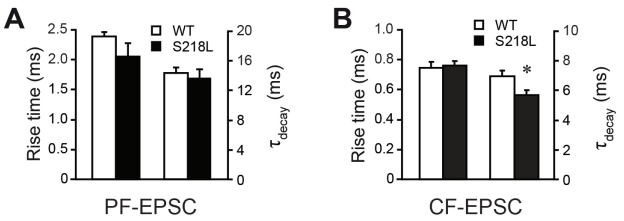

Figure S1. Kinetics of PF- and CF-EPSCs

(A) Quantification of 10 - 90% rise time (left) and τ_{decay} (right) of PF-EPSCs (WT n = 8, Cacna1a^{S218L} n = 10). (B) Quantification of 10 – 90% rise time and τ_{decay} of CF-EPSC (WT n = 21, *Cacna1a*^{S218L} n = 20). Asterisks indicate significant differences ($p < 0.05$).

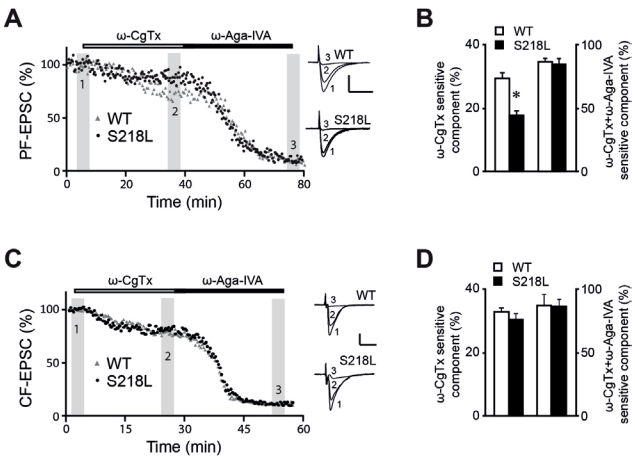

Figure S2. P/Q- and N- type VGCC sensitive fractions of PF-EPSC and CF-EPSC

(A) Representative examples of the time course of PF-EPSC amplitudes of WT (grey triangle) and *Cacna1a*^{S218L} (black dots) Purkinje cells during the subsequent application of 3 µM ω-Conotoxin-GVIA (ω-CgTx) and 0.2 µM ω-Agatoxin-IVA (ω-Aga-IVA). The PF-EPSC amplitudes before toxin application were normalized to 100%. Insets represent example EPSC traces taken from indicated time points (scale bars: vertical 200 pA, horizontal 20 ms). (B) Summarized toxin-sensitive PF-EPSC components (WT n = 5, Cacna1a^{S218L} n = 6). (C, D) Similar to (A, B), the representative time course of CF-EPSC amplitudes and summarized ω-CgTx and ω-Aga-IVA sensitive components of CF-EPSC were presented (WT n = 4, *Cacna1a*^{S218L} n = 4). Asterisks indicate significant differences ($p < 0.05$).

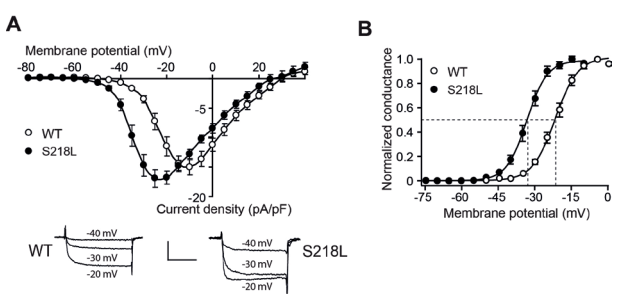

Figure S3. Negative shift of voltage-current relationships of whole-cell Ca^{2+}-currents in p5-6 *Cacna1a*^{S218L} Purkinje cells

(A) Voltage-current relationship of Ca^{2+}-current in WT (n = 14) and *Cacna1a*^{S218L} (n = 13) Purkinje cells. Mean current densities were plotted against depolarizing voltages. Insets show representative traces of Ca^{2+} currents in WT and *Cacna1a*^{S218L} Purkinje cells evoked by 50 ms depolarizing pulses to -40, -30 and -20 mV (holding potential = -80 mV; scale bars: vertical 10 pA/pF, horizontal 20 ms). (B) Normalized Ca^{2+}-conductance at different depolarizing voltages in WT (n = 14) and *Cacna1a*^{S218L} (n = 13) Purkinje cells. Solid curves indicate Boltzmann fits and dashed lines indicate corresponding voltages of half-maximum conductance.

Figure S4. Irregular Purkinje cell activity pattern under various in vitro conditions

(A) Mean second coefficient of variance (CV2) and firing frequency of spontaneous Purkinje cell activities from WT (n = 21) and *Cacna1a*^{S218L} (n = 26) at physiological temperatures in the absence of any blocker. (B) Similar to (A), but now representing pacemaking activity recorded in 3.2 mM K^+ACSF from WT (n = 20) and Cacna1a^{S218L} (n = 18) Purkinje cells. Asterisks indicate significant differences ($p < 0.05$).

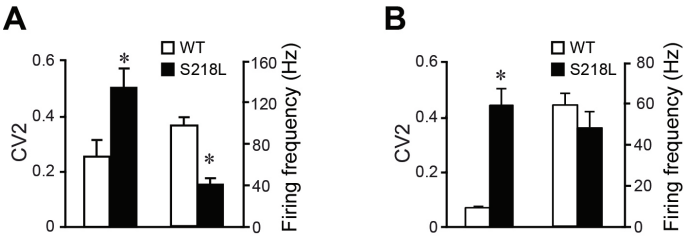

Figure S5. Burst-like simple spike pattern in alert *Cacna1a*^{S218L} mutant mice

Extracellular recording of single unit Purkinje cell activity in alert *Cacna1a*^{S218L} mutant mice. Arrows indicated simple spike burst activities and subsequent pauses (scale bars: vertical 400 µV, horizontal 100 ms).

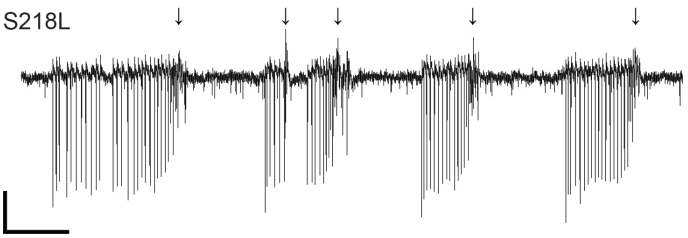

Figure S6. Blocking VGCCs partially restore hyperexcitable action potential threshold in *Cacna1a*^{S218L} Purkinje cells

Bath application of 100 µM $CdCl_2$ restored the mean action potential (AP) threshold in *Cacna1a*^{S218L} Purkinje cells towards the WT level (n = 8 for S218L+$CdCl_2$). For comparison the WT and *Cacna1a*^{S218L} Purkinje cell data are represented again (as in Figure 7). Asterisks indicate significant differences ($p < 0.05$).

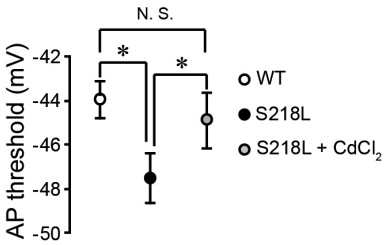

Table S1. Quantification of cerebellar volume, Purkinje cell number and dimensions of individual components of PF-PC synapse

Estimated cerebellar volume in mm^3 and total number of Purkinje cells (n = 4 for both WT and *Cacna1a*^{S218L}). Quantifications (n = 3 for both WT and *Cacna1a*^{S218L}) of Granule cell density per μm^2; density of parallel fiber-Purkinje cell synapses (PF-PC) per 20 μm^2 of molecular layer; Purkinje cell spine density per 20 μm^2 of molecular layer; PFV size; Purkinje cell spine length; spine head size from EM studies. Spine density along PC dendrite (# Spine/µm) and PFV density along granule cell axon (#PFV/µm) were quantified with Golgi-Cox stained specimen (n = 4 for both WT and *Cacna1a*^{S218L}).

	V_{cb} (mm^3)	# PC (x 10^3)	GrC density (#/μm^2)	PF-PC Synapse (#/20 μm^2)	PFV size (μm^2)	Spine neck length (µm)	Spine size (μm^2)	# Spine/µm	# PFV/µm
WT	35.41 ± 3.01	21.76 ± 5.00	3.98 ± 0.14	21.34 ± 1.30	0.22 ± 0.02	0.99 ± 0.03	0.12 ± 0.01	1.37 ± 0.18	0.20 ± 0.09
S218L	36.24 ± 2.10	22.50 ± 5.33	4.08 ± 0.15	20.87 ± 1.36	0.19 ± 0.03	0.98 ± 0.02	0.12 ± 0.01	1.24 ± 0.51	0.18 ± 0.06
T-test	0.84	0.42	0.50	0.62	0.43	0.82	0.63	0.25	0.94

Table S2. Multiple synaptic contacts between PFV and PC spines

Quantification of the proportion of parallel fiber varicosities that contact with multiple Purkinje cell spines.

	Number synapses per PFV (1 to 4)					
	1	***2***	***3***	***4***	***5***	***6***
WT	977	23	0	0	0	0
S218L	844	139	14	1	1	1

Table S3. Action potential kinetics and basic Purkinje cell properties

Absolute amplitude of action potential (AP); half width (HW) (ms) of AP; maximum rising slope (dV/dt) (V/s); maximum repolarizing slope (-dV/dt) (V/s); resting membrane potentials (RMP) and decay time constance (τ_{decay}) of membrane capacitance calculated from 19 WT and 18 *Cacna1a*^{S218L} Purkinje cells.

	AP amplitude (mV)	HW (ms)	dV/dt (V/s)	-dV/dt (V/s)	RMP (mV)	τ_{decay} (ms)
WT	69.89 ± 2.18	0.22 ± 0.01	397.42 ± 19.66	343.32 ± 13.87	-47.96 ± 0.71	11.06 ± 0.37
S218L	66.33 ± 1.64	0.22 ± 0.01	399.87 ± 22.07	369.00 ± 14.27	-50.38 ± 0.81	10.33 ± 0.37
T-test	0.22	0.96	0.93	0.21	0.03	0.64

Stereological quantification

Calbindin and Nissl double-stained tissue was used for stereological quantification of Purkinje cell numbers using an Olympus BH2 Microscope equipped with a motorized stage controlled by a computer running StereoInvestigator 4 software (MBF Bioscience, Williston, VT, USA). To estimate the total volume of the cerebellum, virtual contours were drawn around cerebellar tissue. Within each contour, optical grids (300 × 300 μm^2) including a 3D counting frame (150 × 150 × 15 μm^3) were systematically placed. Purkinje cells with nucleoli inside the counting frame or contacting the upper and right border of the counting frame were included in the counting, according to standardized criteria [1]. The total Purkinje cell number was estimated using the formula:

$$N = \sum Q \cdot (t/h) \cdot (1/asf) \cdot n$$

Where N is the estimation of Purkinje cell number in the cerebellum, $\sum Q$ is the total counted cell number, t is the thickness of the slice, h is the height of the counting frame, asf is the ratio between the area of the frame and the area of the sampling grid and n is the slice sampling interval. The cerebellar volume was estimated by multiplying the total contour area with the section thickness without correcting for shrinkage factors.

Computational modeling

Mechanisms of dendritic calcium spikes were simulated in a single-compartment model of an isolated piece of Purkinje cell dendrite. The model contained the following set of membrane currents: a high threshold voltage-activated P/Q-type calcium channel (CaP), a low-threshold voltage activated T-type Ca^{2+}-channel (CaT), a voltage-activated persistent K^+-channel (KM), a low-affinity calcium-activated voltage dependent K^+-channel (BK) and a high-affinity calcium-activated K^+-channel (SK). Simulations were done in NEURON with an integration time step of 25 μs. BK, CaT and KM channel descriptions were taken from [2] (as implemented in NEURON by [3]). The CaP channel description was taken from [4] and the SK-channel from [5].

The model simulated an isolated piece of Purkinje cell dendrite and consisted of a single cylindrical compartment with length L = 4 μm, diameter d = 2 μm and specific membrane capacitance C_m = 1.64 μF/cm^2. Calcium entering the compartment diffused instantaneously within a thin sub-membrane shell with thickness d_{shell} = 100 nm. The shell defined a volume that was used to compute the intracellular Ca^{2+}-concentration, which was regulated by Ca^{2+}-entry through membrane channels and removal by a first-order mechanism with rate constant β_{Ca} = 0.6 ms^{-1}. The extracellular Ca^{2+}-concentration was 2 mM, and the internal Ca^{2+}-concentration was not allowed to decrease below 100 nM.

For BK, CaT, KM and leak currents, the current density i for was calculated as $i = gm^p h^q z^r (V_m - E)$, where g is the conductance density, m is an activation variable with p order kinetics, h is an optional inactivation variable with q order kinetics, z is an optional Ca^{2+}-dependent activation variable with r order kinetics, V_m is the membrane potential and E is the reversal potential for the ionic species (E_K= *-85 mV*, E_{leak} = *-80 mV*). Channel activation and inactivation variables were expressed in terms of a steady state value $m_\infty(V_m)$ and a time constant $\tau_m(V_m)$. Voltage-dependent gating parameters were

calculated from a first-order reaction scheme with forward rate $\alpha(V_m)$ and backward rate $\beta(V_m)$ as $m_\infty = \alpha/(\alpha+\beta)$ and $\tau_m = 1/(\alpha+\beta)$, except for KM and leak currents, for which they were defined explicitly. Ca^{2+}-dependent gating parameters were calculated as $z_\infty = 1/(1+\alpha_z/[Ca^{2+}])$ and $\tau_z = \beta_z$. The specific settings for each current were as follows.

BK: $g = 80, p = 1, q = 0, r = 2, \alpha = 7.5, \beta = 0.11/\exp((V_m - 35)/14.9), \alpha_z = 40, \beta_z = 10$

CaT: $g = 0.5, p = 1, q = 1, r = 0, \alpha_m = 0.0025/(1+\exp((v+40)/8)), \beta_m = 0.19/(1+\exp(-(v+50)/10)),$
$\alpha_h = 2.6/(1+\exp(-(v+21)/8)), \beta_h = 0.18/(1+\exp((v+40)/4))$

KM:

$g = 0.013, m_\infty = 1/(1+\exp(-(V_m+35)/10)),$
$\tau_m = 3.3(\exp((V_m+35)/40)+\exp(-(V_m+35)/20))/200$

Leak: $g = 0.33, m = 1, h = 1, z = 1$

Conductance densities are in mScm^{-2}, voltages in mV.

The SK-channel was simulated by a Markov-chain scheme with six states, where the conductance was determined by the sum of two open probabilities, multiplied by a factor $g = 0.4$. To account for heterogeneities in submembrane calcium concentration, the effective calcium concentration for SK-channels was set to one third of the global concentration. Details can be found in [5].

For the CaP channel, current density was determined as $i_{CaP} = mI_{GHK}$, with m a voltage-dependent gate and I_{GHK} calculated from the Goldman-Hodgkin-Katz current equation. Definitions were as follows.

$$m_\infty = 1/(1+\exp(-(V_m+19)/5.5))$$

$$\tau_m = \begin{cases} 0.000264 + 0.128\exp(0.103V_m) & V_m \le -35\mathrm{mV} \\ 0.000191 + 0.00376\exp(-((V_m+41.9)/27.8)^2) & V_m > -35\mathrm{mV} \end{cases}$$

$$I_{GHK} = 4P_{Ca^{2+}}\frac{VF^2}{RT}\frac{[Ca^{2+}]_i - [Ca^{2+}]_o\exp(-2FV/RT)}{1-\exp(-2FV/RT)}$$

Where $P_{Ca^{2+}} = 1\times10^{-2}\mathrm{cm/sec}$, $[Ca^{2+}]_i \ge 100\mathrm{nM}$, $[Ca^{2+}]_o = 2\mathrm{mM}$, $T = 310\mathrm{K}$, $F = 9.6485\times10^4\mathrm{C/mol}$ and $R = 8.3145\mathrm{JK^{-1}mol^{-1}}$.

The effects of a mutation in the CaP channel parameters on the initiation of Ca^{2+}-spiking were investigated by introducing a -12 mV offset to the voltage dependent gate m. Parameter space of determinants of spike onset was explored by varying the densities of CaP- and SK- channels and the critical parameter I_{inj}, for both wild-type and Cacna1a^{S218L} mutants. This allowed investigation of the qualitative effects of e.g. certain channel

affecting drugs or potential compensatory mechanisms in Cacna1a^{S218L} Purkinje cell dendrites. Ca^{2+}-spikes in the model were detected by implementing a membrane potential threshold criterium, and the occurrence of three or more consecutive threshold crossings was taken as an indication of sustained spiking. The threshold in both models was V_m = -20 mV.

Supplementary references

1. Gundersen HJ (1986) Stereology of arbitrary particles. A review of unbiased number and size estimators and the presentation of some new ones, in memory of William R. Thompson. J Microsc 143: 3-45.
2. De Schutter E, Bower JM (1994) An active membrane model of the cerebellar Purkinje cell II. Simulation of synaptic responses. J Neurophysiol 71: 401-419.
3. Miyasho T, Takagi H, Suzuki H, Watanabe S, Inoue M, et al. (2001) Low-threshold potassium channels and a low-threshold calcium channel regulate Ca2+ spike firing in the dendrites of cerebellar Purkinje neurons: a modeling study. Brain Res 891: 106-115.
4. Khaliq ZM, Gouwens NW, Raman IM (2003) The contribution of resurgent sodium current to high-frequency firing in Purkinje neurons: an experimental and modeling study. J Neurosci 23: 4899-4912.
5. Solinas S, Forti L, Cesana E, Mapelli J, De Schutter E, et al. (2007) Computational reconstruction of pacemaking and intrinsic electroresponsiveness in cerebellar Golgi cells. Front Cell Neurosci 1: 2.

Chapter 8

Discussion

This thesis describes several aspects of the role of Ca^{2+} mediated signalling in cerebellar function and motor learning. Using genetically modified mouse models, we are able to pin down the involvements of one or several fundamental components in the cerebellar functioning. We show for the first time how dampening the Ca^{2+}-induced transmitter release at parallel fiber – Purkinje cell (PF-PC) synapses provides us a new insight in the properties of the granule cell network (Ch. 3). It suggests a fundamental dissociation between the role of granule cell output in maintaining normal motor performance and the role in consolidating newly learned information. In addition, this thesis emphasizes on the specific forms of cerebellar synaptic plasticity and their potential role in cerebellar learning. We use cell specific manipulation of long-term potentiation and depression (LTP/LTD) at PF-PC synapses, as well as the synaptic transmission and plasticity at molecular layer interneuron – Purkinje cell (MLI-PC) synapses by targeted lesioning of key enzymes or neurotransmitter receptors (Chs. 4-6). These data provide new insights in the involvement of specific synaptic inputs at the Purkinje cell network during synaptic plasticity and motor learning. Last but not least, we show that gain-of-function mutations that enhance Ca^{2+}-influx induce cerebellar ataxia by a similar pathophysiology as loss-of-function mutations. The importance and implication of these findings will be discussed in detail below.

Function of granule cell network: spreading diversity and setting the time-windows

The structure of the granular layer network is well suited for spreading diverse sets of information. The mossy fibers (MF) themselves are derived from many different sources and they cover large parts of the cerebellar lobules innervating many different granule cells (GrCs). The numerosity of GrCs in turn provides ample inputs to large parts of the molecular layer. The Golgi cells, which form a very heterogeneous group of interneurons that are superimposed on the GrCs (Simat et al., 2007), may well serve to further enhance the diversity of the information that they encode. The combination of feedforward and feedback inhibition superimposed by the Golgi cells will allow the granular layer to control spike delay, to increase the firing rate for specific short periods, to induce delays in changes of firing rate, and to generate prolonged periods of increased firing (D'Angelo and De Zeeuw, 2009). In such a process, sufficient number of GrCs is thus critical for generating and maintaining the vast diversity of output patterns from GrC layer networks. Several attempts have been made to answer the question that to what extend the GrCs is needed for proper cerebellar function (Yamamoto et al., 2003; Wada et al., 2007; Kim et al., 2009). These studies target the direct upstream cascade of neurotransmitter release at PF-PC synapses and effective interrupt the GrCs outputs. Both of the strategies reveal similar results that the basal motor performances are severely impaired following the lesion of GrCs outputs. Wada et al. also present the involvement of granule cell output in a cerebellum related learning task, e.g., eye-blink conditioning. Clearly, GrCs are required for the cerebellar functioning since they are the major output neurons that innervate molecular layer networks. However several aspects of the GrCs output and functions remain puzzling. Wada et al. described the absence of PC simple spike firing following the silencing the GrC output, which is contradictive to the intrinsic pacemaking activity of PCs (Raman and Bean, 1999). Although it could be attributed into the involvement of inhibition from intrinsically active MLIs that silence the PCs, it is not consistent with the ample evidence from *In vitro* studies that show the GrCs

outputs to be negligible. Moreover, PCs remain active with and without MLI inputs (Ch. 7). In addition, MLIs are also innervated by GrCs and thus could in theory be equally affected by the absence of GrC output as PCs. It remains to be shown whether the PC simple spike firing is silent in the mice where GrCs outputs are chronically rather than acutely silenced using genetic approach (Kim et al., 2009). Second, GrCs themselves remain silent most of the time and often operate with long brief high frequency bursts (Chadderton et al., 2004; Arenz et al., 2008; Ruigrok et al., 2011). It has been estimated that the majority of energy consumption in the cerebellum is to maintain the metabolism and resting membrane potentials of the cerebellar GrCs (Howarth et al., 2010). It would be extremely energy inefficient to maintain such a system, if not necessary.

In order to answer the question what are the functions of the GrCs outputs in cerebellar learning, we studied the $\alpha6^{Cre}$-*Cacna1a* KO mice, in which the GrC output is dampened but not silenced completely (Ch. 3). In these mice, the synaptic transmission at PF-PC synapses is minimized to < 30% of wt littermates, whereas the basic motor performance is intact. Such a surprising normal basic motor performance contradicts with the previous two studies, which showed that abolishing the PF-PC synaptic transmission result in severe cerebellar ataxia (Wada et al., 2007; Kim et al., 2009). In addition, previous studies on *Cacna1a* mutant mice also suggest that the lack of PF-PC inputs might contribute to the ataxic phenotype, although such studies cannot pin down the origin of ataxia due to the wide spread expression of P/Q-type calcium channels throughout the whole cerebellum (Rhyu et al., 1999; Matsushita et al., 2002). This thesis presents that the ataxia is absent with minimal GrC output (Ch. 3), but is pronounced when PF-PC synaptic input is increased (Ch. 7). Thus, to what extent the reduction of synaptic input at PF-PC synapses contributes to motor deficits remains elusive. Evidently, a certain minimal percentage (although less than 30%) of functional intact GrCs is required for fundamental motor performance. In order to investigate such a bottom limit of GrCs population, several factors have to be addressed experimentally. First, are all the GrCs functionally homogeneous? Although it is feasible to assume that the existence of certain variance in the GrC physiological properties given the extreme numerosity, it is not shown whether GrCs can be categorized into functionally specific subgroups. Second, GrCs receive MF inputs from diverse brain regions, which raises the question whether there is any regional specificity of GrC groups that are reserved for fundamental cerebellar functions? If there is regional specificity, which groups of GrCs full fill what function? Last, what is the exact population of GrCs required to sustain normal motor performance? Future studies should aim at varying the percentage and location of functionally intact GrCs and study the motor performance.

The absence of overnight consolidation of newly acquired procedural memory in the $\alpha6^{Cre}$-*Cacna1a* KO mice (Ch. 3) suggests that a large population of GrCs is essential for stringent cerebellar learning tasks. Randomly silencing the majority of GrC output is likely to affect motor learning in several ways. 1. The reduction of GrC output in a random fashion is likely to minimize the diversity of output patterns, which we proposed to be essential for cerebellar learning in later paragraphs of this chapter. 2. The mosaic organization of the remaining GrC output alters long-term plasticity at PF-PC synapses, which is also essential for memory consolidation (Ch. 4b). 3. Reduction of PF-MLI and potentially

also PF-Golgi cell inputs could disrupt the feedforward and feedback inhibition from GrCs and thus affect the PC firing patterns and ultimately also the memory process. A similar increase in PC simple spike regularity and loss of memory consolidation is also observed in the PC-Δγ2 mice, which lack functional synaptic inhibition at MLI-PC synapses (Ch. 5), which validates our working hypothesis that a complete and dynamic GrC layer network is essential for delicate learning process.

Apart from Purkinje cell spiking activity it remains to be elucidated how spiking patterns in the GrC layer network are modulated. We propose that the various forms of plasticity present in the granule cell network serve to fine-tune and preserve these spatio-temporal patterns of GrC activity. For example, the level of LTP at the MF-GrC synapse may have a prominent impact on the time of occurrence of the first GrC spike in response to a particular MF input. By controlling first spike delay, this form of LTP may allow spikes to fall inside the window set by the feedforward inhibition provided by the Golgi cells, whereas LTD at the MF-GrC synapse may drive the GrC response beyond the window limit. By controlling the exact onset of a time-window and the number of spikes that occur within a time-window such fine-tuning may modify the MF patterns that enter the GrC network (Brickley et al., 1996; Armano et al., 2000). In principle plasticity at the MF-GrC synapse could continuously modify the spike discharge of a group of GrCs operating within a particular time-window. The feedback inhibition provided by the Golgi cells in turn might control the offset of a time-window as well as the duration of the silent period after the time-window of GrCs spiking activity (Fig. 1). In addition, plasticity at the PF-Golgi cell synapse, intrinsic plasticity of GrCs or undiscovered forms of long-term plasticity such as that of the MF-Golgi cell synapse or Golgi cell-GrC synapse may contribute to the same processes that determine the windows of spiking and the intermittent silent periods in between. As potentiation of intrinsic excitability can be achieved at a relatively low threshold in GrCs, it may help to maintain their readiness for generating action potentials in conditions of strong synaptic inhibition and/or weak synaptic excitation (Fregnac, 1998; Daoudal and Debanne, 2003). Since GrCs form relatively compact electrotonic structures with relatively small losses of potential between dendrites and soma, the mutual impact of changes in intrinsic excitability and strength of synaptic inputs may be relatively robust. Thus, if the synergistic roles of both synaptic and intrinsic plasticity in the granular cell network are fully exploited, it may operate as a flexible device for expanding and redistributing spiking information in the spatiotemporal domain.

Function of Purkinje cell network: creating output by selecting input

Several hypotheses have been proposed about how vast amount of inputs from GrCs network could be stored and converted into cerebellar working memory. Among those the Marr-Albus-Ito theory is one of the most influential concepts. In this theory, the synaptic plasticity at PF-PC synapse, to be specific, long-term-depression (LTD) at this synapse, is critical for learning and memory in the cerebellum. The CF fiber input derived from inferior olivary neurons is considered to act as the ‘teaching signal’ that induces LTD at the PF-PC synapses when coincidently activated with PF input, and thus is the considered to act as the cue for memory formation (Ito, 2001). However the recent experimental evidence appears

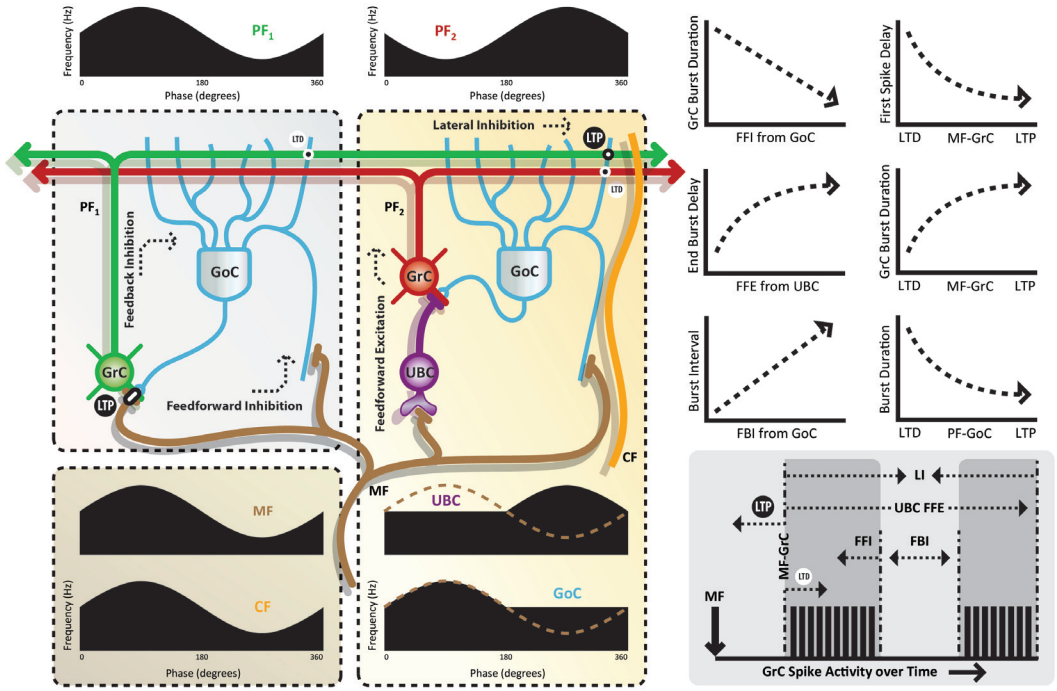

Figure 1; Spreading diversity and setting the time-windows in the granule cell network.

The Left panels illustrate the diagram of connectivity, known sites of plasticity, and phasic activity patterns of cellular components following sinusoidal stimulation. The activity profiles reflect average responses from a group of cells or fibers and do not represent individual activity patterns. Within the glomeruli mossy fiber (MF) rosettes have excitatory effects on granule cells (GrC), unipolar brush cells (UBC) and Golgi cells (GoC) (synapses are displayed separately for clarity). UBCs have excitatory projections on granule cells, which can be prolonged for hundreds of milliseconds. GoCs receive excitatory inputs from GrCs and project back to the glomeruli where they again inhibit GrCs. Together, this constitutes a network in which a combination of feedforward excitation, feedforward inhibition, feedback inhibition and lateral inhibition, conveyed by the MF-UBC, MF-GoC, GrC-GoC and GrC-GoC pathways, respectively (indicated by dashed arrows), controls the timing and diversity of parallel fiber (PF) output. The lower left panel displays phasic activity from the two main inputs to the cerebellum, i.e. MF and climbing fiber (CF) input. In the top part of the left panel it is shown how plasticity can set a time-window in which the GrCs can overcome tonic inhibition from GoCs. Sustained MF activity leads to presynaptic LTP, thereby increasing the driving force onto the GrC. Increased activity in the PF leads to LTD at the PF-GoC synapse, attenuating feedback inhibition and further facilitating transduction of MF signaling into PF activity (PF_1). The middle panel depicts how GrC activity can be altered in the vestibulocerebellum. Although the general anatomical organization in the granular layer is conserved throughout the cerebellar cortex, the predominant presence of UBCs forms the one distinct feature that sets aside the more primitive vestibulocerebellum from the rest. Prolonged and delayed responses from these cells can adjust the time-window of activity in about half of all GrCs. Congruent activity from PFs and CFs may lead to LTP at the PF-GoC synapse, which enforces lateral inhibition to suppress out-of-phase GrC activity creating an opposite phase in the PFs (PF_2). Right panels displays how distinct forms of inhibition and plasticity may modify the firing behaviour in GrCs. A summary is given in the right bottom figure. See main text for further explanation.

to be diverse, some support this notion whereas others contradict (De Zeeuw et al., 1998; Welsh et al., 2005; Hansel et al., 2006; Ke et al., 2009) and (Ch. 4-6). As a matter of fact, the core of this controversy lies in the discussion of the feasibility and significance of LTD at the PF-PC synapses. Several issues have been hotly debated: First: are the CF input and subsequent LTD at the PF-PC synapses essential for cerebellar learning? It has been shown that the CF inputs do not necessarily act as the key signal during learning tasks (Welsh et

al., 2005; Ke et al., 2009). These data argue against the essential role of CF induced LTD in the cerebellar memory formation. Second: is the PF-PC LTD exclusively CF-dependent? The coincident detection of PF-CF inputs by inducing the mGluR1-mediated supralinear Ca^{2+}-influx has been emphasised to support the theory of the CF-dependent LTD induction (Wang et al., 2000). However recent evidence show that the supralinear Ca^{2+}-concentration and LTD at PF-PC synapses can be well induced with high frequency PF inputs, which saturate the local Ca^{2+}-buffering capacity (Hartell, 1996; Canepari and Vogt, 2008). Although one should be cautious to interpret cerebellar learning using *In vitro* evidence, there is a fair chance to reconsider the specificity of the CF input in LTD induction. In addition, it seems to be inefficient use depression and not potentiation of GrCs output, since GrCs remain silent most of the time. Considering that most of the cerebellar neurons are intrinsically active, continuously induced suppression of excitatory inputs at such an autonomous system will result in severe loss of information in the output patterns.

Previous studies utilizing genetically modified mouse models, including the PKC, PKG and CaMKII mutants (De Zeeuw et al., 1998; Feil et al., 2003; Hansel et al., 2006; Ch 6) unambiguously show the positive correlation of the aberrant LTD induction and motor deficits. However this thesis also provides arguments that interruption of PF-PC LTD at the level of AMPA receptors does not interrupt the cerebellar mediated learning, which indicates that the lack of LTD can be compensated for by other mechanisms within/outside of the cerebellar cortex to allow for motor learning to occur (Hansel et al., 2001; Khaliq and Raman, 2005; Bagnall and du Lac, 2006). On the other hand, this thesis also provides evidence that the long-term potentiation (LTP) and intrinsic plasticity at PF-PC synapses, the synaptic inhibition between the MLIs and Purkinje cells are involved in cerebellar learning (Ch. 4b, 5). Since multiple learning mechanisms other than the LTD at PF-PC synapses may play a role in cerebellar learning and memory, we propose a more general concept onhow various types of synaptic input and plasticity may act during learning in the PC network. To start with, it is reasonable to state that the CF input indeed plays a central role in cerebellar learning, although the CF-induced LTD at the PF-PC synapses may not be the only learning mechanism (Ch. 4).

How will the diverse pattern produced from GrC networks be further processed in the PC networks? It is likely that the guiding signals provided by the CF can select and sculpt the codings that are needed to improve behavior. The CF does this by the presence ánd absence of heterosynaptic effects, either directly or via spillover. As explained above, CF activity may not only reduce Purkinje cell activity by inducing LTD at the PF-PC synapse, but also by promoting potentiation at the PF-MLI and MLI-PC synapse (Fig. 2), and probably even at the PF-Golgi cell synapse. Vice versa, the absence of climbing fiber activity can increase Purkinje cell activity by permitting LTP at the PF-PC synapse, and by promoting LTD at the PF–MLI synapse. Since these depressing and potentiating effects, which work in synergy, are all timing-dependent in that they all depend on whether the CF activity coincides within a particular time frame with the PF activity or not (Bell et al., 1997; Han et al., 2000; Wang et al., 2000; Coesmans et al., 2004), it will be critical to have sufficient variety in the temporal codings of the PFs. This variety will allow the CF to drive the simple spike activity of the Purkinje cells into any direction, even into a phase that is

opposite to that of the MFs (compare phase of MFs in Fig. 1 with that of simple spikes in Fig. 2). Interestingly, such an opposite phase in MF activity and Purkinje cell simple spike activity is exactly what has been found on various occasions and what has been considered as enigmatic. For example, during the vestibulo-ocular reflex the vast majority of the vestibular simple spike responses of PCs in the vertical-axis zones of the floccular complex in primates shows a phase that is opposite to that of the majority of the corresponding MF inputs (Lisberger and Fuchs, 1978a, b; Miles et al., 1980). Likewise, during smooth pursuit eye-movement the percentage of Purkinje cell simple spike responses that are excited for rotation of the ipsilateral eye to the ipsilateral side of recording is significantly higher than that of the corresponding MF responses (Lisberger and Fuchs, 1978a, b). Thus, we argue that the combination of diversity spreading in the GrC network and guided selection in the molecular layer provides a powerful mechanism to create the appropriate phase in the PC simple spike output.

Distributed Dynamic Plasticity

We refer to the combination of the main forms of plasticity involved in cerebellar learning as distributed dynamic plasticity; distributed, because it includes various types of synaptic and intrinsic plastic effects in various types of neurons and superimposed interneurons occurring at the same time under similar induction protocols (c.f. Ch. 2), and dynamic, because the plasticity occurs as various, early/late short-term and long-term processes that, since their timescales cannot be separated, move at a functional level smoothly from one learning stage into the other. This concept implies that memory formation and storage in the olivocerebellar system is created in a distributed and dynamic fashion allowing continuous expansion and fine-tuning to the changing body and environment conditions. The CF play a critical role by inducing various forms of heterosynaptic plasticity when they are active, and by permitting various forms of homosynaptic plasticity when they are silent. For instance, simultaneous activation of PF and CF input results in a weakening in the synaptic strength at the PF-PC synapse, a strengthening at the PF-MLI synapse, and possibly also concurrent strengthening of inhibition at the MLI-PC synapse. As a consequence, all these forms of synaptic plasticity function together to reduce the spiking output from PCs. Similarly, PF only input facilitates LTP at PF-PC synapses as well as LTD at the PF-MLI synapse that could ultimately enhance the spiking outputs from PCs. Importantly, all these forms of plasticity are antidirectional including both depressing and potentiating effects, and they are all reinforcing in that the potentiating and depressing effects at the superimposed interneurons operate in synergy with the depressing and potentiating effects at their target neurons, respectively.

Our conceptual model of distributed dynamic plasticity elaborates upon the general concepts initiated by Marr, Albus and Ito (Marr, 1969; Albus, 1971; Ito, 1982), and recently modified by Roberts (Roberts, 2000, 2007) and Dean and colleagues (Dean et al., 2010). Yet, we attribute relatively major roles to plasticity at the input and output of the interneurons superimposed on both GrCs and Purkinje cells, and we argue that potentiation of both the superimposed interneurons and their target neurons forms, at least initially, the dominating type of plasticity. Although LTD may contribute at various levels and might to

some extent even compensate for deficits in potentiation, it is probably not absolutely essential at any location in the chain of events, whereas LTP is more critical at various levels (Fig. 2, 3). One might even speculate that LTP and intrinsic changes in excitability form in principle the fundamental memories that persist and are being used throughout life. It follows the notion that we have an excessive amount of GrCs and even more parallel fiber varicosities, the vast majority of which is silent (Isope and Barbour, 2002; Brunel et al., 2004; Chadderton et al., 2004; Arenz et al., 2008; Barmack and Yakhnitsa, 2008; Ruigrok et al., 2011) and hence tends to be more sensitive to potentiation than depression.

It has been proposed that bidirectional plasticity at the PF-PC synapse is essential to avoid saturation of the synapse by noise and thereby to prevent meaningless modification of synaptic strengths by random activation and to eventually prevent overexcitation or underexcitation of the Purkinje cell involved (Coesmans et al., 2004; Jorntell and Hansel, 2006). Bidirectional plasticity may indeed be helpful in these processes, but in our working hypothesis potentiation at this synapse does not necessarily need to be controlled by

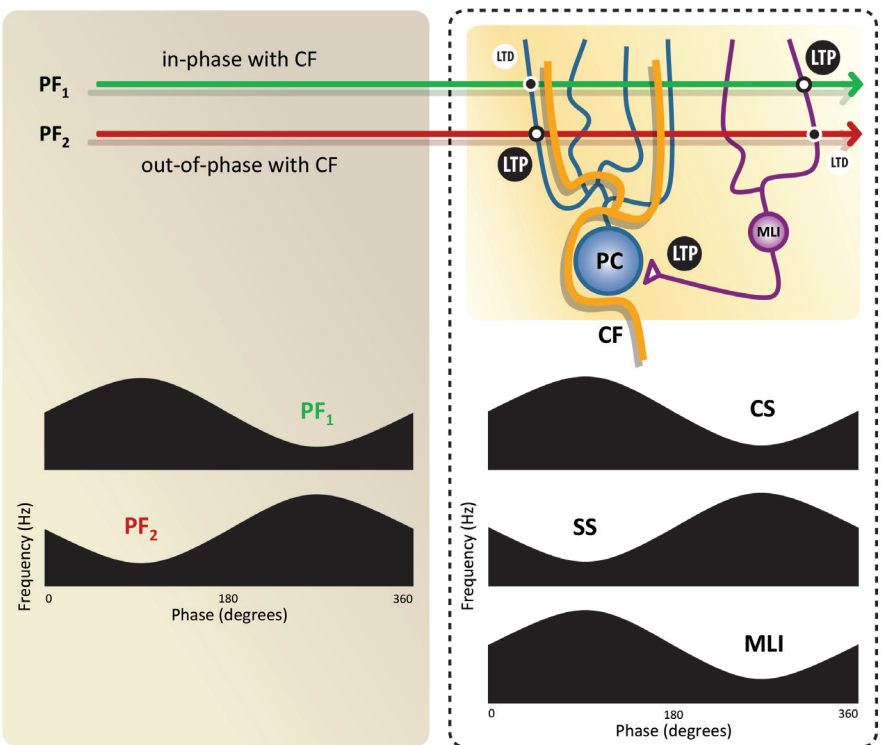

Figure 2; Creating output by selecting input in Purkinje cell network.

By controlling the direction of plasticty at multiple synapses, the climbing fiber links the appropriate PF-phase to the desired target. When CF activity is in-phase with PF-activity, it will promote LTP at the PF-MLI synapse, LTD at the PF-PC synapse, and rebound potentiation at the MLI-PC synapse (for simplicity the rebound potentiation is here also indicated as LTP). Conversely, when CF activity is absent, LTD is induced at the PF-MLI synapse, whereas LTP is induced at the PF-PC synapse. Through this mechanism, the CF can induce opposite phases in the MLI and PC. Ultimately, simple spike activity in PCs is controlled directly by excitatory inputs from out-of-phase PFs (PF_2) and suppression from in-phase PFs (PF_1) through feedforward inhibition from MLIs. As a consequence, the simple spike output of PCs will be out-of-phase with CF activity (indicated as complex spikes, i.e. CSs).

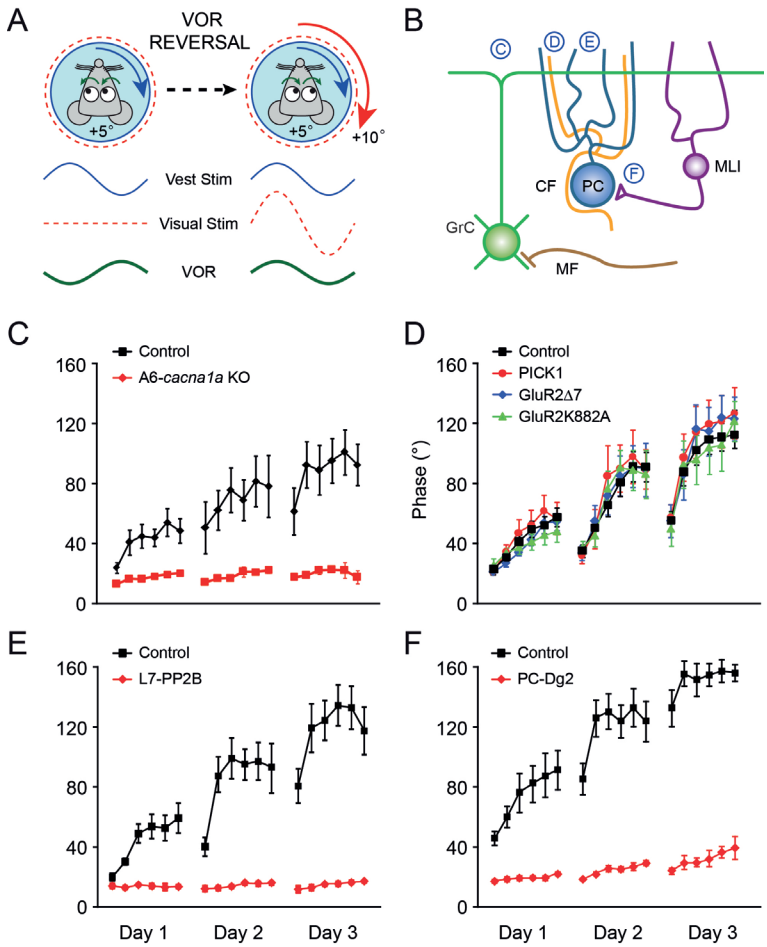

Figure 3; Phase reversal of the vestibulo-ocular reflex; phenotypes in plasticity-deficient preparations. A, Phase reversal of the vestibulo-ocular reflex (VOR) can be obtained following visuovestibular mismatch training during which the optokinetic stimulus is constantly given in phase with the turntable stimulation, but gradually at greater amplitude; here it starts with an optokinetic stimulus that is stationary with an amplitude of zero degrees on day zero (left), and, is, over the course of two to three additional days, cranked up to 10 degrees in phase with the table (right), which kept rotating at 5 degrees throughout the experiments. This mismatch training will ultimately force the mouse to make a compensatory eye movement during vestibular stimulation in the dark that is opposite in direction (green line). B, schematic drawing of the cerebellar cortex and some of its plasticity sites, which are indicated by the letters C to F; these letters refer to synaptic transmission at the parallel fiber (PF) to Purkinje cell (PC) synapse (C), LTD at the PF to PC synapse (D), LTP at the PF-PC synapse (E), and synaptic transmission at the molecular layer interneuron (MLI) to PC synapse (F). The letters correspond to the phenotypes in phase reversal depicted in panels C to F. C, If one dampens the synaptic transmission at the PF-PC synapses, one does observe a deficit in phase reversal learning (Ch. 3). D, If one genetically tackles LTD at the PF-PC synapse selectively downstream at the level of the AMPA receptors (GluR2d7 or GluR2K882A) or its insertion (PICK1) in three different mutants (Ch. 4.1), there is no phenotype, neither in motor performance, nor in motor learning or consolidation. Likewise, if one blocks PF-PC LTD pharmacologically by applying T-588, phase reversal learning is not impaired (Ch. 4.1). E, Instesad, if one block PF to PC LTP and intrinsic plasticity of Purkinje cells simultaneously by deleting PP2B in a Purkinje cell specific manner, there is a prominent phenotype in phase reversal learning (Ch. 4.2). F, Similarly, if one in effect deletes synaptic transmission at the PF-MLI synapse and plasticity at the MLI-PC synapse, there is a phenotype in phase reversal learning (Ch. 5).

PF-PC LTD, because potentiation at the input and output of MLIs can make up for PF-PC LTD maintaining a stable level of excitability (Ch. 5), and because all synapses are in the end controlled by climbing fiber feedback, thereby facilitating stability in the learning pro-

cess (Roberts, 2000, 2007). The fact that a stored procedural memory should in principle be retrievable for the rest of one's life demands a mechanism that can last forever. In this respect the detailed molecular mechanisms underlying LTP at the PF-PC synapse may differ from that at the CA3-CA1 synapse in the hippocampus, which is required for declarative memory formation and which can and needs to be formed more rapidly with more prominent options for extinction (Morris et al., 1986; Myers et al., 2006). Since procedural memories formed at a young age can indeed last forever (Stahl et al., 2006), while the ability to form new procedural memories is affected by aging (Woodruff-Pak et al., 2010), it will be interesting to find out whether the capacity for potentiating PF synapses both at PC and interneurons is diminished over time, and if so, to what extent this is reflected in a saturation of particular GluR subunits at the end of life (Douyard et al., 2007; Kessels and Malinow, 2009).

Taken together, we propose that the options provided by distributed dynamic plasticity in the cerebellar cortex are sufficiently rich to modify phases of activity and behaviour in any direction, and that these acquired behaviours can be preserved and saved for a lifetime in the sets of potentiated inputs to GrC and PCs as well as their superimposed interneurons, while LTD at these synapses might help to handle saturation due to noise issues and to allow for compensation when necessary.

Phase reversal of the vestibulo-ocular reflex explained by distributed dynamic plasticity.

Over the past decade many mouse mutants have been designed to investigate the roles of particular forms of plasticity in various forms of cerebellar motor learning such as eyeblink conditioning, locomotion conditioning and adaptation of the vestibulo-ocular reflex (VOR) (Aiba et al., 1994; Shibuki et al., 1996; De Zeeuw et al., 1998; Miyata et al., 2001; van Alphen and De Zeeuw, 2002; Feil et al., 2003; Hansel et al., 2006; Kishimoto and Kano, 2006; Andreescu et al., 2007). In particular phase reversal of the VOR has been shown to be a sensitive paradigm to detect differences in cerebellar motor learning and consolidation (Ch. 4-6). VOR phase reversal can be obtained following several days of visuovestibular mismatch training during which the optokinetic stimulus is constantly given in phase with the turntable stimulation, but gradually at greater amplitude (Fig. 3). This mismatch training will ultimately force the mouse to make a compensatory eye movement during vestibular stimulation in the dark that is opposite in direction, because the error signals of retinal slip during the training in the light are reversed in direction. This reversal of retinal slip signals will reverse the phase of the climbing fiber activity, which in turn will induce, according to the principles of distributed dynamic plasticity, various changes in neuronal spiking activity. The reversal of the phase of the CF signals will induce potentiation at the PF-PC synapses and the PF-MLI synapses including stellate cells, basket cells and presumably also Golgi cells that were in a silent or depressed state before the reversal. Likewise, it will depress the PF-PC and PF-MLI synapses that were potentiated in the initial state (Fig. 1, 2). Thus, in contrast to real life where new procedural memories are mostly formed by increasing or decreasing the phase of the CF signals, while the direction of the modulation is relatively stable, this paradigm provides the maximum challenge to the system enforcing a complete reversal in the direction of the CF signals. And so ultimately, there will be

a complete reversal of the direction of movements following the same stimulus; whereas the direction of compensatory eye movements during vestibular stimulation in the dark is contraversive before the training paradigm, it will be ipsiversive at identical stimulation parameters after the training (compare green eye movement traces before and after training in Fig. 3).

Since so many different reinforcing forms of plasticity are probably involved simultaneously in this form of motor learning, there must be ample room for compensation in case a single form of plasticity is impaired. Thus, one expects the most prominent phenotypes in mouse mutants in which multiple forms of plasticity are affected. The severity of the deficits in motor learning and consolidation of phase reversal that we have now observed in tens of mutants are in line with this prediction (Fig. 3). For example, if one tackles LTD at the PF-PC synapse selectively downstream at the level of the AMPA receptor or its insertion (Ch. 4.1), there is indeed no phenotype, neither in motor performance, nor in motor learning or consolidation (Fig. 3). However, if one tackles this form of LTD centrally in the metabolic pathways of the PCs by interfering with one of the kinases such as PKC, PKG or CaMKII (De Zeeuw et al., 1998; Feil et al., 2003; Hansel et al., 2006), thereby presumably also affecting postsynaptic plasticity at the MLI-PC synapse (Kano et al., 1996; Song and Messing, 2005) and/or presynaptic plasticity at the PC- cerebellar nuclei neuron synapse (Pedroarena and Schwarz, 2003), motor learning is affected. Likewise, if one blocks the activity of approximately 70% of all GrCs, basic motor performance and motor learning are not affected, while there is a phenotype in consolidation of phase reversal learning (Ch. 3). Instead, if one blocks PF-PC LTP and intrinsic plasticity of Purkinje cells simultaneously by deleting PP2B in a PC specific manner, possibly also affecting plasticity at their inhibitory synapses (Ch. 2, 6.2), there is a prominent phenotype in phase reversal learning (Fig. 3). Similarly, if one in effect deletes plasticity at the PF-MLI synapse and plasticity at the MLI-PC synapse while inducing compensatory effects in excitability of PCs by deleting the GABAA-γ2 receptor specifically in PCs (Ch. 5), there is a phenotype in phase reversal learning and consolidation (Fig. 3). Taken together, it is our working hypothesis that cerebellar learning is only prominently affected when at least two main sites of plasticity are affected, with potentiation at the PF synapses being one of the most dominant players. If one only affects LTD at the PF-PC synapse, there is apparently sufficient compensation at the other sites to take over and allow completely normal cerebellar motor learning. Interesting enough, the memory learning and consolidation could be compensated at other sites inside/outside of the cerebellar cortex. It has been suggested that once acquired, the consolidation motor memory can be stored and extrapolated in the absence of PF inputs (Wada et al., 2007). It is quite plausible that the memory consolidation deficits found in various mouse mutants in this thesis are underestimated due to the compensatory mechanisms at other locations, such as PF-MLI synapses, PC-cerebellar nuclei neuron synapses, or in the vestibular nuclei (Bagnall and du Lac, 2006; Pugh and Raman, 2009; Liu et al., 2010). In this case, development approaches of interrupting specific sites in the cerebellar cortex could reveal more subtle alterations in the cerebellar functioning. Thus it remains to be illustrated what are the functions of various types of synapses in the cerebellar cortex. What is apparent is that synaptic plasticity at various cerebellar neurons, which cannot be masked during development, is essential for motor memory formation and

consolidation.

In this respect, one can hypothesize that the superimposed MLIs, which may have occurred later in evolution than their target neurons, i.e. the PCs and GrCs, have endowed the cerebellar cortex with ample possibilities to compensate for potential deficits in one of the plasticity mechanisms in the target neurons themselves. This development in itself would indicate how important the role of the cerebellar cortex in motor learning and consolidation has become during evolution. Furthermore, the expanding population of the cerebellar cortical neurons and their functional circuits during phylogeny may also be superimposed into the existing, motor function related cerebellar circuits to elaborate their stringent, non-motor related cognitive functions (Scelfo et al., 2008).

Causes and consequences of cerebellar malfunction in ataxia

Previous studies provided clear evidence as to how cerebellar ataxia comes about using loss-of-function *Cacna1a* mutants. Most of these mutants all have prominent ataxia that largely resembles episodic ataxia type 2 (EA2) and spinocerebellar ataxia type 6 (SCA6). Several hallmark features of the cerebellar ataxia, including morphological changes of neurons and synapses, altered synaptic transmissions between neurons, aberrant intrinsic pacemaking activity of PCs as well as altered firing patterns *in vivo* (Rhyu et al., 1999; Matsushita et al., 2002; Hoebeek et al., 2005; Walter et al., 2006) have been shown in these loss-of-function mutants. The selective degeneration of PCs in parasagittal patterns is only found in a small fraction of all these mutants, including the homozygous $Ca_V2.1^{-/-}$ and *la* mice, whereas much milder but clear PC degeneration is also found in 1 year old tg mice (Pietrobon, 2010). However no clear neuronal death has been reported in *rkr* and *rol* mice. The neuronal death in the cerebellum could be related to the extent of reduction in Ca^{2+} current density, since the highest Ca^{2+} current reduction have been found in $Ca_V2.1^{-/-}$ (100%) and la (70%) mice; whereas only 50% reduction in current density are found in other mutants as well as the heterozygous $Ca_V2.1^{-/-}$ mice. To what extend the cerebellum exceeds its threshold to trigger neuronal death remains to be determined. At the ultrastructural level, alterations in PF-PC synaptic formations, including ectopic spines in dendrite and single PF varicosity contacting multiple PC spines are generally found in the loss-of-function mutants (Rhyu et al., 1999). In addition, the global *Cacna1a* KO mice also show multiple CF innervations onto the same PC. These observations have been interpreted as a rescue mechanism to compensate for the loss of synaptic transmission due to the loss of Ca^{2+} influx at presynaptic terminals. Here we show that in the $Cacna1a^{S218L}$ mutants, in which the $Ca_V2.1$ (P/Q-type) mediated Ca^{2+}-influx is increased in both the soma and axon terminals of various neurons (Adams et al., 2010) and PF-PC EPSC appeared to be larger, the malformed PF varicosity contacting multiple spines are also found (Ch. 7)). Since there is no need for such compensation mechanism in $Cacna1a^{S218L}$ mutants, the malformation of PF-PC synapses is likely to be the direct consequence of a abnormal Ca^{2+}-channel functioning.

The increased irregularity of PC pacemaking activity and simple spike firing are considered as the main causes of ataxia (Hoebeek et al., 2005; Walter et al., 2006). Also in $Cacna1a^{S218L}$ mice we found irregular PC firing activities, probably more severe than that

in the tg mice. *In vitro*, *Cacna1a*^{S218L} PCs consistently generate spontaneous bursts that are facilitated by spontaneous dendritic Ca^{2+} spikes. *in vivo*, PCs show similar burst-like activities in the alert *Cacna1a*^{S218L} mice, suggesting a main contribution to the ataxic phenotype. Thus it is not surprising to point out that the *Cacna1a*^{S218L} mice are also more ataxic than the tg mice. Previous studies provide ample evidence that SK- and BK-channels contribute to the intrinsic firing of PCs (Edgerton and Reinhart, 2003; Womack et al., 2004; Alvina and Khodakhah, 2008). In the loss-of-function mutants, the Ca^{2+} activated K^+ channel (SK and BK) functions are compromised thus lead to irregular PC firing patterns (Walter et al., 2006). However it remains enigmatic that reduced SK- and BK-conductance changes the regularity between spikes rather than increases firing frequency in a more homogeneous pattern. It is possible that the Ca^{2+}-influx and the subsequent activation of SK- and BK-channels vary randomly from trial to trail, and such a natural variation could be saturated in the loss-of-function mutants. The *Cacna1a*^{S218L} mutant, on the other hand, shows extremely irregular Purkinje cell firing patterns due to the spontaneously occurring Ca^{2+}-bursts. Thus both reduced and increased Ca^{2+}-influx ultimately leads to irregular PC firing via distinct mechanisms. Interestingly enough, both ataxic phenotypes can be partly rescued by a SK-channel enhancer, which increases the SK mediated AHP thus improve the regularity of PC firing patterns in loss-of-function mutants and reduces the susceptibility of Ca^{2+}-burst firing in the *Cacna1a*^{S218L} mutants. Thus a generalized therapeutic strategy aiming at enhancing SK-channel functions could have a broad application in ataxic patients.

It is worth mentioning that it is generally accepted that PCs have extremely regular pacemaking activity *In vitro*, although several previous studies also show alternating trimodal and bursty intrinsic firings patterns in wild type PCs *In vivo* (Womack and Khodakhah, 2002; Loewenstein et al., 2005). Phamacological studies reveal that the SK- and BK-channels are also involved in the regulation of such burst firing patterns (Womack and Khodakhah, 2002; Womack et al., 2009). Up to date, the occurrence and functional consequences of such irregular PC firing patterns have not been fully characterized. Although operating in various intrinsic pacemaking firing states could enrich the coding patterns of PCs, previous studies unequivocally show that PCs operate constantly in up-states in alert mice and the down-states are largely influenced by the anaesthesia (Loewenstein et al., 2005; Schonewille et al., 2006). It is likely the case, that the PC firing patterns *In vitro* can be further influenced by various factors, including the general health conditions of PCs after slice preparation, the ionic composition of the recording solutions and interference from recording electrodes. Thus future experiments are needed to unravel the conditions that trigger the transition between tonic and burst-like firing patterns in the PCs.

Various mouse models described in this thesis are designed to elucidate the role of long-term plasticity in the cerebellar learning and show different levels of basic motor performances. The α6^{Cre}-*Cacna1a*$^{-/-}$, *PICK1*$^{-/-}$, *GluR2Δ7* and *GluR2K882A* all have normal motor performance (Ch. 3, 4), whereas the *L7-γ2* and *L7-PP2B* have modest motor impairment (Ch, 5) and *βCaMKII*$^{-/-}$ show profound ataxia (Ch, 6.2). Surprisingly, α6^{Cre}-*Cacna1a*$^{-/-}$, in which more than 70% of the GrC output are silenced, have normal motor performance. It seems unlikely that the mild ataxia in *L7-PP2B* mice is primarily induced by reductions in the total PF-PC input, because the reduction of PF-EPSC in the A6-*Cacna1a*$^{-/-}$ is even

more pronounced than that in various Ca^{2+} loss-of-function mutants. Considering the remaining PF-PC inputs are functionally intact (Ch, 3), it is possible that a small fraction of well-preserved PF-PC inputs, but not the generally reduced PF-PC inputs is potent enough to maintain normal motor performance. As a result of reduced PF-PC inputs, an increase rather than decrease in PC firing regularity has been shown in the $\alpha6^{Cre}$-*Cacna1a*$^{-/-}$. In line with this notion, the *L7-γ2* mice, which lack the phasic synaptic inhibition at the MLI–PC synapse, show a more regular PC spiking pattern and virtually intact basal eye movements (Ch, 5). In addition, a previous study shows that a clear ataxic phenotype occurs following the complete silencing of the GrC output probably due to the complete cessation of simple spike firing (Wada et al., 2007). Clearly the PC firing regularity is critical for both motor performance and motor learning, in that the decreased regularity seems to be tightly associated with motor performance deficits and increased regularity might be better attributed to the consolidation impairments. However one should take in mind that the regularity of firing we refer to is a general indication of PC firing pattern over a certain time period. Such mean values of regularity do not contain specific information of the instantaneous changes in PC firing patterns (Shin et al., 2007). To what extend that the PC firing dynamics lead to a loss of motor performance or motor learning deficits remain to be determined.

Synaptic plasticity to maintain motor performance

What is the relation between synaptic plasticity and motor performance? Previous studies using global or cell specific genetically modified mouse models that tackle the key enzymes involved in synaptic plasticity are usually associated with a basal motor deficits (De Zeeuw et al., 1998; Hansel et al., 2006). It is possible that alterations in synaptic plasticity cause cerebellar ataxia by affecting the precision of the synaptic transmission. As mentioned previously, the aberrant long-term plasticity might affect either the strength or the timing of excitatory and/or inhibitory synaptic inputs and consequently an altered regularity of PC simple spike firing patterns. Recent findings presented in this thesis show rather diverse phenotypes, in that global mutants that lack LTD at PF-PC synapses show normal motor performances, the PC-specific mutants that lack LTP at PF-PC synapses and intrinsic plasticity in Purkinje cells show moderate impairment of motor performance, whereas a global *βCaMKII*$^{-/-}$ mice that affect plasticity at both excitatory and inhibitory synapses as a whole show prominent ataxia. The wide range of genetically manipulated mutants in this thesis allow us to further elaborate the discussion on the role of these key enzymes in maintaining normal motor performance. The PKC dependent AMPA receptor internalization mediated by PICK1 protein binding at the C-terminal of AMPA receptors is critical for the postsynaptic form of LTD at PF-PC synapses (Xia et al., 2000). However the LTD deficits per se probably do not contribute to the impaired motor performance, since the ataxic phenotype is not found in the *PICK1*$^{-/-}$ *GluR2Δ7* and *GluR2K882A* mice. Besides the AMPA receptors, a large number of substrates can also be phosphorylated by PKC in PCs. It remains to be illustrated which downstream targets of PKC dependent phosphorylation are involved in the pathogenesis of ataxia. Similarly, PP2B mediated dephosporylation plays critical roles in LTP at PF-PC synapses, intrinsic plasticity in PCs as well as iLTP at MLI-PC synapses. These synaptic changes could individually or simultaneously contribute

to the moderate motor deficits in the *L7-PP2B* mice. Up to now it is rudimentary to conclude the involvements of LTP or intrinsic plasticity in maintaining motor performance. Future studies should be conducted to dissect their unique contribution by specifically affecting individual types of synaptic plasticity in PCs. When one considers the results presented in Ch. 6, it is interesting to point out that α and *βCaMKII*$^{-/-}$ mice have distinct phenotypes. Deleting βCaMKII causes severe ataxia whereas little motor dysfunction is found in *αCaMKII*$^{-/-}$ mice, although the learning of new motor tasks is abnormal (Hansel et al ., 2006). This difference could be contributed by both the spatial and functional differences between these two isoforms. αCaMKII is exclusively expressed in the PCs in cerebellum, whereas βCaMKII is expressed throughout the cerebellum in most of the neurons. Thus deleting βCaMKII might have broader impact on various sites in the cerebellum than deleting αCaMKII. Furthermore, Ch. 6 suggests functional difference between α and βCaMKII in mediating synaptic plasticity at both excitatory and inhibitory synapses. At the PF-PC synapses, deleting αCaMKII impair LTD induction without affecting LTP, whereas LTP/LTD induction roles are inverted in the βCaMKII KO mice. Likewise, at the molecular layer interneuron-PC synapses, deleting αCaMKII completely abolishes the enzymatic power of the CaMKII holoenzyme and deleting βCaMKII shifts the induction threshold. These results suggest that αCaMKII serves a pure enzymatic role and βCaMKII fulfils both enzymatic and structural functions. What are the functional consequences of genetically ablating αCaMKII or βCaMKII in simple spike output and motor performance? As is commonly found in various ataxic mouse models, the regularity of PC simple spike firing plays a critical role in maintaining normal motor performance. It is indeed the case that the irregular PC firing patterns are found in the *βCaMKII*$^{-/-}$ but not *αCaMKII*$^{-/-}$ mice (Hoebeek, personal communication). Up to date, little evidence of PC firing regularity has been shown in other mutants with concurrent reversal of synaptic plasticity and motor performance deficits; it would be interesting to dissect the synaptic plasticity component in the induction of ataxia.

References

Adams PJ, Rungta RL, Garcia E, van den Maagdenberg AM, MacVicar BA, Snutch TP (2010) Contribution of calcium-dependent facilitation to synaptic plasticity revealed by migraine mutations in the P/Q-type calcium channel. Proc Natl Acad Sci U S A 107:18694-18699.

Aiba A, Kano M, Chen C, Stanton ME, Fox GD, Herrup K, Zwingman TA, Tonegawa S (1994) Deficient cerebellar long-term depression and impaired motor learning in mGluR1 mutant mice. Cell 79:377-388.

Albus JS (1971) A theory of cerebellar function. Math Biosci 10:25-61.

Alvina K, Khodakhah K (2008) Selective regulation of spontaneous activity of neurons of the deep cerebellar nuclei by N-type calcium channels in juvenile rats. J Physiol 586:2523-2538.

Andreescu CE, Milojkovic BA, Haasdijk ED, Kramer P, De Jong FH, Krust A, De Zeeuw CI, De Jeu MT (2007) Estradiol improves cerebellar memory formation by activating estrogen receptor beta. J Neurosci 27:10832-10839.

Arenz A, Silver RA, Schaefer AT, Margrie TW (2008) The contribution of single synapses to sensory representation *in vivo*. Science 321:977-980.

Armano S, Rossi P, Taglietti V, D'Angelo E (2000) Long-term potentiation of intrinsic excitability at the mossy fiber-granule cell synapse of rat cerebellum. J Neurosci 20:5208-5216.

Bagnall MW, du Lac S (2006) A new locus for synaptic plasticity in cerebellar circuits. Neuron 51:5-7.

Barmack NH, Yakhnitsa V (2008) Functions of interneurons in mouse cerebellum. J Neurosci 28:1140-1152.

Bell CC, Han VZ, Sugawara Y, Grant K (1997) Synaptic plasticity in a cerebellum-like structure depends on temporal order. Nature 387:278-281.

Brickley SG, Cull-Candy SG, Farrant M (1996) Development of a tonic form of synaptic inhibition in rat cerebellar granule cells resulting from persistent activation of GABAA receptors. J Physiol 497 (Pt 3):753-759.

Brunel N, Hakim V, Isope P, Nadal JP, Barbour B (2004) Optimal information storage and the distribution of synaptic weights: perceptron versus Purkinje cell. Neuron 43:745-757.

Canepari M, Vogt KE (2008) Dendritic spike saturation of endogenous calcium buffer and induction of postsynaptic cerebellar LTP. PLoS One 3:e4011.

Chadderton P, Margrie TW, Hausser M (2004) Integration of quanta in cerebellar granule cells during sensory processing. Nature 428:856-860.

Coesmans M, Weber JT, De Zeeuw CI, Hansel C (2004) Bidirectional parallel fiber plasticity in the cerebellum under climbing fiber control. Neuron 44:691-700.

D'Angelo E, De Zeeuw CI (2009) Timing and plasticity in the cerebellum: focus on the granular layer. Trends Neurosci 32:30-40.

Daoudal G, Debanne D (2003) Long-term plasticity of intrinsic excitability: learning rules and mechanisms. Learn Mem 10:456-465.

De Zeeuw CI, Hansel C, Bian F, Koekkoek SK, van Alphen AM, Linden DJ, Oberdick J (1998) Expression of a protein kinase C inhibitor in Purkinje cells blocks cerebel-

lar LTD and adaptation of the vestibulo-ocular reflex. Neuron 20:495-508.
Dean P, Porrill J, Ekerot CF, Jorntell H (2010) The cerebellar microcircuit as an adaptive filter: experimental and computational evidence. Nat Rev Neurosci 11:30-43.
Douyard J, Shen L, Huganir RL, Rubio ME (2007) Differential neuronal and glial expression of GluR1 AMPA receptor subunit and the scaffolding proteins SAP97 and 4.1N during rat cerebellar development. J Comp Neurol 502:141-156.
Edgerton JR, Reinhart PH (2003) Distinct contributions of small and large conductance Ca2+-activated K+ channels to rat Purkinje neuron function. J Physiol 548:53-69.
Feil R, Hartmann J, Luo C, Wolfsgruber W, Schilling K, Feil S, Barski JJ, Meyer M, Konnerth A, De Zeeuw CI, Hofmann F (2003) Impairment of LTD and cerebellar learning by Purkinje cell-specific ablation of cGMP-dependent protein kinase I. J Cell Biol 163:295-302.
Fregnac Y (1998) Homeostasis or synaptic plasticity? Nature 391:845-846.
Han VZ, Grant K, Bell CC (2000) Reversible associative depression and nonassociative potentiation at a parallel fiber synapse. Neuron 27:611-622.
Hansel C, Linden DJ, D'Angelo E (2001) Beyond parallel fiber LTD: the diversity of synaptic and non-synaptic plasticity in the cerebellum. Nat Neurosci 4:467-475.
Hansel C, de Jeu M, Belmeguenai A, Houtman SH, Buitendijk GH, Andreev D, De Zeeuw CI, Elgersma Y (2006) alphaCaMKII Is essential for cerebellar LTD and motor learning. Neuron 51:835-843.
Hartell NA (1996) Strong activation of parallel fibers produces localized calcium transients and a form of LTD that spreads to distant synapses. Neuron 16:601-610.
Hoebeek FE, Stahl JS, van Alphen AM, Schonewille M, Luo C, Rutteman M, van den Maagdenberg AM, Molenaar PC, Goossens HH, Frens MA, De Zeeuw CI (2005) Increased noise level of purkinje cell activities minimizes impact of their modulation during sensorimotor control. Neuron 45:953-965.
Howarth C, Peppiatt-Wildman CM, Attwell D (2010) The energy use associated with neural computation in the cerebellum. J Cereb Blood Flow Metab 30:403-414.
Isope P, Barbour B (2002) Properties of unitary granule cell-->Purkinje cell synapses in adult rat cerebellar slices. J Neurosci 22:9668-9678.
Ito M (1982) Cerebellar control of the vestibulo-ocular reflex--around the flocculus hypothesis. Annu Rev Neurosci 5:275-296.
Ito M (2001) Cerebellar long-term depression: characterization, signal transduction, and functional roles. Physiol Rev 81:1143-1195.
Jorntell H, Hansel C (2006) Synaptic memories upside down: bidirectional plasticity at cerebellar parallel fiber-Purkinje cell synapses. Neuron 52:227-238.
Kano M, Fukunaga K, Konnerth A (1996) Ca(2+)-induced rebound potentiation of gamma-aminobutyric acid-mediated currents requires activation of Ca2+/calmodulin-dependent kinase II. Proc Natl Acad Sci U S A 93:13351-13356.
Ke MC, Guo CC, Raymond JL (2009) Elimination of climbing fiber instructive signals during motor learning. Nat Neurosci 12:1171-1179.
Kessels HW, Malinow R (2009) Synaptic AMPA receptor plasticity and behavior. Neuron 61:340-350.
Khaliq ZM, Raman IM (2005) Axonal propagation of simple and complex spikes in cer-

ebellar Purkinje neurons. J Neurosci 25:454-463.
Kim JC, Cook MN, Carey MR, Shen C, Regehr WG, Dymecki SM (2009) Linking genetically defined neurons to behavior through a broadly applicable silencing allele. Neuron 63:305-315.
Kishimoto Y, Kano M (2006) Endogenous cannabinoid signaling through the CB1 receptor is essential for cerebellum-dependent discrete motor learning. J Neurosci 26:8829-8837.
Lisberger SG, Fuchs AF (1978a) Role of primate flocculus during rapid behavioral modification of vestibuloocular reflex. I. Purkinje cell activity during visually guided horizontal smooth-pursuit eye movements and passive head rotation. J Neurophysiol 41:733-763.
Lisberger SG, Fuchs AF (1978b) Role of primate flocculus during rapid behavioral modification of vestibuloocular reflex. II. Mossy fiber firing patterns during horizontal head rotation and eye movement. J Neurophysiol 41:764-777.
Liu Y, Formisano L, Savtchouk I, Takayasu Y, Szabo G, Zukin RS, Liu SJ (2010) A single fear-inducing stimulus induces a transcription-dependent switch in synaptic AMPAR phenotype. Nat Neurosci 13:223-231.
Loewenstein Y, Mahon S, Chadderton P, Kitamura K, Sompolinsky H, Yarom Y, Hausser M (2005) Bistability of cerebellar Purkinje cells modulated by sensory stimulation. Nat Neurosci 8:202-211.
Marr D (1969) A theory of cerebellar cortex. J Physiol 202:437-470.
Matsushita K, Wakamori M, Rhyu IJ, Arii T, Oda S, Mori Y, Imoto K (2002) Bidirectional alterations in cerebellar synaptic transmission of tottering and rolling Ca2+ channel mutant mice. J Neurosci 22:4388-4398.
Miles FA, Fuller JH, Braitman DJ, Dow BM (1980) Long-term adaptive changes in primate vestibuloocular reflex. III. Electrophysiological observations in flocculus of normal monkeys. J Neurophysiol 43:1437-1476.
Miyata M, Kim HT, Hashimoto K, Lee TK, Cho SY, Jiang H, Wu Y, Jun K, Wu D, Kano M, Shin HS (2001) Deficient long-term synaptic depression in the rostral cerebellum correlated with impaired motor learning in phospholipase C beta4 mutant mice. Eur J Neurosci 13:1945-1954.
Morris RG, Hagan JJ, Rawlins JN (1986) Allocentric spatial learning by hippocampectomised rats: a further test of the "spatial mapping" and "working memory" theories of hippocampal function. Q J Exp Psychol B 38:365-395.
Myers KM, Ressler KJ, Davis M (2006) Different mechanisms of fear extinction dependent on length of time since fear acquisition. Learn Mem 13:216-223.
Pedroarena CM, Schwarz C (2003) Efficacy and short-term plasticity at GABAergic synapses between Purkinje and cerebellar nuclei neurons. J Neurophysiol 89:704-715.
Pietrobon D (2010) CaV2.1 channelopathies. Pflugers Arch 460:375-393.
Pugh JR, Raman IM (2009) Nothing can be coincidence: synaptic inhibition and plasticity in the cerebellar nuclei. Trends Neurosci 32:170-177.
Raman IM, Bean BP (1999) Ionic currents underlying spontaneous action potentials in isolated cerebellar Purkinje neurons. J Neurosci 19:1663-1674.
Rhyu IJ, Abbott LC, Walker DB, Sotelo C (1999) An ultrastructural study of granule cell/

Purkinje cell synapses in tottering (tg/tg), leaner (tg(la)/tg(la)) and compound heterozygous tottering/leaner (tg/tg(la)) mice. Neuroscience 90:717-728.
Roberts PD (2000) Modeling inhibitory plasticity in the electrosensory system of mormyrid electric fish. J Neurophysiol 84:2035-2047.
Roberts PD (2007) Stability of complex spike timing-dependent plasticity in cerebellar learning. J Comput Neurosci 22:283-296.
Ruigrok TJ, Hensbroek RA, Simpson JI (2011) Spontaneous activity signatures of morphologically identified interneurons in the vestibulocerebellum. J Neurosci 31:712-724.
Scelfo B, Sacchetti B, Strata P (2008) Learning-related long-term potentiation of inhibitory synapses in the cerebellar cortex. Proc Natl Acad Sci U S A 105:769-774.
Schonewille M, Khosrovani S, Winkelman BH, Hoebeek FE, De Jeu MT, Larsen IM, Van der Burg J, Schmolesky MT, Frens MA, De Zeeuw CI (2006) Purkinje cells in awake behaving animals operate at the upstate membrane potential. Nat Neurosci 9:459-461; author reply 461.
Shibuki K, Gomi H, Chen L, Bao S, Kim JJ, Wakatsuki H, Fujisaki T, Fujimoto K, Katoh A, Ikeda T, Chen C, Thompson RF, Itohara S (1996) Deficient cerebellar long-term depression, impaired eyeblink conditioning, and normal motor coordination in GFAP mutant mice. Neuron 16:587-599.
Shin SL, Hoebeek FE, Schonewille M, De Zeeuw CI, Aertsen A, De Schutter E (2007) Regular patterns in cerebellar Purkinje cell simple spike trains. PLoS One 2:e485.
Simat M, Parpan F, Fritschy JM (2007) Heterogeneity of glycinergic and gabaergic interneurons in the granule cell layer of mouse cerebellum. J Comp Neurol 500:71-83.
Song M, Messing RO (2005) Protein kinase C regulation of GABAA receptors. Cell Mol Life Sci 62:119-127.
Stahl JS, James RA, Oommen BS, Hoebeek FE, De Zeeuw CI (2006) Eye movements of the murine P/Q calcium channel mutant tottering, and the impact of aging. J Neurophysiol 95:1588-1607.
van Alphen AM, De Zeeuw CI (2002) Cerebellar LTD facilitates but is not essential for long-term adaptation of the vestibulo-ocular reflex. Eur J Neurosci 16:486-490.
Wada N, Kishimoto Y, Watanabe D, Kano M, Hirano T, Funabiki K, Nakanishi S (2007) Conditioned eyeblink learning is formed and stored without cerebellar granule cell transmission. Proc Natl Acad Sci U S A 104:16690-16695.
Walter JT, Alvina K, Womack MD, Chevez C, Khodakhah K (2006) Decreases in the precision of Purkinje cell pacemaking cause cerebellar dysfunction and ataxia. Nat Neurosci 9:389-397.
Wang SS, Denk W, Hausser M (2000) Coincidence detection in single dendritic spines mediated by calcium release. Nat Neurosci 3:1266-1273.
Welsh JP, Yamaguchi H, Zeng XH, Kojo M, Nakada Y, Takagi A, Sugimori M, Llinas RR (2005) Normal motor learning during pharmacological prevention of Purkinje cell long-term depression. Proc Natl Acad Sci U S A 102:17166-17171.
Womack M, Khodakhah K (2002) Active contribution of dendrites to the tonic and trimodal patterns of activity in cerebellar Purkinje neurons. J Neurosci 22:10603-10612.
Womack MD, Chevez C, Khodakhah K (2004) Calcium-activated potassium channels are

selectively coupled to P/Q-type calcium channels in cerebellar Purkinje neurons. J Neurosci 24:8818-8822.

Womack MD, Hoang C, Khodakhah K (2009) Large conductance calcium-activated potassium channels affect both spontaneous firing and intracellular calcium concentration in cerebellar Purkinje neurons. Neuroscience 162:989-1000.

Woodruff-Pak DS, Foy MR, Akopian GG, Lee KH, Zach J, Nguyen KP, Comalli DM, Kennard JA, Agelan A, Thompson RF (2010) Differential effects and rates of normal aging in cerebellum and hippocampus. Proc Natl Acad Sci U S A 107:1624-1629.

Xia J, Chung HJ, Wihler C, Huganir RL, Linden DJ (2000) Cerebellar long-term depression requires PKC-regulated interactions between GluR2/3 and PDZ domain-containing proteins. Neuron 28:499-510.

Yamamoto M, Wada N, Kitabatake Y, Watanabe D, Anzai M, Yokoyama M, Teranishi Y, Nakanishi S (2003) Reversible suppression of glutamatergic neurotransmission of cerebellar granule cells *in vivo* by genetically manipulated expression of tetanus neurotoxin light chain. J Neurosci 23:6759-6767.

SUMMARY

The calcium influx and calcium dependent signalling cascades play essential roles in the proper neuronal functions, such as mediating neurotransmitter release, facilitating carious forms of synaptic plasticity and controlling neuronal spike firings. In cerebellum, these functions are well tuned to maintain high specificity and precession during motor performance and learning. This thesis attempts to dissect the fundamental roles of calcium related pathways in cerebellar learning and functions. To do so we combined the genetically manipulated mouse models that specifically target certain cascades of the calcium signalling, with the molecular, electrophysiological and behavioural examinations.

Chapter 3 demonstrate that the deleting P/Q type voltage gated calcium channels specifically at the parallel fiber to Purkinje cell (PF-PC) synapses using a cre-loxP system results in silencing of the majority of the cerebellar granule cells. Stochastic reduction of the synaptic inputs from granule cells up to 70% does not affect the basal motor performance of the mice, but rather disrupts the overnight memory consolidation. We further show this loss of consolidation is correlated with reduced dynamic range of PC simple spike firing pattern and impaired long term synaptic plasticity. Thus our results suggest that the majority of the cerebellar granule cells do not contribute to the fundamental motor performance, but participate in more sophisticated, memory consolidation process. In order to study the underlining mechanisms of such motor learning and memory consolidation at the PF-PC synapses, we further examine the involvements of long term synaptic plasticity at this synapse.

Long term depression (LTD) at the PF-PC synapses has been suggested to be one of the best candidate mechanisms for cerebellar learning. In Chapter 4.1 we show a rather unexpected but extremely interesting result that genetically blocking LTD induction does not affect the motor learning in mouse models. We do so by affecting the target at the very downstream cascades of LTD induction, the internalization of AMPA receptors and examine the VOR adaptation, the eye blink conditioning, as well as the performance on the Erasmus ladder of these mutants. All three mutants perform equally well as the control groups, challenging the classical LTD hypothesis as the main learning mechanism in the cerebellum. Further, we provide an alternative suggestion, that the LTP and intrinsic plasticity might be also important for proper cerebellar learning in Chapter 4.2. The mutant mice with PC specific ablation of the protein phosphotase 2B (L7-PP2B) show impaired LTP at the PF-PC synapses and intrinsic plasticity in PCs, however normal LTD. These mice have mild motor performance deficits but severely aberrant short and long term learning abilities, which could be caused by more regular simple spike firing at lower frequencies.

The positive correlation between increased regularity of simple spike firing and motor learning/memory problems are observed not only in those mutants that PF-PC synapses are affected, but also in the mouse model that lack phasic inhibition from molecular layer interneurons (MLIs, Chapter 5). The PC specific deletion of the γ2 subunits in $GABA_A$ receptors prevents $GABA_A$ receptors from entering the synapses. This results in a severe loss in inhibitory synaptic transmission and thus a more regular PC firing pattern. A computational simulation further supports that the inhibition from MLIs is involved in the fine tuning of the temporal patterns of PCs, which is necessary for the consolidation of newly acquired memory.

CaMKII mediates the long term plasticity at both the excitatory and inhibitory synapses in the cerebellum. Chapter 6 focuses on differentiating the roles of the two main isoforms of CaMKII, the α and βCaMKII in synaptic plasticity. We for the first time generate the βCaMKII null-mutants and studied the induction of LTP and LTD conditions in this mouse (Chapter 6.1). This study shows that the βCaMKII plays an essential role in controlling the direction of synaptic plasticity at the PF-PC synapses. A LTP induction protocol results in LTD in the βCaMKII knockout PCs, whereas a LTD induction protocol in turn induces LTP. These data suggest that the βCaMKII plays an additional structural role that controls the activity of the CaMKII holoenzyme in response to different levels of the calcium signals during synaptic plasticity induction. In Chapter 6.2 we further study the role of α and βCaMKII isoforms in controlling synaptic plasticity at inhibitory synapses. We show that both a- and bCaMKII are essential for LTP at the MLI-PC synapses. However, each of the CaMKII isoforms has a specific role: aCaMKII controls the enzymatic function that enables inhibitory plasticity whereas bCaMKII has a more structural role. In the absence of bCaMKII, the suppressing effect of coincident pre- and postsynaptic activity is reversed to a potentiating effect by means of a novel molecular cascade. Together our findings pioneer the differentiation of a- and bCaMKII in mediating inhibitory plasticity and reveal that these individual roles are consistent for both inhibitory and excitatory synapses.

In Chapter 7 we study the pathogenesis in gain-of-function P/Q type voltage gated calcium channel mutant mice. Both the morphology and synaptic transmission are altered in this mutant, which together with the burst firing patterns in the PCs, could cause impairment in motor performance. Further study on the burst firing pattern not only reveals the involvement of SK channel in regulating the threshold of burst firings in the PCs, but also suggests rescuing effects on PC spiking patterns and motor performance using SK channel enhancers. These data explore the consequence of a gain-of-function calcium channel mutant and suggest several common hallmarks in the pathogenesis shared by both loss- and gain-of-function mutants.

Taken together, this thesis describes the consequences of genetically manipulating calcium mediated signalling cascades on the cerebellar learning and functions. It helps to further understand how various critical neuronal functions can be well controlled by a single calcium ion.

Samenvatting

Neuronale functies zoals neurotransmissie, synaptische plasticiteit en actiepotentiaal generatie worden voor een belangrijk deel gereguleerd door de instroom van calcium ionen en de secundaire effecten hiervan. In de kleine hersenen (cerebellum) zijn de calcium instroom en de hieropvolgende effecten zo afgesteld dat ze de neuronale functies optimaliseren welke nodig zijn voor de regulatie van de motoriek. Mijn proefschrift tracht om de precieze rol van calcium mechanismen in het optimaliseren van cerebellaire functies te verduidelijken. We hebben hiervoor gebruik gemaakt van genetisch gemanipuleerde muizen waarin specifieke calcium mechanismen zijn aangedaan en ook van moleculaire, elektrofysiologische en gedragsexperimenten.

Hoofdstuk 3 maakt duidelijk dat het verwijderen van P/Q-type voltage-gevoelige calcium kanalen uit de synaps tussen parallel vezels en Purkinje cellen door middel van het Cre-LoxP systeem de meeste korrelcellen het zwijgen oplegt. Na stimulatie van de korrelcellen blijkt dat ongeveer 70% geen output meer teweeg kan brengen door de afwezigheid van P/Q-type calciumkanalen. Deze mutatie resulteert in een statische parallel vezel – Purkinje cel synapse: Synaptische plasticiteit van deze specifieke synaps is sterk aangedaan. Het effect op het gedrag van deze mutante muizen is echter miniem: Alleen het onthouden van nieuwe motorische taken is aangedaan, terwijl de het aanleren van deze nieuwe taken wel goed verloopt. Ook het effect op de activiteit van Purkinje cellen is beperkt: Alleen de regelmatigheid van de Purkinje cel activiteit is verhoogd. Onze resultaten geven aan dat wanneer 70% van de korrelcellen monddood wordt gemaakt, er vrijwel geen effekten te meten zijn in het basale functioneren van het cerebellum. Alleen specifieke gedragstesten wijzen uit dat het onthouden, maar niet het aanleren van een nieuwe motorische taak aangedaan is. Om de correlatie tussen aanpassingen van de motoriek en synaptische plasticiteit in de cerebellaire schors beter te bestuderen, hebben we vervolgens de afzonderlijke vormen van plasticiteit gemodificeerd.

Synaptische plasticiteit van de parallel vezel – Purkinje cel verbinding is traditiegetrouw een veel bestudeerd mechanisme in het onderzoek naar de regulatie van motoriek. Met namen ‘long-term depression’, de verzwakking van de parallel vezel – Purkinje cel verbinding op lange termijn, werd sinds de 60-er jaren van de vorige eeuw gezien als hét functionele mechanisme achter motorisch leren. Hoofdstuk 4.1 laat echter zien dat wanneer alleen long-term depression van de parallel vezel – Purkinje cel verbinding is aangedaan, er geen effect is op het motorisch leren. Verandering van de verantwoordelijke neurotransmitter receptoren in deze synaptische verbinding hadden namelijk geen effect op het aanleren of onthouden van veranderde oogbewegingreflexen of oogknipperreflexen. Ook de scores bij de Erasmus ladder tests lieten geen afwijkingen zien. Long-term depression blijkt dus niet het neuronale substraat te zijn voor aanpassing van de motoriek. Hoofdstuk 4.2 laat zien dat ‘long-term potentiation’, de versterking van de parallel vezel – Purkinje cel verbinding op lange termijn, een beter alternatief is als neuronaal substraat van motorisch leren. De Purkinje cel specifieke verwijdering van het enzym ‘proteinfosfatase 2 B’ (PP2B) voorkomt long-term potentiation, maar heeft geen effect op long-term depression. Deze ‘PP2B’-muizen hebben verstoorde motoriek. Het aanleren van nieuwe motorische taken lukt wel, maar het onthouden niet. Onze resultaten laten zien dat behalve het gedrag en de plasticiteit van de parallel vezel – Purkinje cel verbinding ook de activiteit van Purkinje cellen is veranderd in PP2B-muizen: actiepotentialen komen minder vaak voor, maar zijn

wel regelmatiger.

De positieve correlatie tussen de toename in regelmaat van actiepotentialen in Purkinje cellen en motorisch leren blijkt niet alleen voor te komen wanneer de parallel vezel – Purkinje cel verbinding is veranderd, maar ook wanneer de interneuron – Purkinje cel verbinding is veranderd. In hoofdstuk 5 staat beschreven dat wanneer de inhibitoire, synaptische verbindingen niet meer functioneren door het verwijderen van een essentieel component van zg. GABA-erge receptoren, de Purkinje cel activiteit regelmatiger is dan normaal. Door middel van een computersimulatie tonen we aan dat het gebrek aan functionele inhibitoire synapsen in Purkinje cellen en de toename van regelmaat in de output van de cerebellaire schors, oftewel in de Purkinje cel activiteit, leidt tot een probleem met het onthouden van aangeleerde motorische taken, zoals bepaalde oogbewegingreflexen.

Een van de belangrijkste moleculen die geactiveerd wordt door calcium is 'CaMKII'. Dit zg. Kinase-enzym is essentieel voor synaptische plasticiteit van zowel excitatoire als inhibitoire synapsen in Purkinje cellen. Hoofdstuk 6 tracht de verschillende functies van αCaMKII en βCaMKII te onderscheiden in excitatoire plasticiteit (hoofdstuk 6.1) en inhibitoire plasticiteit (hoofdstuk 6.2). In hoofdstuk 6.1 laten we zien dat βCaMKII essentieel is voor het induceren van zowel long-term potentiation als long-term depression van de parallel vezel – Purkinje cel verbindingen, terwijl αCaMKII alleen noodzakelijk is voor long-term depression. Deze resultaten laten zien dat βCaMKII naast een kinase-activiteit ook nog een structurele rol heeft die essentieel is voor αCaMKII om normaal te functioneren bij het moduleren van de synaptische plasticiteit van de excitatoire verbindingen in een Purkinje cel. In hoofdstuk 6.2 beschrijven we eenzelfde essentiele rol voor βCaMKII in de modulatie van synaptische plasticiteit van inhibitoire verbindingen in Purkinje cellen. Wanneer βCaMKII afwezig is, schaadt dat de functie van αCaMKII. Tezamen vormen de resultaten uit hoofdstuk 6 de eerste differentiatie van de functies van αCaMKII en βCaMKII in het reguleren van synaptische plasticiteit in Purkinje cellen.

Hoofdstuk 7 beschrijft welke effecten van de zg. S218L puntmutatie in het Cacna1a gen, dat codeert voor een essentieel deel van de P/Q-type calcium kanalen, ataxie veroorzaken. Zowel de morfologie als de sterkte van de parallel vezel – Purkinje cel verbindingen is verhoogd in deze *Cacna1a*^{S218L} mutante muizen. Purkinje cellen laten ook een versterkte respons zien op synaptische en elektrische stimulaties, waaruit blijkt dat Purkinje cellen hyper-excitabel zijn. De Purkinje cel activiteit gemeten *in vivo* is dan ook erg onregelmatig. Echter, door het stimuleren van calciumafhankelijke kalium kanalen wordt niet alleen het onregelmatig vuren van de Purkinje cellen verminderd, maar ook de ataxie. Bij een gedragstest genaamd rotarod, waarbij de muizen op een horizontale, roterende balk moeten lopen, blijkt dat de *Cacna1a*^{S218L} deze test beter uit kunnen voeren wanneer ze het medicijn Chlorzoxazone, dat calciumafhankelijke kalium kanalen stimuleert, toegediend krijgen via hun drinkwater. Dezelfde therapeutische strategie is ook effectief bij andere muismodellen met een mutatie in het *Cacna1a* gen.

Dit proefschrift beschrijft de consequenties van genetische manipulering van calcium mechanismen met betrekking op het functioneren van de cerbellaire cortex. De resultaten dragen bij aan een verduidelijking hoe het calcium ion de vele verschillende neuronale functies beïnvloedt.

Curriculum Vitae

Name:	Zhenyu Gao 高振宇
Date of birth:	01 June 1982
Place of birth:	Shanghai, China

Education and Experience

2011-	Postdoc Erasmus MC, Department of Neuroscience Rotterdam, the Netherlands
2006-2011	PhD student Erasmus MC, Department of Neuroscience Rotterdam, the Netherlands
2004-2006	Neuroscience (MSc) Vrije Universiteit Amsterdam, the Netherlands
2003-2004	Research assistant Institute of Brain Science Fudan University Shanghai, China
1999-2003	Biotechnology (BSc) Shanghai Jiao Tong University Shanghai, China

List of Publications

Gao Z, Todorov B, Barrett CF, van Dorp S, Ferrari MD, van den Maagdenberg AM, De Zeeuw CI and Hoebeek FE *Effects of enhanced granule cell-Purkinje cell transmission and Purkinje cell excitability in Cacna1a^{S218L} mutants Rescued by SK-channel activators.* Submitted

Gao Z, van Woerden GM, Elgersma Y, De Zeeuw CI and Hoebeek FE *Interactions between specific CaMKII subtypes and $GABA_B$*-receptors *control long-term potentiation at inhibitory synapses.* Submitted

Gao Z*, van Beugen B*, De Zeeuw CI *Cerebellar Cortical Plasticity Cut into Cellular Components.* Submitted

Hoebeek FE*, Galliano E*, **Gao Z***, Schonewille S, Todorov B, Pop AS, D'Angelo E, Maagdenberg AM., De Zeeuw CI *Silencing the majority: The essence of cerebellar granule cells.* Submitted

Schonewille M*, **Gao Z***, Boele HJ*, Vinueza Veloz MF*, Amerika WE, Simek AA, De Jeu MT, Steinberg JP, Takamiya K, Hoebeek FE, Linden DJ, Huganir RL, De Zeeuw CI (2011) *Re-evaluating the Role of LTD in Cerebellar Motor Learnin*g. **Neuron** 70:43-50.

van Woerden GM*, Hoebeek FE*, **Gao Z**, Nagaraja RY, Hoogenraad CC, Kushner SA, Hansel C, De Zeeuw CI, Elgersma Y (2009) betaCaMKII controls the direction of plasticity at parallel fiber-Purkinje cell synapses. **Nat Neurosci** 12:823-825.

Schonewille M*, Belmeguenai A*, Koekkoek SK*, Houtman SH*, Boele HJ, van Beugen BJ, **Gao Z**, Badura A, Ohtsuki G, Amerika WE, Hosy E, Hoebeek FE, Elgersma Y, Hansel C, De Zeeuw CI (2010) *Purkinje cell-specific knockout of the protein phosphatase PP2B impairs potentiation and cerebellar motor learning*. **Neuron** 67:618-628.

Wulff P*, Schonewille M*, Renzi M, Viltono L, Sassoe-Pognetto M, Badura A, **Gao Z**, Hoebeek FE, van Dorp S, Wisden W, Farrant M, De Zeeuw CI (2009) *Synaptic inhibition of Purkinje cells mediates consolidation of vestibulo-cerebellar motor learning*. **Nat Neurosci** 12:1042-1049.

van den Maagdenberg AM*, Pizzorusso T*, Kaja S*, Terpolilli N*, Shapovalova M, Hoebeek FE, Barrett CF, Gherardini L, van de Ven RC, Todorov B, Broos LA, Tottene A, **Gao Z**, Fodor M, De Zeeuw CI, Frants RR, Plesnila N, Plomp JJ, Pietrobon D, Ferrari MD (2010) *High cortical spreading depression susceptibility and migraine-associated symptoms in Ca(v)2.1 S218L mice.* **Ann Neurol** 67:85-98.

(* Authors contributed equally)

Acknowledgments

As the PhD journey approaching its end, all the obstacles on the way became the milestones of achievements. Like other parts of the day life, research is full of fun, happiness, satisfaction as well as blood, sweat and tears. It was the countless amount of helps in hand from many people, that supported me to reach the wonderful end. Hereby I would like to thank all who taught me, helped me or offered moral support.

First I would like to thank my promoter Professor Chris I. De Zeeuw. Dear Chris, thank you very much for offering me an opportunity to work in this department, to learn from you, and to have the best environment to continue my scientific career. You gave the best example how a good scientist combines the hard working ethics with true passion for science. I am lucky to have you as my promoter.

Many thanks go to my co-promoter, Dr. Freek. E. Hoebeek. Dear Freek, I can not express enough gratitude to you for your great efforts in helping me for almost everything. It was a privilege of becoming the first member of the 'Hoebeek lab'; and since then we spent wonderful time together both inside and outside the lab. Thank you so much for teaching me all the techniques, discussing the results and plans and always encouraging me to pursuit my interests. You are truly a great mentor and the best friend. This thesis would not be possible without your help.

During these years I have received many generous help and comments from other professors from the Neuroscience department. Dear Gerard, I would like to thank you for all your intellectual inputs and constructive comments. Thank you for teaching me the knowledge about electrophysiology and showing me how I should interpret the data with extra caution. Dear Ype, due to the nice collaboration, I was often rushing into your office asking many silly questions. Thanks you very much for all the patients, helps and comments on the projects. In addition, thank you both for being the small committee and reviewing my thesis. The same thanks go to another committee, Dr Adriaan Houtsmuller for reviewing my work. I am deeply impressed by the beautiful imaging techniques from you, and hopefully we can work together in the future. I would also like to thank all the other thesis committee for reviewing my thesis and participating the promotion.

Naturally I would like to thank two people that played important parts during my PhD time, and now are also my 'paranimfen'. Dear Elisa, it has been an honour having you as a colleague since the very beginning. We worked back in back on the setups, and enjoyed all the fun in the lab. You are not only a great scientist, but also a wonderful friend (and cook)! Thank you very much for arranging all the

things for me! And dear Boyan, thank you for accepting being my paranimf even you are always busy flying all over the world. I am glad our project worked out so nicely and I had you as a friend. It was always fun to have dinner and hang out with you, and surely many more will come.

I always believe people need luck to have the best lab members; obviously I was the lucky one. First of all, I would like to thank two fabulous ladies. Dear Mandy and Petra, the 'Gao's angels', you've been always extremely kind and caring to me. You made my staying in the Netherlands so much easier that it felt like a second home. A thank you is absolutely not enough to press all my gratitude for your help! To Boeke, thank you for all your great discussion and debates on science, sports, music and almost every topic. You as a critical mind in our lab, definitely brought great ideas and boosted our productivity. And we are so going to have the lobsters together. For the new members in the lab, Oscar and Lieke, it was great to have you in the lab; we shared such a nice time. Oscar, I wish you all the best in your medical training, although I believe you will be also a great scientist. Lieke, I know the start of a PhD is tough, but sure you will handle it just fine. Stijn, it was a shame that you could not stay in Rotterdam for a longer period, but we had great time and I wish you all the best at NIN. And for other former members of the lab, thank you very much for all the helps.

Several other labs helped me extensively during my PhD period. Firstly, I would like to thank the fast growing Schonewille lab. Dear Martijn, we started collaboration on the LTD project the very first day when I started my PhD time. You've been more concerned about my data than myself at that time :). Thanks you for all the great works and help from you that have yielded or will become the fatnastic publications. And for playing football together that we were able to teach other departments how to play from time to time.... Dear Aleksandra, thank you for the discussion and help on various projects and great trips together to Geneva and Chicago. I wish you all the best in your future research. Dear Rogerio, thank you for your weird but interesting conversations, you made the lab unique from any others worldwide. Kai, your Chinese is as impressive as your Matlab skills, good luck for your PhD. Since Martijn taught too many students in his lab, I can not list all the names, but thank you all for the conversations and help.

There are many people from the Elgersma lab I would like to acknowledge. First of all to some former members: Dear Geeske, the only Geeske, you told me almost everything about the CaMKII. Thank you for generating all these fantastic mice that we learned tremendously from. There is no doubt you are the best of the best. Dear Nils, you were actually the first one that helped me to improve my slice quality when I started my PhD. Thank you for telling me about the last stage of thesis writing, indeed it was quite a task. Dear Miki, there was a long period that

we had to share the same mouse on daily basis, thank you for the help and the wonderful Italian smile. Stathis thank you for all the friendly conversations and vivid demonstrations of how a mouse should behave. It's a pity that all you guys can not join the defence, but no matter where you are, thank you. Dear Minetta, Laura and Mehrnoush, thank you so much for always arranging the mice for me and tolerating the constant questions about the breeding speed. Dear Azar, I really appreciate all your suggestions and help on electrophysiology. For Susan, good luck for your PhD, now I can say the last year will be intense, but sure you can do it. Dear Caroline, I hope you still remember how to patch a Purkinje cell, then you are better than lots of the hippocampal people. Wish you all the luck for your future research. Dear Thijs, it was always nice to find you in the lab late in the evenings and weekends for a good conversation and a cool beer.

I would like to thank Arn and Curtis from Leiden University. Dear Arn, thank you for your good advices on many of our collaborating projects, and more importantly thank you for squeezing time squeezing time out of your busy schedule for my promotion. Curtis, I learned a lot from you about electrophysiology, especially about calcium channels, all the best for your new career!

Many thanks to the two 'living libraries', Tom and Jerry. Thank you Tom for your amazing knowledge about cerebellum, I can always find the answer at your place if I have any anatomical question. Dear Jerry, thank you so much for all the discussions over these years, I learned from you not only about cerebellum but also wonderful insights about life. For sure we will meet again soon.

To the members of the big De Zeeuw lab; Bas, Laurens, Henk-Jan, Mafer and Cullen and others. Thank you for the helps in experiments and wish you all the best in the future. Also, I would like to say thank you to the colleagues from NIN. Dear Laurens thanks for those fun time about science and about wine. Sure we will find great stuff from the cerebellar nuclei. Beerend and Jornt, thank you for your hospitality at NIN.

Dear Ru, Arrrrrr for the Igor, Arrrrrr for the internal and chemicals, Arrrrrr for the great discussions and Arrrrrrr. John, your cheerful attitude always impresses me, thank you for all the nice conversation. Also for Tom, Silviu and Heico, thank you all for your helps. To Arthur and the members of Houweling lab, thank you all for the nice conversations.

Many thanks to the Kushner lab for their help with mice and behaviour tests. Dear Steven, you always had brilliant comments on our seminars, I learned a lot from you. For the lab members: to Denise for your generous offers of CaMKII mice; to Laurie-Anne for the help with the puller, and for Femke for the kind help with culture protocols.

A big “thank you” to the members of Marcel de Jeu’s lab. Dear Marcel, thank you for the constructive comments on the experiments and setups. Bazzi, thank you so much for your help in imaging and even more for all your jokes and nick names, you are indeed also a really talented comedian. And Sheena, for your kind helps on staining and microscope.

Dear Dick, talking with you is really interesting, there is no way I can predict what you are going to say. That however is the reason I really enjoy talk with you! Sorry though for laying back in teaching eyes and ears though. Dear Vera, for all the friendly conversations in the histology lab.

I would like to thank the people who were always kind enough to give me a crush course about molecular biology. Dear Casper, thank you for all the comments on my projects and nice suggestions. To the members of the Casper lab, Esther, Karin, Marijn, Kah Wai, Myrrhe, Max, Nanda and Phebe, thank you for the conversation with you guys, it was particularly fun after a few bottles of beer. In addition, thank you Robert and Lukas for the suggestions on culture and imaging techniques.

To my form neighbours from the Hansel lab. Dear Christian, thank you for sharing your wonderful knowledge about the Purkinje cell plasticity. For Genny, Eric, Amor and Simone, thank you for all the laugh we had in your office.

There are a group of people that offered me the best supports I can ever imagine. Let us to be honest, we can not do much without help from them. Dear Erika and Elize, thank you not only because I could always count on you for the perfect histology and EM, but also for the huge amount of “Bitterballen” I had. Dear Hans, you are the magician in our department, who virtually fixed all the broken pieces I brought to you. Thank you Edith, Loes and Suzan for arranging all the documents, applications, forms and other really annoying but important works for me. And big thank you to Kenneth, Annette, Jurgen and Ria for making sure my orders always went through and I had enough money to buy bitterballen.

I was the only Chinese people in the department when I started, but now I can always talk in Chinese. So I would like to thank you all here, for the fast expending Chinese group：亲爱的同志们，战友们，帅哥美女们，很高兴能在荷兰认识你们，这也算是缘分吧。祝你们今后工作顺利，事事顺心。

Last but not least, I would like to thank my family for their infinite love. 亲爱的爸爸妈妈，虽然我离开家已经这么多年了，你们还是一样的操心，谢谢你们对我做的一切的一切，没有你们就没有我。亲爱的胡君，谢谢你能在我身边，感谢你对我这么多年的包容和牺牲。我们共同经历了很不寻常的七年，这里面有太多的故事太多的感动，但 这一切都是因为有你才这么美丽。